

THE EFFECT OF MOBILITY IMPAIRMENT ON FEMORAL CORTICAL AND
TRABECULAR STRUCTURE

by

Devora Gleiber, BA

A thesis submitted to the Graduate Council of
Texas State University in partial fulfillment
of the requirements for the degree of
Master of Arts
with a Major in Anthropology
May 2017

Committee Members:

Daniel Wescott, Chair

Deborah Cunningham

Kate Spradley

COPYRIGHT

by

Devora Gleiber

2017

FAIR USE AND AUTHOR'S PERMISSION STATEMENT

Fair Use

This work is protected by the Copyright Laws of the United States (Public Law 94-553, section 107). Consistent with fair use as defined in the Copyright Laws, brief quotations from this material are allowed with proper acknowledgment. Use of this material for financial gain without the author's express written permission is not allowed.

Duplication Permission

As the copyright holder of this work I, Devora Gleiber, refuse permission to copy in excess of the "Fair Use" exemption without my written permission.

ACKNOWLEDGEMENTS

I would like to thank my advisor, Dr. Daniel Wescott, for all of his support, assistance, and guidance with this research and every day throughout my time in the graduate program. Thank you to my committee members, Dr. Deborah Cunningham and Dr. Kate Spradley, for all of their support and guidance in planning, executing, and completing this thesis work. I would like to thank my incredible cohort, Lauren Meckel, Justin Pyle, Courtney Siegert, Alexis Goots, Chloe McDanel, and Alejandra Ayala Bas, for their incredible support, brainpower, and everlasting friendship. I could not have made it through this program without them.

Thank you to Dr. Dawnie Steadman at the University of Tennessee, Knoxville, for allowing me to borrow femora for my mobility impaired sample from the William M. Bass Donated Skeletal Collection. I would like to thank Dr. Tim Ryan at Penn State University for welcoming me to his lab and training me in conducting trabecular analysis. Thank you to the Graduate College, the Grady Early Fellowship, and the Anthropology Department for the funding I received, which enabled my execution and completion of this research project. This research is also supported in part through instrumentation funded by the National Science Foundation under Grant NSF:MRI 1338044.

Lastly, and most importantly I would like to thank the individuals and their families who have donated their remains to the willed body donation programs at both the Forensic Anthropology Center at Texas State and at the University of Tennessee, Knoxville. Without their generous gift I could not have conducted such skeletal research.

TABLE OF CONTENTS

	Page
ACKNOWLEDGEMENTS.....	iv
LIST OF TABLES.....	vii
LIST OF FIGURES.....	viii
LIST OF ABBREVIATIONS.....	x
CHAPTER	
1. INTRODUCTION.....	1
Research Questions.....	2
Bone Microstructure and Biomechanics.....	3
Trabecular Architecture.....	5
Cortical Bone.....	6
Previous Studies.....	8
Disuse.....	8
Mobility.....	11
2. MATERIALS AND METHODS.....	14
Study Population.....	14
Reconstruction of Bone Mechanical Properties.....	15
Fixturing and Scanning.....	16
Volumes of Interest.....	19
Trabecular Bone Analysis.....	21
Cortical Bone Analysis.....	22
External Bone Dimensions.....	25
Statistical Analysis.....	26
3. RESULTS.....	29
Parametric or Nonparametric.....	29
Mobility Impaired vs. Normal Mobility.....	30
Mobility Impaired vs. Normal Mobility by Sex.....	33
Visual Assessment.....	35

Sex Differences	37
Males vs. Females Combined Mobility	37
Males vs. Females by Mobility	38
Age Correlation.....	40
Mobility Impaired Left vs. Right	41
Mobility Impairment Time Dispersal	43
 4. DISCUSSION AND CONCLUSION.....	 44
Trabecular Architecture	44
Cortical Bone	46
Mobility Impairment Time Dispersal	51
Bioarchaeological application.....	51
Conclusion	52
 APPENDIX SECTION.....	 54
 REFERENCES	 130

LIST OF TABLES

Table	Page
2.1. Trabecular bone properties	22
2.2. Cortical bone cross-sectional properties	25
3.1. Normality and homoscedasticity of the trabecular and cortical variables and whether a parametric or nonparametric test is appropriate	29
3.2. Mobility differences for each trabecular variable	34
3.3. Mobility differences for each cross-sectional variable with sexes combined and separate	34
3.4. Sex differences for each trabecular variable for the combined and separated mobility groups	39
3.5. Sex differences for each cortical bone cross-sectional variable for the combined and separated mobility groups	39

LIST OF FIGURES

Figure	Page
2.1. Complete femur and amputated femur with plastic BBs at neck midpoint, subtrochanteric, and midshaft	16
2.2. The fixtures used for scanning the femoral head, femoral shaft, and femoral shaft with a femoral amputation site	17
2.3. Orientation for the femoral head reconstructions	18
2.4. Representative Avizo isosurface of the high-resolution μ CT scan of a left proximal femur, with the ROI box aligned around the femoral head	20
2.5. Position of the VOI within the trabeculae of the femoral head and subsequent VOI isosurface of a mobility impaired and normal mobility individual	20
2.6. External measurements taken on the proximal femur: maximum femoral head diameter, neck midpoint breadth, and neck midpoint length	26
3.1. Boxplots of trabecular properties for mobility impaired and normal mobility individuals	31
3.2. Boxplots of the significant %CA and CAstd. LBM of the midshaft and subtrochanteric slices, and MA, MAstd., and MAstd. LBM of the midshaft slices comparing the mobility impaired and normal mobility individuals	32
3.3. Femoral midshaft slices from a mobility impaired (D47-2013) left and right femora, and the normal mobility match (D21-2011) left femur	36
3.4. Neck midpoint slices from UT14-92D left and right femora, and the normal mobility match (D49-2014) left femur	36
3.5. Boxplot of significant difference in ConnD for males and females in for the mobility samples combined	38
3.6. Boxplots of differences in Tb.Th and midshaft TAst. between the amputated leg and complete leg femora of single amputees	41

3.7. Femoral midshaft slices of a mobility impaired individual with bilateral disuse from double amputation with matching patterns of remodeling between the left and right femora, and the matched normal mobility individual (D49-2014) left femoral slice	42
3.8. Femoral midshaft slices of a single amputee (UT60-09D) with a left leg amputation, the non-amputated leg, and the matched normal mobility individual left femur	42
4.1. Scatterplot regressing I_{\min} against I_{\max} for the mobility impaired samples separated by impairment type and the normal mobility samples.....	50

LIST OF ABBREVIATIONS

Abbreviation	Description
μ CT	micro-computed tomography
SMA _s	second moments of area
TXSTDSC	Texas State University Donated Skeletal Collection
BMI	body mass index
NSI	North Star Imaging, Inc.
BB	ball bearing
μ m	microns
VOI	volume of interest
ROI	region of interest
BV/TV	bone volume fraction\
BV	bone volume
TV	total volume
Tb.Th	trabecular thickness
Tb.Sp	trabecular spacing
ConnD	connectivity density
DA	degree of anisotropy
I_{\min}	second moment of area around minor axis
I_{\max}	second moment of area around major axis
Θ	theta
Z_{\min}	section modulus around minor axis
Z_{\max}	section modulus around major axis
Z_p	polar section modulus
J	polar second moment of area
I_{\max}/I_{\min}	cross-sectional shape ratio
TA	total area
CA	cortical area
TAstd.	total area standardized for body mass
CAstd.	cortical area standardized for body mass
LBM	lean body mass
MA	medullary area
%CA	percent cortical area
ANOVA	analysis of variance
MAstd.	medullary area standardized for body mass
Subtroch	subtrochanteric
M.Obese	morbidly obese
Ances.	ancestry

1. INTRODUCTION

Bone is a dynamic tissue that responds to mechanical force by increasing (high loads) or decreasing (disuse) in mass (Huiskes et al. 2000; Hazelwood et al. 2001). Therefore, a relationship exists between bone architecture and mechanical usage (Rubin and Rubin 2006; Ruff et al. 2006; Skerry 2008). While anthropologists frequently examine long bone structure to reconstruct mobility patterns in past populations (Holt 2003; Stock 2006; Tardieu 2010; Ryan and Shaw 2015), structural changes in the lower limb bones associated with conditions that result in reduced mobility have received far less attention (Wescott 2014).). Understanding the patterns expressed from unloading in individuals who have experienced disuse is critical to correctly interpreting various loading signatures. Reduced mobility or long-term immobility results in diminished muscular stress and normal weight bearing on the lower limb bones. Therefore, reduced ambulatory ability should be reflected in the structure of these bones.

Being able to recognize and diagnose long-term mobility impairment from human skeletal remains has significant implications within bioarchaeology, forensic anthropology, and bone biology. Within bioarchaeology, patterns of mobility are often interpreted using trabecular and cortical bone architecture and geometry. This research serves to bolster the accuracy of such interpretations by exploring the patterns in bone that occur when vertical loading forces are entirely removed during one's life. Furthermore, it serves as a basis and guide for inferring and possibly diagnosing instances of mobility impairment in the bioarchaeological record. Similarly, within forensic anthropology this research aids in identifying indicators of mobility impairment during life, which may assist in identification of the individual. In addition, there are

biomechanical and biomedical implications for bone use correlation with disuse and for exploring types of impairment in life that can cause evidence of limb disuse in the bone. Mobility impairment can result from multiple causes, such as injury, disease, or neurological and muscular disorders. The results of this study add to the knowledge of how bone remodels after an event that leads to disuse of one or both lower limbs, but in cases of retained muscle function.

Research Questions

This research investigates the effect of disuse on the cross-sectional geometry and trabecular bone structure (i.e., thickness and orientation) of the lower limbs, and in particular, the femur. Comparisons of the cortical bone structure and geometry, and trabecular architecture was made between individuals with known lower limb mobility impairment during life and individuals with no known mobility impairment. Such individuals with no known mobility impairment will be referred to as having normal mobility. High resolution images of the bone were obtained using micro-computed tomography (μ CT). High resolution imaging of the bone allows for non-destructive investigation of the internal and external structure of the bone.

The main research question investigated in this research is how does cortical and trabecular bone remodel, (i.e., change in orientation and/or strut thickness) in response to unloading from disuse? Furthermore, can these changes be used to diagnose individuals with long-term mobility impairment in medicolegal cases and bioarchaeological investigations? Therefore, the null hypothesis is that there is no quantifiable difference in the cortical bone geometry or trabecular thickness and orientation in the femora of mobility impaired individuals compared to those of normal mobility individuals. The

alternative hypotheses are that 1) femoral bone density will be reduced in mobility impaired individuals compared to that of normal mobility individuals in both the cortical bone area and trabeculae, 2) the trabecular orientation and structure is different in mobility impaired individuals compared to that of normal mobility individuals, and 3) the cortical bone geometry will be different and more varied in mobility impaired individuals. Additionally, any affect that sex or age might have on the trabecular and cortical properties was also investigated.

Bone Microstructure and Biomechanics

Anthropologists have long used mechanical principles to explain skeletal structure and variation of both past and present populations. In particular, it is often used to reconstruct behavioral and mobility patterns among human populations (Ruff 2008). The concept that mechanical loading influences bone structure is often referred to as Wolff's Law, although many anthropologists now prefer to instead use the term "bone functional adaptation" (Ruff et al. 2006a ; Ruff 2008). This is the idea that there exists a simple feedback model based on the mechanical deformation of bone tissue under external mechanical loading. The amount a material deforms in response to the application of force and relative to the material's original length is the strain (Rubin and Rubin 2006; Skerry 2008). The force causing such strain is defined as the stress being placed on the object (Rubin and Rubin 2006).

Bone response to mechanical usage is a result of bone having osteocytes integrated into its matrix and connected by a network of canaliculi. These cells are the bone's mechanosensory system. Osteocytes sense strain and signal bone formation cells (osteoblasts) and bone resorption cells (osteoclasts) to correct the imbalance (Sievänen

2010). When an excess amount of stress is placed on bone, osteoblasts will begin to lay down more bone in response. When there is very little external stress placed upon the bone, osteoclasts resorb more bone than is being laid down by osteoblasts. A qualification to the general feedback loop is that strain levels the bone is accustomed to is not constant, but varies depending on its anatomical location and factors such as diet, disease, age, hormonal factors, and genetic background (Ruff 2008). Additionally, the type of strain, its frequency, and the loading history of the bone cells influence the magnitude of the bone response (Ruff et al. 2006). Stress or lack thereof can even lead to a change in the cells themselves that are present in the bone. For example, the exposure to microgravity conditions during space flight results not just in bone loss, but also in a decrease in number of osteoblasts (Rubin and Rubin 2006). It has been found that strain actually reduces the rate of osteocyte apoptosis, thus matrix deformation is critical to the survival of osteocytes (Gross et al. 2001; Rubin and Rubin 2006).

The bone mechanostat theory, first outlined by Frost (1996) then reiterated and updated by him (2003), describes the adaptation of bony tissue to its mechanical environment (Lerebours and Buenzli 2016). This hypothesis originates from the observation that healthy load-bearing bones and the trabeculae of any contemporary bony vertebrate contain “more strength than is needed to keep typical peak voluntary mechanical loads on them from causing nontraumatic fractures” (Frost 2003:1081). This indicates that additional forces are causing bone formation and remodeling other than the basic structure needed to keep the bone from spontaneously fracturing. Frost proposed a simple feedback loop in which regions of bone experiencing high mechanical loads

become reinforced and strengthened, while those under low mechanical loads are removed (Lerebours and Buenzli 2016).

Lerebours and Buenzli (2016) have recently elaborated on this basic concept to create a cell-based mechanostat theory of bone. They discuss that having a mechanostat relies on there being a “mechanical reference state” or setpoint. Above this point the tissue experiences mechanical overuse and below it mechanical disuse. Bone remodeling is sensitive to changes in strain magnitude, number of loading cycles, distribution of the loading, and the rate of strain. In order to influence the bone cell response, the signal must be dynamic, or time-varying; static loads are ignored by the skeleton (Rubin and Rubin 2006). Therefore, this setpoint varies in space and time, as well as local loading history, load timing and rest periods, and influences the bone adaptation. Thus, the nature of the osteocyte response depends on the magnitude of the difference between the habitual strain signal and that in the new situation. The cellular basis of mechanosensation should not be forgotten, and an accurate mechanostat theory accounts for both osteocyte signaling to osteoclasts and osteoblasts, and the desensitization of osteocytes to the mechanical stimulus.

Trabecular Architecture

Trabecular bone is the porous bone found within articulating joints and vertebral bodies. Its architecture combines suitable strength and stiffness with minimal weight, and thus provides optimal load transfer (Huiskes et al. 2000). It is also thought to be primarily adapted to sustain compressive loads along its main trabecular orientation (Sanyal et al. 2012). A distinct characteristic of trabecular architecture is its ability to adjust its orientation. Huiskes et al. (2000) used computational modeling to evaluate local strain

and confirm that remodeling in trabeculae is governed by feedback from mechanical load transfer. They found that no matter the original trabecular configuration, when a similar stress was applied, a similar architecture was eventually obtained, confirming the stability of the process. For example, when the external load being applied to the architecture was rotated by 30°, the trabeculae gradually reorientated to again align with the external load. Additionally, when external loading was reduced by 20%, trabecular thickness was reduced, resulting in a bone mass loss of 15.8%, similar to that observed in individuals subjected to disuse (Zerwekh et al. 1998; Huiskes et al. 2000). These functions and responsiveness of trabecular bone to mechanical loading makes it the ideal material to analyze when assessing the effects of loading or disuse on bone.

Utilizing high resolution μ CT technology allows the microarchitecture of trabecular bone to be visualized and quantified. Analysis of the three-dimensional morphology of trabeculae examines several key parameters, such as bone volume fraction, average trabecular thickness and separation, connectivity of the trabeculae, which can be used as a proxy for the number of trabeculae, and structural anisotropy, a measure of the extent to which trabeculae are similarly aligned (Fajardo and Müller 2001). These trabecular properties have been used to quantify trabecular bone in a number of studies of various species and anatomical locations, such as vertebrae, proximal and distal femur and tibia, iliac crest, metacarpals, and calcaneus (Turunen et al. 2013).

Cortical Bone

Cortical bone, also known as compact or lamellar bone, is the dense outer surface of most bones and composes the diaphyses of long bones. It is composed of closely

packed osteons containing a central haversian canal that is surrounded by concentric rings of bony matrix. Cortical bone cross-sections, particularly from long bone diaphyses, are commonly used to study the loading history of individuals and populations. Since long bone diaphyses behave much like engineering beams when mechanically loaded (Huiskes 1982; Ruff 2008), they can thus be similarly analyzed. In such a beam model, the amount of bone and its distribution from externally applied forces can be calculated to estimate the direction of loads and the strength of the bone using cross-sectional geometric properties of the beam. When strain reaches a certain point the beam will fail, or fracture. The ability of the structure to resist fracture is the strength, and the resistance of it to deformation, prior to failure, is the rigidity (Martin et al. 1998). There are also different types of loading that act on the bone: axial compression and tension, which act along the bone's long axis and compress or pull it apart; bending, producing both compression and tension on opposite surfaces of the cross section; and torsion, which is produced from the bone being twisted about its long axis and causing diagonal, or shearing, stresses (Ruff 2008).

With computed tomography and now even higher resolution μ CT imaging available, cortical bone cross-sections can be visualized and geometric properties assessed non-destructively. The cross-sectional geometric properties that can be used to assess the bone is response to the above listed forces and evaluate the rigidity and strength of the bone are listed in Table 2.2. Under pure compression and tension, the rigidity and strength of the bone are proportional to the cortical bone cross-sectional area. However, that simplistic model of mechanical loading is not often the case. More important and realistic is to assess bending and torsion. The cross-sectional properties

known as second moments of area (SMAs) are proportional to bending and torsion rigidity. The related strength properties are called section moduli and are calculated by dividing the SMAs by half the diameter of the section. It is obvious that in such mechanical analyses, the distribution of bone is very important, such that “the same bone area distributed further from the center of the section will result in a much greater bending and torsional rigidity and strength” (Ruff 2008:186). Another measurement, although of morphological rather than biomechanical significance, is the total subperiosteal area and medullary area, which can be used to calculate the cortical area and the percent cortical area. Of course, true mechanical loading situations are more complex than the simple beam modeling discussed; however, these properties are the best available for assessing and giving some estimate of the bone’s mechanical properties and loading environment (Ruff 2008).

Previous Studies

Disuse

Many of the experimental studies investigating the effect of unloading in a disuse model has been conducted using rats. This is likely due to their small size and thus quicker bone response, which makes them easier to handle, adjust their mobility, and study significant changes over a shorter period of time. Studies on the unloading of rat hind limbs, using tail suspension, shows that the resorption activity is unchanged, but the formation activity significantly reduced (Vico et al. 1998; Simske et al. 1992; Baiotto et al. 2009). This indicates that the main response to unloading is a decrease in osteoblast activity. Bouvard et al. (2012) studied the bone microarchitecture and macroarchitecture of the tibia in a disuse model of growing rats by injecting a muscle paralytic into the right

hind limb of twenty-five rats. Over the course of the study they found that the unaffected left hind limb significantly increased in cortical thickness, cross sectional total area and growth in length due to the sudden overuse required. Comparatively, in the paralyzed right hind limb, bone trabecular volume and cortical thickness significantly decreased as soon as day 14. There was also an associated increase in cortical porosity in the paralyzed limb. Growth in length did not differ between sides, and while the total area of the cross section did not increase, the right limb cross section did acquire a more rounded shape. While it is uncertain how similarly human and rat bones remodel, this study indicates that there will be significant differences between loaded and unloaded limbs, and indicates that both trabecular and cortical should be affected.

Studies conducted on paraplegic individuals (Biering-Sorensen et al. 1990; Frey-Rindova et al. 2000; Eser et al. 2004; Dionyssiotis et al. 2007) show that cortical and trabecular bone loss responds differently during various intervals of time post-injury. Dionyssiotis et al. (2007) found that the trabecular bone was more affected in those individuals in their study with a mean paralysis duration of 5.7 years. Eser et al. (2004) studied eighty-nine combined paraplegic and tetraplegic patients with a paralysis duration of 2 months to 50 years. They found that only trabecular bone mineral density decreased; the cortical wall of the femur and tibia became thinner, but no less dense. Additionally, when they analyzed data with a time post-paralysis of less than 5 years, they found a significant linear decrease of cortical bone mineral density, with an overall decrease in the epiphyses and shaft by 50-60%. There was an initial decrease in cortical bone in the shaft based on endosteal resorption, after which new levels of stability were reached after around 5-7 years (Eser et al. 2004). This clearly indicates that bone response to disuse is

more complicated than simple resorption and loss, and that cortical and trabecular bone likely respond differently in time and degree.

At the extreme of unloading environments is that of microgravity experienced by individuals in space flight and on long-term space missions. Accumulated data from over 40 years of space exploration show that this has a very detrimental effect on bone and muscle (Qin et al. 2013). It was found that astronauts lose bone mineral in the lower limbs at a rate nearing 2% per month. The greatest bone mineral density losses from time in space have been observed in the skeleton of the lower body. This is in agreement with general studies of osteopenia, a disease characterized by long term bone tissue loss, particularly in the weight-bearing skeletal elements. Even in an experimental 7-day bed rest model for microgravity, a decreased bone formation rate in the iliac crest was observed (Qin et al. 2013).

The femur is an accurate bone to study for unloading effects because it is of greater importance for maintained function of the body. This helps eliminate possible confounding variables of health that may affect bone. For example, calcium deprivation can cause skeletal bone loss, however sites most affected are more likely to be those of lesser importance for maintained function, such as the distal extremities rather than those closer to the trunk of the body or the skull (Skerry 2008). Therefore, any bone loss or changes observed in the proximal femur of individuals with known mobility impairment are most likely to be the result of unloading from disuse, rather than a confounding health factor.

It is important to remember that overloading and disuse are the increase and reduction in activity from that which the skeleton is currently habituated, and therefore

are relative terms. There are no absolute levels of activity that constitute overuse or disuse. Thus, disuse is not assessable purely in terms of levels of activity. One person may gain bone under the same conditions that another loses it because each is habituated to a different previous level (Skerry 2008).

Mobility

The other side of this concept of a dynamic, self-regulating skeleton that tunes its mass and architecture to the prevailing demands of habitual activity (Skerry 2008) is that this allows for inference of mobility patterns from the trabecular and cortical architecture. Furthermore, when studying past populations, populational differences in mobility can be used by bioarchaeologists for inferring such important information as subsistence strategy, division of labor, demography, trade, and territoriality (Wescott 2014). The femur is most commonly used for such studies. In human archaeological populations, femoral diaphyseal cross-sectional shaft is often used for interpretation of terrestrial logistic mobility. This is the daily land distance covered by individuals or groups. Variation in this shape is also influenced by lower limb habitual activities, body physique, and terrain type amongst others (Wescott 2014). Diaphyseal cross-sectional geometric properties have been used to investigate populations over a broad span of time. Such studies have investigated the evolution of bipedalism (Tardieu 2010), increasing sedentism in Upper Paleolithic and Mesolithic Europeans with the onset of the Last Glacial Maximum (Holt 2003), the robusticity of hunter-gatherers relative to climate and habitual behavior (Stock 2006), and differences in pre- and protohistoric Great Plains populations due to subsistence practice and geography (Wescott 2008).

More recently, with the increasing use of high resolution μ CT, researchers have begun utilizing analyses of trabecular architecture for studies on mobility and subsistence. Of much interest has been the relative gracility of the modern human skeleton despite having an enlarged body size and lower limb joint surfaces in comparison with extant primates. To investigate this, trabecular analysis has been conducted comparing modern humans, non-human primates, various fossil hominins, hunter-gatherer and agriculturalist populations (Chirchir et al. 2012; Ryan and Shaw 2015; Chirchir et al. 2017). Chirchir et al. (2012) found that only recent modern humans have low trabecular density throughout the limb joints, while extinct hominins and pre-Holocene *Homo sapiens* retain the high levels of trabecular density seen in nonhuman primates. Additionally, Ryan and Shaw (2015) found that the relative gracility of the modern human skeleton is the result of decreased biomechanical loading. Chirchir et al. (2017), compared more sedentary Holocene agricultural with Holocene forager populations, and agreed with Ryan and Shaw (2015) results. They found that a decline in activity levels associated with agriculture significantly contributed to the reduction in trabecular bone volume.

With the increasing use of trabecular analysis for interpreting mobility, understanding how the bone responds to unloading from disuse can in turn indicate how use maintains bone growth and density, and confirm the accuracy of interpreting mobility patterns among past populations. Wescott (2014) did this with diaphyseal shape, comparing that of five individuals with long-term limited mobility to those with normal mobility, and thus examine temporal trends in Native American and modern United States populations. He found that the mobility impaired individuals exhibited a reduction

in bending rigidity in both the I_{\max} and I_{\min} planes compared to that of the mobile groups composed of Paleolithic European hunter-gatherers, Arikara, Inuit, and modern American Blacks and Whites. The research presented in this paper similarly examines differences between individuals with normal mobility and those with mobility impairment. However, with the use of μ CT imaging the trabecular architecture was able to be analyzed as well as the cortical area and cross-sectional geometry.

2. MATERIALS AND METHODS

Study Population

The study population is made up of twenty-eight mobility impaired and twenty-eight fully mobile individuals (Appendix A). Within each mobility group nineteen of the individuals are male and nine are female, with a mean age of 66 years. The mobility impaired sample includes a variety of individuals across a gradient of mobility impairment, including two wheelchair bound individuals, nine double amputees, fifteen single amputees, one individual with cerebral palsy, and one individual who was immobile to the bed/couch for five years before death. The mobility impaired sample (n = 28 individuals; 55 femora) was acquired from the Texas State University Donated Skeletal Collection (TXSTDSC: n = 9), the William M. Bass Donated Skeletal Collection housed at the University of Tennessee, Knoxville (n = 18), and the University of Missouri (n = 1). The normal mobility sample (n = 28) is composed of individuals from the TXSTDSC that were sex and age matched as closely as possible to the mobility impaired individuals. Ancestry and body mass index (BMI) range were also matched when possible.

While it is known that bone responds to mechanical loading, there are other factors that can affect the response to loading and disuse. The most tangible of these factors are sex, age, genetic constitution, and nutrition. Males and females respond differently to loading related events, and age can affect the initial density of the bone (Skerry 2008). Following this, each individual in my study population was age and sex matched with a normal mobility individual for comparisons in order to control for the confounding variables of age and sex. Another possible confounding variable is the

length of time an individual was mobility impaired. This was accounted for as much as possible by assessing individuals with known histories. The amount of time of disuse is known for fourteen of the twenty-eight individuals and ranges from about 4 months to 15 years (Appendix A). All of the individuals became mobility impaired as adults.

Both femora were acquired and analyzed for the mobility impaired individuals, and one femora (left side whenever possible) was chosen from the normal mobility individuals. There were two mobility impaired individuals in my sample for which only one femur was either able to be acquired or was usable for scanning. The right femoral head of UT06-02D was a metal replacement; thus, no femoral head scan could be acquired or analyzed for this study. However, the shaft below the metal replacement was scanned and an estimated femoral midshaft slice was used in the cortical bone analysis. Only the left femur of the individual with cerebral palsy (MUA042208) was able to be acquired.

Reconstruction of Bone Mechanical Properties

Micro-computed tomography (μ CT) is a non-destructive imaging method that creates high resolution images that can be used to reconstruct the bone in three-dimensional space and to analyze the internal structure of bone (Fajardo and Müller 2001). In this project, a North Star Imaging, Inc. (NSI) X5000 μ CT system was used to image the proximal end and shaft of femora of both mobility impaired and normal mobility individuals. Before scanning, 0.12-gram green plastic airsoft ball bearings (BBs), 6mm in diameter, were hot glued to the bone in three locations (Figure 2.1): 1) midpoint of the femoral neck, 2) 20cm below the lesser trochanter, and 3) midshaft of the

femoral diaphysis. Midshaft was determined as half of the maximum femoral length.

These were placed to mark which slices would be analyzed for cortical bone properties.

In the case of single femoral amputees, midshaft was estimated on the partially amputated femora using the other complete femur from the same individual.



Figure 2.1. Complete femur (left) and amputated femur (right) with plastic BBs at neck midpoint, subtrochanteric, and midshaft.

Fixturing and Scanning

For scanning of the femoral heads, the femora were fixtured to a wedge made out of green florist foam and held in place with rubber bands (Figure 2.2A). For most of the femoral shaft scans, the distal end of the femur was fixtured in a cut out white foam piece inside of a tall plastic cylinder (Figure 2.2B). For those femora with amputation sites, the proximal ends were either fitted into the same white foam and tall plastic cylinder as used for the distal ends (Figure 2.2C) or fixtured on green foam inside of a large plastic cylinder and secured with other foam pieces. Florist's foam was used since it has a low density and can be easily filtered out of the μ CT scans and subsequent reconstructions;

however, any time a plastic cylinder was used, the area of the bone being scanned had to be above the container so that the cylinder was not captured in the scan.

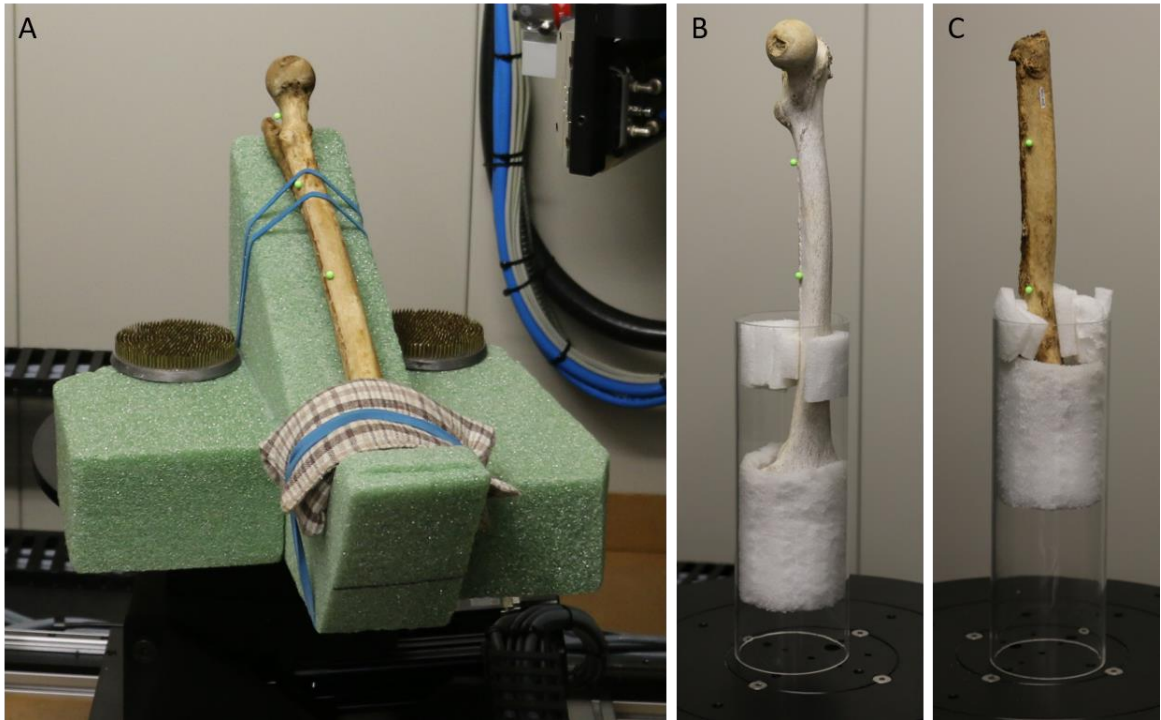


Figure 2.2. The fixtures used for scanning the A) femoral head, B) femoral shaft, and C) femoral shaft with a femoral amputation site.

The scans were conducted using the NSI efX_{DR} program (North Star Imaging, Inc.). Some of the basic settings for the scanning were as follows: focal spot of 7 microns (μm), 3060-3090 projections for the femoral heads and 950-1750 projections for the shafts, 3 frames averaged, a 15ms delay between each rotation, voltage ranging from 102-106kV, and a current range of 172-205 μA . There is a recommended minimum voxel to object size ratio of two (Bouxsein et al. 2010). Since human trabeculae commonly range from 200-400 μm (Mullender et al. 1996), a resolution of 50 μm or less is recommended when scanning human bone for trabecular analysis to ensure that the trabecular visualization is accurate for subsequent analyses. In this study, all femoral head scans had a resolution of 32-43 μm . The femoral shaft scans, which were used for analysis of

cortical bone slices, do not require such a high resolution, and thus image resolutions ranged from 73-88 μm . However, there were six femoral shaft scans with resolutions of between 110 μm and 115 μm obtained in order to include the amputation site in the scan. Lastly, there is one scan with a resolution of 143 μm , which was done to include the entire metal rod within the femoral shaft for data collection overlap on another research project.

When conducting μCT it is important to calibrate the image. Following the scanning of each object, or any time the imaging geometry is changed, CT calibration was run to “establish key parameters such as true length scale and beam geometry” (North Star Imaging, Inc.). This is what accurately sets the voxel size during reconstruction. A large 15mm calibration tool was used for all of the CT calibrations.

All of the scans were reconstructed using the NSI efX_{CT} program (North Star Imaging, Inc.). During reconstruction, the femoral head scans were oriented along the axes of the bone and with the top of the reconstruction box (green box) parallel to the slice orientation through the neck midpoint (Figure 2.3). Slices from the reconstructions were exported as 8-bit tiff files.

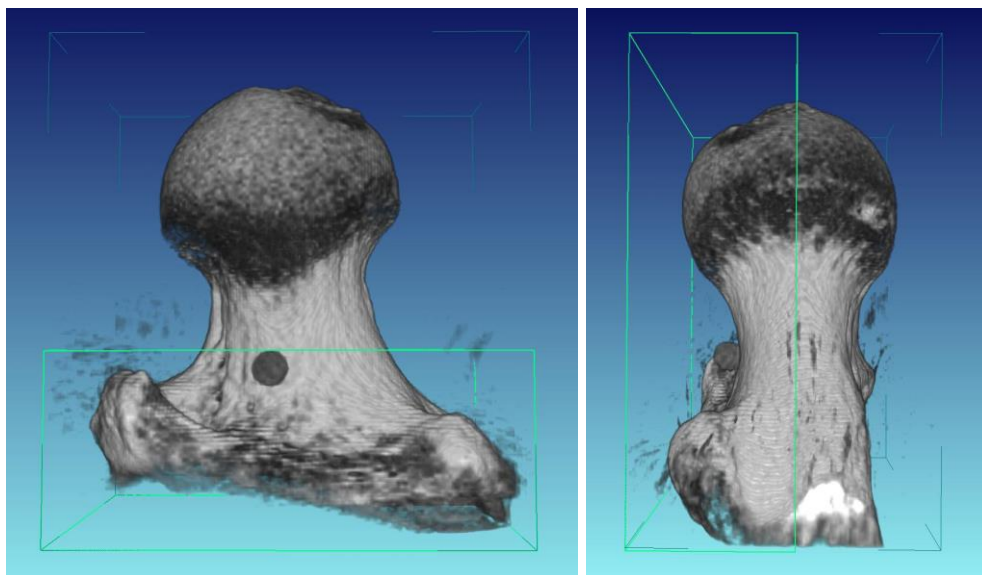


Figure 2.3. Orientation for the femoral head reconstructions.

Volumes of Interest

The femoral head trabecular bone volumes of interest (VOIs) were obtained using the program Avizo Lite 9.2.0 (FEI Visualization Sciences Group). First, isosurface renderings were created to determine the ideal threshold for viewing the scan, then an actual isosurface was made using that threshold and including 4x4x4 downsampling to make the program run quicker. The bone was oriented in the xy plane looking directly at the articular surface. In order to accurately create the VOIs in all of the femoral heads, each femoral head needed to be oriented with the xy orthoslice running through the long axis of the bone. Thus, transform editor was used to first rotate the bone 90° in the x plane, and then on to 100° in the y plane, resulting in a rotation setting of -0.385207x, -0.385207y, and 0.838589z.

A script made and provided to me by Dr. Tim Ryan at Penn State University was attached to the open data and used to first create a region of interest (ROI) box. This was manually narrowed in around the articular surface of the femoral head (Figure 2.4). The mobility impaired femoral heads are quite variable and often had extra ossifications, resulting in a need for slight estimation on some when creating the VOIs. In these instances, an orthoslice was used to view the slices for a more accurate placement of the ROI. Next, a cubic VOI was created that is 50% the size of the shortest length of the ROI and placed directly in the center of the ROI (Figure 2.5) using the VOI “proximal femur” and then “create” buttons of the script program. Lastly, slices of the VOI were exported from Avizo as DICOM files.

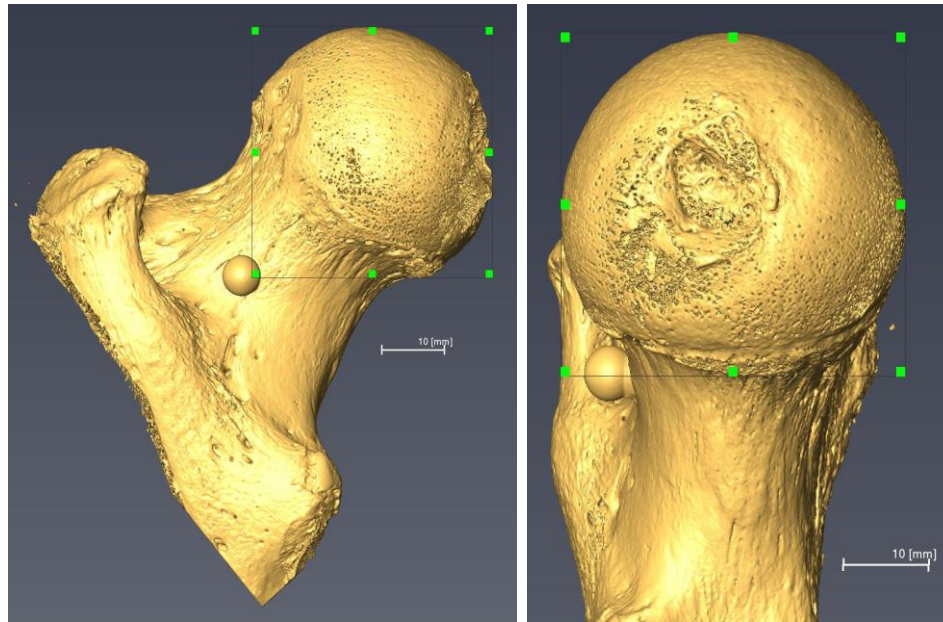


Figure 2.4. Representative Avizo isosurface of the high-resolution μ CT scan of a left proximal femur, with the ROI box (defined by the green squares and connecting lines) aligned around the femoral head. (Scale bars, 10mm.)

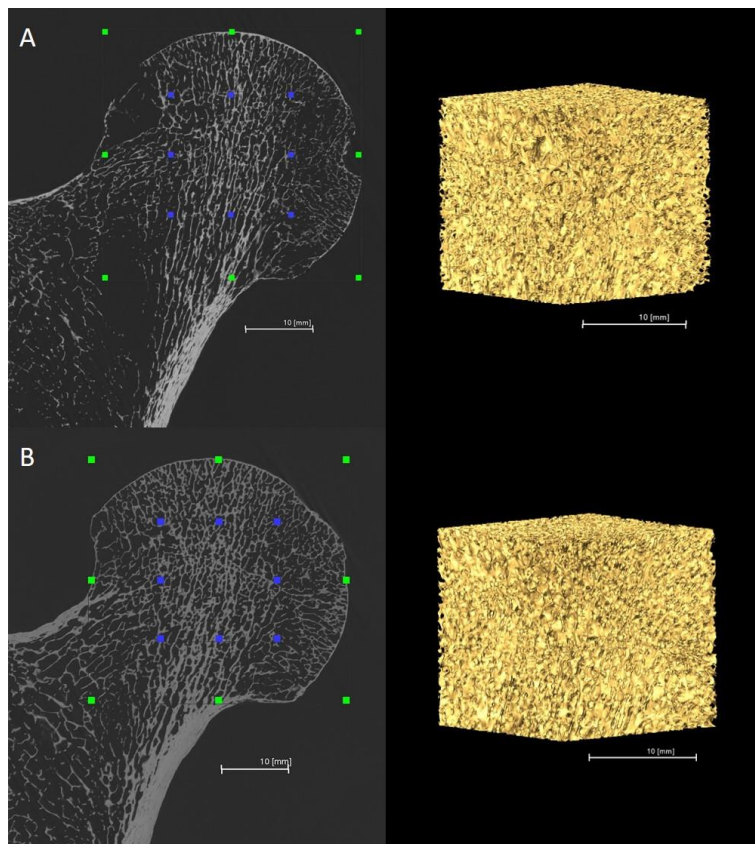


Figure 2.5. Position of the VOI (blue squares and connecting lines) within the trabeculae of the femoral head (left) and subsequent VOI isosurface (right) of a mobility impaired (A) and normal mobility (B) individual. (Scale bars, 10mm.)

Trabecular Bone Analysis

The VOI DICOM files were each loaded into ImageJ and a macro (also created by Dr. Ryan and adjusted by me) was used to run through all of the trabecular bone analyses in BoneJ version 1.4.2 (Doube et al. 2010). BoneJ is a plugin for ImageJ and was directed with the macro to first convert the image into the necessary binary format using the “optimise threshold” option, following which the volume fraction, thickness, structure model index, purify, connectivity, and anisotropy options were run. The resultant relevant data from BoneJ includes bone volume fraction (BV/TV), which is a ratio of the volume of bone present (BV) in a particular region compared to the total volume of interest (TV; Fajardo and Müller 2001). BoneJ also provides the trabecular thickness (Tb.Th) and trabecular spacing (Tb.Sp.), which are measures of the thickness of the trabeculae and spacing between the trabeculae, respectively. Connectivity density (ConnD) was also measured and acts as a proxy for the number of trabeculae per unit volume (Odgaard and Gundersen 1993). The orientation of the trabeculae was assessed with the degree of structural anisotropy (DA), which is a measure of the alignment similarity of the trabeculae (Fajardo and Müller 2001; Fajardo et al. 2007; Table 2.1). All of these components describe the thickness and orientation of the trabecular struts, as well as the bone volume of the region. These measurements were used to analyze how the trabecular bone remodels via differences in orientation, strut thickness, spacing, or number in response to disuse from mobility impairment.

Table 2.1. Trabecular bone properties (Shaw and Ryan 2012; Ryan and Shaw 2015).

Property	Abbreviation	Units	Definition
Bone volume fraction	BV/TV	ratio	relative trabecular bone volume in the VOI
Trabecular thickness mean	Tb.Th	mm	mean thickness of trabecular struts
Trabecular spacing mean	Tb.Sp	mm	mean distance between adjacent trabeculae
Connectivity density	ConnD	mm ⁻³	the number of interconnections among trabeculae
Degree of anisotropy	DA	ratio	how highly oriented trabeculae are within the VOI (1 - short axis/long axis); 0 = isotropic, 1 = anisotropic

Cortical Bone Analysis

Cortical bone cross-sections were selected for visual comparison at midshaft of the femoral diaphysis, subtrochanteric, and midpoint of the femoral neck (Appendices B-D). As explained above, all of these landmarks were marked with a plastic BB, and thus found in the slices exported from the reconstruction program by loading the slices as a stack into ImageJ and locating the slice number directly above the top edge of the BB for the femoral neck midpoint and midshaft of the femur, and directly below the bottom edge of the BB for the subtrochanteric location.

For the purposes of this study, cortical area and cross-sectional geometrical properties were analyzed only for the subtrochanteric and midshaft slices since those are most often analyzed for biomechanical studies. Each midshaft and subtrochanteric slice was imported into the program ImageJ, the scale was set in pixels/mm based on each scan's resolution, and the image was adjusted to a black and white threshold. A number of steps were taken manually within ImageJ to most accurately calculate the cortical area

of each midshaft slice. First, the wand tool was used to select the entire circumference of the bone, the area of which was measured by clicking “analyze” and “measure”. This was then repeated, but using the wand tool to select only the medullary cavity. These measurements were all recorded in an excel table and the cortical area was calculated by subtracting the medullary area from the total area.

To analyze the cross-sectional geometric properties of each slice, the “Slice Geometry” option in BoneJ was used. This calculates multiple measurements; those relevant to the study are the minimum (I_{\min}) and maximum (I_{\max}) bending moments, the minor axis angle (θ), the minimum (Z_{\min}) and maximum (Z_{\max}) bending moments, and the polar section modulus (Z_p ; Table 2.2). I_{\min} and I_{\max} were added together to calculate the torsional rigidity of the bone (J), and I_{\max} was divided by I_{\min} to obtain the shape ratio (I_{\max}/I_{\min}). An I_{\max}/I_{\min} of 1 means that the cross-section is perfectly round.

The left femur midshaft slice for the UT55-10D disuse sample has non-bone residue inside the medullary cavity that appears the same as bone when thresholded. This residue was manually erased using the brush tool in ImageJ prior to running Slice Geometry. The left femur of D06-2013 has a metal rod running through the center, as well as pathological bone growth along the outside of the cortical bone. The ImageJ brush tool was used to cover the metal rod and the pencil tool was used to outline the cortical bone in order for the cortical area to be accurately calculated and Slice Geometry run.

In order to accurately compare bone structural properties between different individuals, body size must be controlled for since body size constitutes a mechanical load and is related to other factors that influence mechanical loading, such as muscle size

(Ruff 2008). Thus it is necessary to standardize each of the above cross-sectional measurements for body mass. This was done in one of three ways (Ruff 2008): the cross-sectional areas were divided by body mass (weight in kg), the second moments of area (SMAs) were divided by [body mass x bone length²], and the section moduli were divided by [body mass x bone length]. In order to have more manageable numbers, the standardized SMAs and section moduli were then divided by 1000. Both the unstandardized (TA and CA) and body mass standardized (TAstd. and CAstd.) measurements were analyzed.

Three individuals in the sample did not have a known body mass. Thus, the Ruff et al. (1991) sex specific equations to estimate body mass from the femoral head diameter were used (Auerbach and Ruff 2004). These equations estimate lean body mass (LBM), which is often different from the known measured or estimated body mass of the individual during life. Therefore, it was additionally investigated as to whether it makes a difference to standardize using the known body mass or the calculated LBM. Statistics were run on the cortical bone and cross-sectional properties standardized using both the known body mass and the LBM (demarcated by “LBM” following the variable). The SMA and section moduli standardizations require knowing the maximum femoral length. However, several of the individuals in the sample are femoral amputees. For the femoral single amputees, the length of the complete femur was used for both sides. Three of the individuals in the sample are femoral double amputees with no way to acquire a maximum femoral length. It was found that, of the measurements recorded during data collection, femoral neck midpoint length multiplied by femoral neck minimum breadth is most correlated with maximum femoral length ($r^2 = 0.4408$). Thus, the equation of this

regression ($y = 0.0903x + 366.55$) was used to calculate an estimated femoral maximum length for the three femoral double amputees. Although this is not ideal, it was deemed an acceptable solution since only three of the individuals required femoral length estimation in this way.

Table 2.2. Cortical bone cross-sectional properties (Ruff 2008).

Property	Abbr.	Units	Definition
Cortical area	CA	mm ²	compressive/tensile strength
Total area	TA	mm ²	area within outer (subperiosteal) surface
Medullary area	MA	mm ²	area of the medullary cavity
Percent cortical area	%CA	%	(CA/TA) x 100
Second moment of area around major axis	I _{max}	mm ⁴	maximum bending rigidity
Second moment of area around minor axis	I _{min}	mm ⁴	minimum bending rigidity
Polar second moment of area	J	mm ⁴	torsional and (twice) average bending rigidity (I _{min} +I _{max})
Theta	θ	degrees	orientation of maximum bending rigidity
Section modulus around major axis	Z _{max}	mm ³	maximum bending strength
Section modulus around minor axis	Z _{min}	mm ³	minimum bending strength
Polar section modulus	Z _p	mm ³	torsional and (twice) average bending strength

External Bone Dimensions

Prior to scanning the bones, calipers were used to record metric measurements of the maximum superior-inferior femoral head diameter, minimum neck breadth, neck midpoint breadth, and neck length (Figure 2.6). The maximum femoral lengths, excepting the femoral amputees, were also recorded when marking the midshaft for BB placement.

These measurements were necessary for accurate placement of the cortical bone slice BBs, and were used in the standardization of the cortical bone properties. They could also later be used to estimate the lever arm length, which is necessary when comparing biomechanical properties.

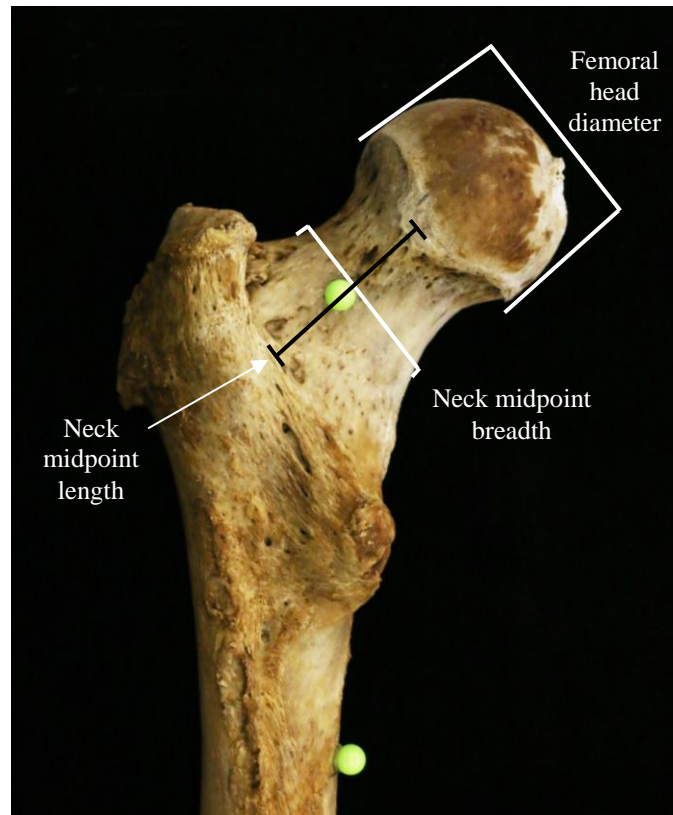


Figure 2.6. External measurements taken on the proximal femur: maximum femoral head diameter, neck midpoint breadth, and neck midpoint length. Minimum neck breadth was also measured at the narrowest part of the neck.

Statistical Analysis

Parametric statistical tests assume a normal distribution and equal variance of the variables. A Shapiro-Wilk W test was first applied to test if the variables for each group were normally distributed. A Levene's test was used to determine if the variances were equal. Not all of the variables met the assumption of normal distribution and equal

variance, and thus nonparametric and parametric statistical tests were used appropriately. A significance level of $\alpha = 0.05$ was used for all statistical tests.

The first test of population differences was to address the overall hypothesis of whether there is a difference in the femoral bone structure between mobility impaired and normal mobility individuals. This was conducted using parametric analysis of variance (ANOVA) and non-parametric equivalent Kruskal-Wallis tests to compare the mobility impaired samples to the normal mobility samples for all of the trabecular and cortical properties measured. ANOVA is used to analyze the differences among group means and the variation among and between groups. The assumptions of this test are that all of the samples are independent of one another, that the data is normally distributed and that it has equal variance. For the data that does not follow all of these assumptions, the non-parametric equivalent, Kruskal-Wallis one-way analysis of variance, was used to test for whether samples originate from the same distribution, comparing group medians rather than means.

ANOVA and Kruskal-Wallis tests were also used to compare the mobility impaired sample to the normal mobility sample, but including sex as an interaction term to investigate whether males and females differ in their pattern of use. Differences in the variables based solely on sex were also investigated using ANOVA and Kruskal-Wallis tests for all of the samples combined, as well as separated by mobility type. Boxplots were made comparing mobility, sex, and mobility by sex for all of the variables to visualize the differences between the groups compared (Appendix E).

A Wilcoxon signed-rank test is a non-parametric test used when comparing two related samples, matched samples, or repeated measurements on a single sample to assess

whether their population mean ranks differ. For this reason, this test was chosen to run on all of the mobility impaired individuals' femora, as well as just those with single amputations to compare the femur of the amputated limb to that of the non-amputated limb to explore any possible patterns. If one leg being amputated causes an overall lack of mobility, then it is expected that there will be no significance in these results, since both femora will have similarly remodeled due to disuse. However, if the individual was still able to ambulate with only one limb amputated, then a significant difference in the remodeling of the two femora is expected.

Regression analysis is used to estimate the relationship among variables and determine if there are any correlations between a dependent variable and one or more predictor variables. For those individuals with a known amount of time of impaired mobility during life, a multiple regression was run to look for any correlation between the time an individual was mobility impaired and the trabecular and cortical properties measured. Multiple regressions were also run to investigate any correlations between the trabecular and cortical properties and age of the individuals separately for both the mobility impaired and normal mobility individuals. Scatterplots of these regressions are included in Appendices H and I.

3. RESULTS

Parametric or Nonparametric

The Shapiro-Wilks W test for normality showed that many of the variables are not normally distributed (Table 3.1). A Levene's test also showed that many variables do not have equal variance between mobility impaired and normal mobility individuals (Table 3.1). Therefore, nonparametric statistical tests were used for analysis of the variables exhibiting a non-normal distribution and/or unequal variance. Parametric statistical tests were able to be used for all of the other variables (Table 3.1).

Table 3.1. Normality and homoscedasticity of the trabecular and cortical variables and whether a parametric or non-parametric test is appropriate.

Bone Variable	Normally Distributed	Equal Variance	Parametric	Nonparametric
BV/TV	Yes	No		✓
Tb.Th	Yes	Yes	✓	
Tb.Sp	No	No		✓
ConnD	No	Yes		✓
DA	Yes	Yes	✓	
%CA	No	No		✓
TA	Yes	Yes	✓	
CA	Yes	No		✓
MA	No	No		✓
TAstd.	No	Yes		✓
CAstd.	Midshaft – No; Subtroch – Yes	Yes	✓Subtroch	✓Midshaft
MAstd.	No	No		✓
TAstd.LBM	Yes	Yes	✓	
CAstd.LBM	Yes	No		✓
MAstd.LBM	No	No		✓
θ	No	Midshaft – No; Subtroch – Yes		✓
I_{max}	No	Yes		✓
I_{min}	Yes	Yes	✓	
I_{max}/I_{min}	Midshaft – No; Subtroch – Yes	Yes	✓Subtroch	✓Midshaft
J	Midshaft – No; Subtroch – Yes	Yes	✓Subtroch	✓Midshaft

Table 3.1 (continued). Normality and homoscedasticity of the trabecular and cortical variables and whether a parametric or non-parametric test is appropriate.

Bone Variable	Normally Distributed	Equal Variance	Parametric	Nonparametric
Z _{max}	Midshaft – No; Subtroch – Yes	Yes	✓Subtroch	✓Midshaft
Z _{min}	Yes	Yes	✓	
Z _p	No	Yes		✓
I _{max} LBM	Midshaft – Yes; subtroch – No	Yes	✓Midshaft	✓Subtroch
I _{min} LBM	Yes	Yes	✓	
J LBM	Midshaft – Yes; Subtroch – No	Yes	✓Midshaft	✓Subtroch
Z _{max} LBM	Yes	Midshaft – Yes; Subtroch – No	✓Midshaft	✓Subtroch
Z _{min} LBM	Yes	Yes	✓	
Z _p LBM	Yes	Midshaft – Yes; Subtroch – No	✓Midshaft	✓Subtroch

Mobility Impaired vs. Normal Mobility

The first analysis run was to test whether a significant difference is present overall between the mobility impaired and the normal mobility samples (Tables 3.2 and 3.3). ANOVA and Kruskal-Wallis tests show that BV/TV ($p = 0.0014$), Tb.Th ($p = 0.0079$) and Tb.Sp ($p = 0.0261$) are all significantly different for mobility impaired and normal mobility samples. Mobility impaired individuals exhibit lower BV/TV and Tb.Th, but greater Tb.Sp (Figure 3.1A,B,C). ConnD ($p=0.9766$), and DA ($p=0.1713$) do not show a significant difference (Figure 3.1D,C).

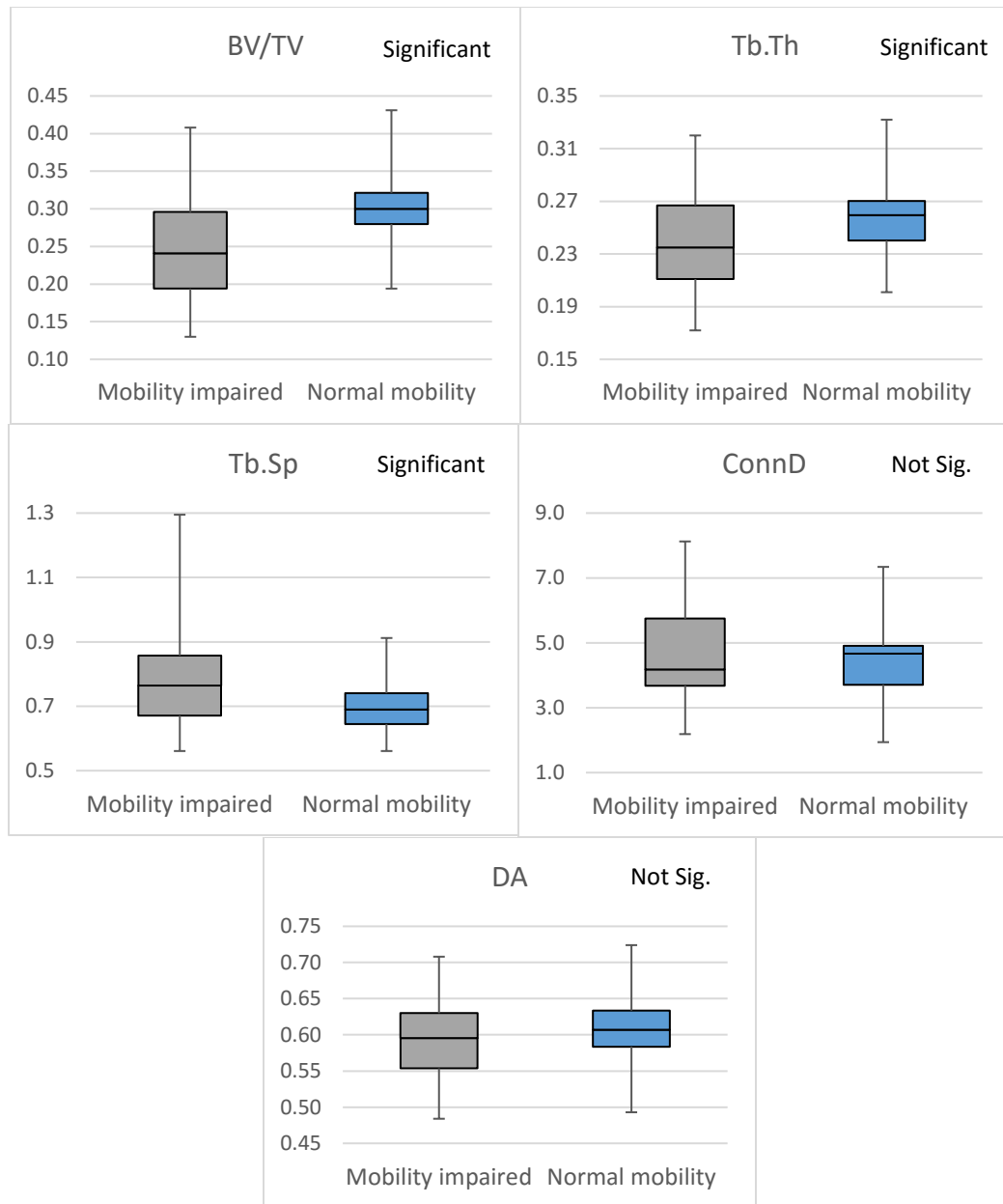


Figure 3.1. Boxplots of trabecular properties for mobility impaired and normal mobility individuals – A) BV/TV, B) Tb.Th, C) Tb.Sp, D) ConnD, E) DA.

For both the midshaft and subtrochanteric slices, %CA (midshaft: $p = 0.0006$; subtrochanteric: $p = 0.0216$) and CAstd. LBM ($p = 0.0095$ and 0.0440) show a significant decrease in the mobility impaired compared to normal mobility individuals (Figure 3.2). Accordingly, MA ($p = 0.0035$), MAstd. ($p = 0.0127$), and MAstd. LBM ($p = .0095$) also

show a significant increase in the midshaft slices of mobility impaired individuals (Figure 3.2), and MA ($p = 0.0675$) and MAstd. LBM ($p = 0.0591$) show a nearly significant increase in the mobility impaired subtrochanteric slices. TA, TAst., TAst. LBM, CAstd., and subtrochanteric CA and MAstd. show no significant difference. Midshaft CA is reduced in mobility impaired individuals with a nearly significant difference ($p = 0.0540$; Appendix E).

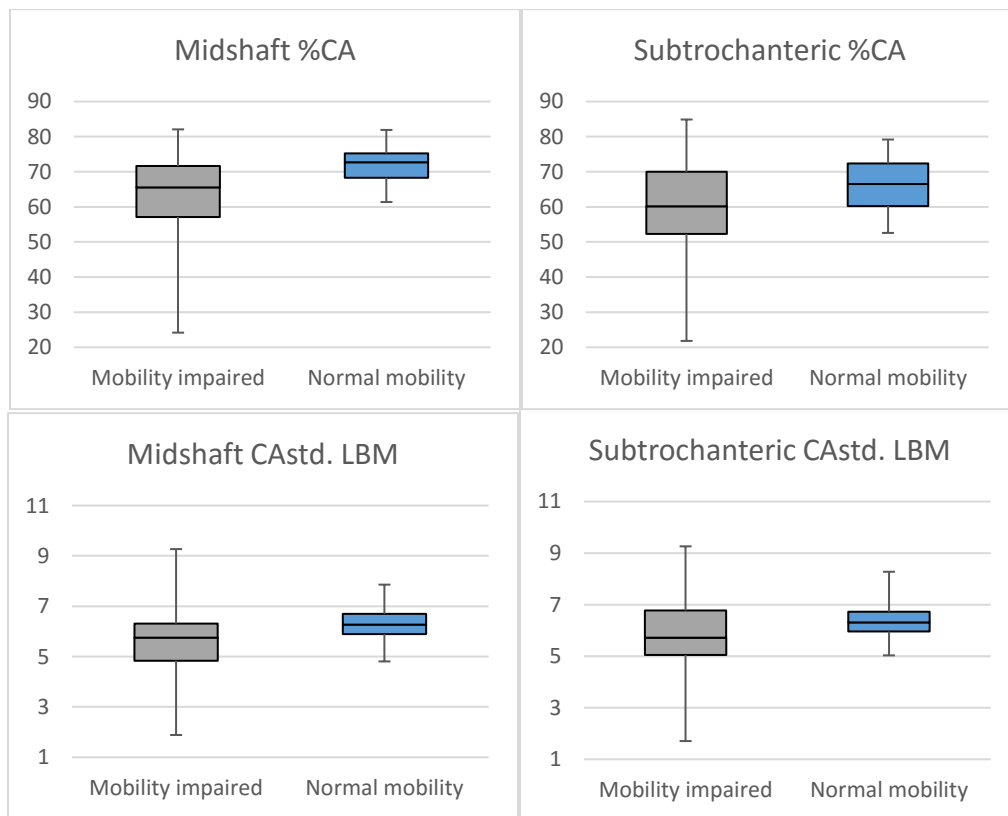


Figure 3.2. Boxplots of the significant %CA and CAstd. LBM of the midshaft and subtrochanteric slices, and MA, MAstd., and MAstd. LBM of the midshaft slices comparing the mobility impaired and normal mobility individuals.

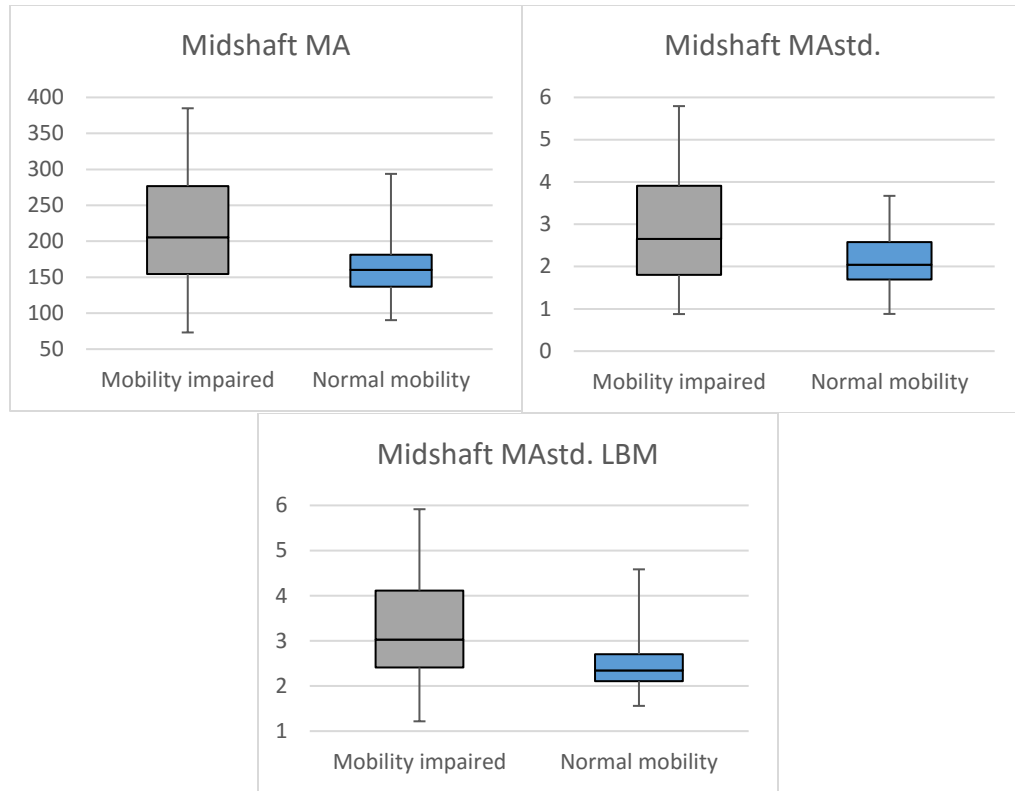


Figure 3.2 (continued). Boxplots of the significant %CA and CAstd. LBM of the midshaft and subtrochanteric slices, and MA, MAstd., and MAstd. LBM of the midshaft slices comparing the mobility impaired and normal mobility individuals.

Cortical geometry is not significantly different between mobility impaired and normal mobility individuals for any of the geometric properties (i.e., I_{max} , I_{min} , I_{max}/I_{min} , J , Z_{max} , Z_{min} , Z_p) in either the midshaft or subtrochanteric slices. There is a nearly significant difference in midshaft θ ($p = 0.0660$) between mobility types, with mobility impaired individuals exhibiting greater angles.

Mobility Impaired vs. Normal Mobility by Sex

When separated first by sex and then tested for differences between mobility types (Tables 3.2 and 3.3) there is no significant difference in females between mobility impaired and normal mobility samples for any of the trabecular properties. In males, BV/TV ($p = 0.0043$), Tb.Th ($p = 0.0040$), and Tb.Sp ($p = 0.0169$) are significantly

different. In females, there is a nearly significant difference between mobility types in both the midshaft and subtrochanteric slices for CAstd. ($p = 0.0710$ and 0.0627), with mobility impaired individuals having lower body mass standardized cortical area, and a nearly significant difference in female midshaft %CA. In males, midshaft %CA ($p = 0.0028$), CAstd. LBM ($p = 0.0269$), MA ($p = 0.0108$), MAstd. ($p = 0.0049$), and MAstd. LBM ($p = 0.0186$) are significantly different. There is no significant difference between mobility impaired and normal mobility samples in cortical geometry, TA, CA, MA or TAstd. within the midshaft or subtrochanteric slices for either males or females. There is a nearly significant difference within female midshaft slices in I_{max} ($p = 0.0630$) and Z_{max} ($p = 0.0710$), and in male midshaft and subtrochanteric θ ($p = 0.0628$ and 0.0867).

Boxplots for all of these results can be found in Appendix F.

Table 3.2. Mobility differences for each trabecular variable.

Variable	Combined Sexes		Males		Females	
	Sig.	Not Sig.	Sig.	Not Sig.	Sig.	Not Sig.
BV/TV	✓		✓			✓
Tb.Th	✓		✓			✓
Tb.Sp	✓		✓			✓
ConnD		✓		✓		✓
DA		✓		✓		✓

Table 3.3. Mobility differences for each cross-sectional variable with sexes combined and separate. A checkmark in both the sig. and not sig. columns means the variable is nearly significant. [Subtroch = subtrochanteric slices]

Variable	Combined Mobility				Male				Female			
	Midshaft		Subtroch		Midshaft		Subtroch		Midshaft		Subtroch	
	Sig.	Not Sig.	Sig.	Not Sig.	Sig.	Not Sig.	Sig.	Not Sig.	Sig.	Not Sig.	Sig.	Not Sig.
TA		✓		✓		✓		✓		✓		✓
CA		✓		✓		✓		✓		✓		✓
MA	✓		✓		✓			✓		✓		✓
TAstd.		✓		✓		✓		✓		✓		✓
CAstd.		✓		✓		✓		✓	✓		✓	
MAstd.	✓			✓	✓			✓		✓		✓
TAstd. LBM		✓		✓		✓		✓		✓		✓

Table 3.3 (continued). Mobility differences for each cross-sectional variable with sexes combined and separate. A checkmark in both the sig. and not sig. columns means the variable is nearly significant. [Subtroch = subtrochanteric slices]

Variable	Combined Mobility				Male				Female			
	Midshaft		Subtroch		Midshaft		Subtroch		Midshaft		Subtroch	
	Sig.	Not Sig.	Sig.	Not Sig.	Sig.	Not Sig.	Sig.	Not Sig.	Sig.	Not Sig.	Sig.	Not Sig.
CAstd. LBM	✓		✓		✓		✓			✓		✓
MAstd. LBM	✓			✓	✓			✓		✓		✓
% CA	✓		✓		✓			✓	✓	✓		✓
θ	✓	✓		✓	✓	✓	✓	✓		✓		✓
I_{min}		✓		✓		✓		✓		✓		✓
I_{max}		✓		✓		✓		✓	✓	✓		✓
I_{max}/I_{min}		✓		✓		✓		✓		✓		✓
J		✓		✓		✓		✓		✓		✓
Z_{min}		✓		✓		✓		✓		✓		✓
Z_{max}		✓		✓		✓		✓	✓	✓		✓
Z_p		✓		✓		✓		✓		✓		✓
I_{min} LBM		✓		✓		✓		✓		✓		✓
I_{max} LBM		✓		✓		✓		✓		✓		✓
J LBM		✓		✓		✓		✓		✓		✓
Z_{min} LBM		✓		✓		✓		✓		✓		✓
Z_{max} LBM		✓		✓		✓		✓		✓		✓
Z_p LBM		✓		✓		✓		✓		✓		✓

Visual Assessment

It is also important to note that visually when scrolling through the stacks of femoral VOI slices in ImageJ, those of the normal mobility individuals all look much more similar, with the same pattern. Those of the mobility impaired individuals are much more variable, often with larger gaps in some places and more bone in others. Within the cortical bone slices (Appendices B-D), very clear is not only the decreased width of the cortical bone, but also the increased porosity within the cortical area. This is particularly visible in the femoral midshaft slices (Figure 3.3; Appendix B). The neck midpoint slices were selected for visual assessment, but not quantified in this study due to limitations of the current programs available for assessing the cortical area and cross-sectional

geometric properties within such high resolution images with clear gaps in the cortical outline and trabecular bone present within the slice. Visually observable in the neck midpoint slices (Appendix D) is that variation is present when comparing the mobility impaired slices to those of the normal mobility match. The mobility impaired individuals generally have less cortical area than that of the matched normal mobility slice, whether from a decrease in cortical thickness and/or increased porosity (Figure 3.4), although there are some exceptions. Additionally, in some of the mobility impaired individuals there is also less trabecular bone present (Figure 3.4).

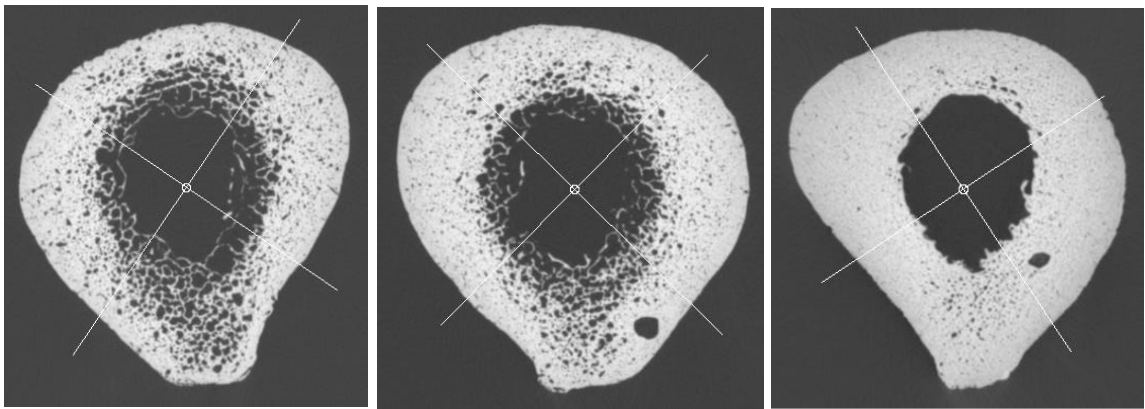


Figure 3.3. Femoral midshaft slices from a mobility impaired (D47-2013) left (left) and right (center) femora, and the normal mobility match (D21-2011) left femur (right).

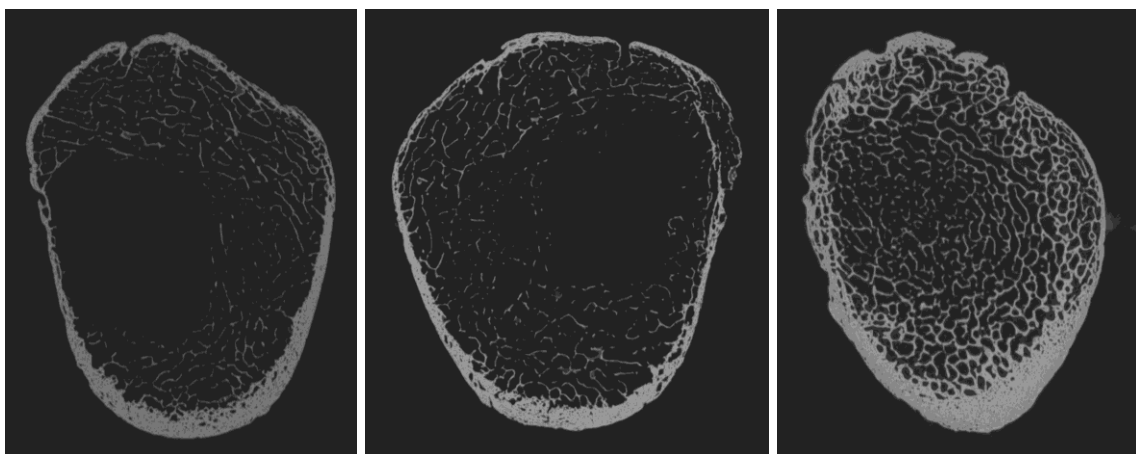


Figure 3.4. Neck midpoint slices from UT14-92D left (left) and right (center) femora, and the normal mobility match (D49-2014) left femur (right). Notice the decreased cortical area and trabecular bone of the mobility impaired compared to normal mobility individual.

Sex Differences

Males vs. Females Combined Mobility

Sex effects for the combined mobility groups were tested using ANOVA and Kruskal-Wallis tests (Tables 3.4 and 3.5). There are no significant differences between males and females for BV/TV, Tb.Th, Tb.Sp, or DA, but there is a significant difference for ConnD ($p=0.0330$), with females having more connectivity than males (Figure 3.5). In both the midshaft and subtrochanteric slices, TA ($p = <0.0001$ for both), TAstd. ($p = 0.0080$ and 0.0168), TAstd. LBM ($p = 0.0359$ and 0.0292), CA ($p = <0.0001$ and 0.0002), and MA ($p = 0.0452$) are all significantly different between males and females, with males having greater total area, cortical area, and medullary area (Appendix G). CAstd. is significantly different between sexes in the midshaft slices ($p = 0.0031$) and has near significance in the subtrochanteric slices ($p = 0.0520$), and CAstd. LBM has near significance ($p = 0.0546$) in the midshaft slices, with males having slightly greater standardized cortical area. There are no significant sex differences in %CA, MAstd., or MAstd. LBM in either the midshaft or subtrochanteric slices (Appendix G). In the midshaft slices, all of the cross-sectional geometric properties, except for θ , are significantly different between males and females (Appendix G). In the subtrochanteric slices, all of the cross-sectional geometric properties, except for θ , I_{\max} LBM, I_{\max}/I_{\min} , J LBM, and Z_{\max} are significantly different between males and females (Appendix G).

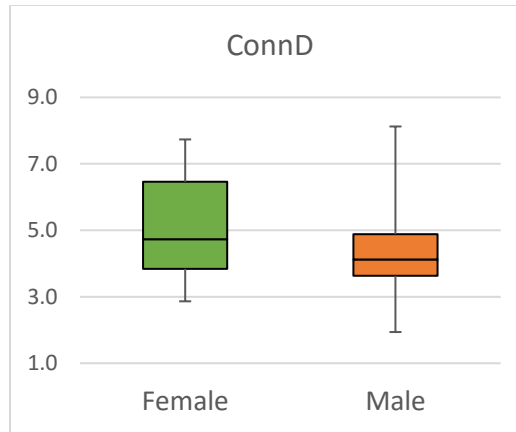


Figure 3.5. Boxplot of significant difference in ConnD for males and females in for the mobility samples combined.

Males vs. Females by Mobility

When separated first by mobility and then tested for sex differences (Tables 3.4 and 3.5) there was no significant difference in any of the trabecular characteristics for either mobility type (Table 3.4), although ConnD did approach significance between males and females in the mobility impaired sample ($p=0.0539$; Appendix F). Within the mobility impaired samples there were significant differences found in both the midshaft and subtrochanteric slices for TA, CA, TAstd., CAstd., I_{min} , I_{max} , J, Z_{max} , Z_{min} and Z_p . In the midshaft slices there is also a significant difference in I_{max} LBM, J LBM, and Z_{max} LBM, and in the subtrochanteric slices in I_{max} . There is a nearly significant difference based on sex in MAstd., Z_{min} LBM, and midshaft I_{min} LBM and Z_p LBM. There is no significant difference between males and females for %CA, MA, TAstd. LBM, CAstd. LBM, MAstd. LBM, θ , or I_{max}/I_{min} in either the midshaft or subtrochanteric slices. In the subtrochanteric slices there is no significance for MAstd., I_{min} LBM, I_{max} LBM, J LBM, Z_{max} LBM, or Z_p LBM.

Within the normal mobility samples there is a significant difference between males and females in TA and CA for both the midshaft and subtrochanteric slices.

Additionally, for the midshaft slices I_{\min} LBM, J LBM, Z_{\max} LBM, Z_{\min} LBM, and Z_p LBM are all significantly different and I_{\max} LBM is nearly significantly different for males and females. For the subtrochanteric slices, MA and TAs_{td}. LBM are also significantly different between males and females. None of the cross-sectional geometric properties are significant in the subtrochanteric slices, although I_{\min} LBM, Z_{\min} LBM, Z_p LBM are nearly significant. There is no significant difference in sex in the normal mobility samples for %CA, TAs_{td}., CA_{std}., CA_{std}. LBM, MA_{std}., MA_{std}. LBM, or midshaft MA.

Table 3.4. Sex differences for each trabecular variable for the combined and separated mobility groups. A checkmark in both the sig. and not sig. column means the variable is nearly significant.

Variable	Combined Mobility		Mobility Impaired		Normal Mobility	
	Sig.	Not Sig.	Sig.	Not Sig.	Sig.	Not Sig.
BV/TV		✓		✓		✓
Tb.Th		✓		✓		✓
Tb.Sp		✓		✓		✓
ConnD	✓	✓	✓	✓		✓
DA		✓		✓		✓

Table 3.5. Sex differences for each cortical bone cross-sectional variable for the combined and separated mobility groups. A checkmark in both the sig. and not sig. column means the variable is nearly significant.

Variable	Combined Mobility				Mobility Impaired				Normal Mobility			
	Midshaft		Subtroch		Midshaft		Subtroch		Midshaft		Subtroch	
	Sig.	Not Sig.	Sig.	Not Sig.	Sig.	Not Sig.	Sig.	Not Sig.	Sig.	Not Sig.	Sig.	Not Sig.
TA	✓		✓		✓		✓		✓		✓	
CA	✓		✓		✓		✓		✓		✓	
MA	✓		✓			✓		✓		✓	✓	
TAs _{td} .	✓		✓		✓		✓			✓		✓
CA _{std} .	✓		✓	✓	✓		✓			✓		✓
MA _{std} .		✓		✓	✓	✓		✓		✓		✓
TAs _{td} . LBM	✓		✓			✓		✓		✓	✓	
CA _{std} . LBM	✓	✓		✓		✓		✓		✓		✓
MA _{std} . LBM		✓		✓		✓		✓		✓		✓
% CA		✓		✓		✓		✓		✓		✓

Table 3.5 (continued). Sex differences for each cortical bone cross-sectional variable for the combined and separated mobility groups. A checkmark in both the sig. and not sig. column means the variable is nearly significant.

Variable	Combined Mobility				Mobility Impaired				Normal Mobility			
	Midshaft		Subtroch		Midshaft		Subtroch		Midshaft		Subtroch	
	Sig.	Not Sig.	Sig.	Not Sig.	Sig.	Not Sig.	Sig.	Not Sig.	Sig.	Not Sig.	Sig.	Not Sig.
θ		✓		✓		✓		✓		✓		✓
I_{min}	✓		✓		✓		✓			✓		✓
I_{max}	✓		✓		✓		✓			✓		✓
I_{max}/I_{min}	✓			✓		✓		✓		✓		✓
J	✓		✓		✓		✓			✓		✓
Z_{min}	✓		✓		✓		✓			✓		✓
Z_{max}	✓			✓	✓		✓			✓		✓
Z_p	✓		✓		✓		✓			✓		✓
I_{min} LBM	✓		✓		✓	✓		✓	✓		✓	✓
I_{max} LBM	✓			✓	✓			✓	✓	✓		✓
J LBM	✓			✓	✓			✓	✓			✓
Z_{min} LBM	✓		✓		✓	✓	✓	✓	✓		✓	✓
Z_{max} LBM	✓		✓		✓			✓	✓			✓
Z_p LBM	✓		✓		✓	✓		✓	✓		✓	✓

Age Correlation

Multiple regressions were run to test whether there is any significant correlation between the trabecular and cortical variables and the age of the individuals. This was done separately for both the mobility impaired individuals and the normal mobility individuals. No significant correlation was found between any of the variables and age of the individuals for either mobility type, with the regressions explaining no more than 10% of the variability for any of the properties (all $R^2 \leq 0.0984$). Scatterplots of these results can be found in Appendix H.

Mobility Impaired Left vs. Right

To test whether there is a significant difference between the left and right femora for the disuse samples, a Wilcoxon signed-rank test was run for all of the trabecular and cortical parameters. These tests found that there are no significant differences in any of the trabecular or cortical properties between the two femora of each individual, either when including all of the mobility impaired samples ($n = 26$), or when running only the single amputees ($n = 11$). Although, for single amputees only, Tb.Th and TAsTd. of the midshaft slices were nearly significant when comparing the amputated leg and complete leg (Tb.Th statistic of 13 and a two-tailed $\alpha=0.05$ critical value of 10; TAsTd. test statistic of 103 and a two-tailed $\alpha=0.05$ critical value of 98). For both variables, the amputated leg exhibited reduced values (Figure 3.6).

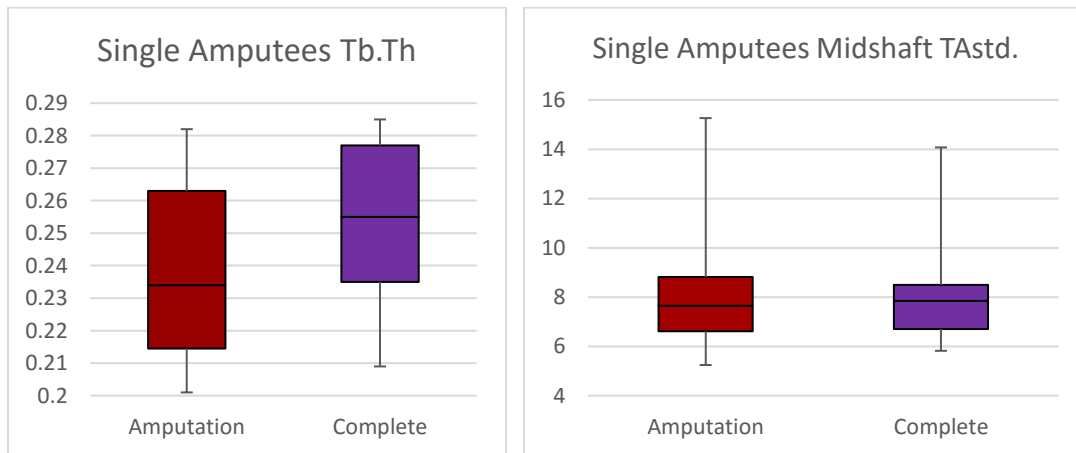


Figure 3.6. Boxplots of differences in Tb.Th (left) and midshaft TAsTd. (right) between the amputated leg (red) and complete leg (purple) femora of single amputees.

Although statistically there is no significant difference in the cortical area of the amputated leg and the complete leg, differences are observable through visual assessment of the slices, and in particular those from the femoral midshaft. The individuals with bilateral disuse from immobility (D32-2014), being wheelchair-bound (D47-2013 and

D56-2013), and several of the double amputees (D04-2014, D28-2015, UT06-02D, UT14-92D, UT55-10D) have very similar patterns of cortical thickness and porosity between the right and left sides, and very clear signs of cortical loss compared to each of their normal mobility matches (example shown in Figure 3.7). In contrast, many of the single amputees do show very different levels of remodeling on each side, with the amputated leg femur having more cortical loss than the complete leg femur. Figure 3.8 shows an extreme example of this pattern.

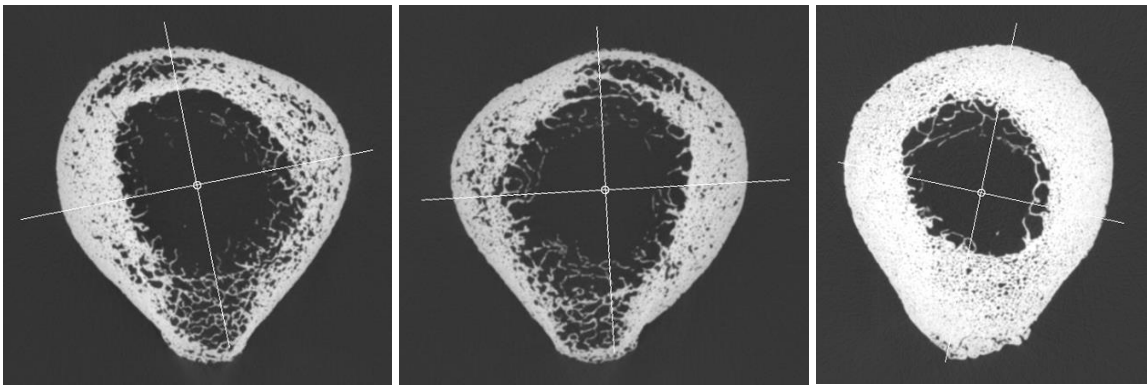


Figure 3.7. Femoral midshaft slices of a mobility impaired individual with bilateral disuse from double amputation with matching patterns of remodeling between the left (left) and right (center) femora, and the matched normal mobility individual (D49-2014) left femoral slice (right).

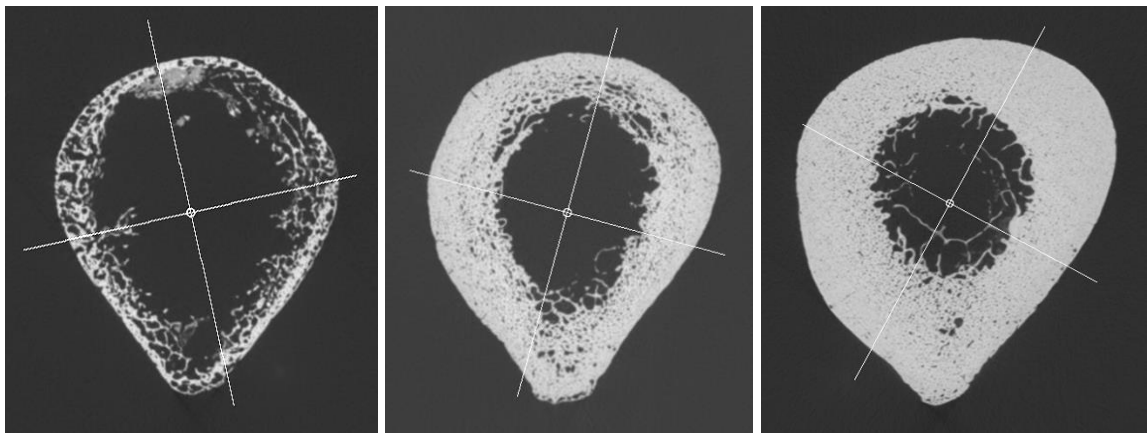


Figure 3.8. Femoral midshaft slices of a single amputee (UT60-09D) with a left leg amputation (left), the non-amputated leg (middle), and the matched normal mobility individual (D65-2013) left femur.

Mobility Impairment Time Dispersal

A multiple regression was run to test whether there is any significant correlation between the trabecular variables and the amount of time of mobility impairment. The amount of time of mobility impairment is known for fourteen individuals, ranging from six months to fifteen years. It was found that there is no significant correlation between any of the trabecular variables and how long the individual was mobility impaired. Two of the double amputees had amputations that occurred at different dates, and thus have different disuse times for each leg. The correlation was tested both with each femur of these individuals having different disuse timings, as well as using the longer amount of time for both femora; no difference was found in the results using either iteration.

Scatterplots were created showing the spread of the variables (Appendix E). A mean and distribution of the trabecular variables from the matched normal mobility femora to these fourteen individuals as a baseline zero amount of time of limb disuse is included in each graph.

4. DISCUSSION AND CONCLUSION

The results of this research show that mobility impairment does have a visible and quantifiably statistically significant effect on the trabecular and cortical bone of the femur. However, some of the differences expected were not observed.

Trabecular Architecture

In the femoral head, the mobility impaired individuals have a lower bone volume fraction (BV/TV) and trabecular thickness (Tb.Th) and greater trabecular spacing (Tb.Sp) than the normal mobility individuals. This indicates that the lower bone volume present in the mobility impaired trabecular architecture is from bone loss from each trabecular strut across the entire VOI, rather than from entire struts having been lost. The mobility impaired individuals have lost bone thickness from the struts, but not the number of trabeculae.

Ryan and Shaw (2015) found a similar pattern of significance in trabecular properties when comparing those of human groups with different subsistence strategies as well as those observed in nonhuman primates. They found that forager and agriculturalist groups' trabecular structure differed based on BV/TV, Tb.Th, and an additional ratio used in their study but not here, bone surface to bone volume. The forager population had significantly higher bone volume fraction, thicker trabeculae, and consequently lower relative bone surface area compared with the two agriculturalist groups. This agrees with my results in terms of the properties influenced by mobility, since foraging is a subsistence strategy that involves a greater daily land distance covered and thus an increased mobility (Wescott 2014), while agriculturalists are relatively more sedentary. Additionally, Ryan and Shaw (2015) found no significant difference in trabecular number

(similar to the measure of connectivity density (ConnD)) or spacing despite the differing loading patterns of foragers and agriculturalists, suggesting that these traits are more conservative across activity levels.

These trabecular results are the opposite of what has been preliminarily found when comparing the proximal tibia of obese individuals and those with a normal body mass index (BMI; Gleiber et al. 2016). In obese individuals, it is the addition of trabeculae that causes a difference in bone volume. There is also a difference in the degree of anisotropy (DA), with obese individuals having less uniformly oriented trabeculae than normal BMI individuals. These are interesting, though not surprising, differences from the results when comparing mobility impaired and normal mobility individuals, since it is variation in loading force that leads to different trabecular orientation (Huiskes et al. 2000).

For mobility impaired individuals there is no loading force, and thus no driving force to change the trabecular orientation. Therefore, it would be expected that the trabeculae of individuals mobility impaired later in life (as is the case in the current study sample) would retain the orientation they had prior to the disuse event. The results of the current study having no significant difference in ConnD or DA agree with this hypothesis, showing no significant variation in the amount of trabecular organization present between mobility impaired and normal mobility individuals. However, this result is actually contrary to my initial hypothesis that the trabecular orientation and structure is different in mobility impaired individuals compared to that of normal mobility individuals. The bone volume, trabecular thickness, and spacing are different, but the number of trabeculae and level of trabecular orientation is not.

The trabecular properties showed no significant sex differences. These results, along with the fact that all of the normal mobility samples were sex matched with the mobility impaired samples to eliminate sex biases, shows that there is no sex interaction factor occurring, and thus the results achieved with both sexes run together are accurate. Dividing the sample to investigate differences based on sex is interesting; however, since the samples were chosen based on mobility impairment rather than sex of the individual, the sample sizes for males and females are very different. Having only nine females in the sample, these results must be viewed with caution as any significance or lack thereof between mobility types within the female samples alone may be the result of a small sample size. This likelihood is supported by the results of the male samples being very similar to those observed in both sexes analyzed together.

Cortical Bone

The cortical bone results show that there is significantly less cortical bone present in mobility impaired than normal mobility individuals. This is the case in both the midshaft and subtrochanteric slices, and thus can be inferred to be true for the entire femoral diaphysis. Along with less cortical area, is a significantly larger medullary cavity in the mobility impaired individuals, thus confirming that cortical bone is being lost endosteally. Furthermore, the loss of cortical bone density in mobility impaired individuals is likely even more significant than the statistical results indicate, since visual assessment of the slices shows a general trend of greater porosity within the cortical bone of the mobility impaired individuals (Appendices B-D). This porosity was not able to be quantified in this study due to method and program constraints, however, it is a factor to be further investigated in the future. These results give real world and human validity to

those observed by Bouvard et al. (2012) in their experimental disuse model of artificial limb paralysis in rats.

Sex differences were found within the measures of cross-sectional total and cortical area, with males having greater area. This is simply an artifact of males generally having larger femora; this does not confound the mobility results since %CA shows no significance based on sex and even when split by sex and then tested for mobility types %CA shows a significance or near significance in both sexes. The only geometric property that showed a near significance in mobility is θ , which has no significant difference in sex.

The results show no significant correlation between the trabecular and cortical properties and the age of the individual within either the mobility impaired samples or the normal mobility samples. It is somewhat surprising that the medullary area shows no significance based on age in either mobility group considering it is known that as an individual ages the medullary cavity increases in size (Ericksen 1979). This lack of medullary size correlation with age indicates that while this remodeling occurs in each individual, there is no visible trend across different individuals, and thus there is more variability within each individual than between ages. It should be noted that the changes seen in mobility impaired individuals—loss of cortical bone, increased medullary cavity, and greater cortical porosity—are similar to those seen as an individual ages, just increased in scale and sped up. This supports the idea that mechanical activity works to mitigate the process of bone degradation and resorption as an individual ages.

In the present study, cortical geometry showed no significance in mobility types. It made no difference in significance as to whether the measurements were standardized

using known body mass or calculated lean body mass. There was a near significance in theta, with greater angles in the mobility impaired individuals. This indicates that there might be some small differences in cortical geometry, however this result is likely due to the greater variation present in the mobility impaired individuals' angles. While it might at first seem surprising that the cortical geometry is conserved with mobility impairment despite the decrease in cortical bone density, it is important to remember that nearly all of the individuals in this study's sample experienced mobility impairment only later in life. Since changes in geometry are highly correlated with changes in loading forces on the bone (Wescott 2014), the lack of vertical loading while experiencing mobility impairment explains these result and the retention of the cortical geometry the individual had prior to the disuse event. Additionally, it is important to note that most of these mobility impaired individuals, though likely atrophied, did retained muscle function. Although these individuals did not experience vertical loading from standing and walking, they were likely still regularly contracting the lower limb muscles during everyday movements, and thus would have muscle forces continuing to act upon the bone. This may have helped to mitigate any effect on cortical geometry that might otherwise occur in individuals with paralysis.

While nearly all of the individuals in the current study experienced mobility impairment only later in life, hypotheses can be made from the results as to how trabecular and cortical bone would differ in individuals with limited or impaired mobility from a young age and during growth. Trabecular orientation would likely be affected such that these individuals would have greatly anisotropic or unorganized trabeculae, with the struts having been deposited under conditions of unloading. Additionally, such

individuals would likely have statistically significant results in cross-sectional geometry compared to individuals with normal mobility, something not seen in the current study sample. This can be inferred from the results of Wescott (2014), comparing five modern mobility-impaired individuals, two of which acquired mobility impairment at a young age, as well as those from studies on disuse in young growing rats (Bouvard et al. 2012). In the rats, the paralyzed limb acquired a more rounded diaphysis in comparison to the non-paralyzed limb even over the course of 35 days. Similarly, Wescott (2014) found that the individuals who had impaired mobility since childhood exhibited obvious wasting and more circular femoral diaphyses. These hypotheses will be investigated in future research since not only will it add to the knowledge of various iterations of mobility impairment, but will also delve into the default condition and genetic predisposition of bone growth without loading forces involved.

One individual in the present study that does show evidence of geometric differences is MUA042208 who had Cerebral Palsy. This neurological disorder results in progressive musculoskeletal pathology, including contractions of the muscle-tendon units, bony torsional deformity and instability of the joints (Robin et al. 2008). Thus, this individual's gait and mobility were progressively affected throughout life with it known that the individual walked with both legs bent and required some combination of using a cane, walker, or wheelchair by around age 30 (though this individual only lived until age 35). Externally there is clear mediolateral wasting of the femoral diaphysis, and the cross-sectional geometric results show that the standardized I_{\min} and I_{\max} values are lower than many of the individuals in the sample (Figure 4.1) with a subsequently higher I_{\max}/I_{\min} ratio. This further bolsters the hypothesis of mobility differences or impairment during

growth affecting the cross-sectional geometry, but that individuals who acquire mobility impairment later in life are unlikely to acquire such changes and instead retain the geometry already established from normal mobility previous to the disuse event.

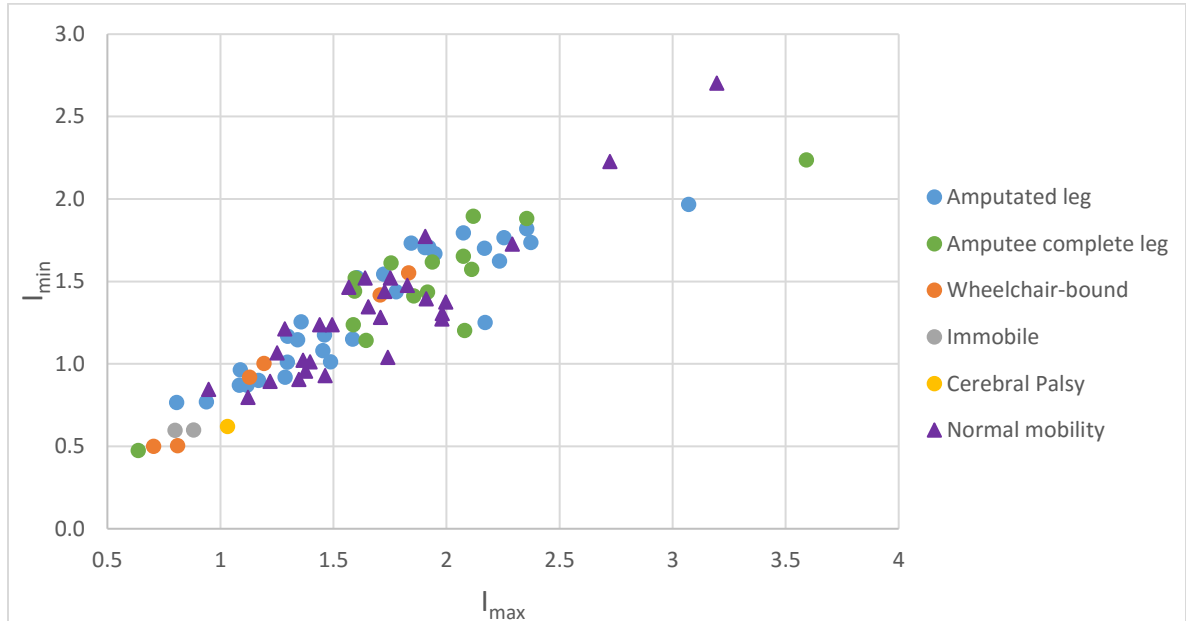


Figure 4.1. Scatterplot regressing I_{min} against I_{max} for the mobility impaired samples separated by impairment type and the normal mobility samples.

There is a general pattern in the results of the mobility impaired samples having a broader range for the many variables. This is possibly due to there being twice the number of femora in the mobility impaired sample, with both sides of each individual being used, as opposed to the normal mobility sample. However, it is also likely that mobility impairment causes a variable response in the different individuals and due to various impairment types. This agrees with the idea of the habitualized strain reference state being different for each individual (Rubin and Rubin 2006; Lerebours and Buenzli 2016), and thus each mobility impaired individual might have been at a slightly different setpoint when remodeling from disuse began.

Mobility Impairment Time Dispersal

The reduced sample size of femora from individuals with known amount of time of mobility impairment (n = 26 femora; 13 individuals) may account for the overall lack of correlation between amount of time of mobility impairment and the trabecular properties. It is also possible that the various other factors, such as age, individual health, strain starting setpoint, etc. that affect bone remodeling may play a greater role in how quickly the effects of mobility impairment can be detected in the trabeculae of each individual rather than how long the individual has had impaired mobility. One factor that cannot be accounted for is individual genetic effects, as there may be genome-specific sensitivities to mechanical loading that predisposes some individuals to higher risk (Judex et al. 2002; Rubin and Rubin 2006). Additionally, Lerebours and Buenzli (2016) discuss the possibility of a new setpoint being reached during periods of unloading. Thus, it is possible that after a certain amount of time there is less bone remodeling occurring and the femur of an individual who was mobility impaired for over 10 years, for example, might have a very similar signature to one who was mobility impaired for 5 years.

Bioarchaeological application

Bioarchaeological application of this research is possible. However, when using these results to investigate the presence of mobility impairment in bioarchaeological remains, particularly prehistoric remains, it is important to remember that prehistoric disuse will likely never match what is seen in our modern populations. With the overall increasing gracility and trabecular loss in modern sedentary populations (Chirchir et al. 2012, 2015), individuals from varying time periods and of varying subsistence strategies will have bone habituated to different activity levels. However, from the results of this

study it can be inferred that individuals with low BV/TV and Tb.Th, and higher Tb.Sp relative to those of individuals from the same population or of the same subsistence strategy, may indicate the presence of mobility impairment.

Conclusion

Mobility impairment does have a visible and significant effect on the trabecular and cortical bone of the femur. Mobility impairment as an adult results in an overall loss of bone in the trabecular struts, quantified by a loss in trabecular thickness and increased spacing between the trabeculae, but has no effect on the trabecular number or orientation. Within the femoral diaphysis, there is a clear loss in cortical bone along the endosteal surface, resulting in an increased medullary area. There was also increased porosity of the cortical bone of the mobility impaired individuals.

The findings of this study have significant implications in both bioarchaeology and forensic anthropology. The results provide a method for recognizing and diagnosing mobility impairment from human skeletal remains. Most importantly the results add to our understanding of how bone responds to mechanical use. This research bolsters the accuracy of utilizing trabecular architecture to interpret past terrestrial logistic mobility and thus subsistence strategies. Unloading does affect the same properties that show significance when comparing more mobile to more sedentary populations (Ryan and Shaw 2015). Additionally, because most of the mobility impaired individuals in this study do maintain muscular function, this research is in essence a model of extreme sedentism that can be used as a minimum to bracket the range of possible values when trabeculae are being used for mobility level comparisons.

This research continues to add to the understanding of bone remodeling and biomechanics during times of unloading; however, there is always more to be done. Future research will include investigating cortical and trabecular bone differences in individuals who had impaired mobility during growth and development. Additionally, the increased cortical porosity observed in the mobility impaired individuals will be further investigated with plans to develop a method to quantify these results. Similarly, since the remodeling observed in mobility impaired individuals is similar to that observed with aging, methods used in bone histology (Gocha and Agnew 2016) observing spatial variation in intracortical remodeling rates due to age may provide a method of examining areas of greater or lesser strain magnitudes.

Understanding how bone responds in instances of disuse and unloading provides valuable information about bone biology, bone growth, the genetic predisposition of bone, how mechanical loading forces actually influence bone cells, bone loss and remodeling patterns, interpreting mobility patterns and subsistence strategies, and diagnosing mobility impairment in skeletal remains. This research has begun to explore this incredibly useful and often lesser studied aspect of bone biology and biomechanics with very interesting results.

APPENDIX SECTION

Appendix A. Mobility impaired and normal mobility match sample demographics.
 [M.Obese = Morbidly Obese; Ances. = Ancestry]

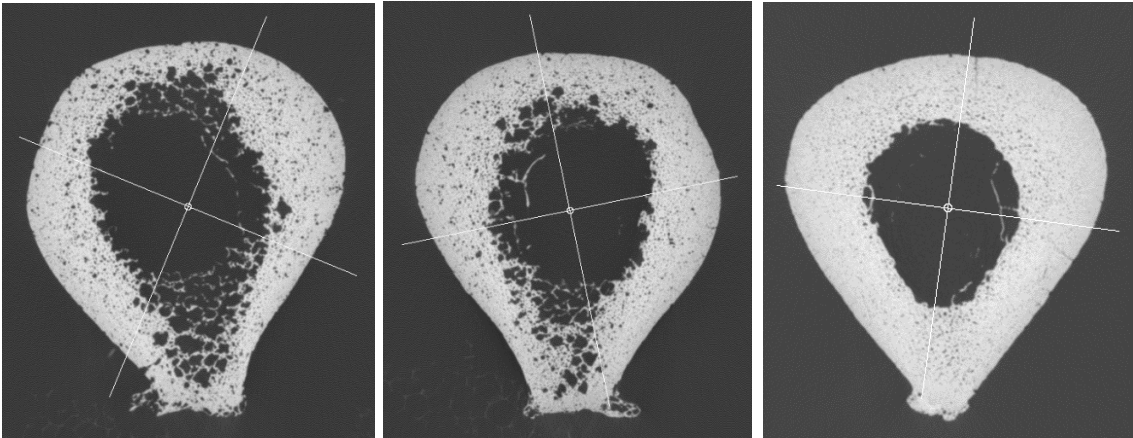
Mobility Impaired	Collection	Disuse Type	Disuse Side	Amputation site	Amt. of time of disuse	Sex	Age (yrs)	Ances.	BMI
D04-2014	TXSTDSC	Double amputation	Both	Tibiae and fibulae	Unknown	M	63	W	N/A
D06-2013	TXSTDSC	R Amputation & L mishealed fracture with metal rod	Both	R femur	R - 4 years	M	68	W	43.5 - M.Obese
D22-2012	TXSTDSC	Amputation	R	Femoral midshaft	15 years	M	78	W	47.1 - M.Obese
D28-2015	TXSTDSC	Double amputation	Both	Tibiae and fibulae	L. leg 7 years, R. leg 5 years	F	76	W	N/A [267 lbs ~ Obese]
D32-2014	TXSTDSC	Immobile	Both	N/A	5 years	F	69	W	62.9 - M.Obese
D47-2013	TXSTDSC	Wheelchair	Both	N/A	Unknown	F	56	W	35.0 - Obese
D51-2014	TXSTDSC	Amputation	L	Tibia and fibula	~11 months	M	74	W	29.6 - Overweight
D54-2015	TXSTDSC	Double amputation	Both	R - distal femur; L - metatarsal	L foot - 9 years, 3 months	F	78	W	49.0 - M.Obese
D56-2013	TXSTDSC	Wheelchair - Scoliosis and MS	Both	N/A	8 years	F	63	W	23.8 - Normal
UT05-00D	UTK Bass	Amputation	R	Tibia and fibula	Unknown	M	88	W	Unknown
UT05-09D	UTK Bass	Amputation	L	Metatarsals	Unknown	M	59	W	27.4 - Overweight
UT05-97D	UTK Bass	Amputation	R	Tibia and fibula	Unknown	F	67	W	Unknown
UT06-02D	UTK Bass	Double Amputation	Both	Femoral midshafts	Unknown	M	77	B	Unknown
UT14-92D	UTK Bass	Double Amputation; paralysis	Both	Tibiae and fibulae	Paralysis R side: ~5years	M	56	W	Unknown
UT17-07D	UTK Bass	Amputation	L	Femur	Unknown	M	75	W	[104 lbs ~ Normal]
UT20-99D	UTK Bass	Amputation	L	Tibia and fibula	Unknown	M	55	W	Unknown
UT23-99D	UTK Bass	Double Amputation	Both	L - femoral midshaft; R - metatarsals	Unknown	M	79	W	Unknown
UT47-01D	UTK Bass	Amputation	R	Tibia and fibula	Unknown	F	56	W	31.9 - Obese
UT53-08D	UTK Bass	Amputation	L	2nd and 3rd metatarsals	Unknown	M	65	W	29.5 - Overweight
UT55-10D	UTK Bass	Double Amputation	Both	Femoral midshafts	~ 7 years	M	49	W	[105 lbs ~ Normal]

Mobility Impaired	Collection	Disuse Type	Disuse Side	Amputation site	Amt. of time of disuse	Sex	Age (yrs)	Ancestry	BMI
UT60-09D	UTK Bass	Amputation	L	Femoral midshaft	L leg - 9 years	M	62	W	26.9 - Overweight
UT64-05D	UTK Bass	Amputation	L	Tibia and fibula; infection of and metal plate in distal femur	Unknown	M	51	W	20.6 - Normal
UT70-08D	UTK Bass	Double Amputation	Both	Midshaft-distal femora	4 years	M	63	W	45.3 - M.Obese
UT73-09D	UTK Bass	Amputation	R	Femoral midshaft	~4 months	F	86	W	23.4 - Normal
UT75-05D	UTK Bass	Double Amputation	Both	L - femoral midshaft; R - tibia and fibula	Unknown	M	59	W	Unknown
UT76-09D	UTK Bass	Amputation	R	Tibia and fibula	~2 years; only ~4 months before prosthetics	M	54	W	24.4 - Normal
UT104-09D	UTK Bass	R foot Amputation & L mishealed fracture	Both	R - 2nd metatarsal	Unknown	M	69	W	29.5 - Overweight
MUA042208	UMO	cerebral palsy, wheelchair and walker	Both; only L acquired	N/A	~2 years	F	35	W	20.4 - Normal

Mobility Impaired	Normal Mobility Match	Sex	Age (yrs.)	Ancestry	BMI	Side
D04-2014	D23-2013	M	63	W	22.2 - Normal	L
D06-2013	D42-2012	M	68	W	38.2 - Obese	L
D22-2012	D07-2013	M	76	W	43.2 - M.Obese	L
D28-2015	D10-2009	F	76	W	25.3 - Overweight	R
D32-2014	D04-2011	F	68	W	38.8 - Obese	L
D47-2013	D21-2011	F	56	W	29.4 - Overweight	L
D51-2014	D28-2012	M	75	W	24.7 - Normal	L
D54-2015	D03-2012	F	78	W	22.7 - Normal	L
D56-2013	D04-2012	F	63	W	27.3 - Normal	L
UT05-00D	D36-2013	M	88	W	21.4 - Normal	L
UT05-09D	D41-2012	M	60	W	23.5 - Normal	L
UT05-97D	D23-2011	F	66	W	23.4 - Normal	L
UT06-02D	D14-2014	M	78	W	28.2 - Overweight	L
UT14-92D	D49-2014	M	56	W	27.8 - Overweight	L

Mobility Impaired	Normal Mobility	Sex	Age (yrs.)	Ancestry	BMI	Side
UT17-07D	D30-2012	M	74	W	34.5 - Obese	R
UT20-99D	D46-2013	M	55	W	35.1 - Obese	L
UT23-99D	D05-2012	M	79	W	25.8 - Overweight	L
UT47-01D	D12-2011	F	53	W	34.6 - Obese	L
UT53-08D	D20-2013	M	67	W	25.3 - Overweight	L
UT55-10D	D01-2009	M	49	W	20.9 - Normal	L
UT60-09D	D65-2013	M	61	W	27.8 - Overweight	L
UT64-05D	D33-2013	M	52	W	22.2 - Normal	R
UT70-08D	D10-2015	M	66	W	43.8 - M.Obese	L
UT73-09D	D12-2013	F	89	Lebanese	22.3 - Normal	L
UT75-05D	D14-2013	M	58	W	20.7 - Normal	L
UT76-09D	D02-2013	M	53	W	24.5 - Normal	L
UT104-09D	D27-2013	M	69	W	28.2 - Overweight	L
MUA042208	D05-2015	F	39	W	18.6 - Normal	R

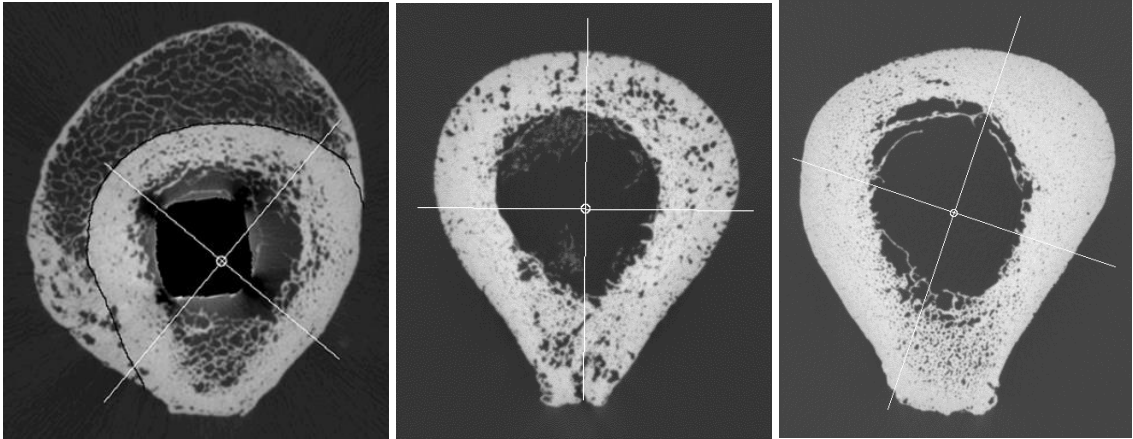
Appendix B. Mobility impaired left, right, and normal mobility match midshaft cortical bone slices with the principal and secondary orientations annotated. [amp. = the amputated leg]



D04-2014 L (amp.)

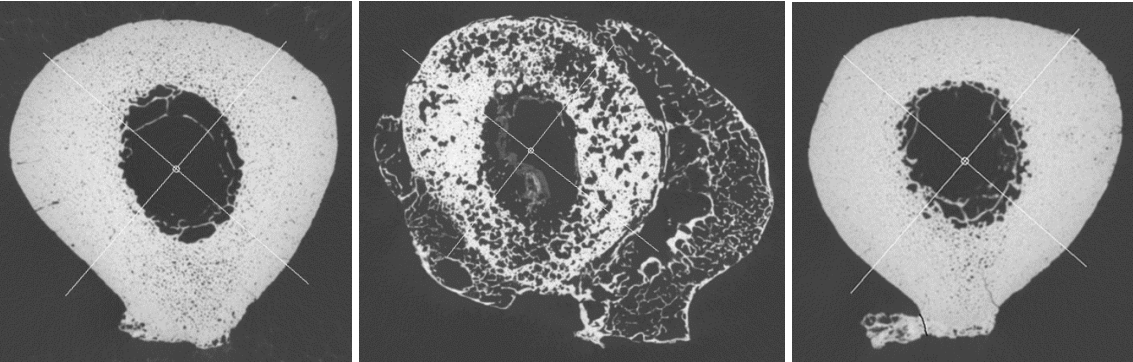
R (amp.)

D23-2013 L



D06-2013 L (fracture/metal rod) R (amp.)

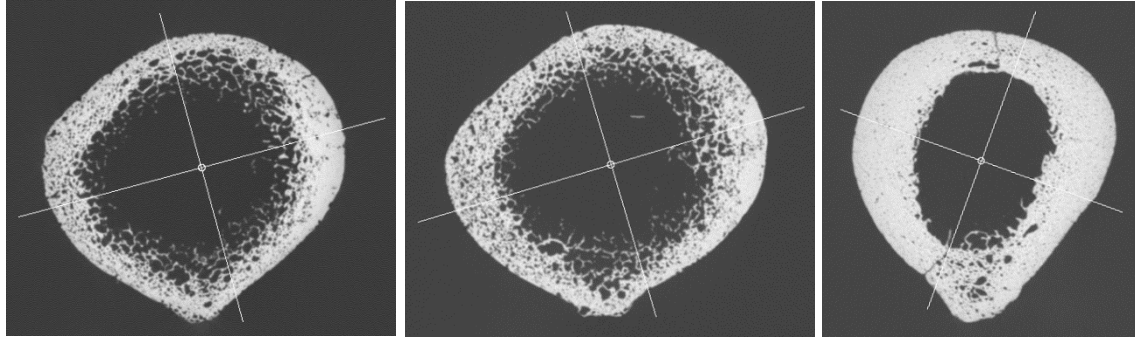
D42-2012 L



D22-2012 L

R (amp.)

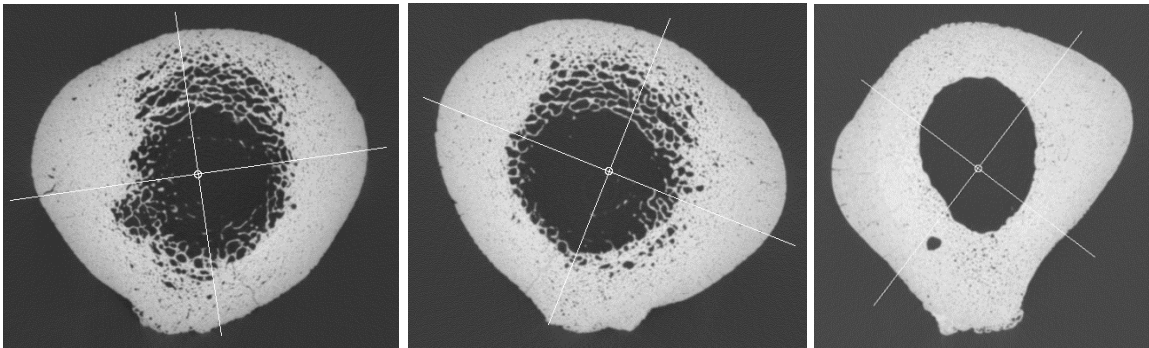
D07-2013 L



D28-2015 L (amp.)

R (amp.)

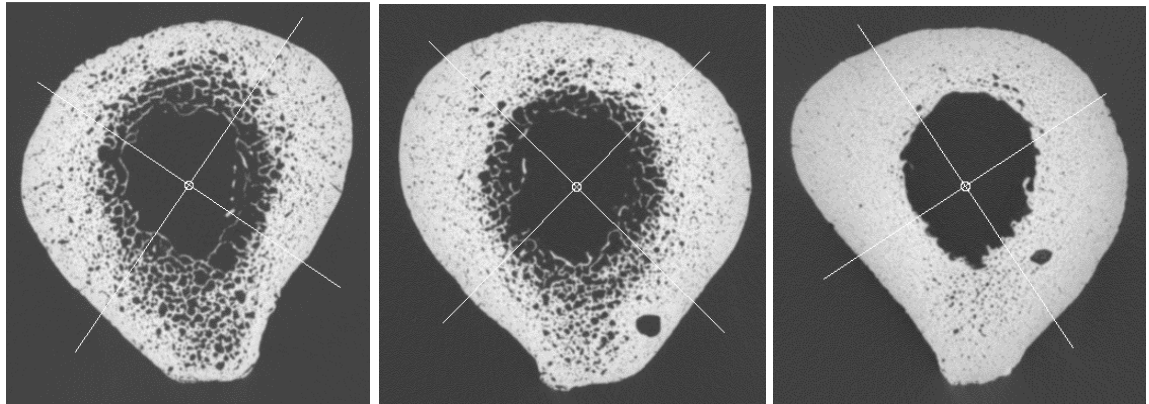
D10-2009 R



D32-2014 L (immobile)

R (immobile)

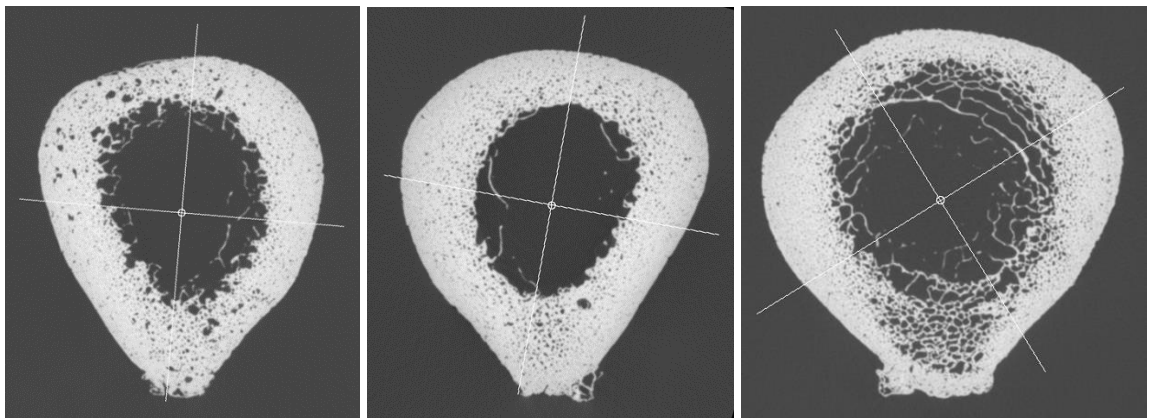
D04-2011 L



D47-2013 L (wheelchair)

R (wheelchair)

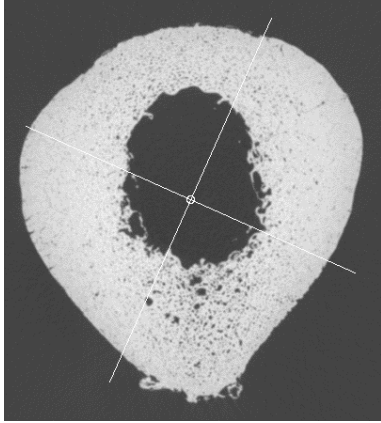
D21-2011 L



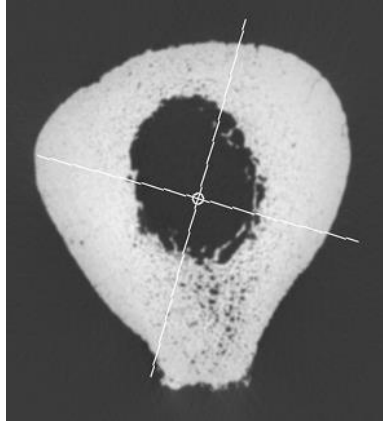
D51-2014 L (amp.)

R

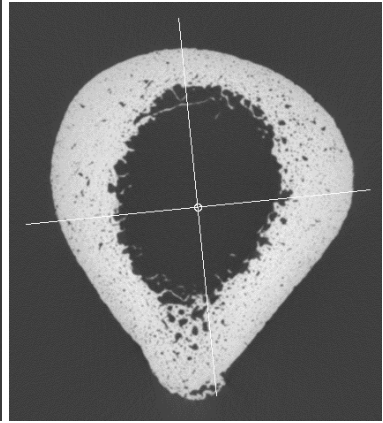
D28-2012 L



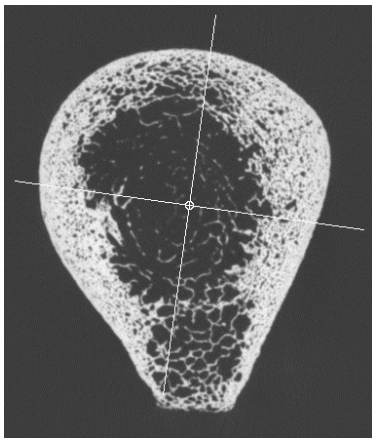
D54-2015 L (amp.)



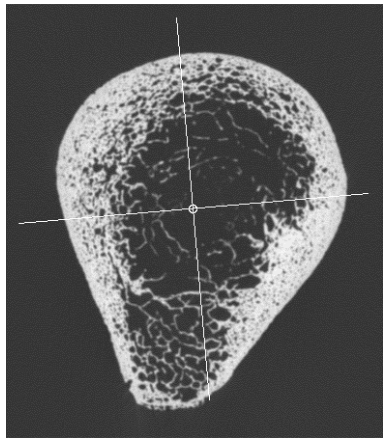
R (amp.)



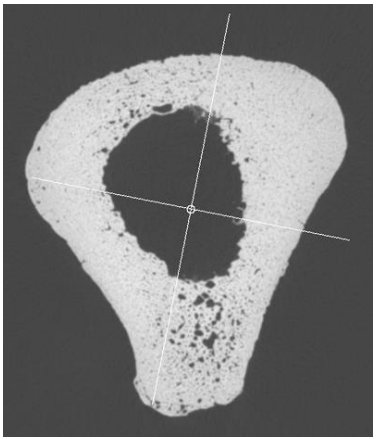
D03-2012 L



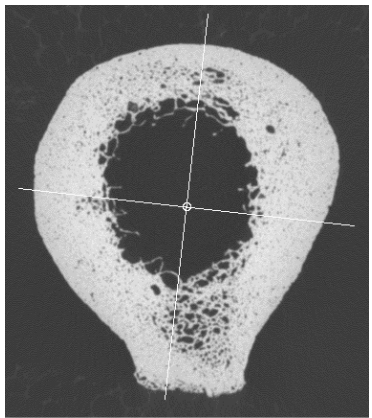
D56-2013 L (wheelchair)



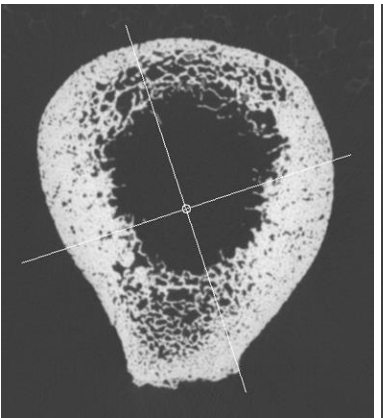
R (wheelchair)



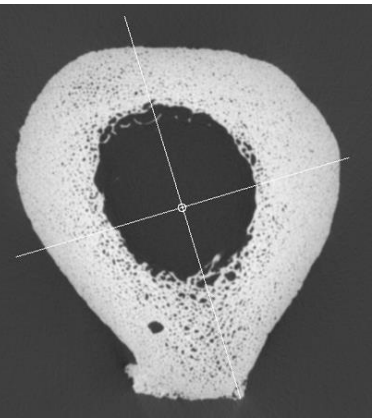
D04-2012 L



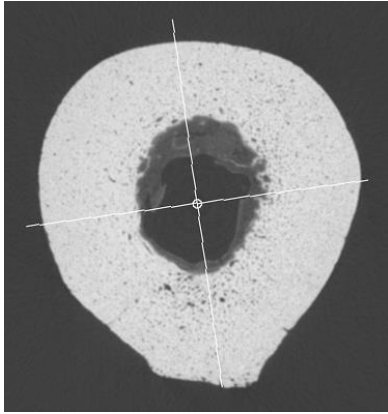
UT05-00D L



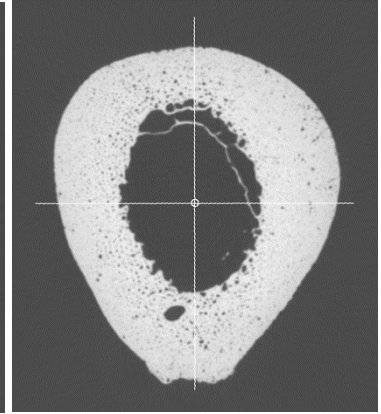
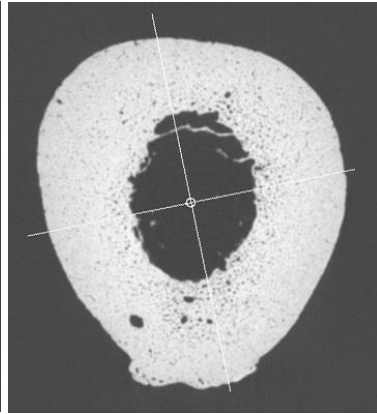
R (amp.)



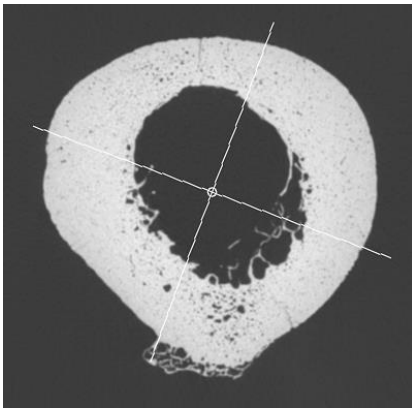
D36-2013 L



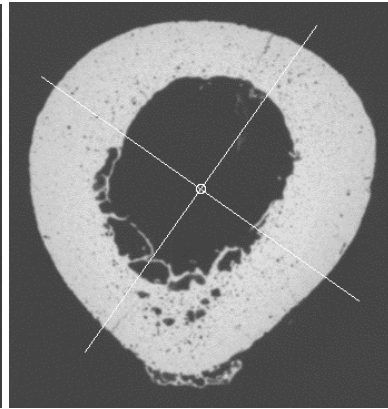
UT05-09D L (amp.- foot) R



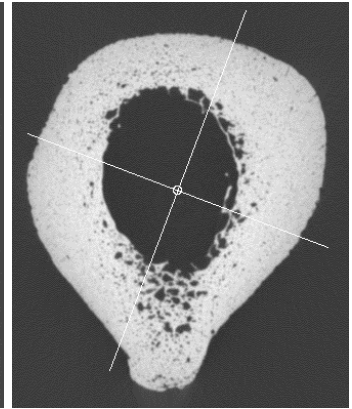
D41-2012 L



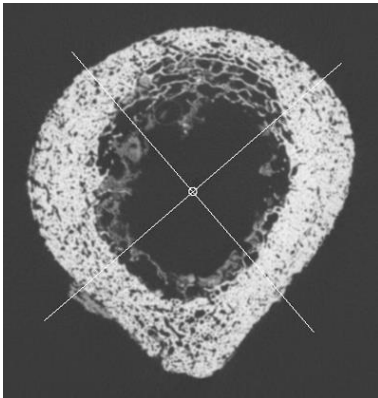
UT05-97D L



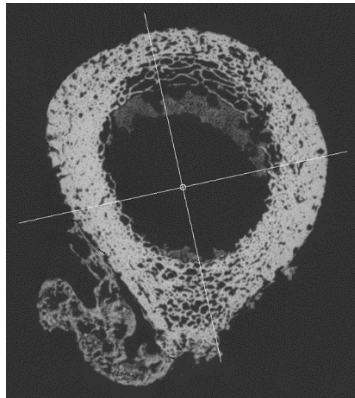
R (amp.)



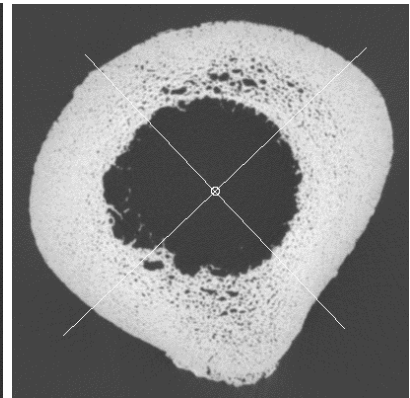
D23-2011 L



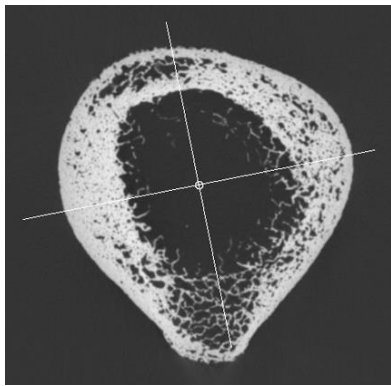
UT06-02D L (amp.)



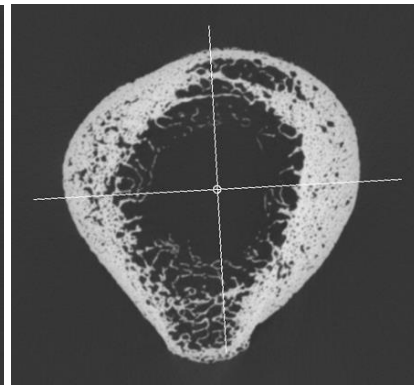
R (amp.)



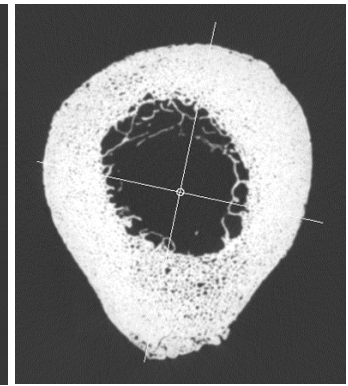
D14-2014 L



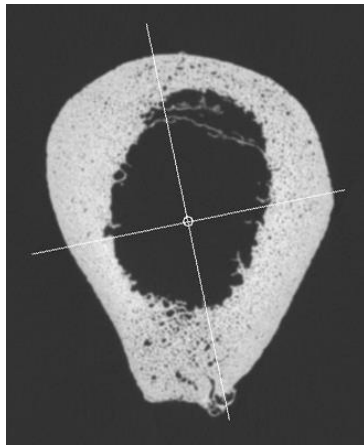
UT14-92D L (amp.)



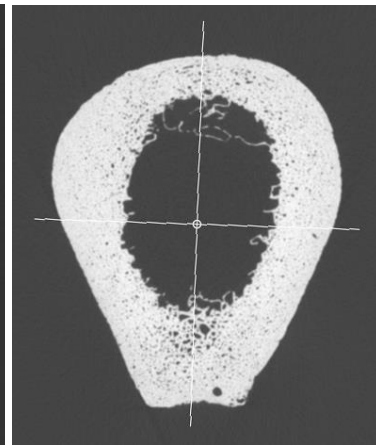
R (amp.)



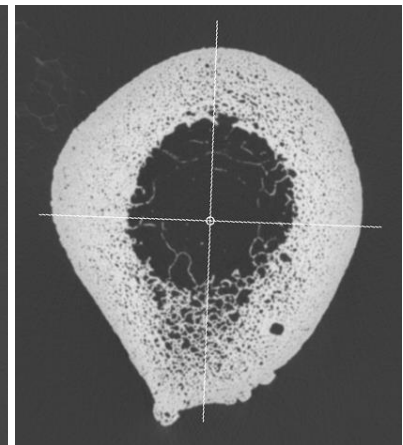
D49-2014 L



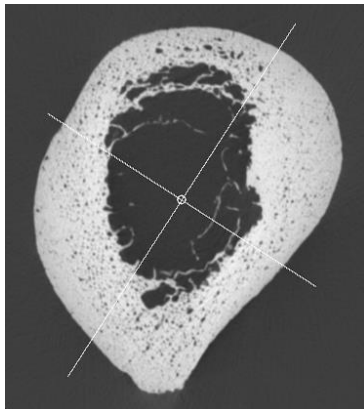
UT17-07D L (amp.)



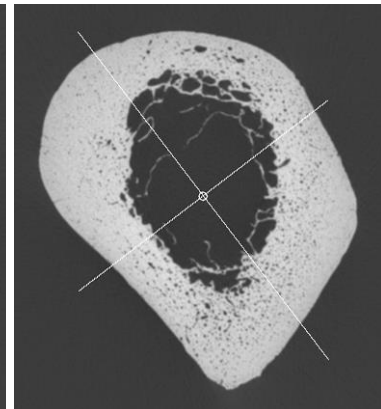
R



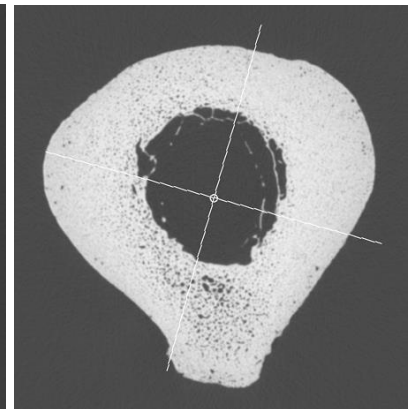
D30-2012 R



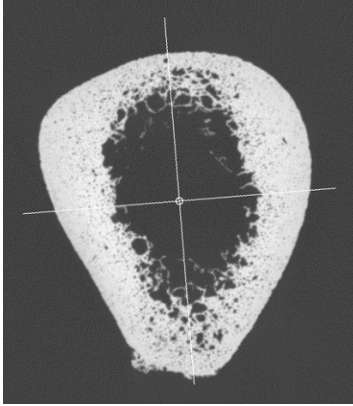
UT20-99D L (amp.)



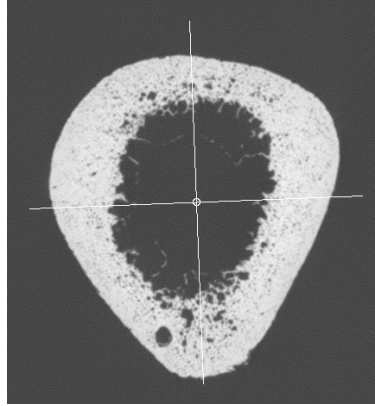
R



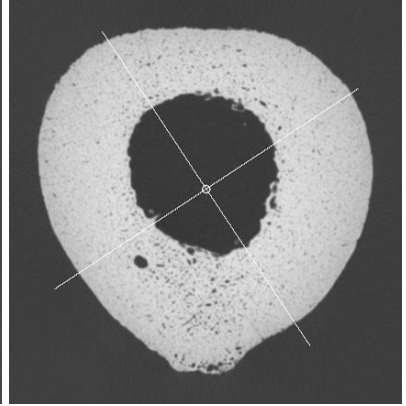
D46-2013 L



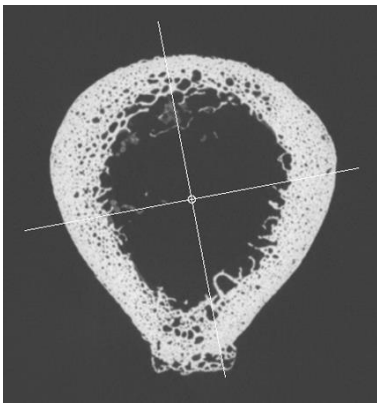
UT23-99D L (amp.)



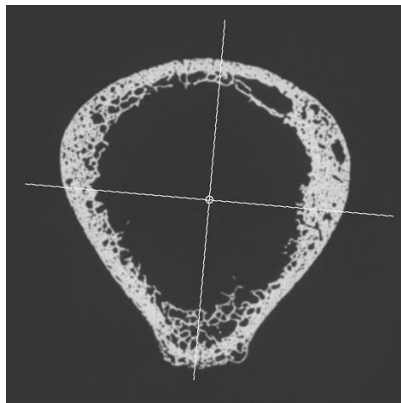
R (amp.- foot)



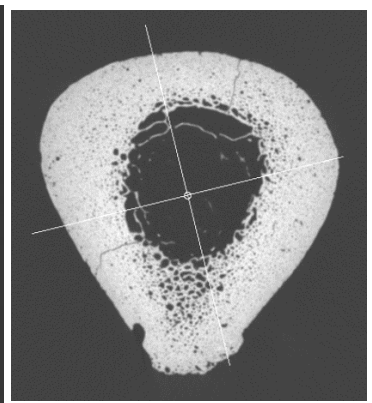
D05-2012 L



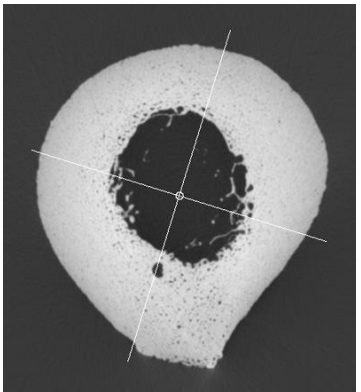
UT47-01D L



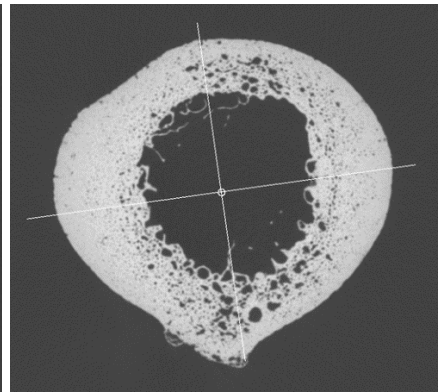
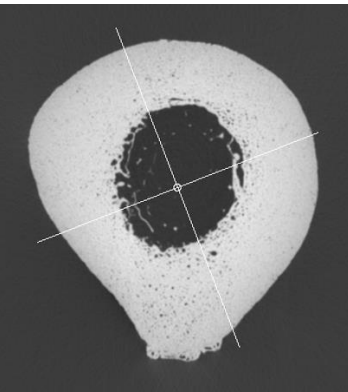
R (amp.)



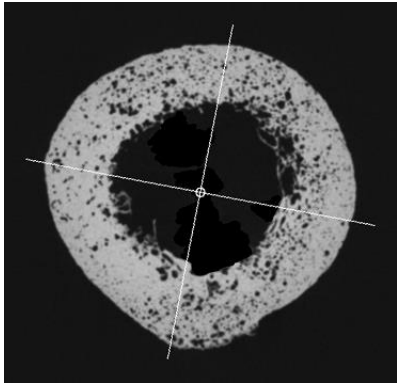
D12-2011 L



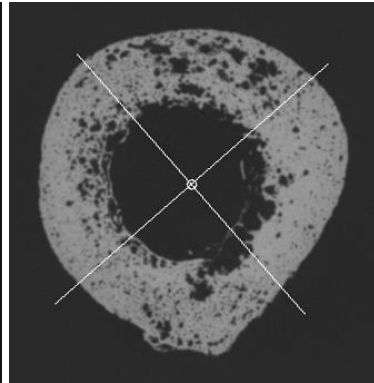
UT53-08D L (amp.- foot) R



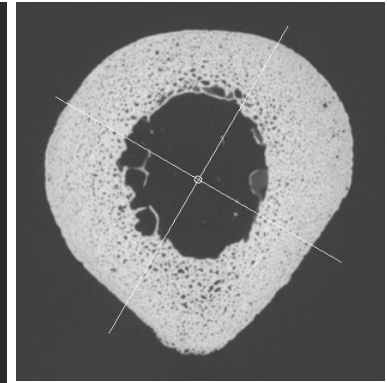
D20-2013 L



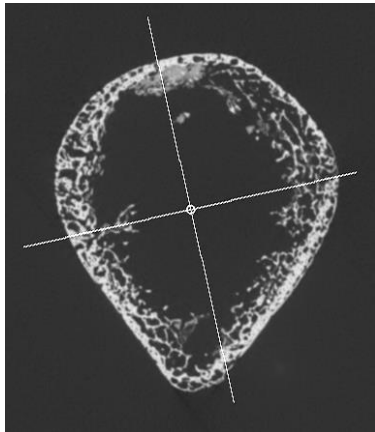
UT55-10D L (amp.)



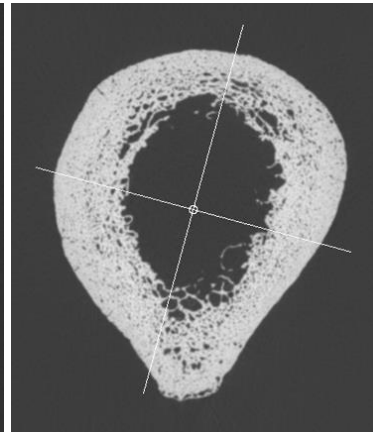
R (amp.)



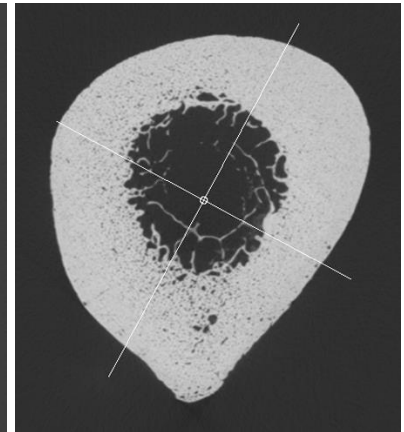
D01-2009 L



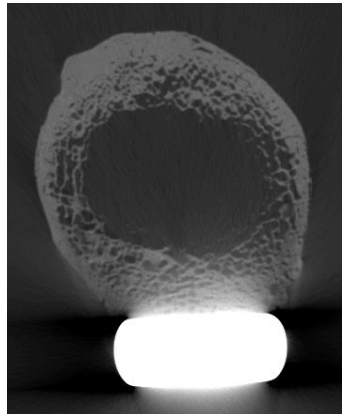
UT60-09D L (amp.)



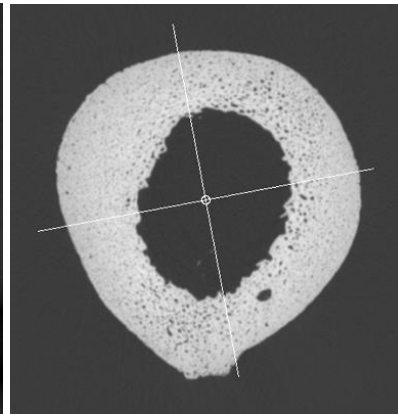
R



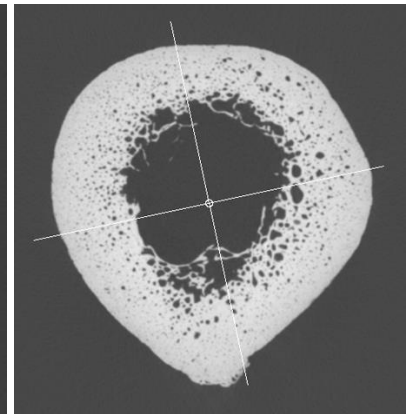
D65-2013 L



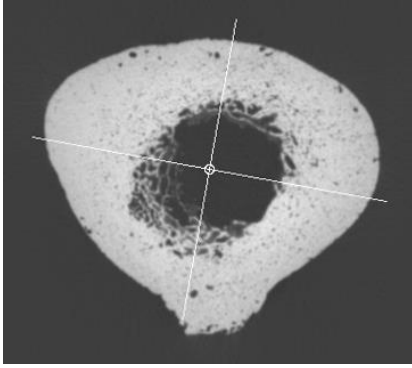
UT64-05D L (amp.)



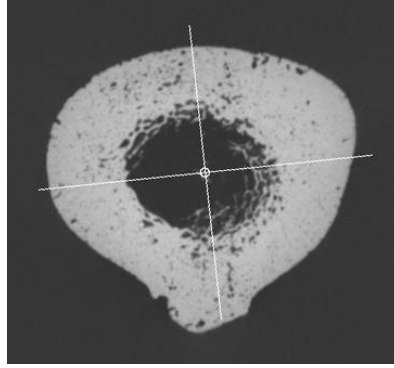
R



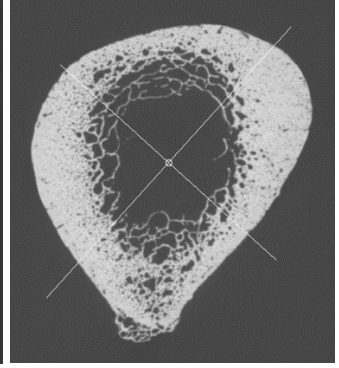
D33-2013 R



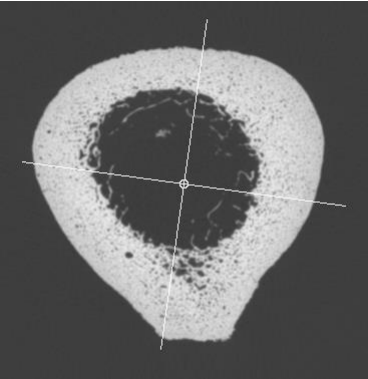
UT70-08D L (amp.)



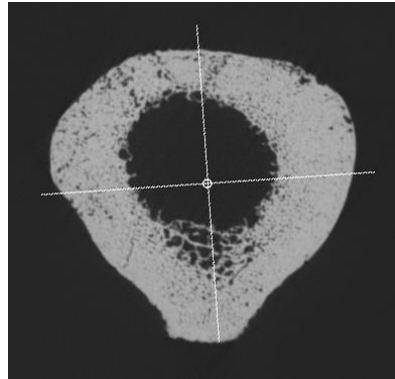
R (amp.)



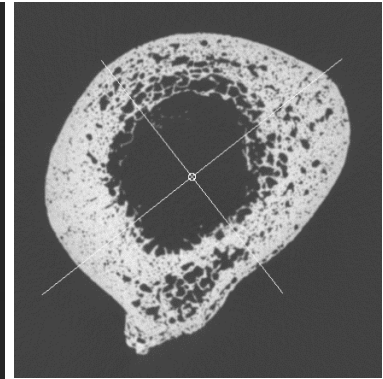
D10-2015 L



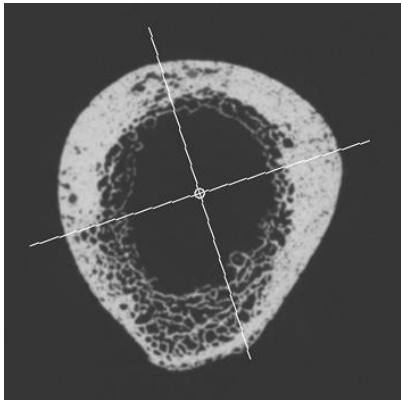
UT73-09D L



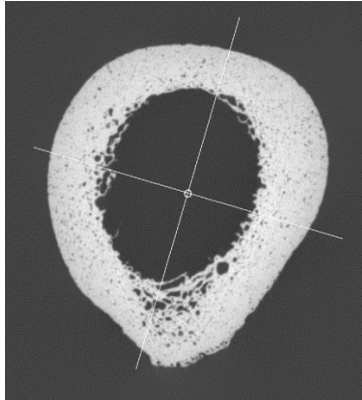
R (amp.)



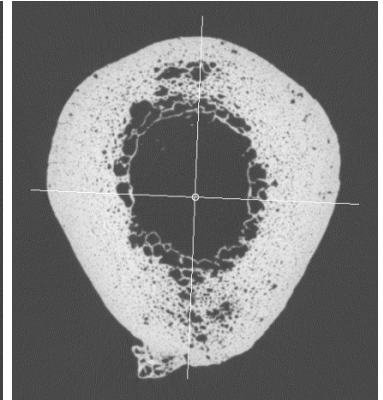
D12-2013 L



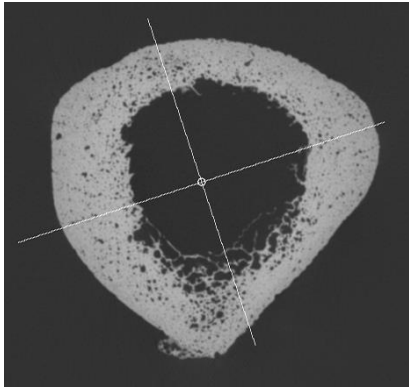
UT75-05D L (amp.)



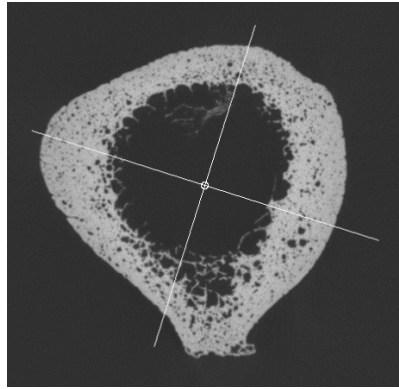
R (amp.)



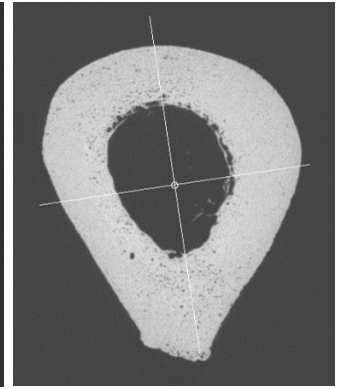
D14-2013 L



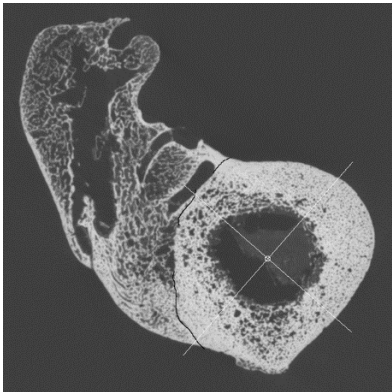
UT76-09D L



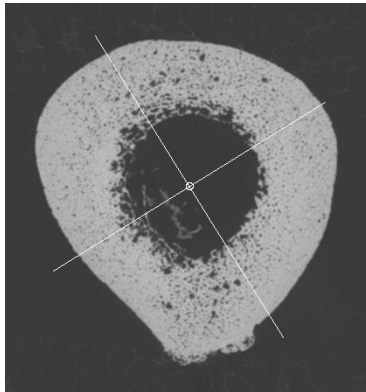
R (amp.)



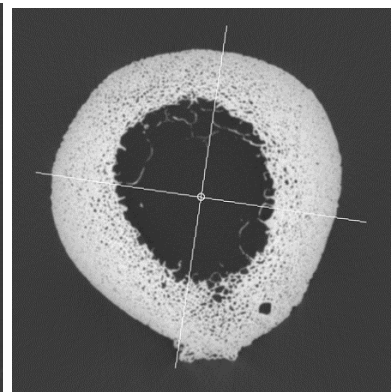
D02-2013 L



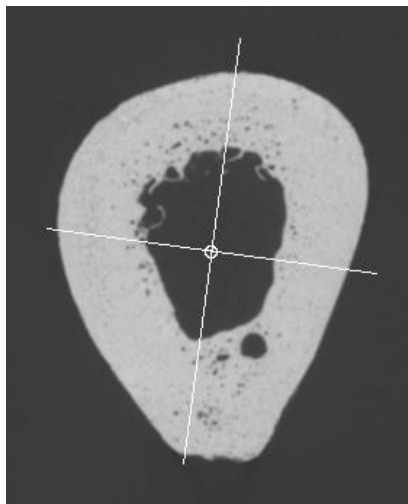
UT104-09D L (fracture)



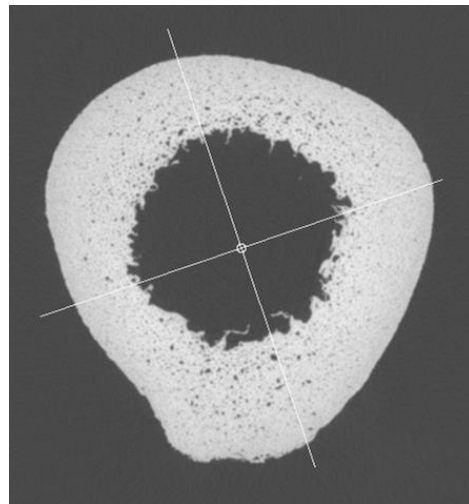
R (amp.- foot)



D27-2013 L

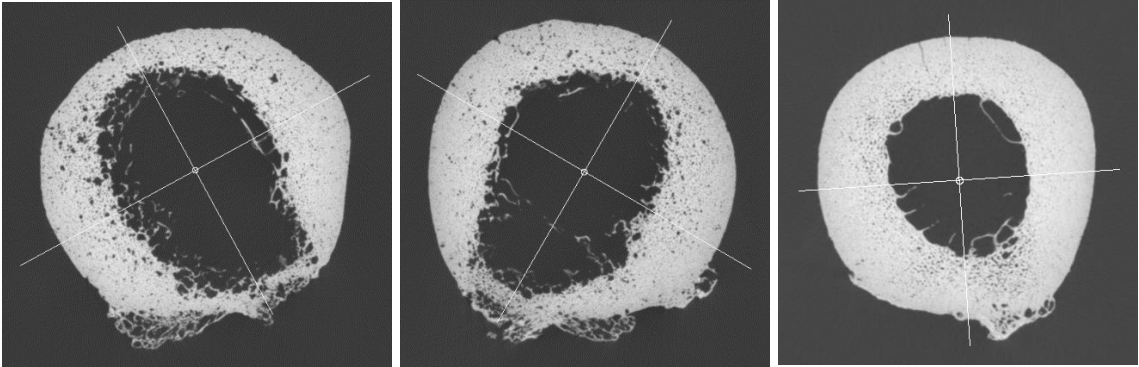


MUA042208 L (CP)



D05-2015 R

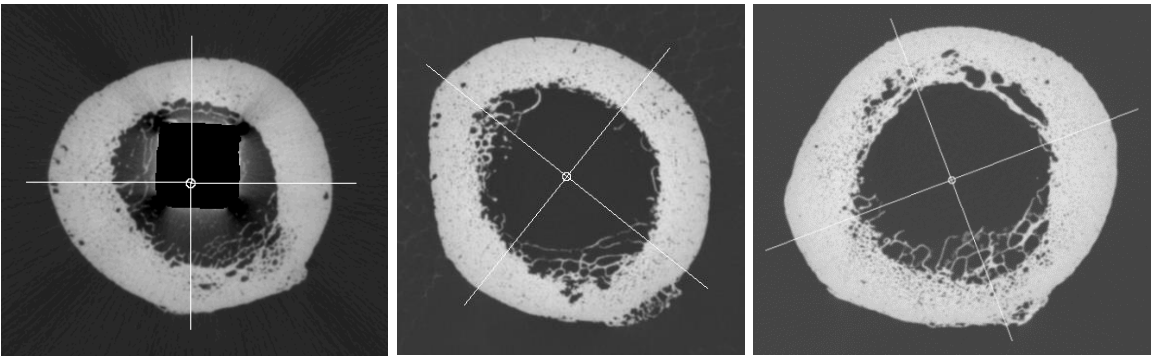
Appendix C. Mobility impaired left, right, and normal mobility match subtrochanteric cortical bone slices with BoneJ Slice Geometry annotations.



D04-2014 L

R

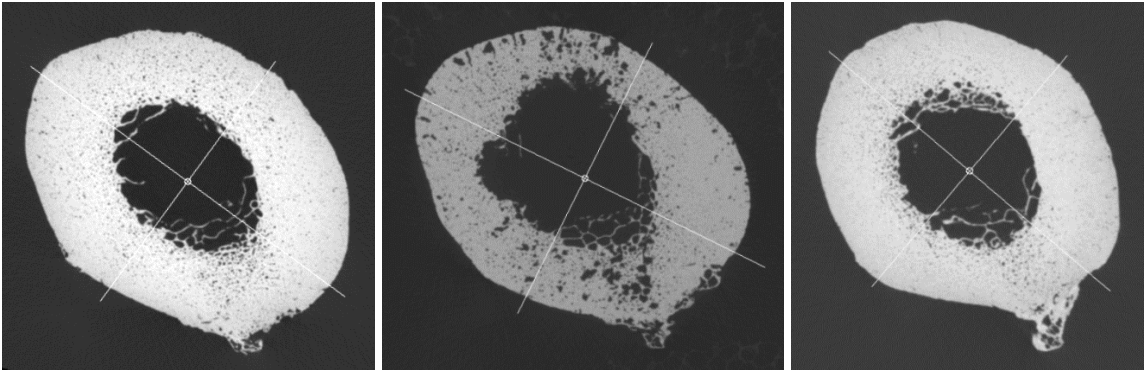
D23-2013



D06-2013 L

R

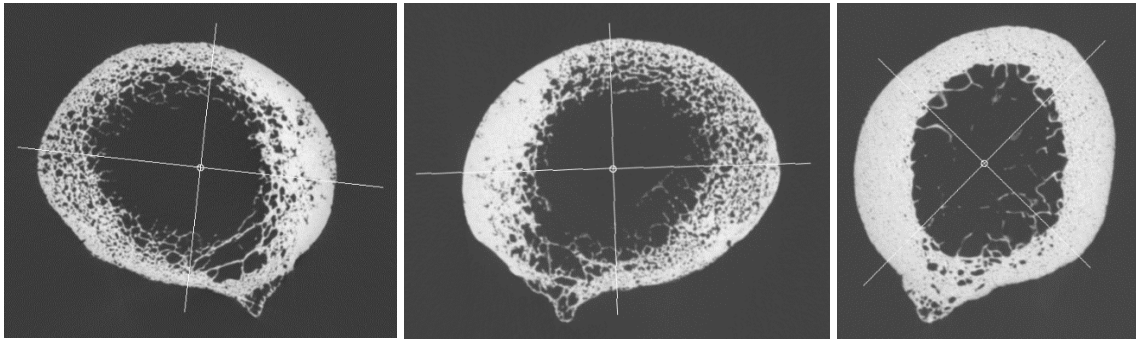
D42-2012



D22-2012 L

R

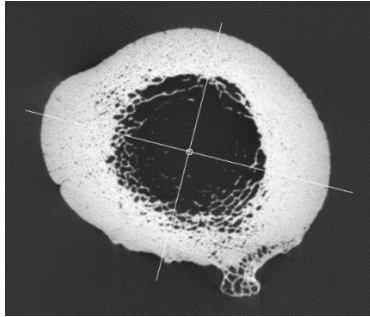
D07-2013



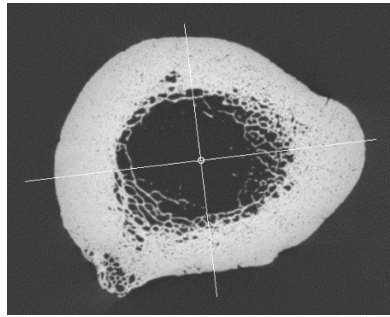
D28-2015 L

R

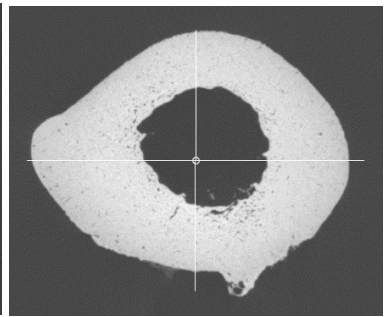
D10-2009



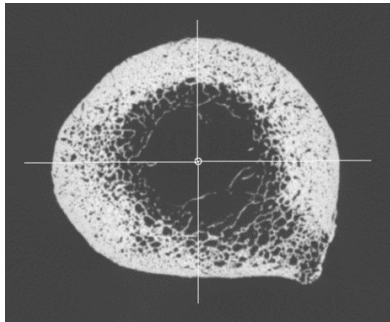
D32-2014 L



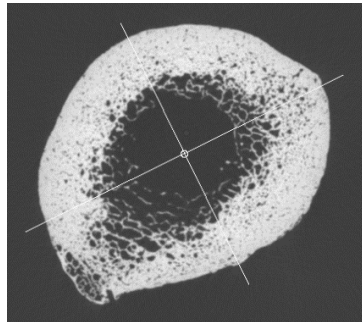
R



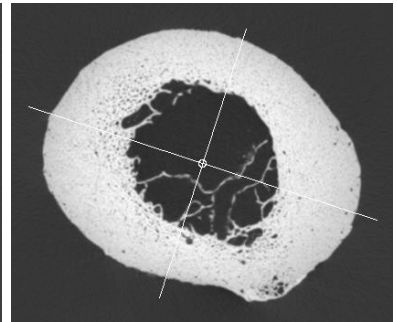
D04-2011



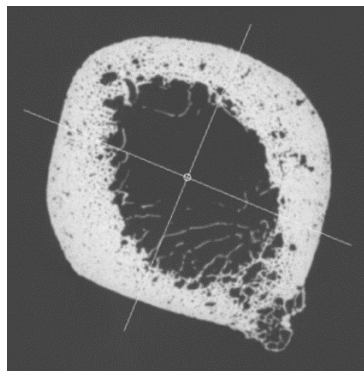
D47-2013 L



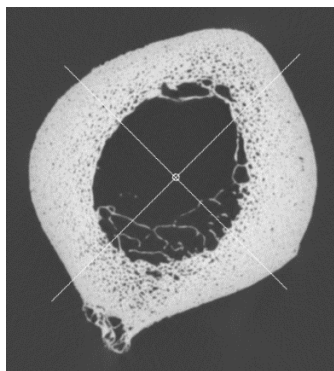
R



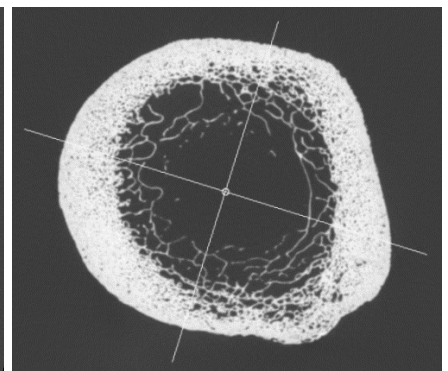
D21-2011



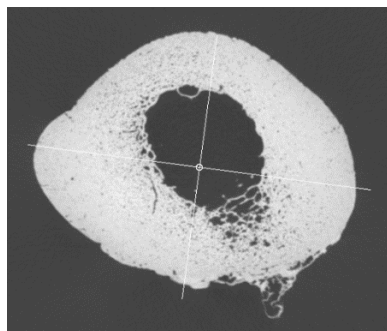
D51-2014 L



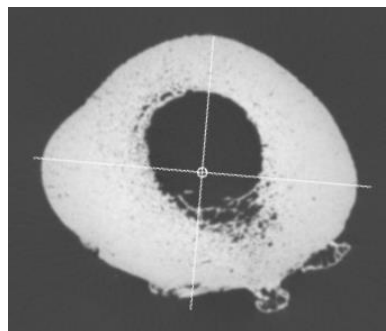
R



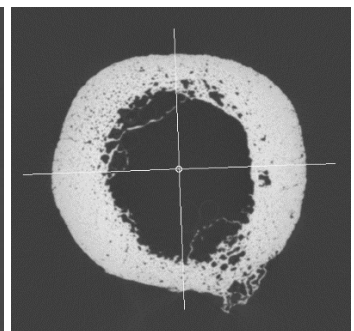
D28-2012 L



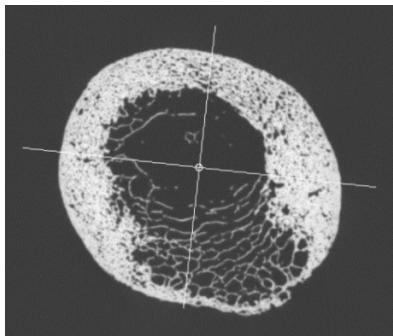
D54-2015 L



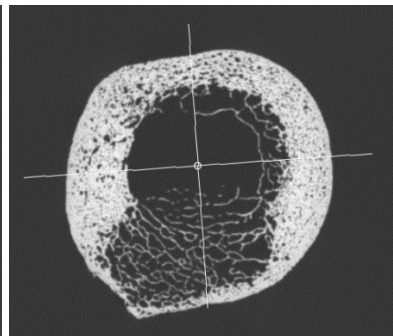
R



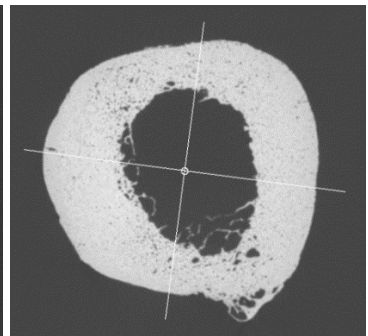
D03-2012



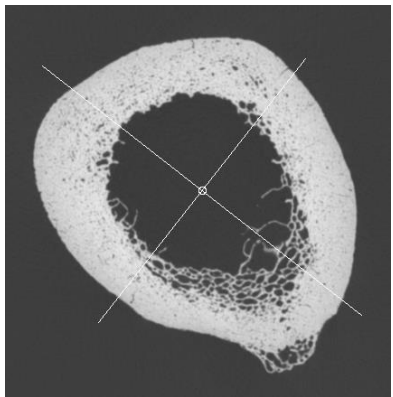
D56-2013 L



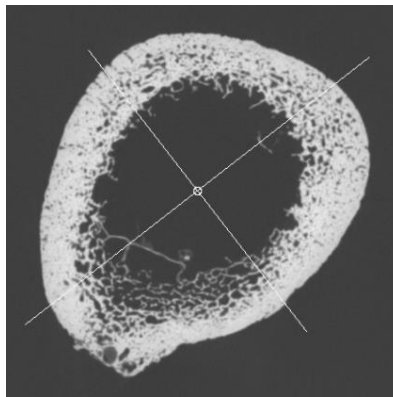
R



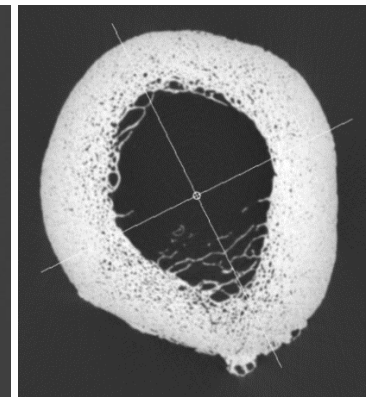
D04-2012 L



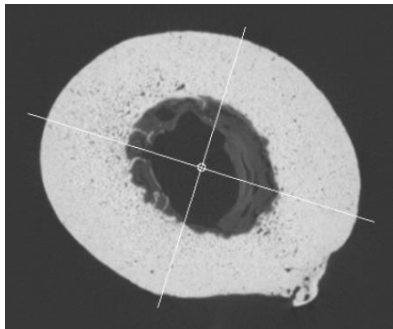
UT05-00D L



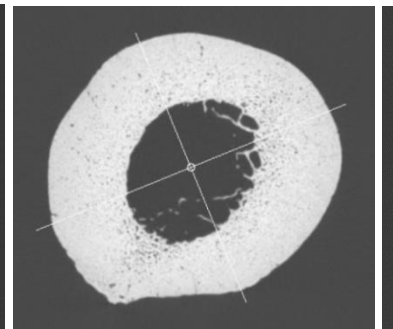
R



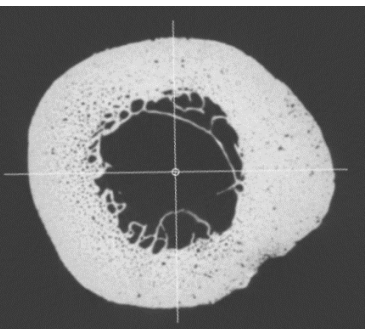
D36-3013 L



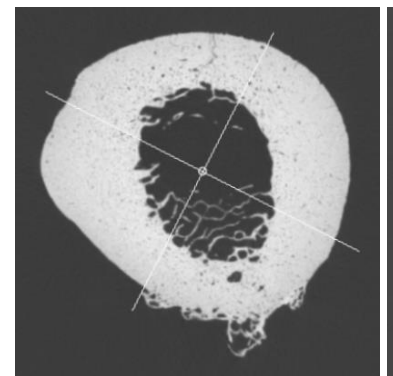
UT05-09D L



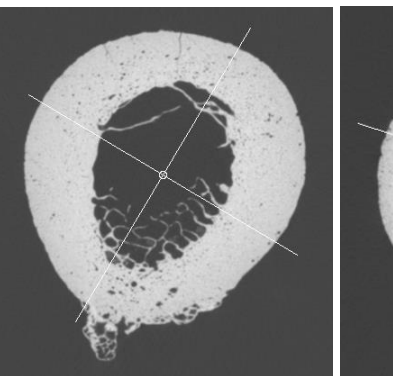
R



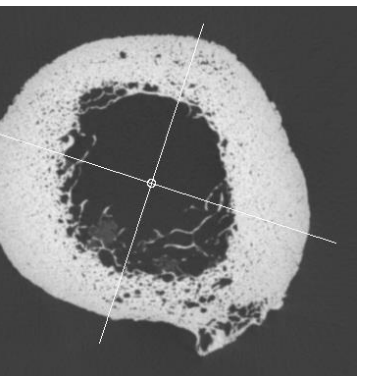
D41-2012



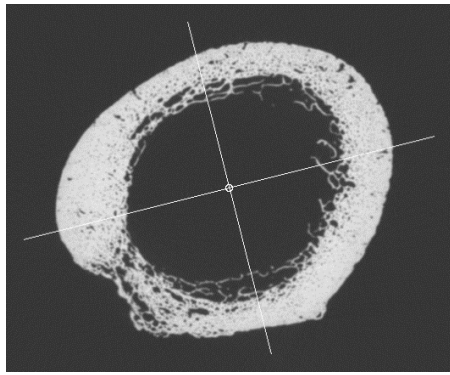
UT05-97D L



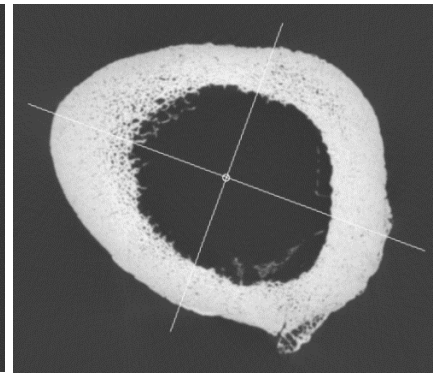
R



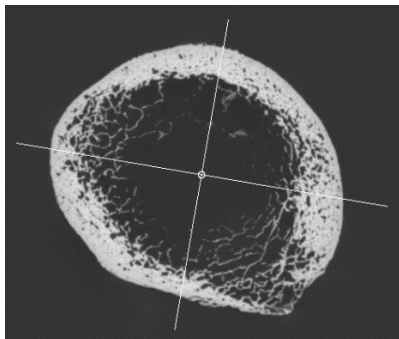
D23-2011 L



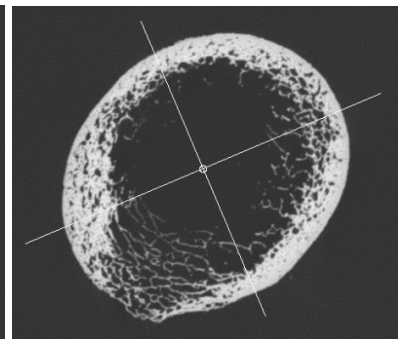
UT06-02D L



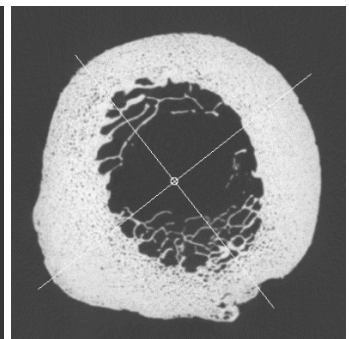
D14-2014 L



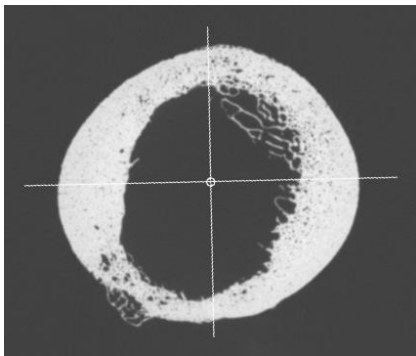
UT14-92D L



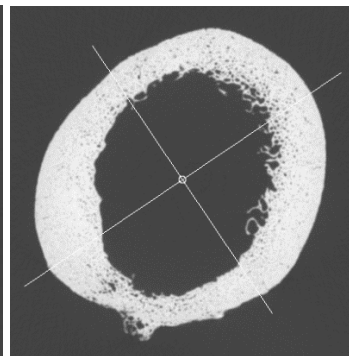
R



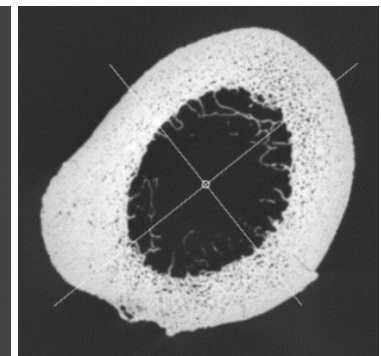
D49-2014 L



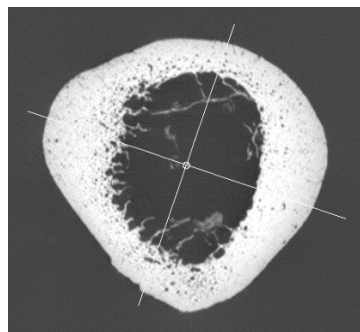
UT17-07D L



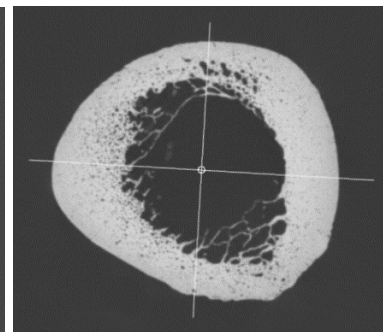
R



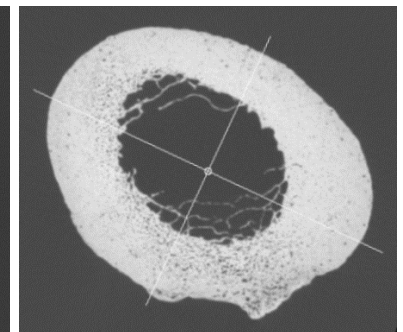
D30-2012 R



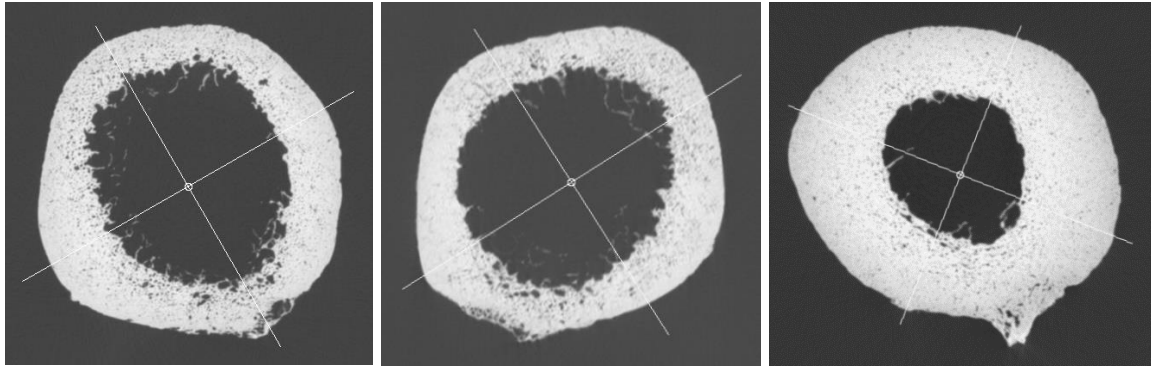
UT20-99D L



R



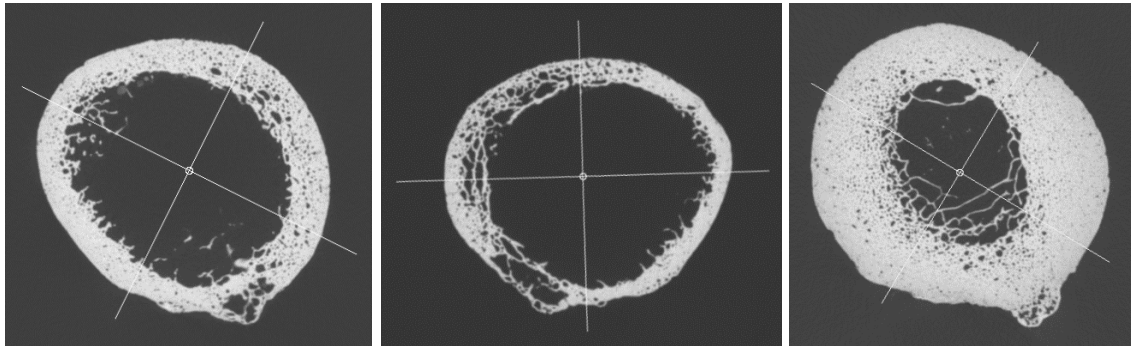
D46-2013 L



UT23-99D L

R

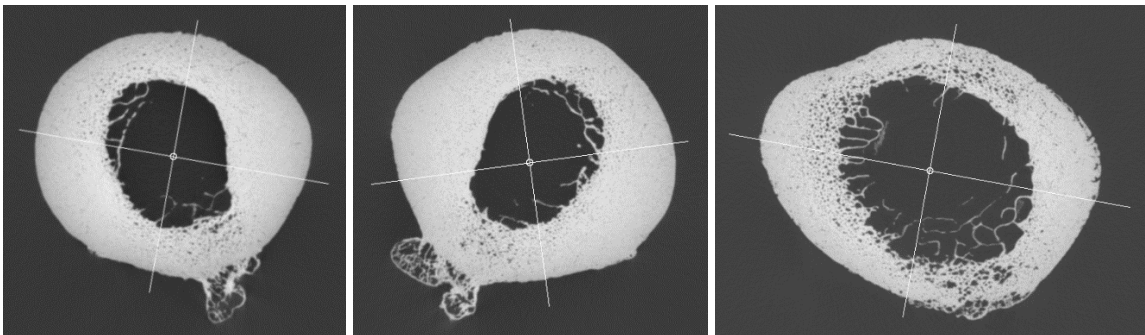
D05-2012



UT47-01D L

R

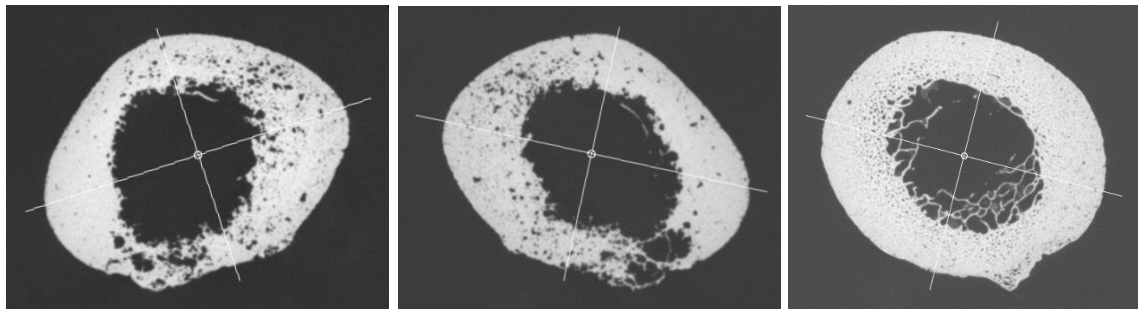
D12-2011 L



UT53-08D L

R

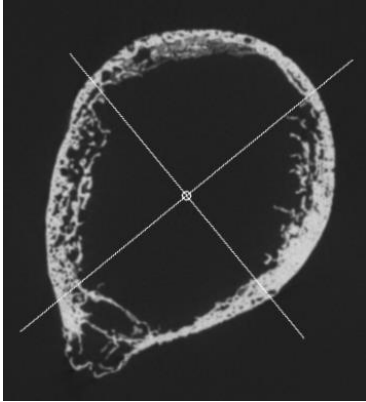
D20-2013 L



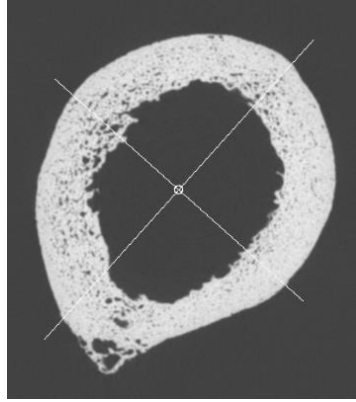
UT55-10D L

R

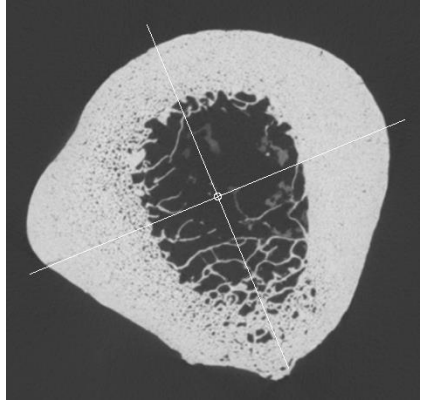
D01-2009 L



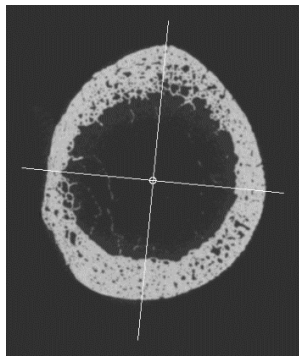
UT60-09D L



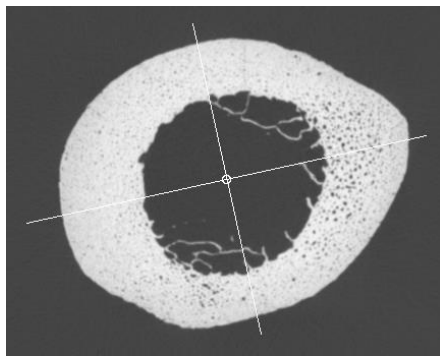
R



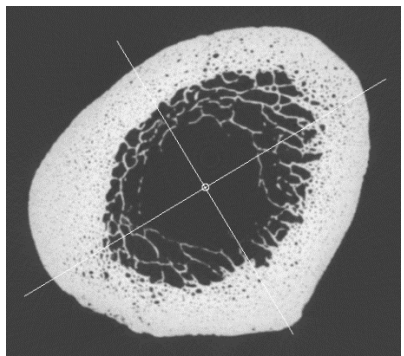
D65-2013 L



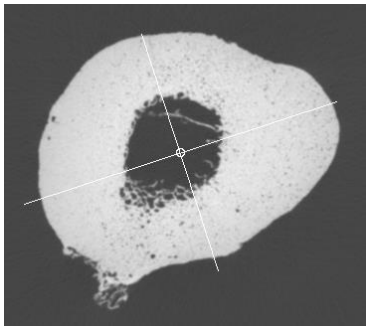
UT64-05D L



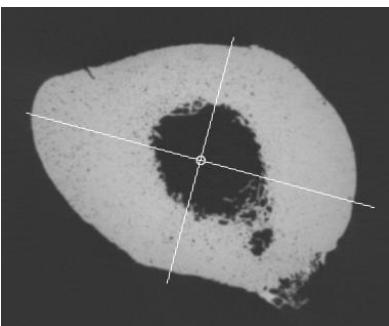
R



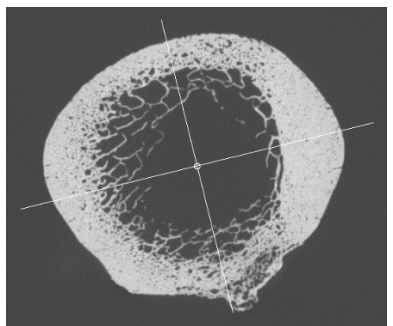
D33-2013 R



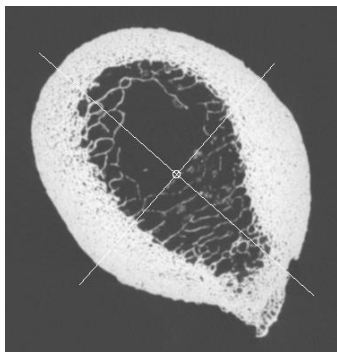
UT70-08D L



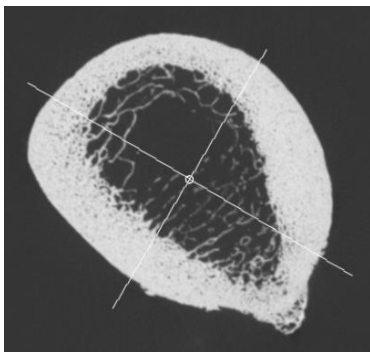
R



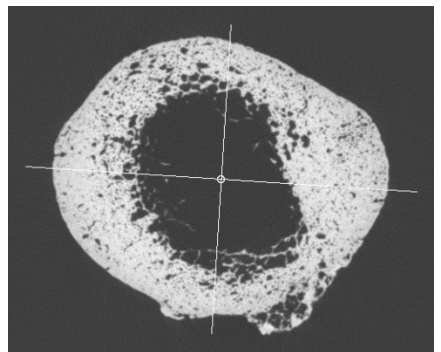
D10-2015 L



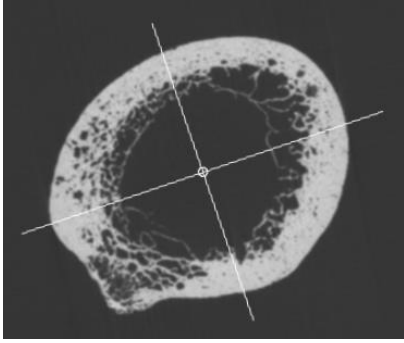
UT73-09D L



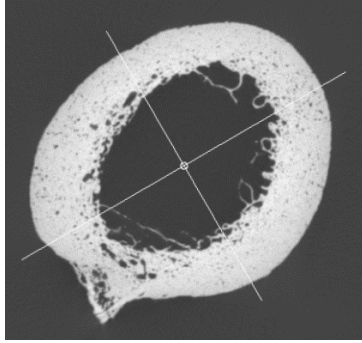
R



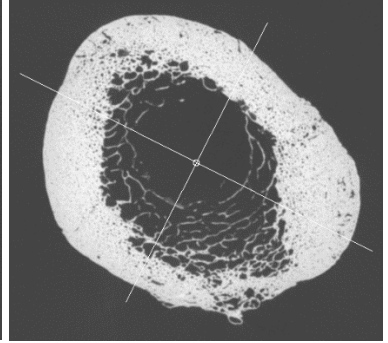
D12-2013 L



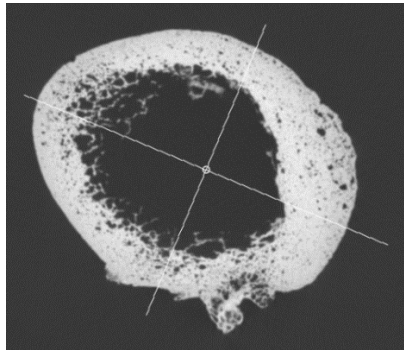
UT75-05D L



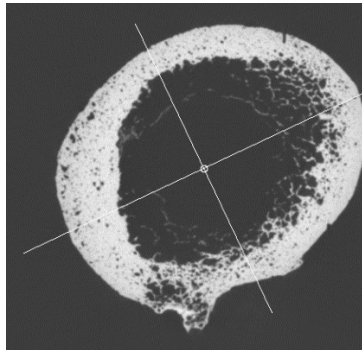
R



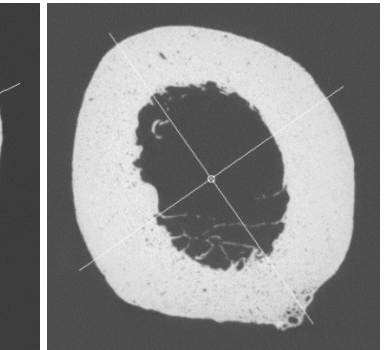
D14-2013 L



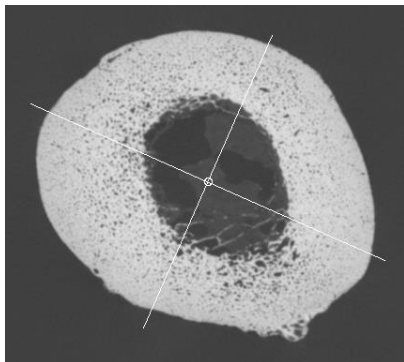
UT76-09D L



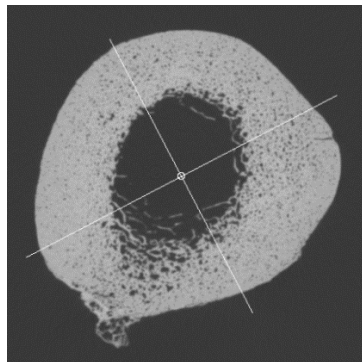
R



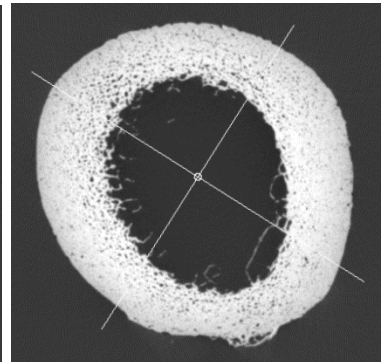
D02-2013 L



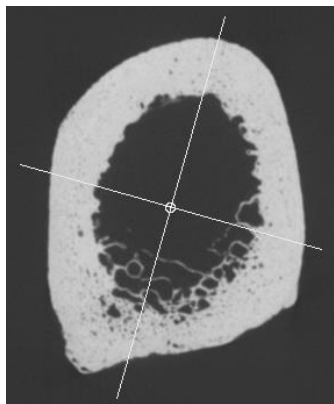
UT104-09D L



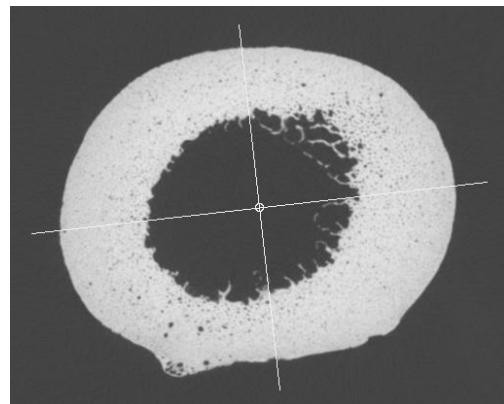
R



D27-2013 L

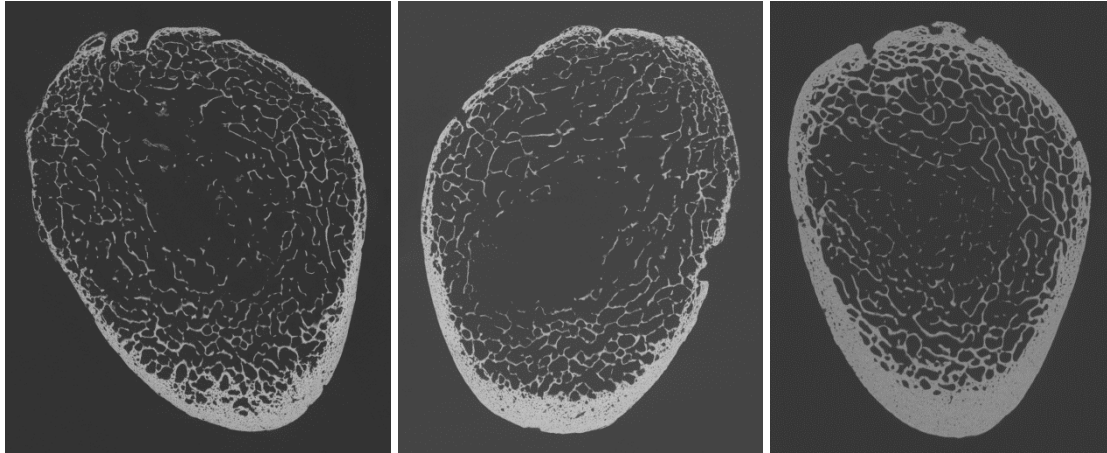


MUA042208 L



D05-2015 R

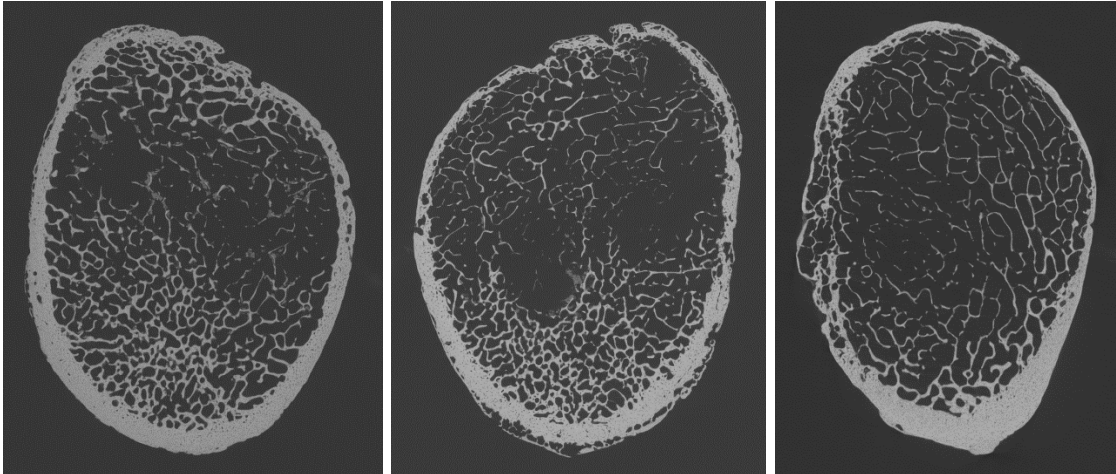
Appendix D. Mobility impaired left, right, and normal mobility match femoral neck midpoint cortical bone slices with BoneJ Slice Geometry annotations.



D04-2014 L

R

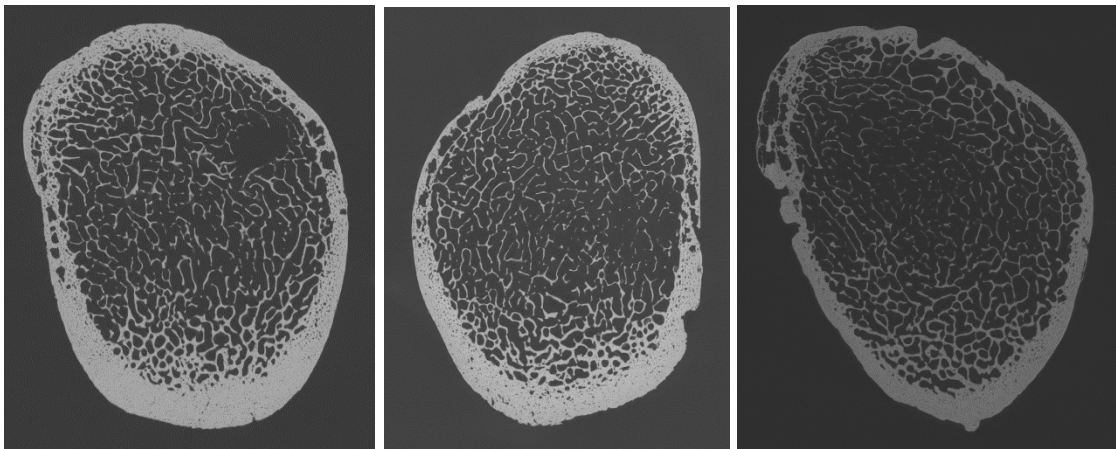
D23-2013 L



D06-2013 L

R

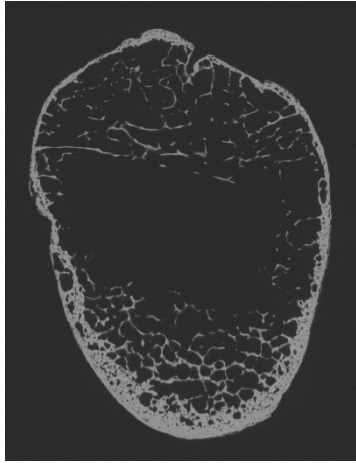
D42-2012 L



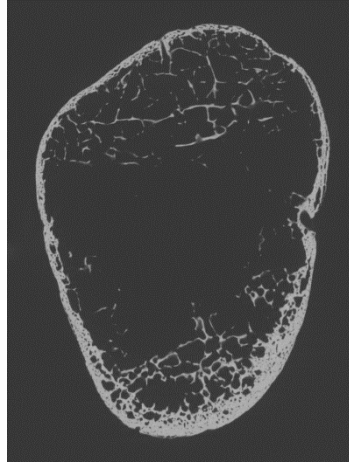
D22-2012 L

R

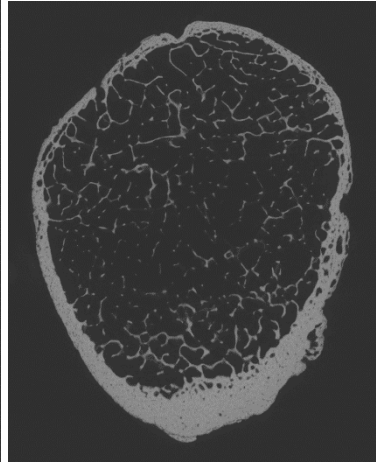
D07-2013 L



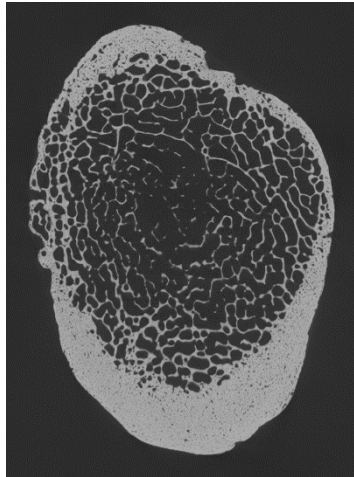
D28-2015 L



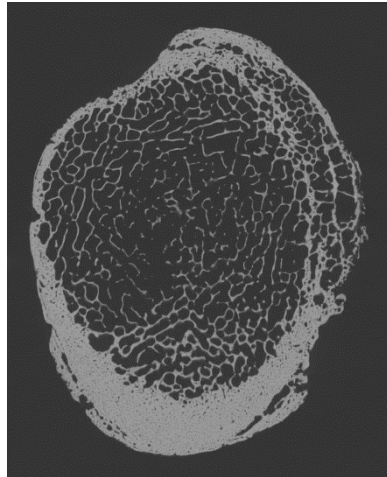
R



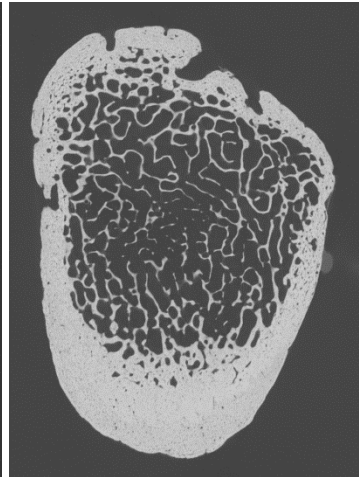
D10-2009 R



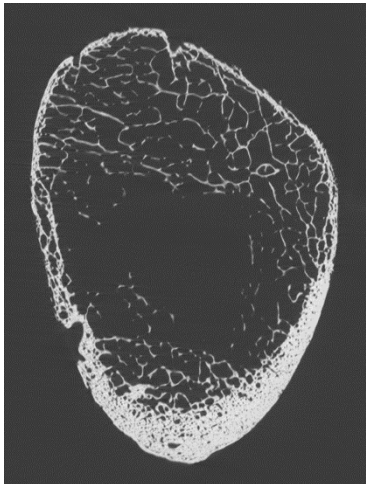
D32-2014 L



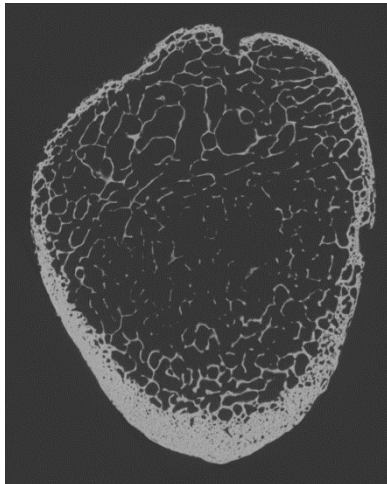
R



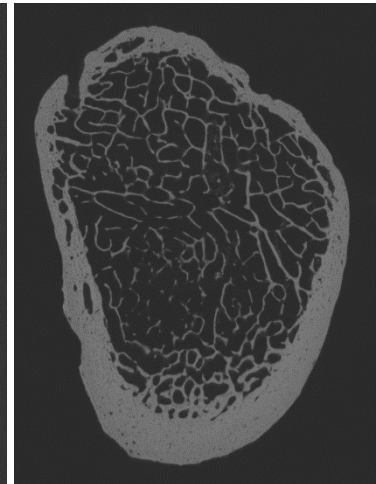
D04-2011 L



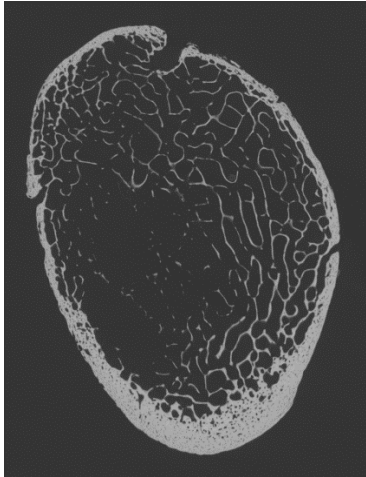
D47-2013 L



R



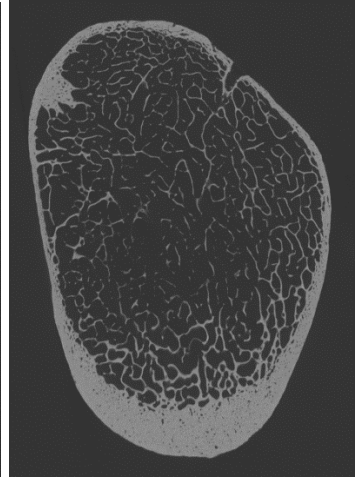
D21-2011 L



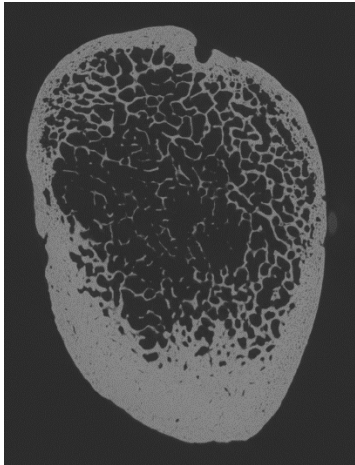
D51-2014 L



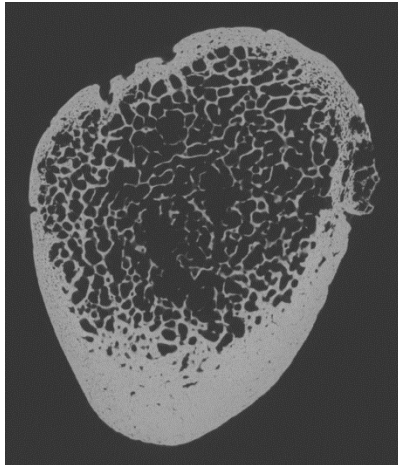
R



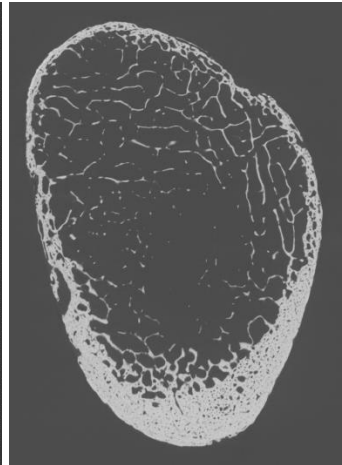
D28-2012



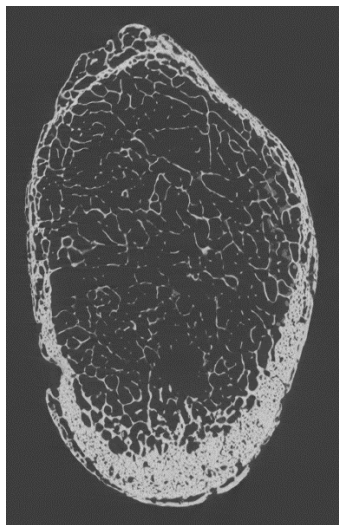
D54-2015 L



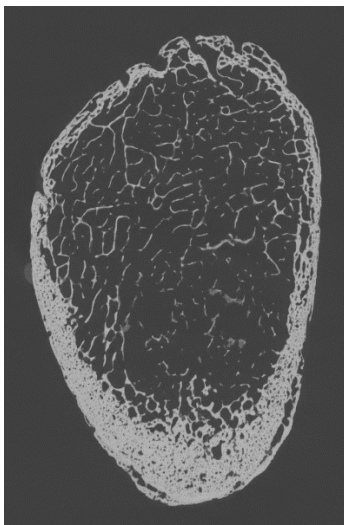
R



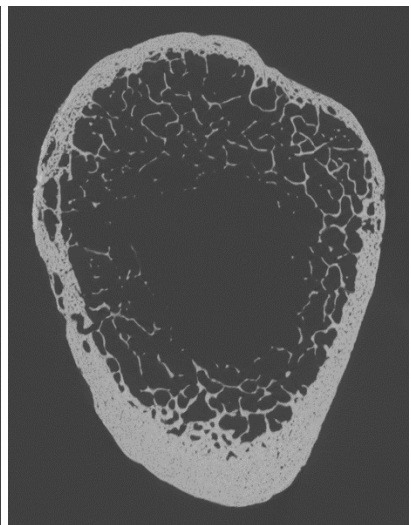
D03-2012 L



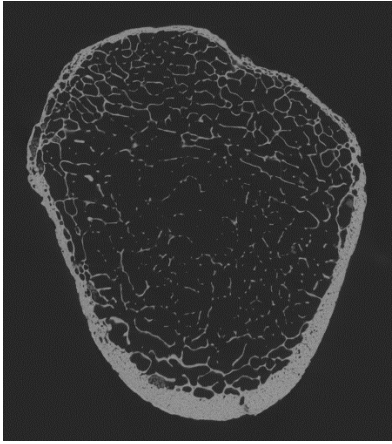
D56-2013 L



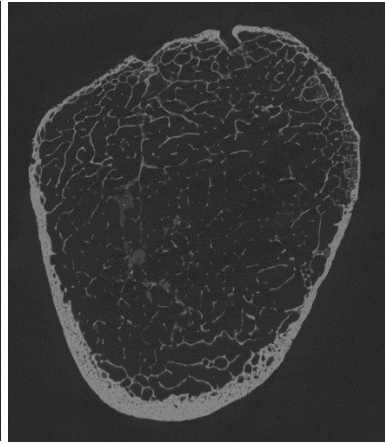
R



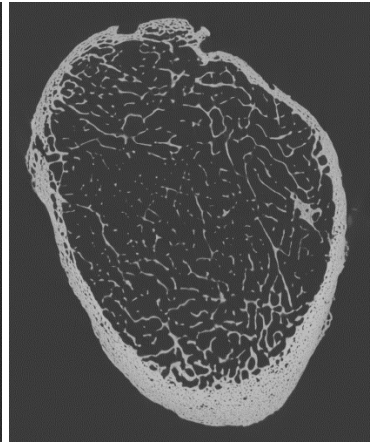
D04-2012 L



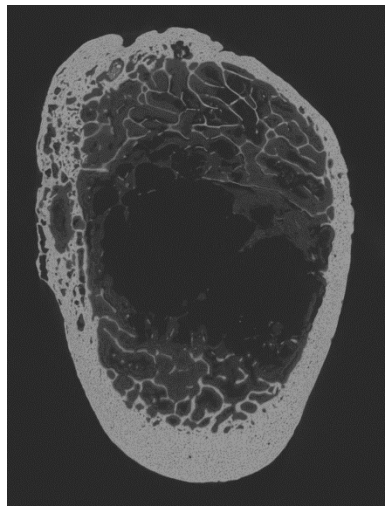
UT05-00D L



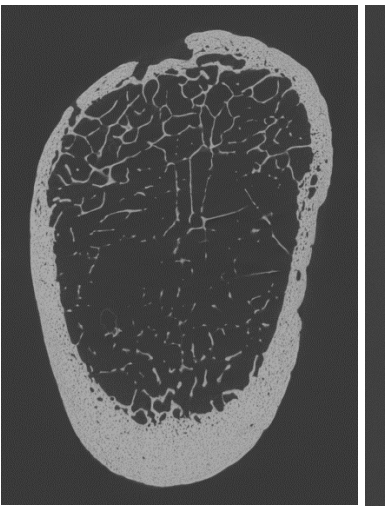
R



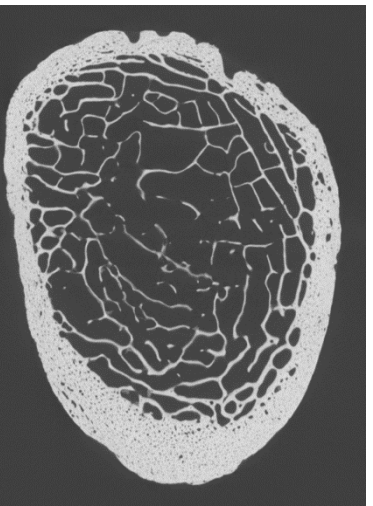
D36-2013 L



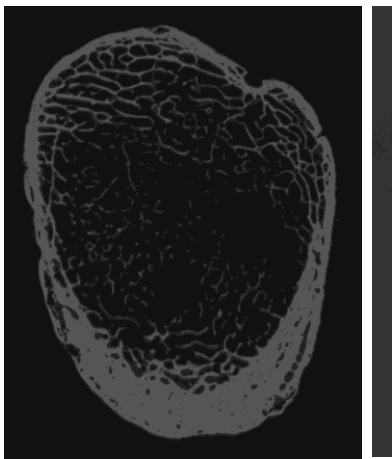
UT05-09D L



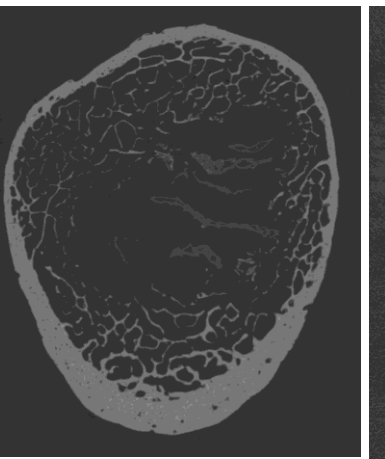
R



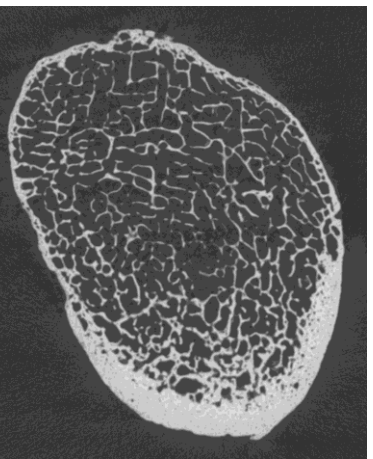
D41-2012 L



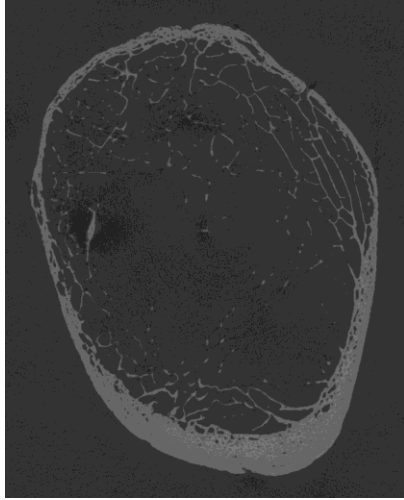
UT05-97D L



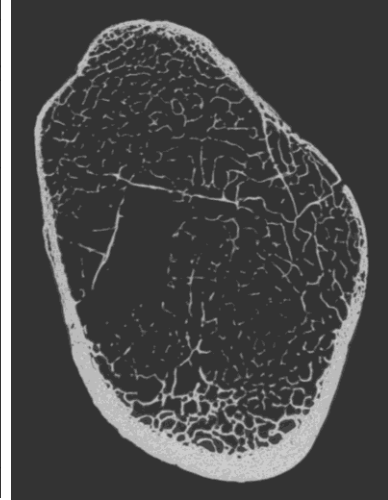
R



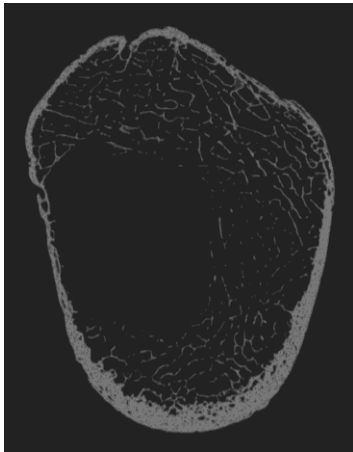
D23-2011 L



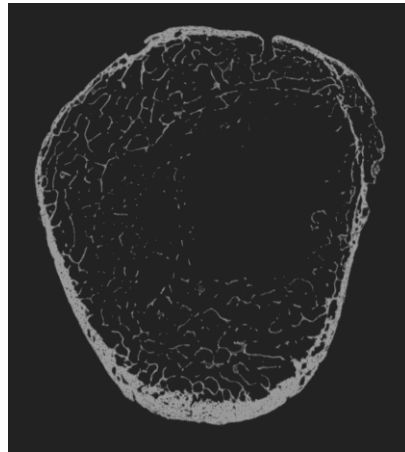
UT06-02D L



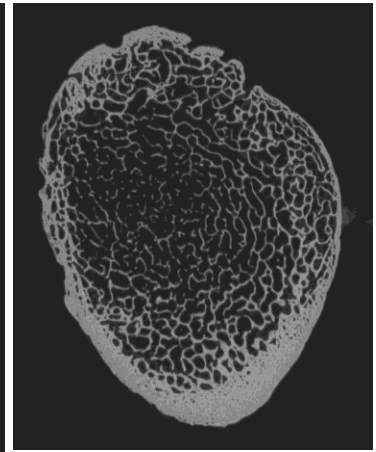
D14-2014 L



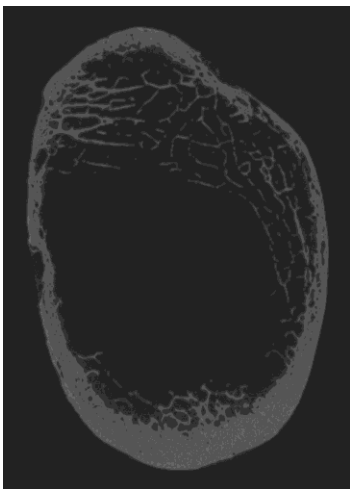
UT14-92D L



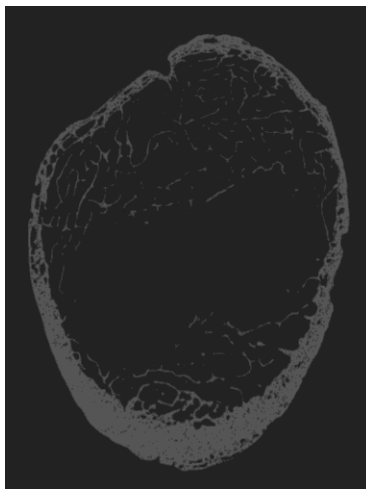
R



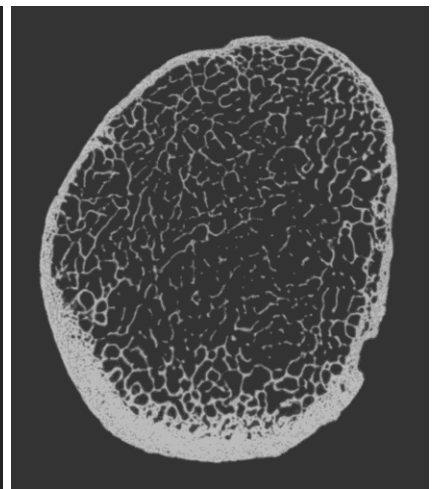
D49-2014 L



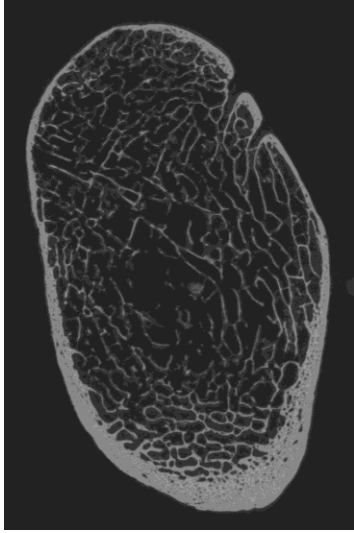
UT17-07D L



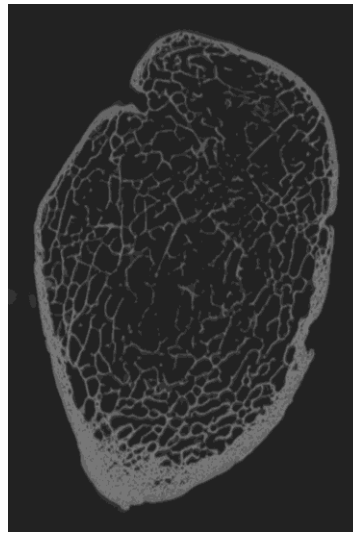
R



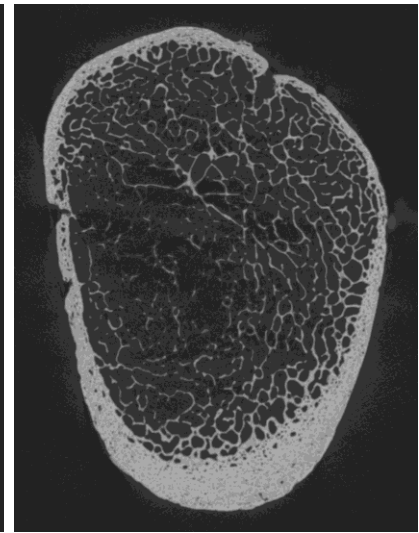
D30-2012 R



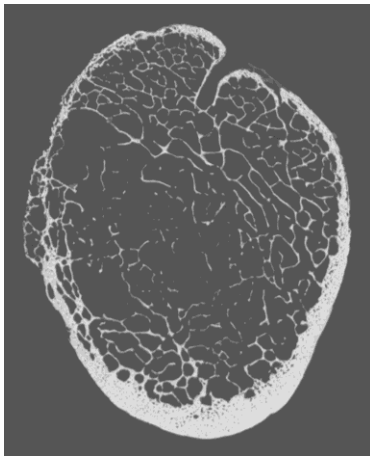
UT20-99D L



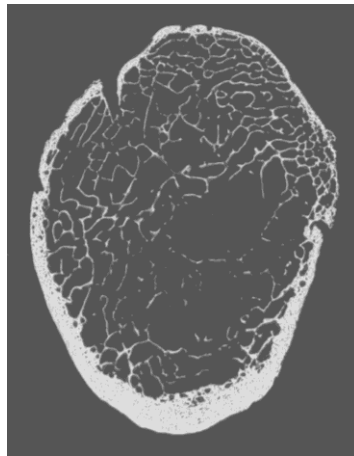
R



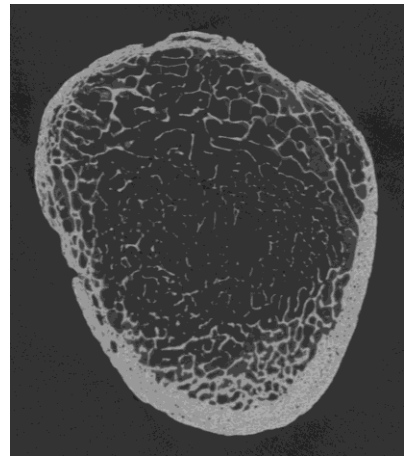
D46-2013 L



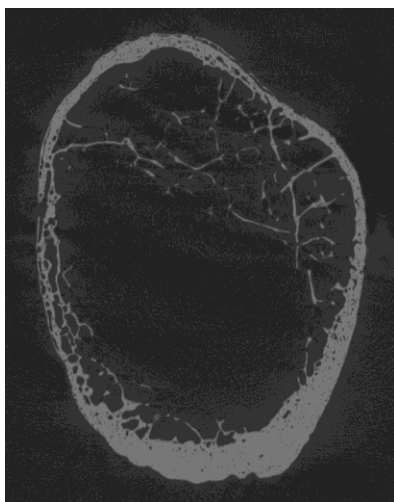
UT23-99D L



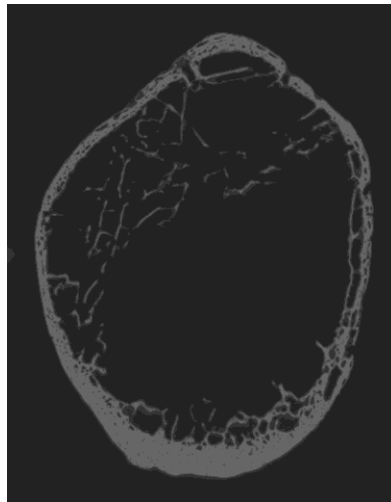
R



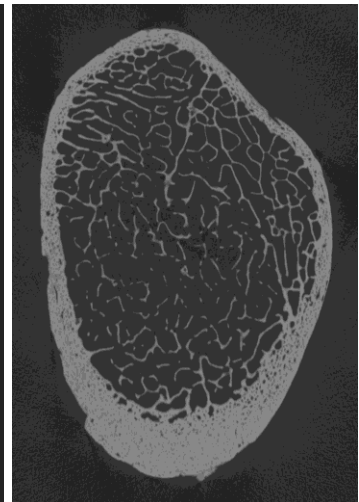
D05-2012 L



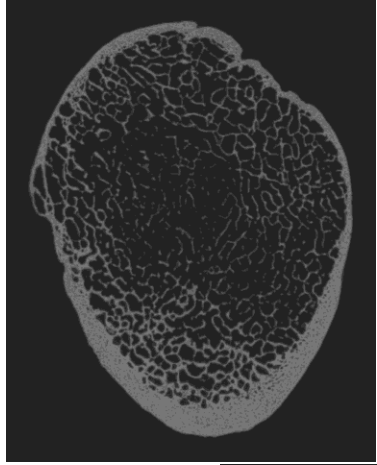
UT47-01D L



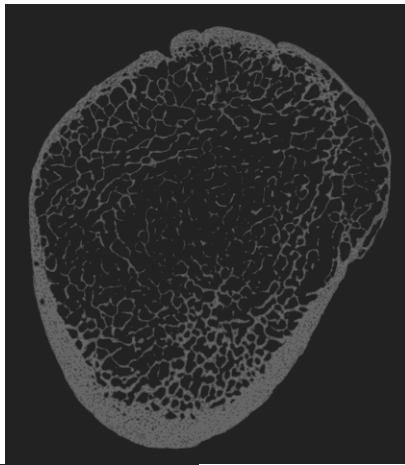
R



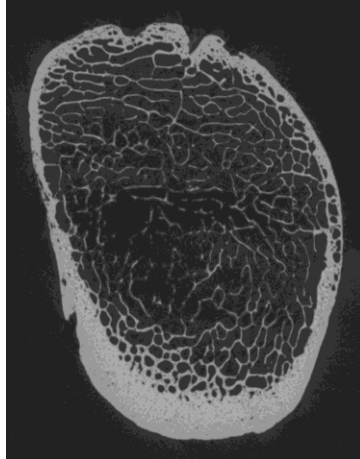
D12-2011 L



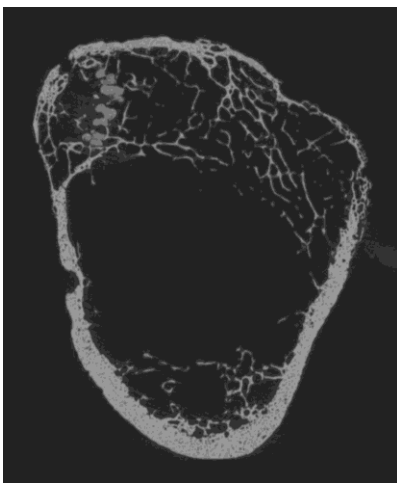
UT53-08D L



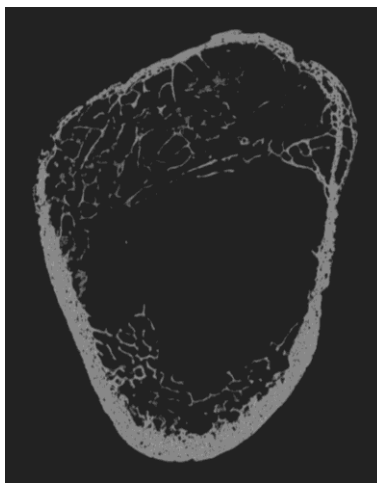
D20-2013 L



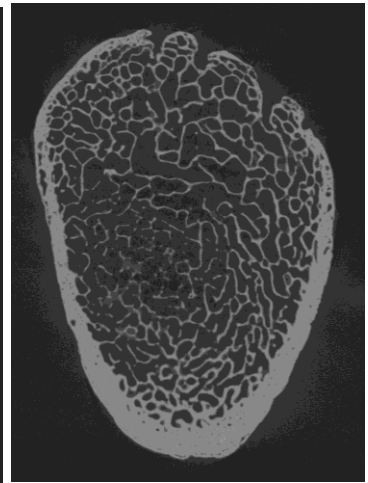
R



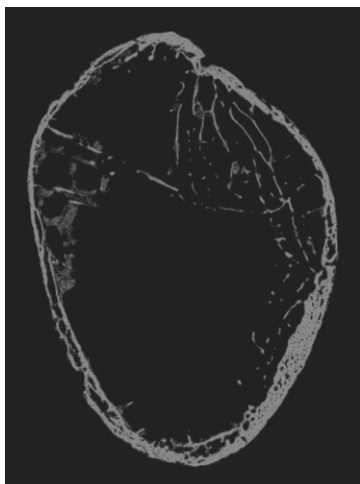
UT55-10D L



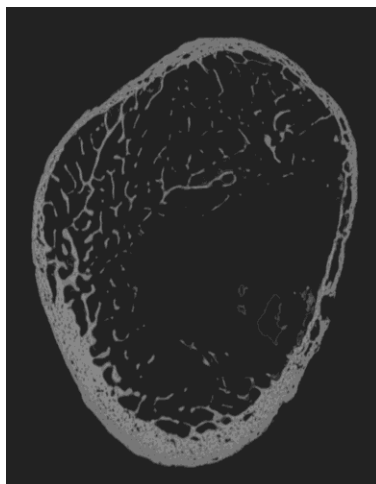
R



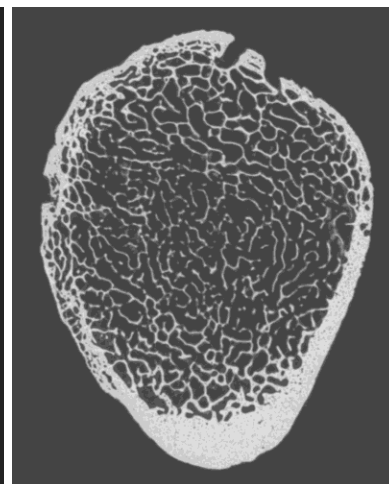
D01-2009 L



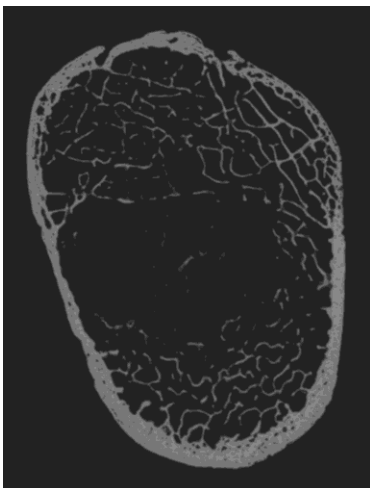
UT60-09D L



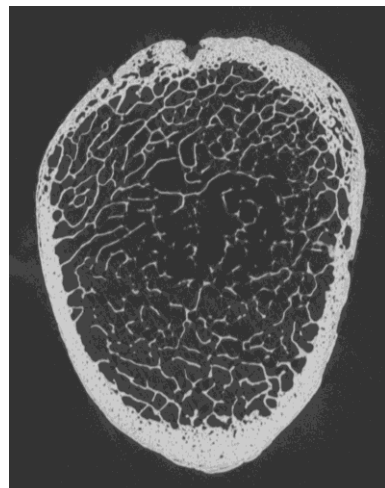
R



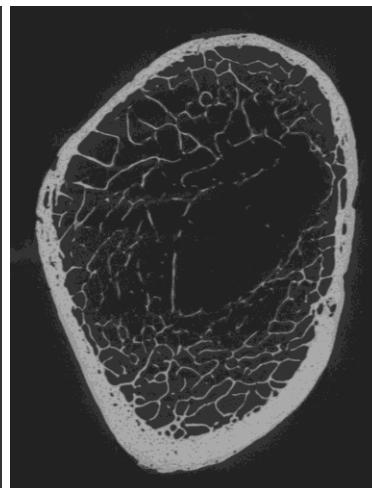
D65-2013 L



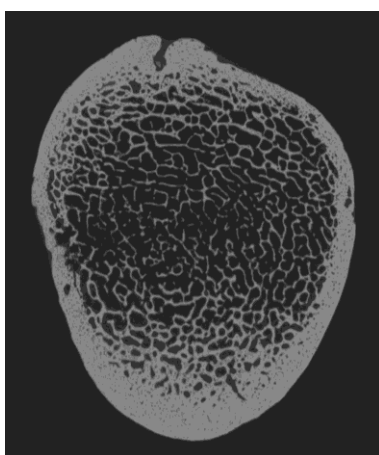
UT64-05D L



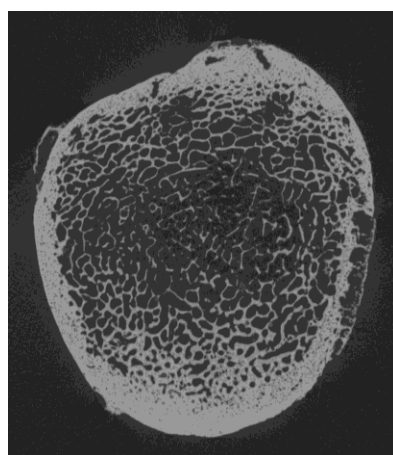
R



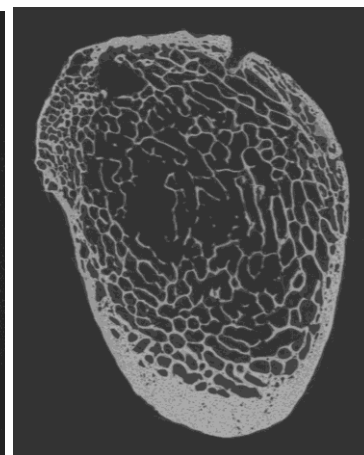
D33-2013 R



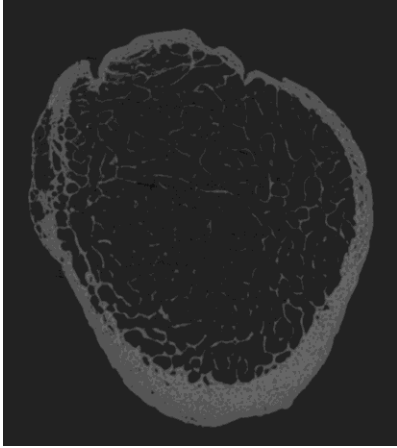
UT70-08D L



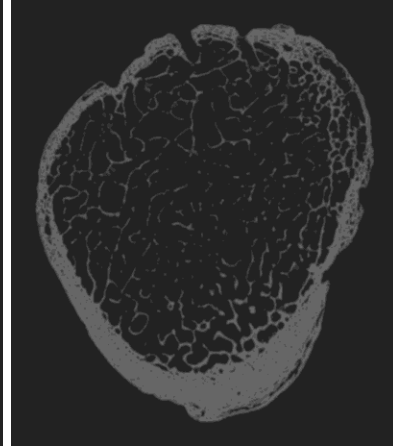
R



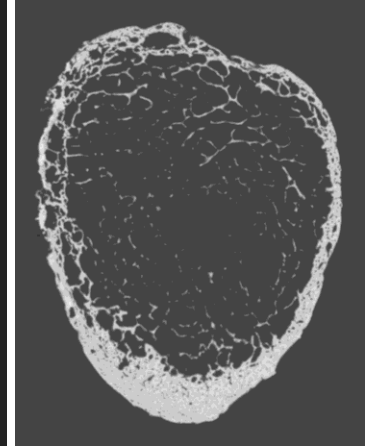
D10-2015 L



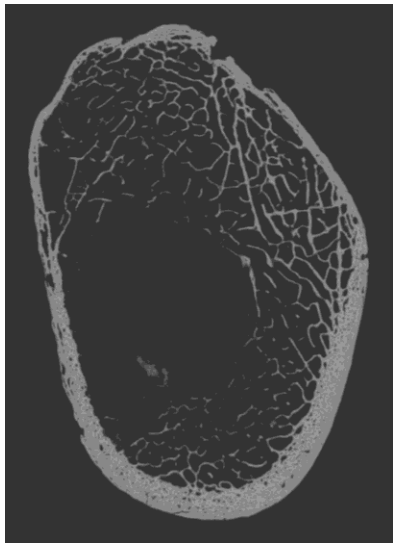
UT73-09D L



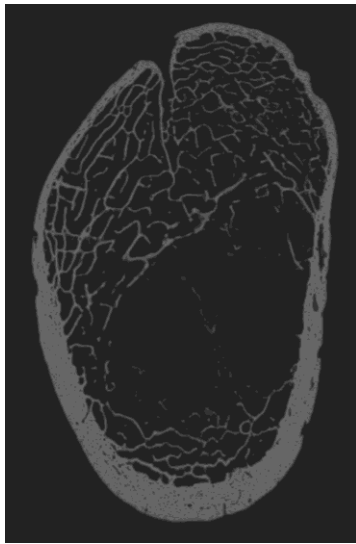
R



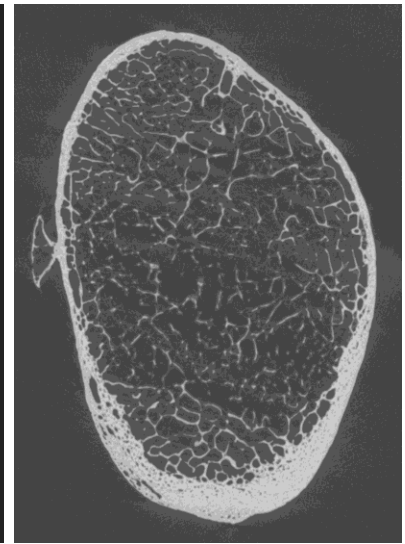
D12-2013 L



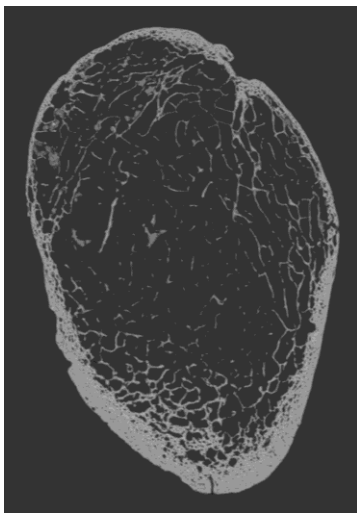
UT75-05D L



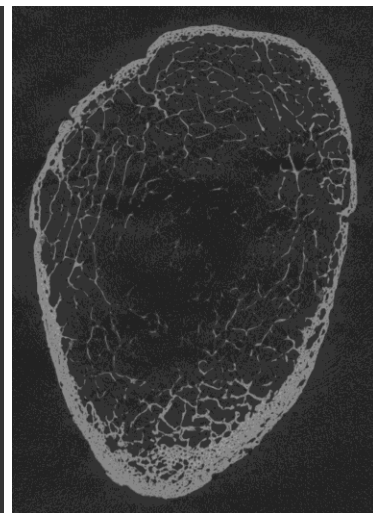
R



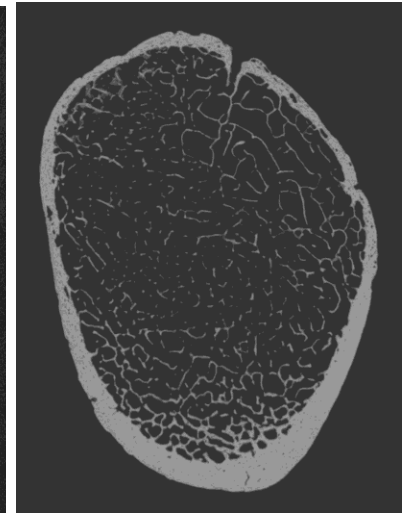
D14-2013 L



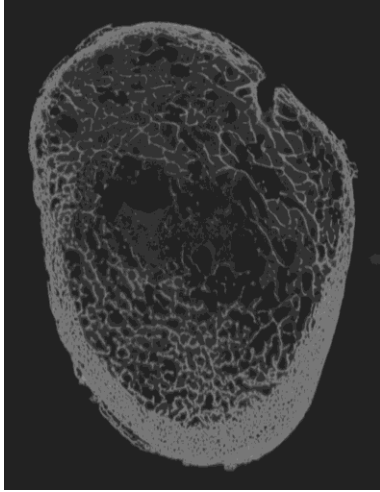
UT76-09D L



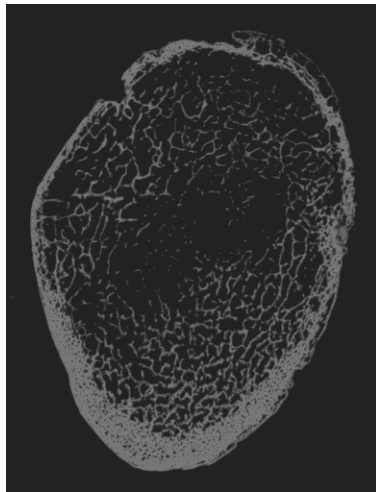
R



D02-2013 L



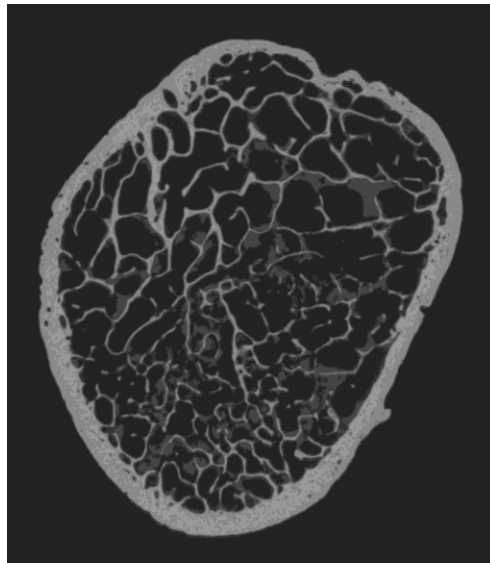
UT104-09D L



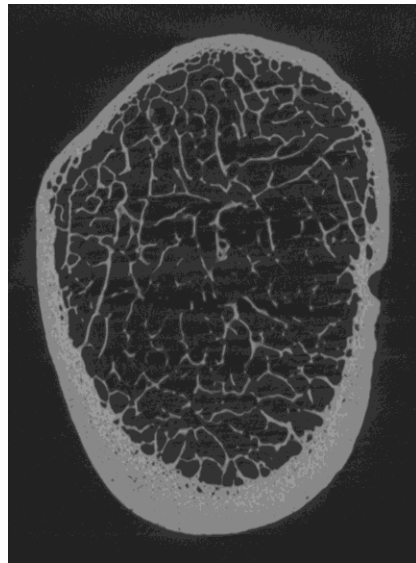
R



D27-2013 L

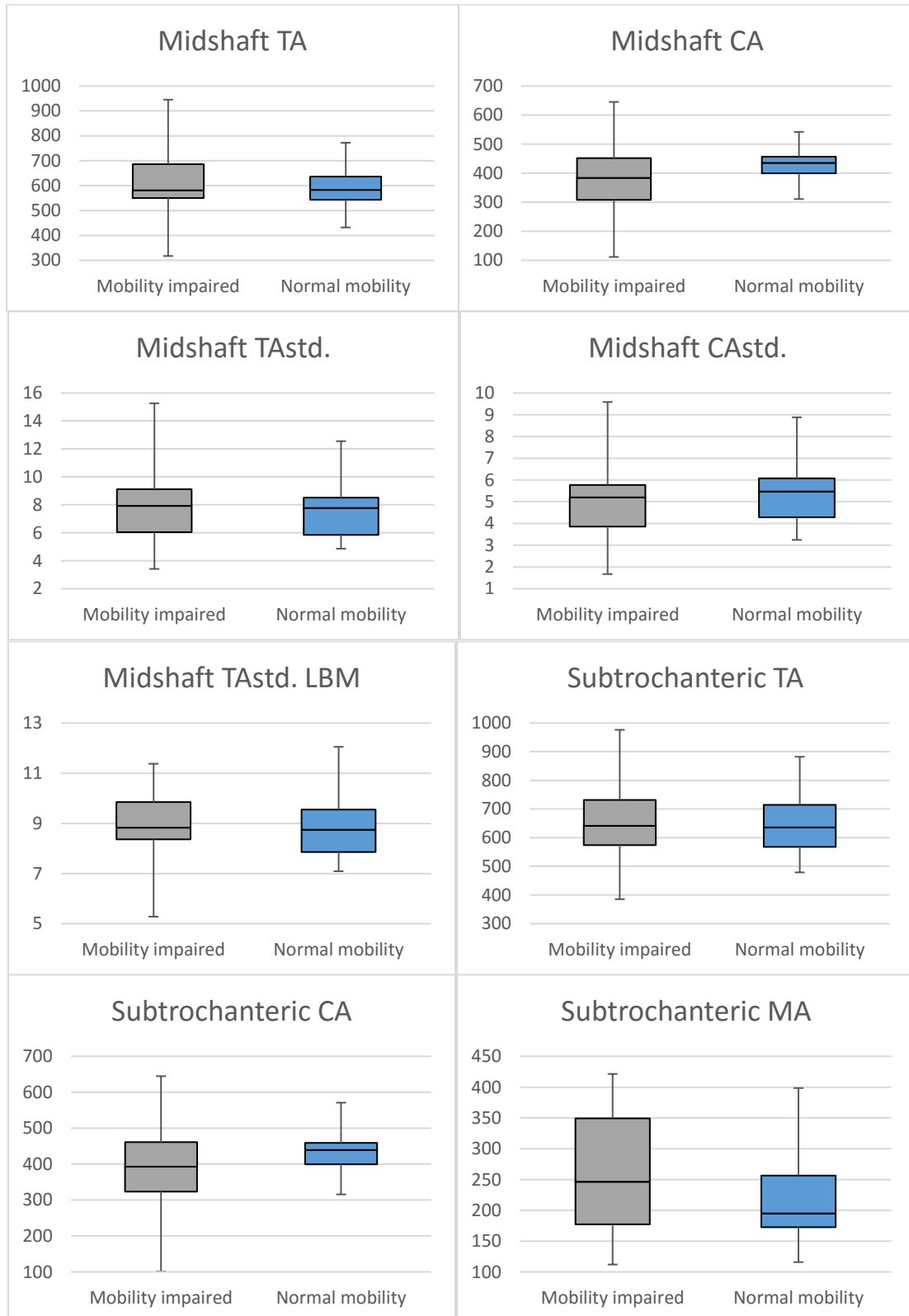


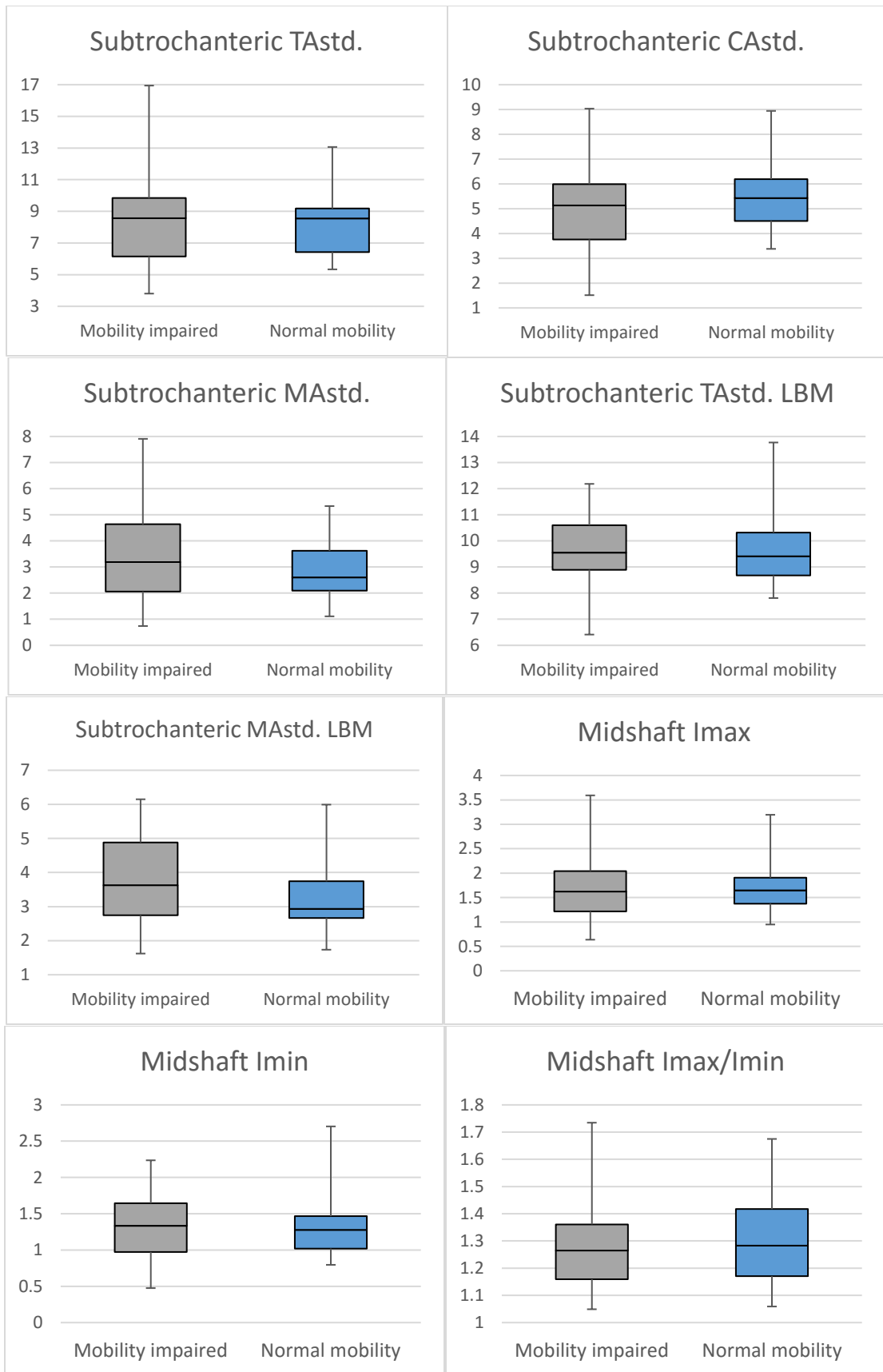
MUA042208 L

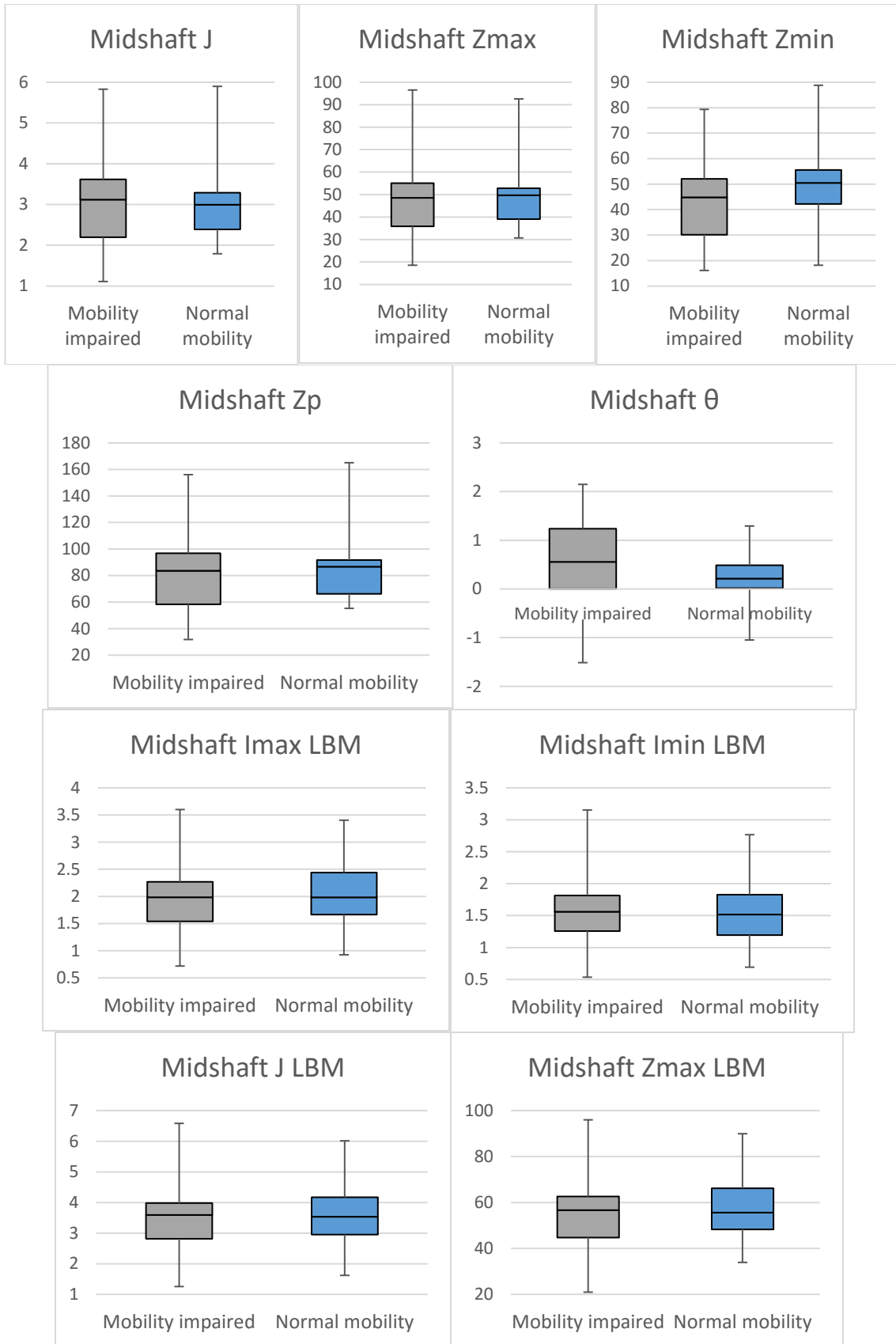


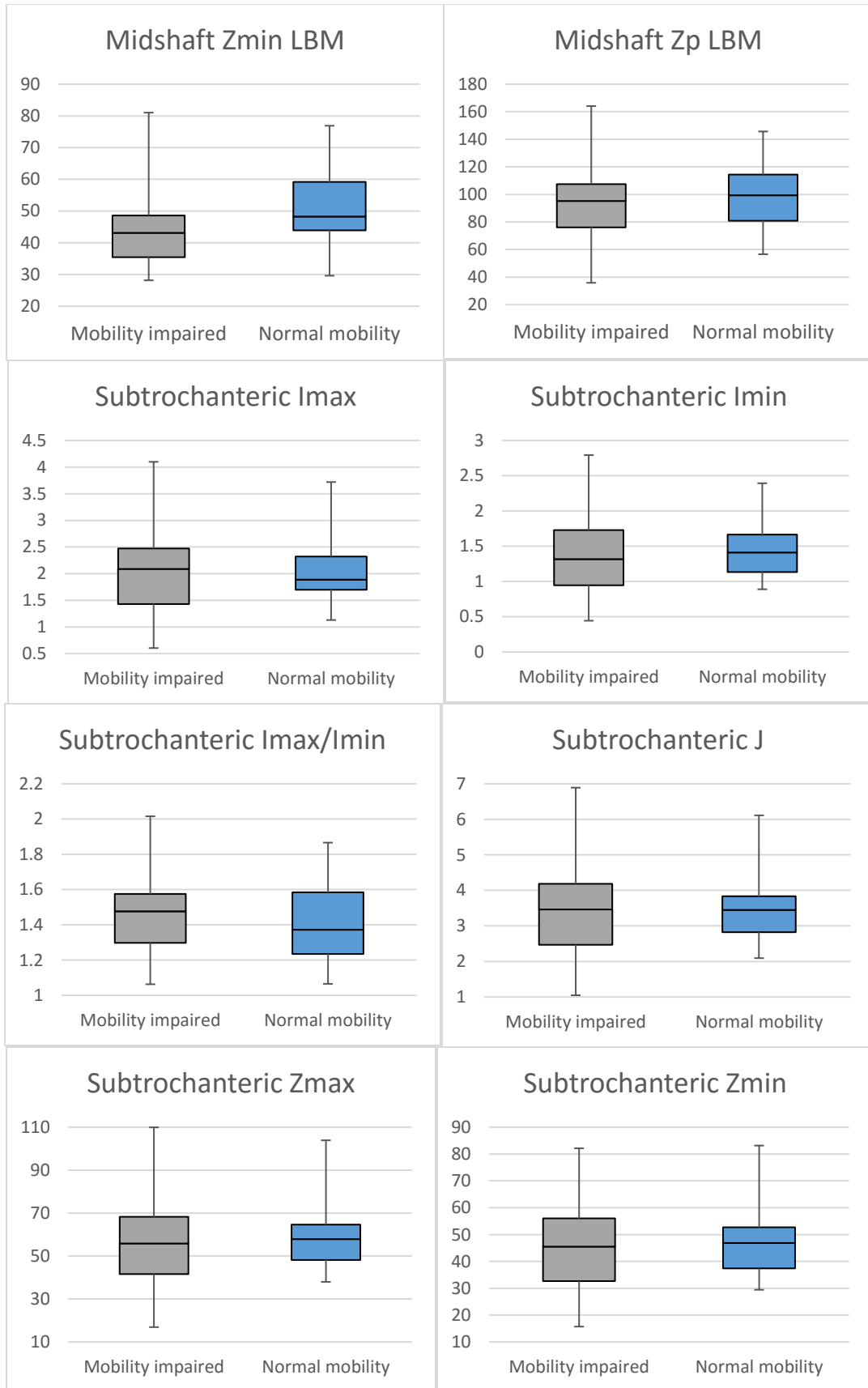
D05-2015 R

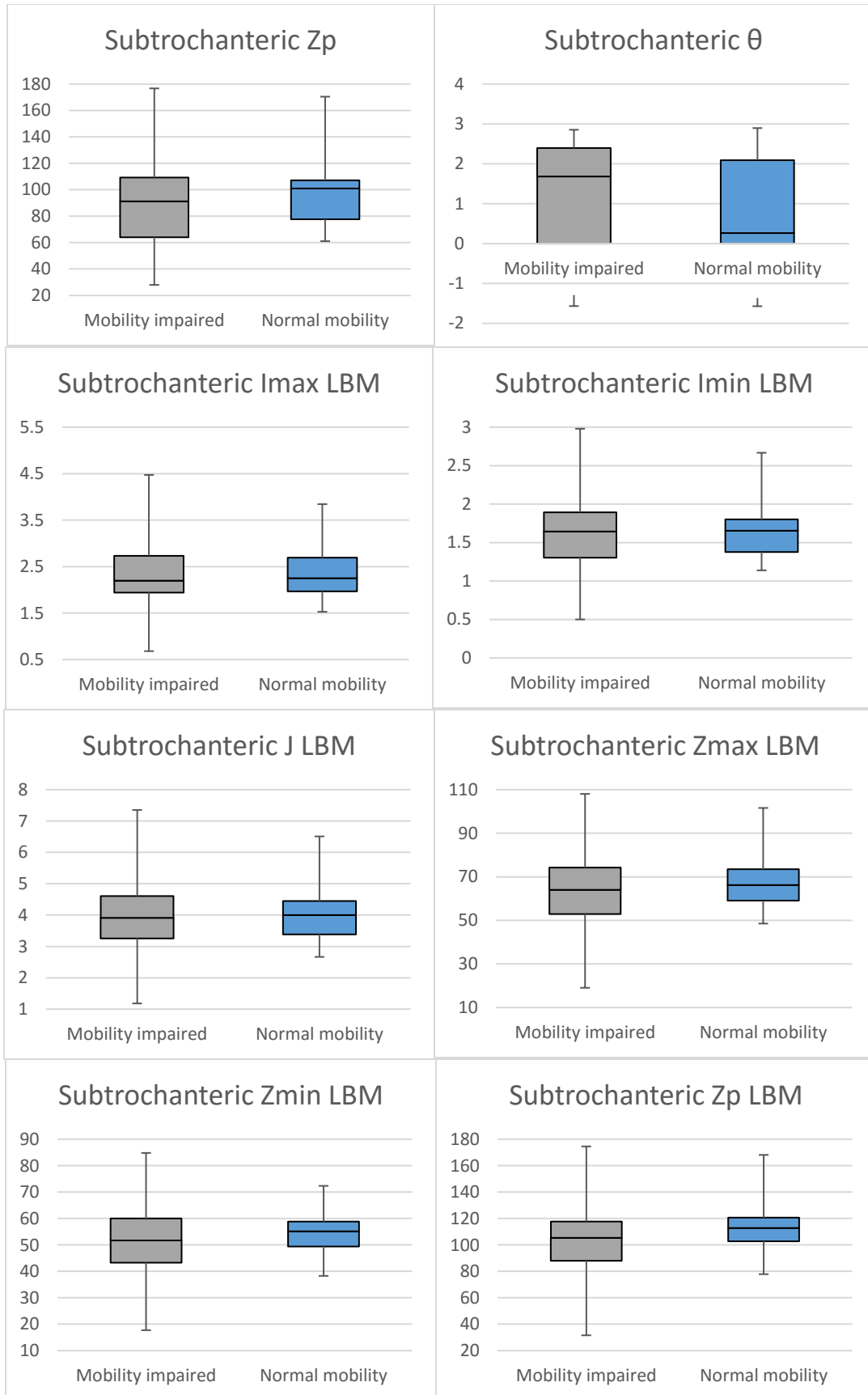
Appendix E. Boxplots of the nearly and non-significant cortical bone and cross-sectional properties for mobility impaired and normal mobility individuals.



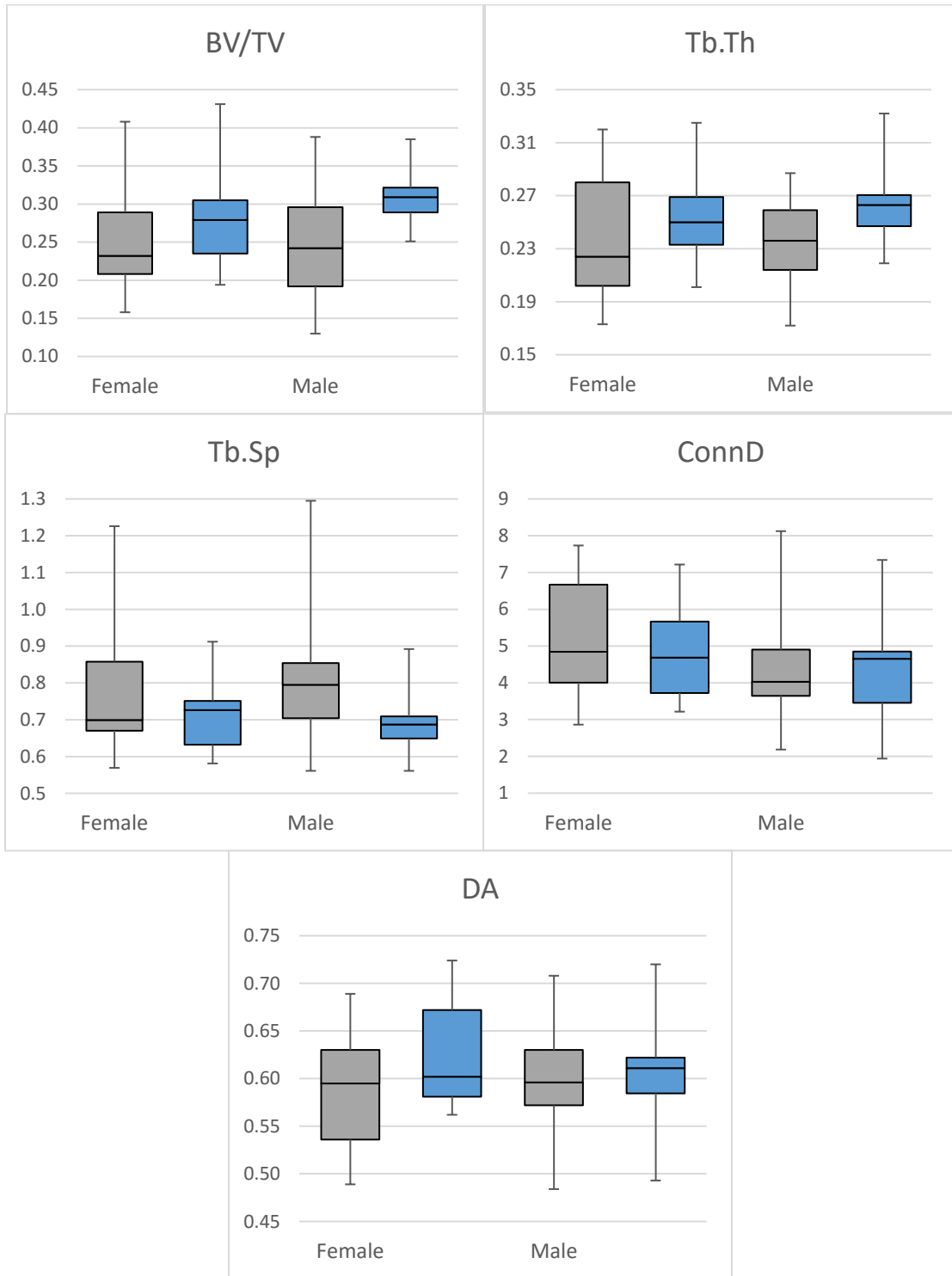


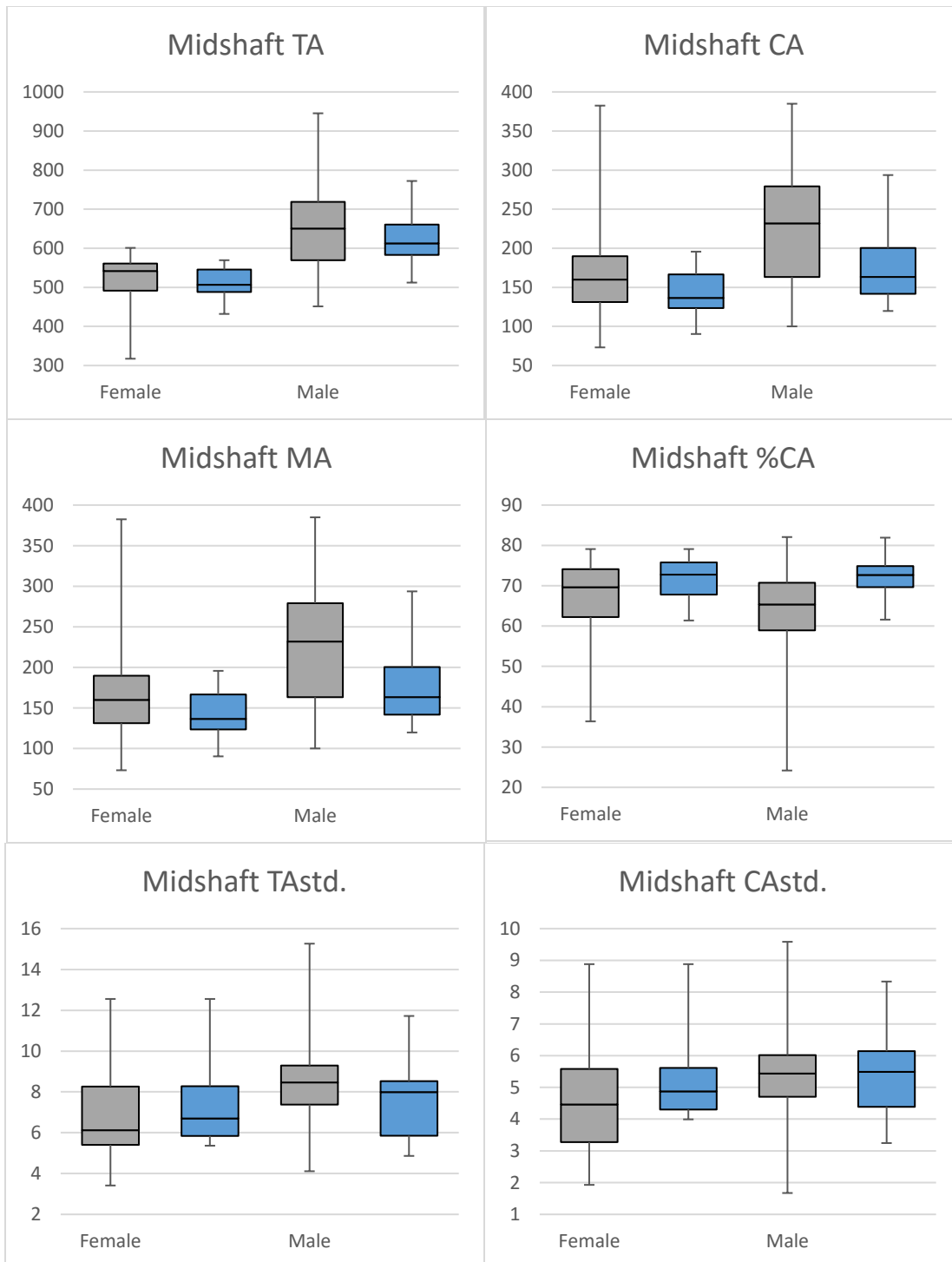


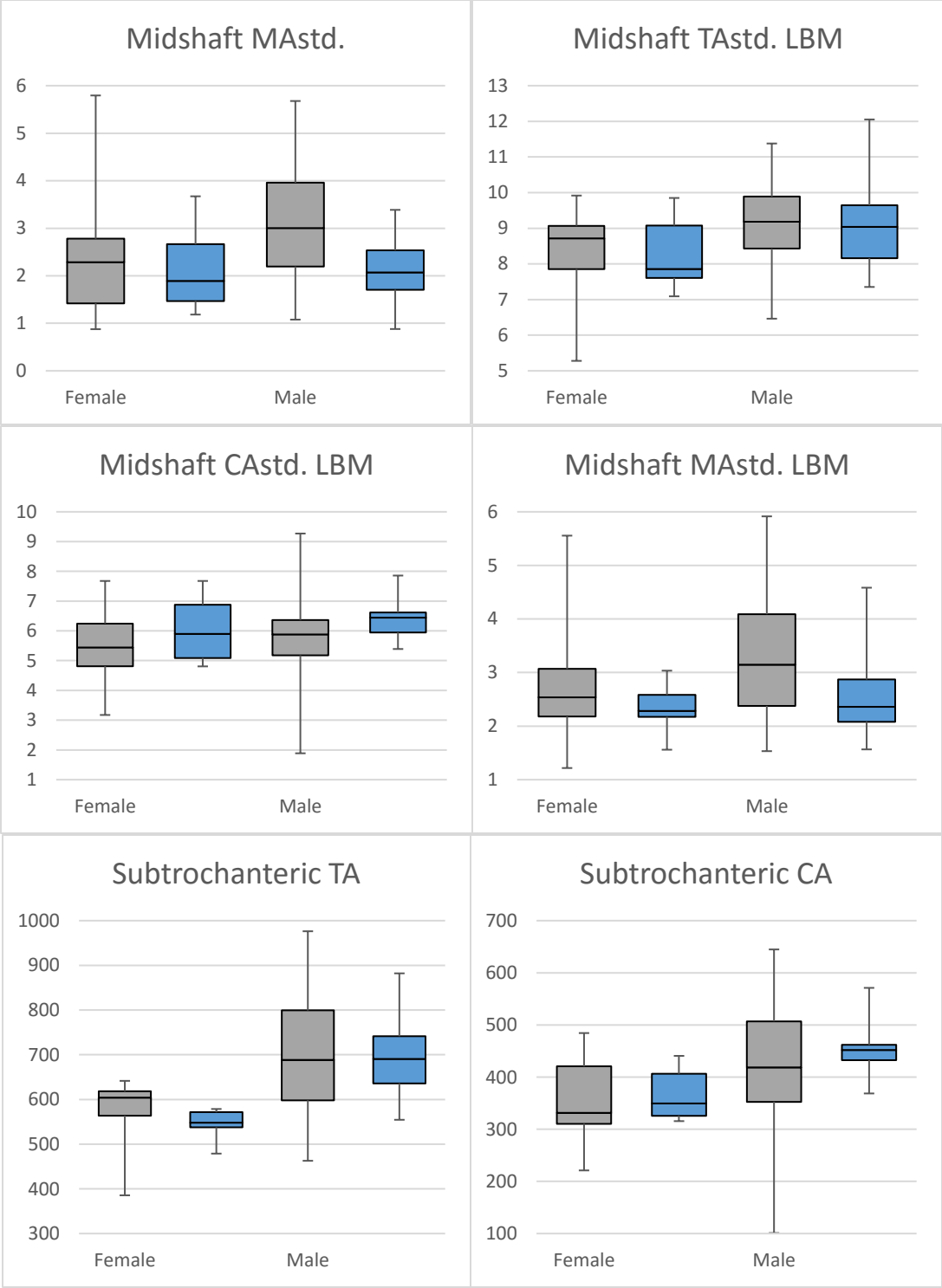


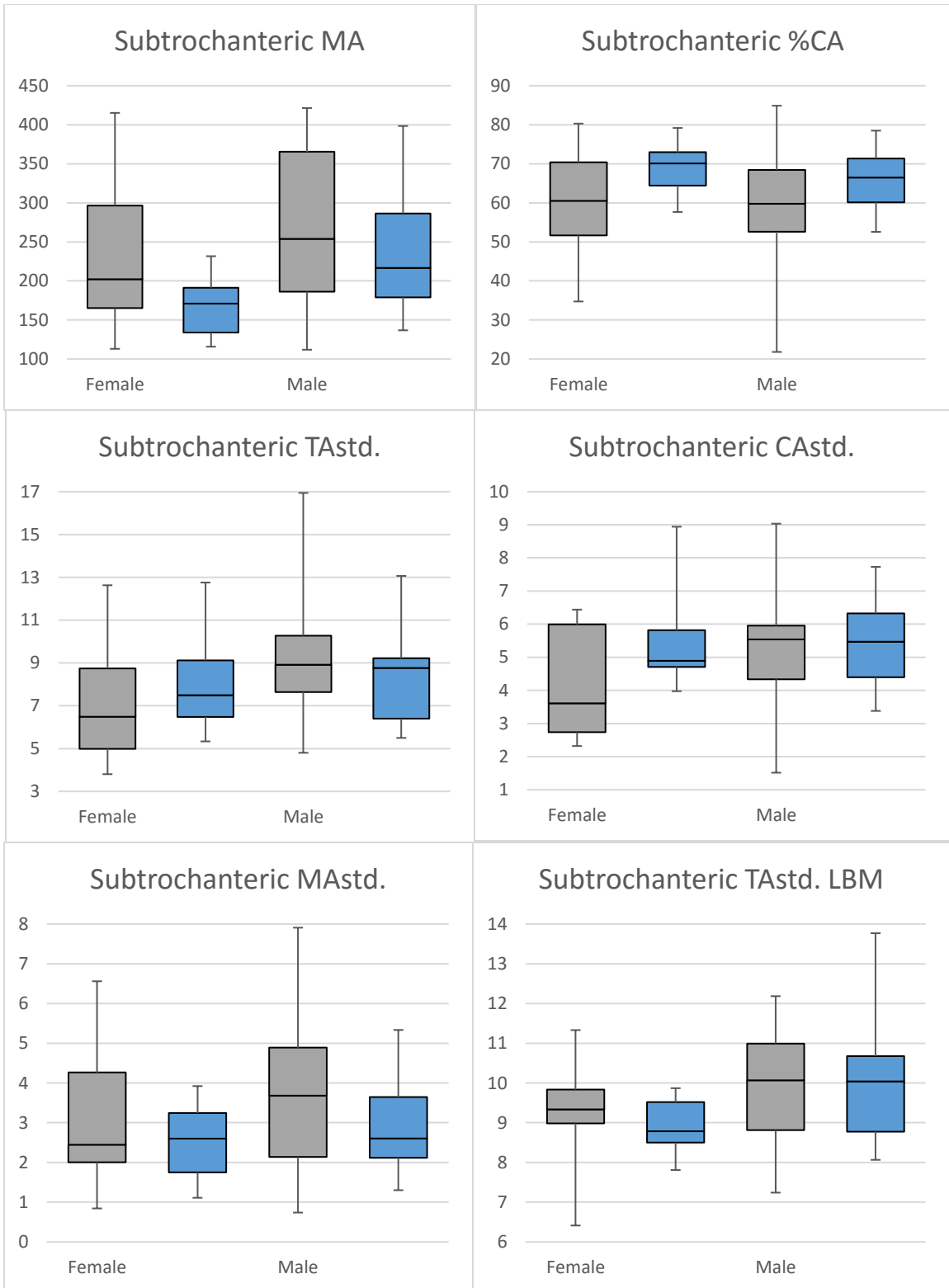


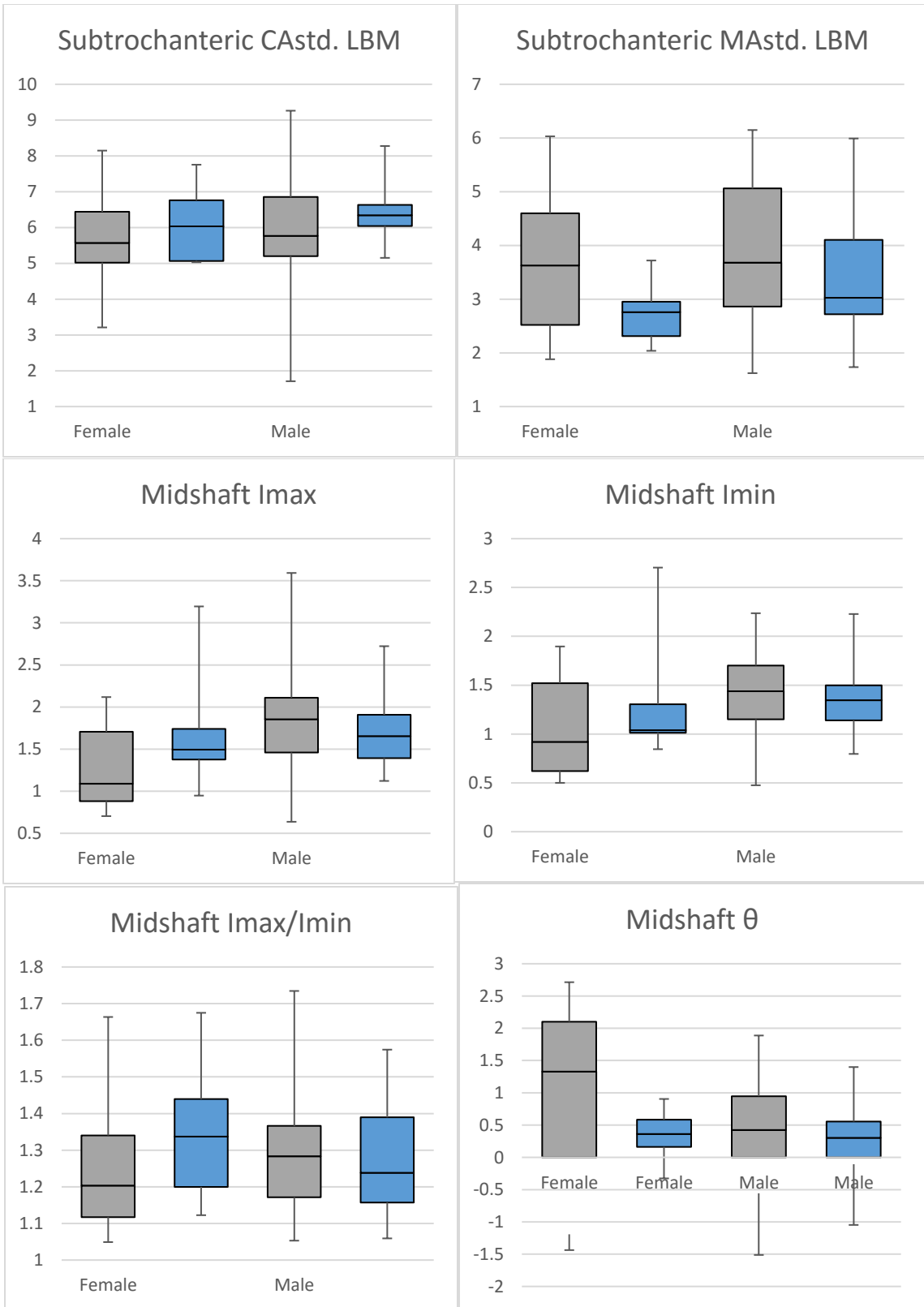
Appendix F. Boxplots comparing the mobility impaired (gray) and normal mobility (blue) samples divided by sex.

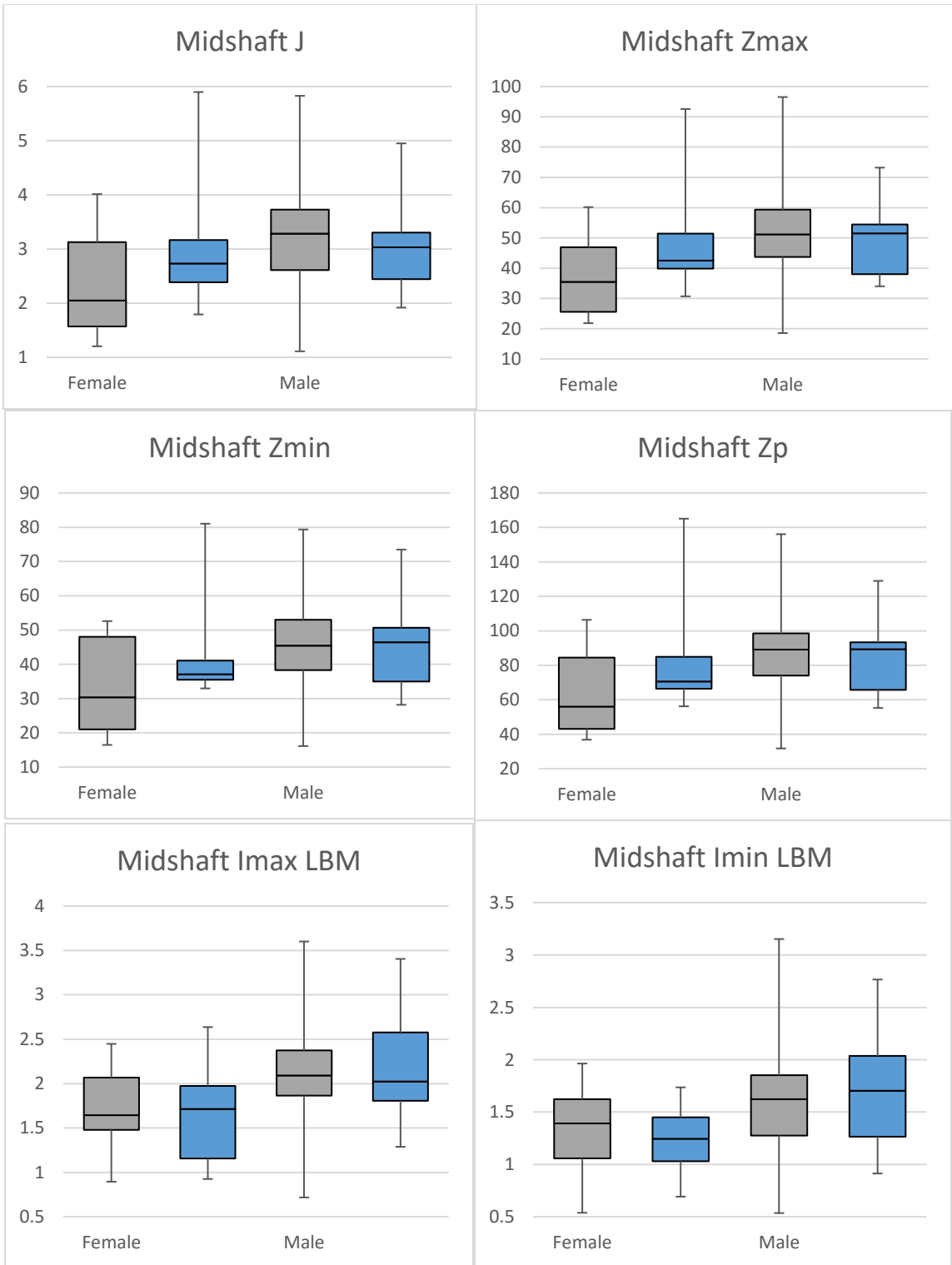


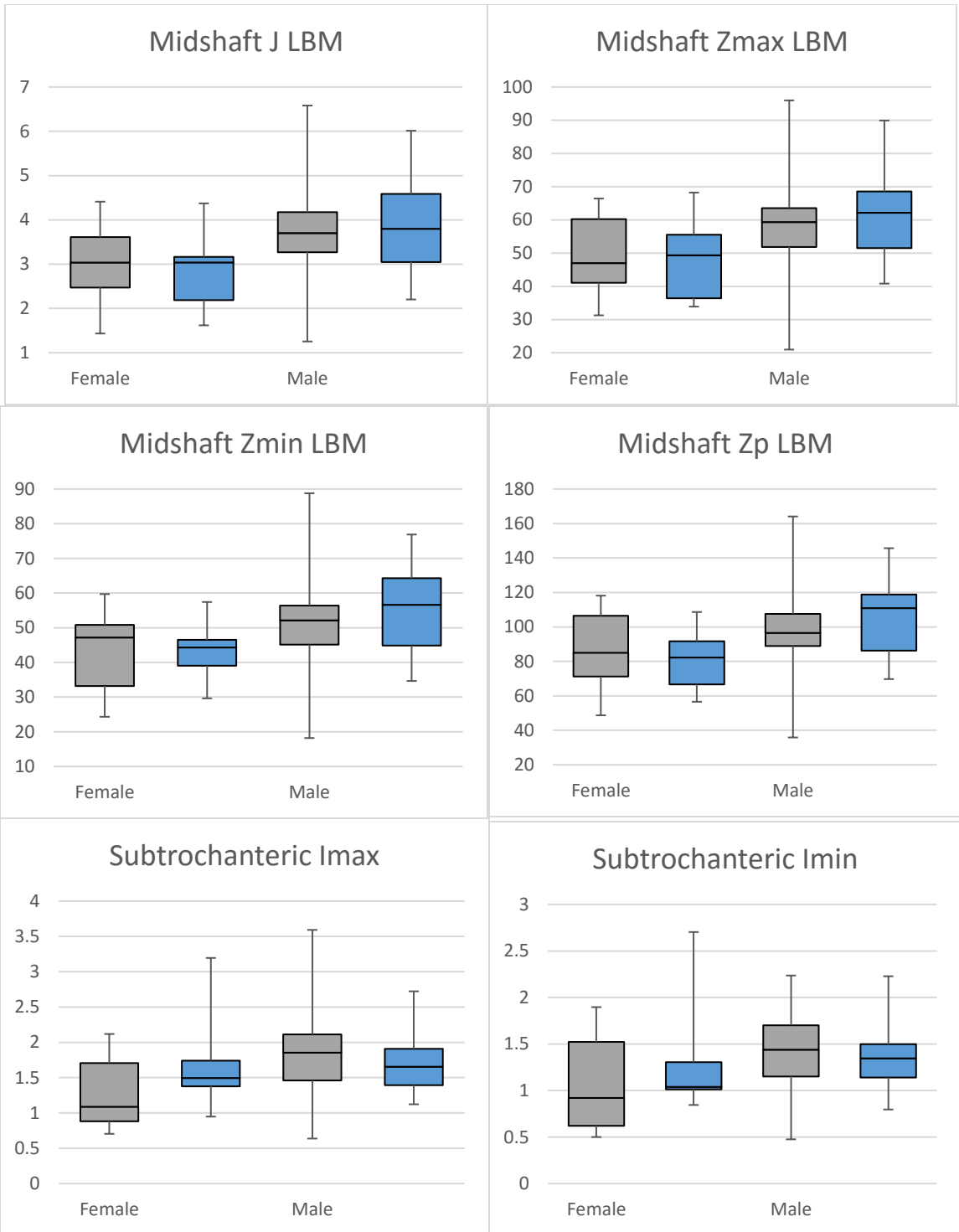


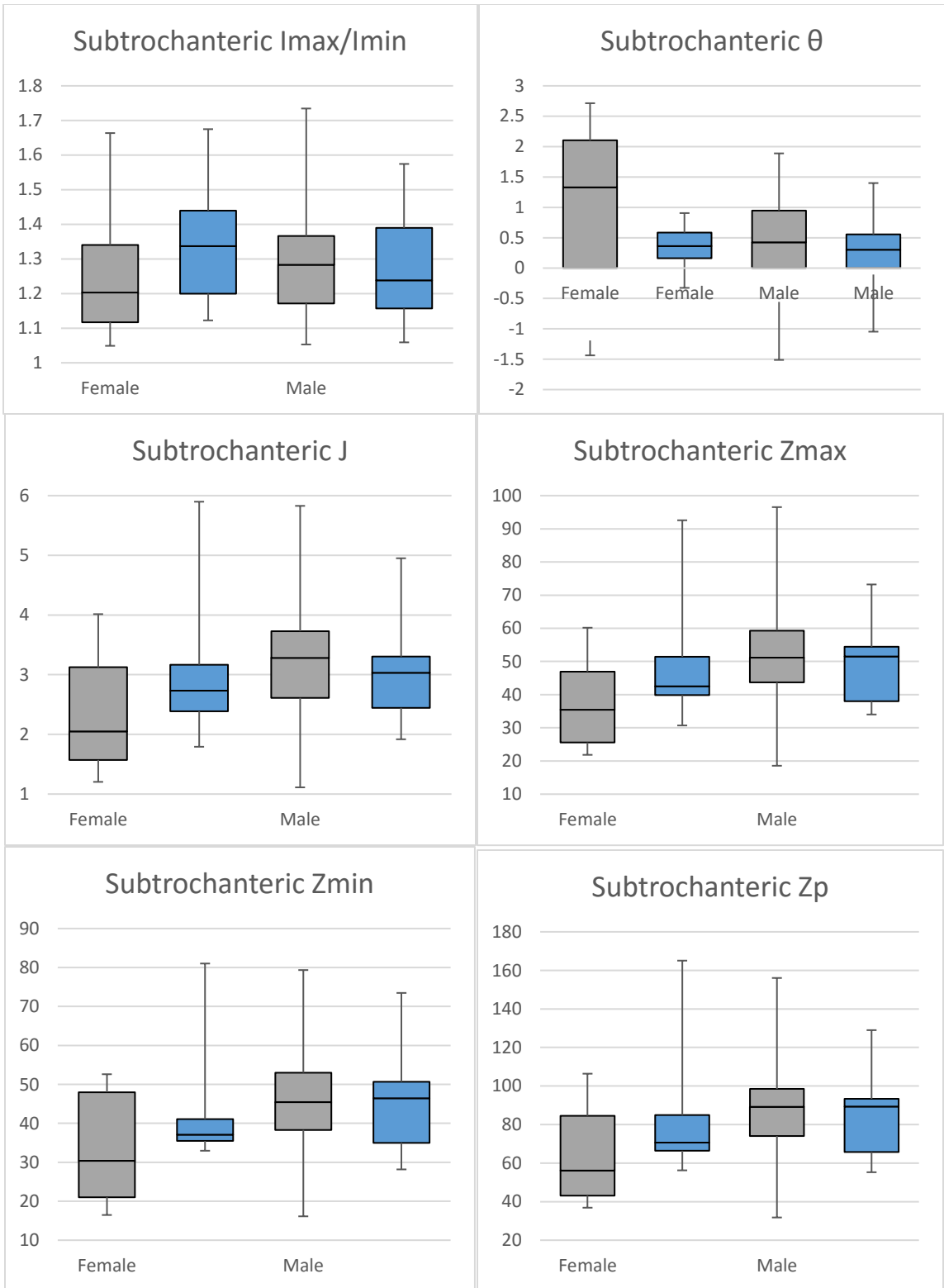


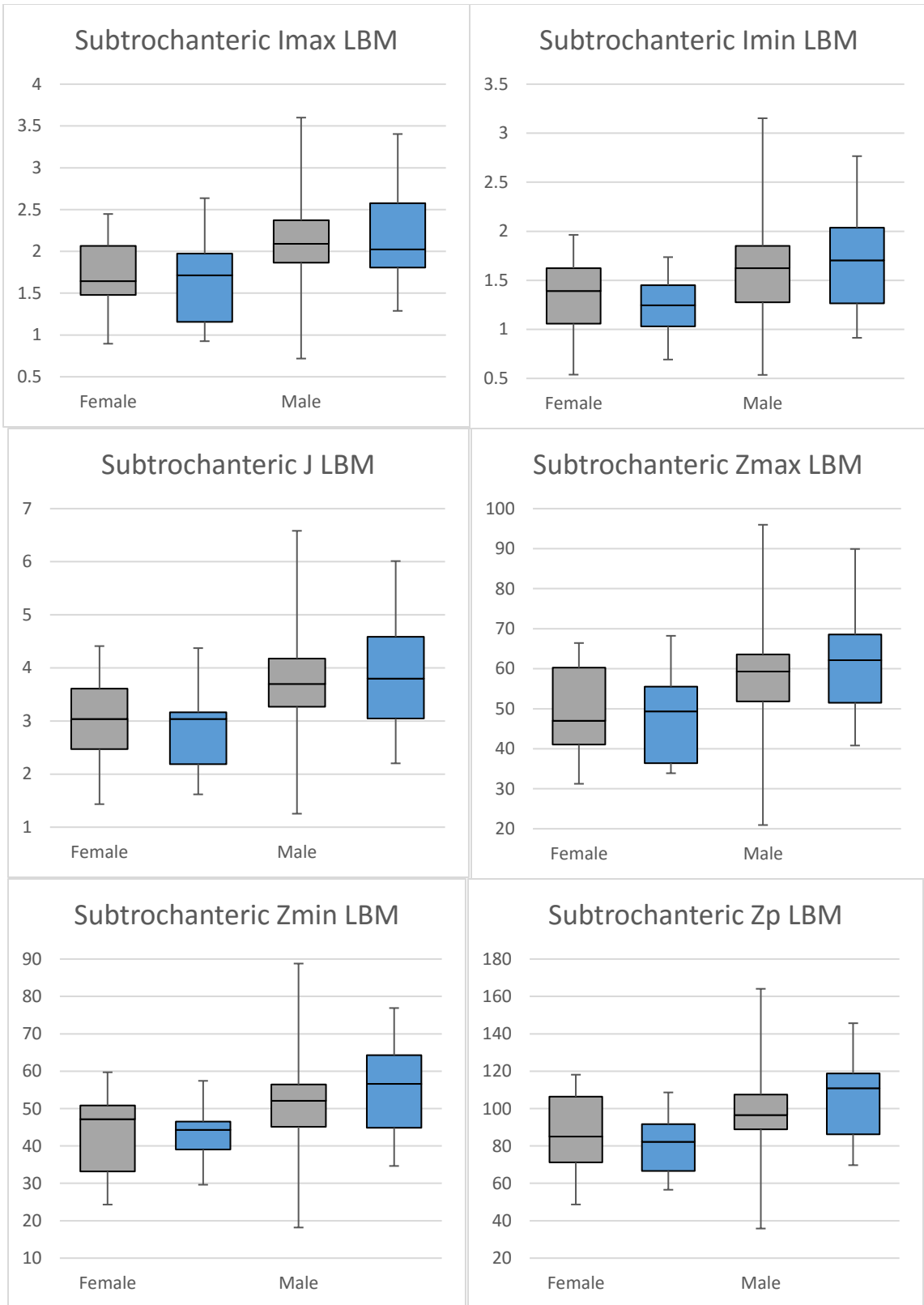




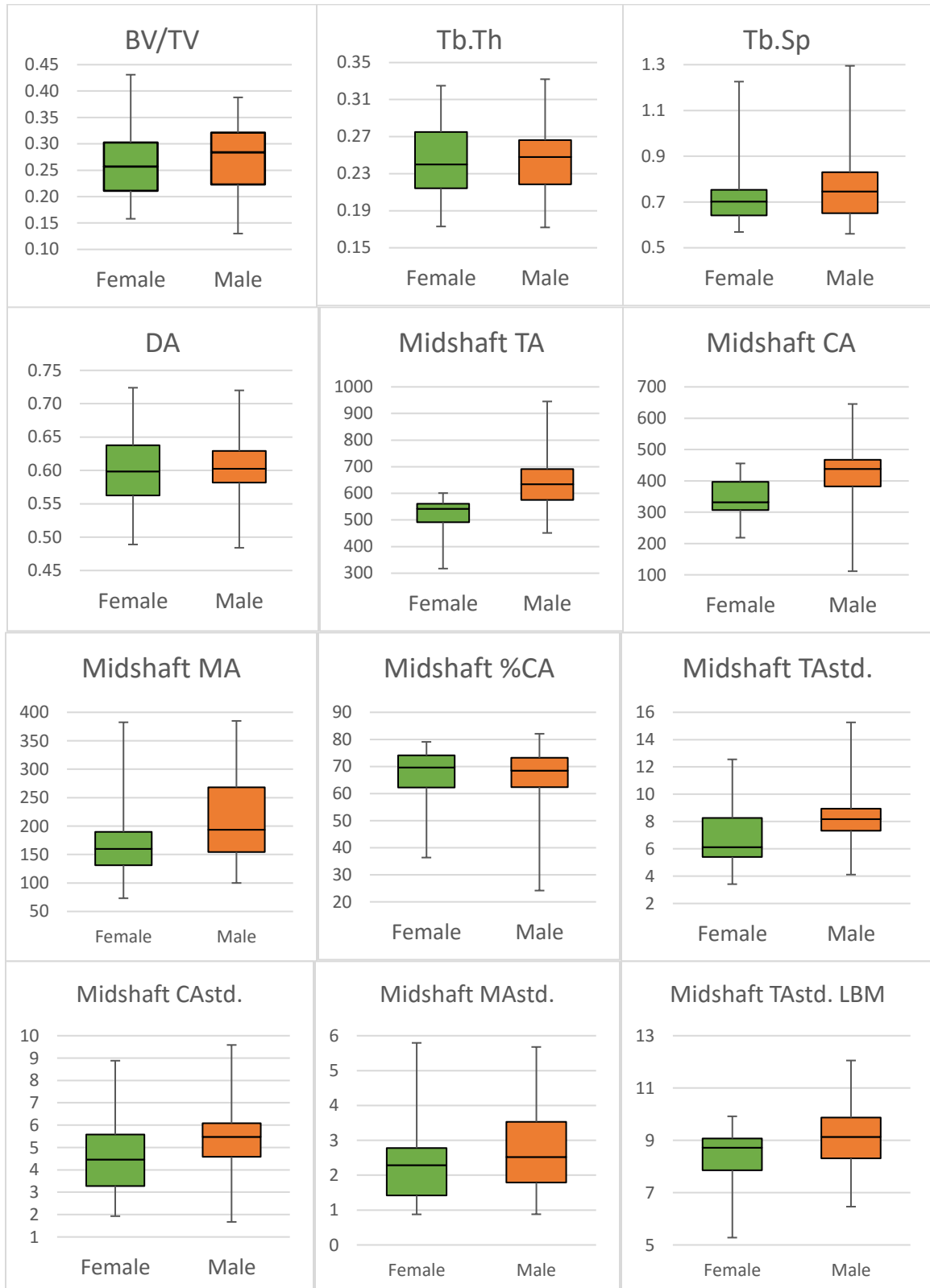


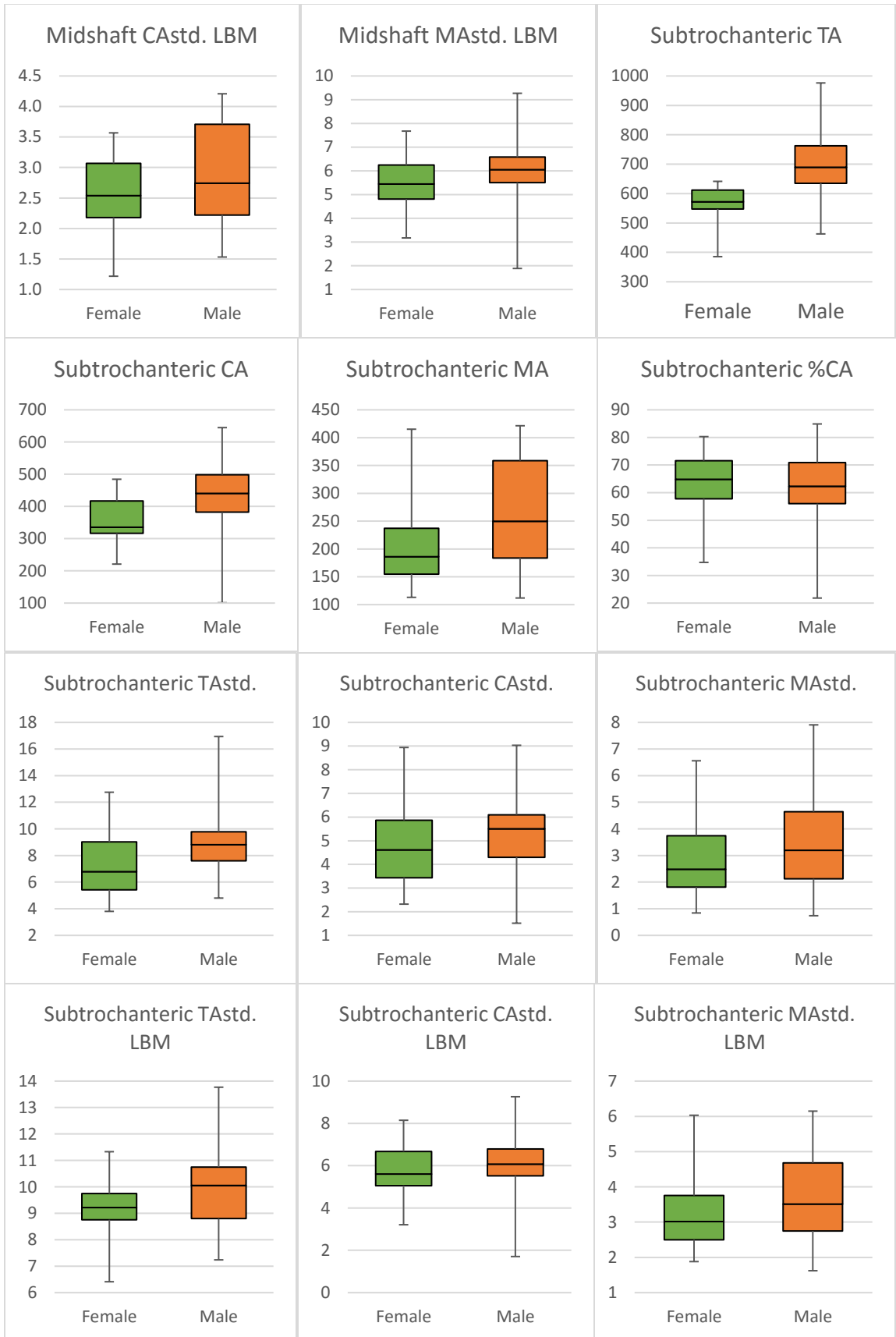


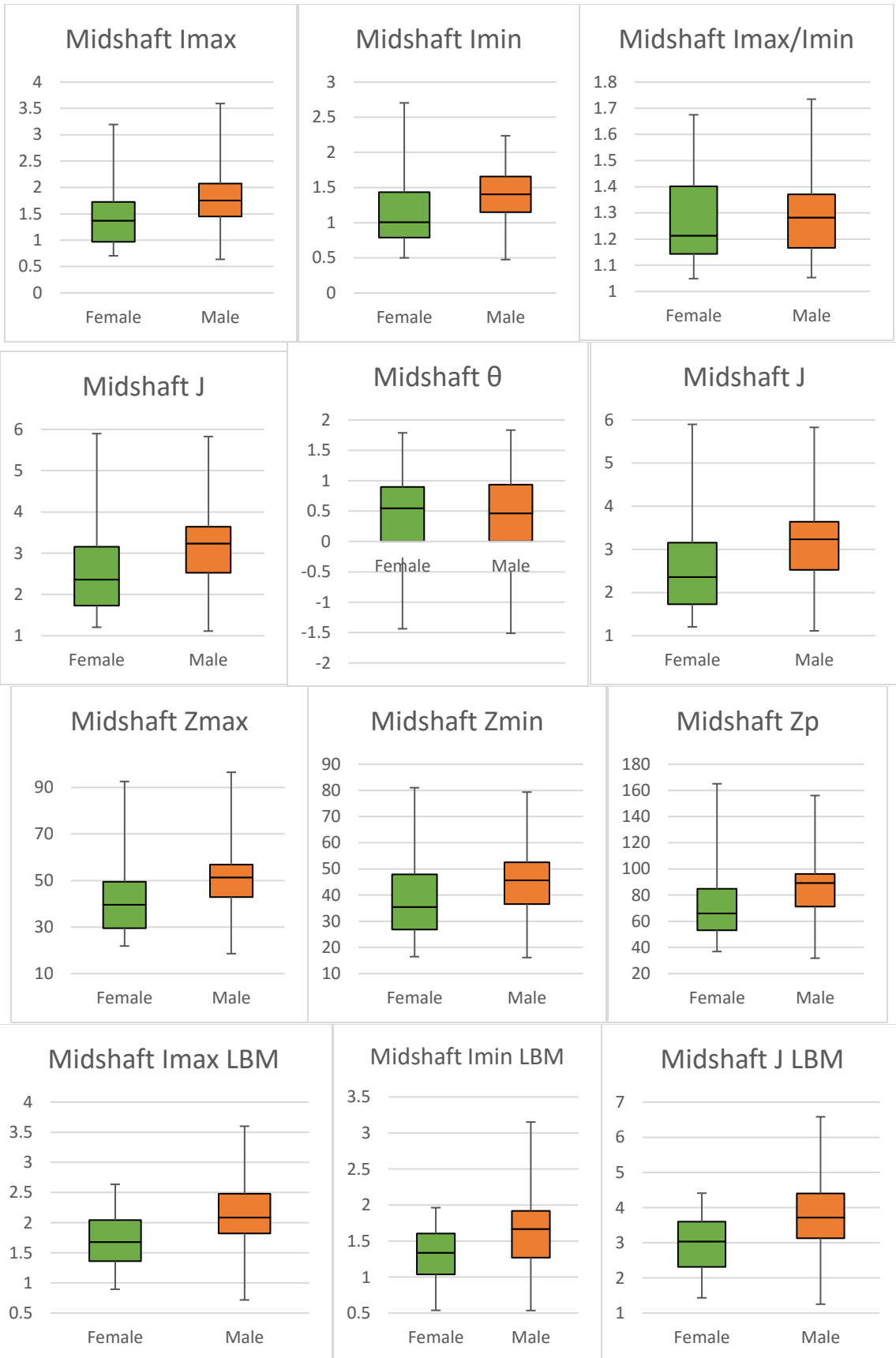


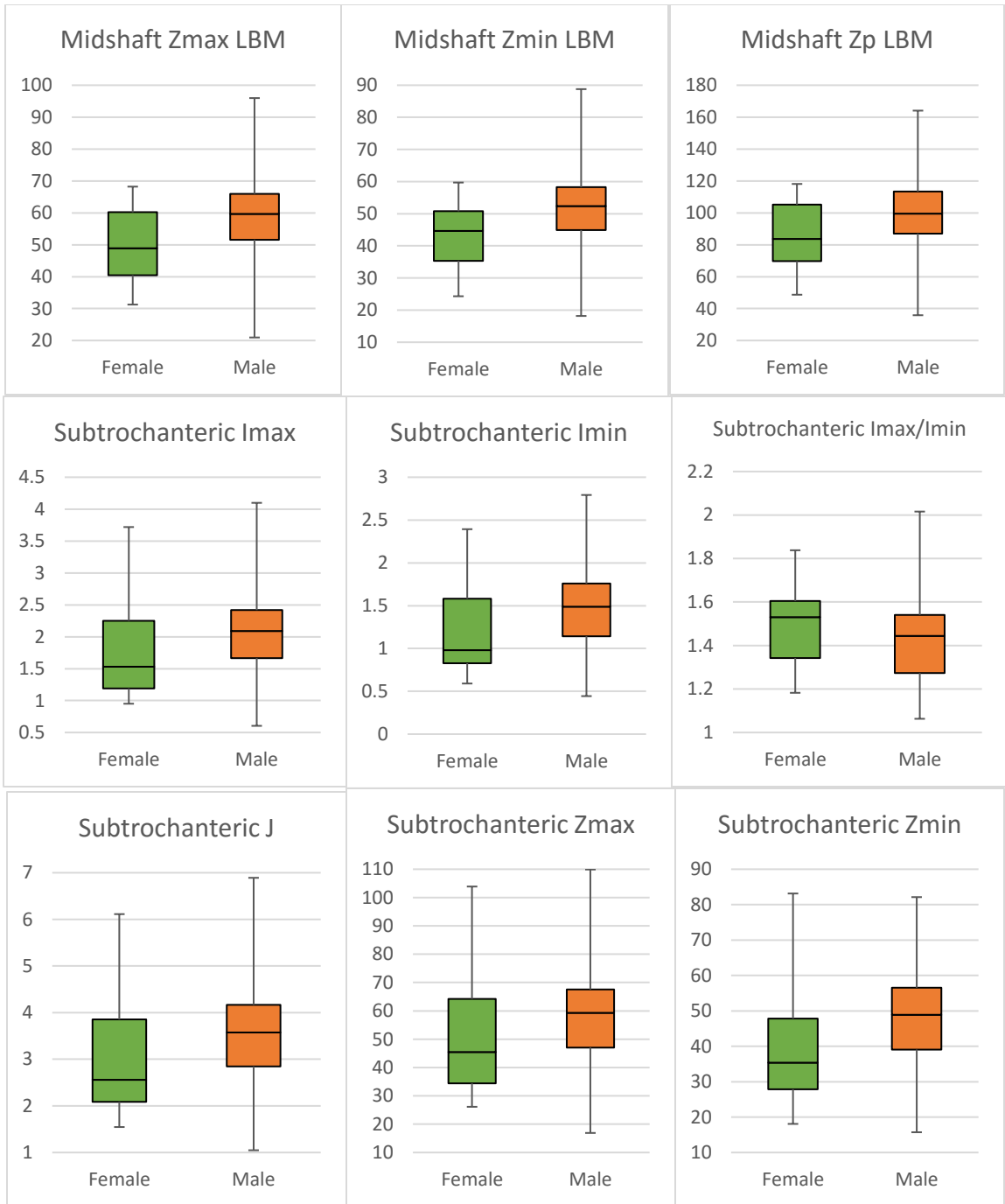


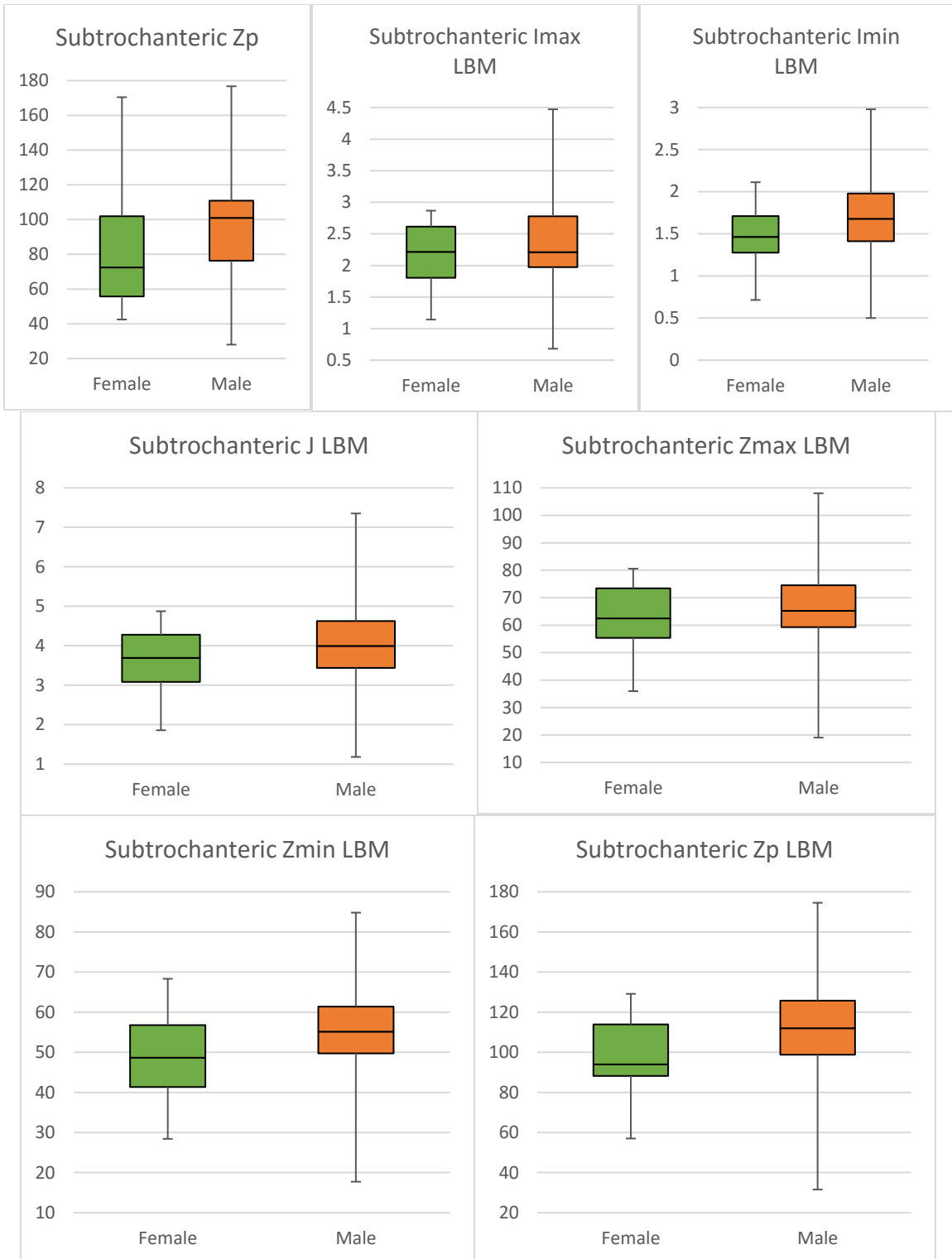
Appendix G. Boxplots of the trabecular and cortical properties with the mobility groups combined and the samples divided by sex.



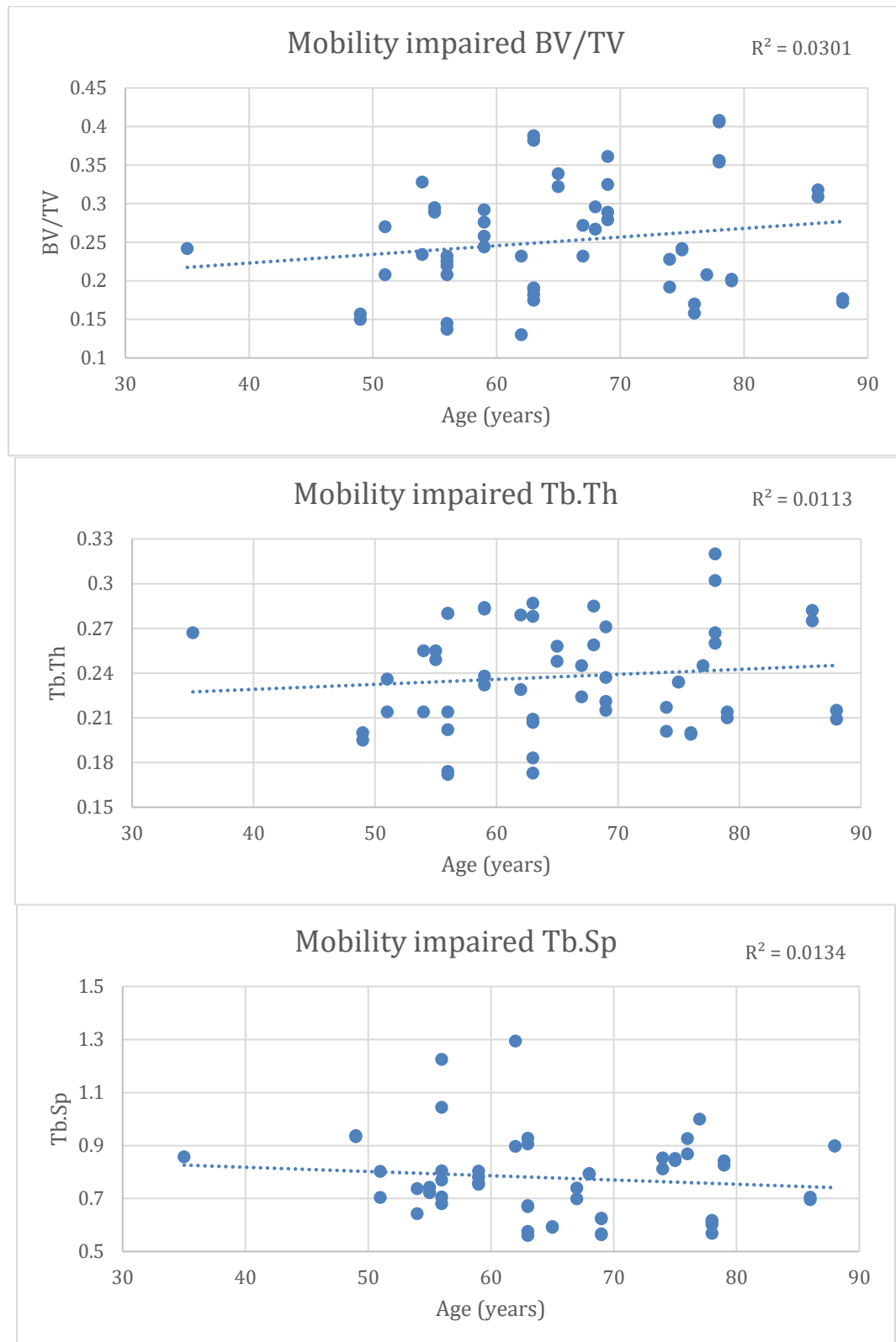


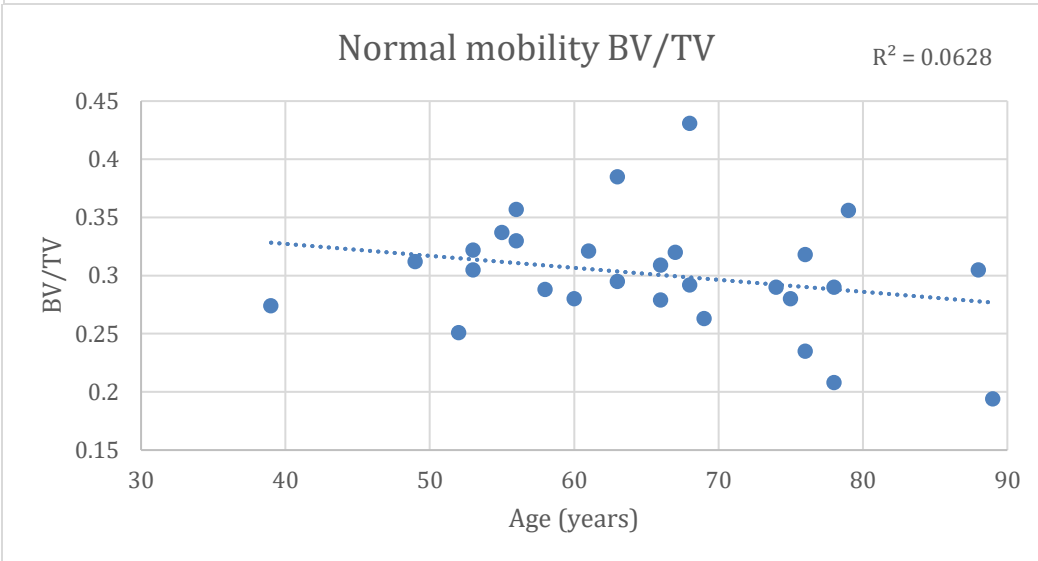
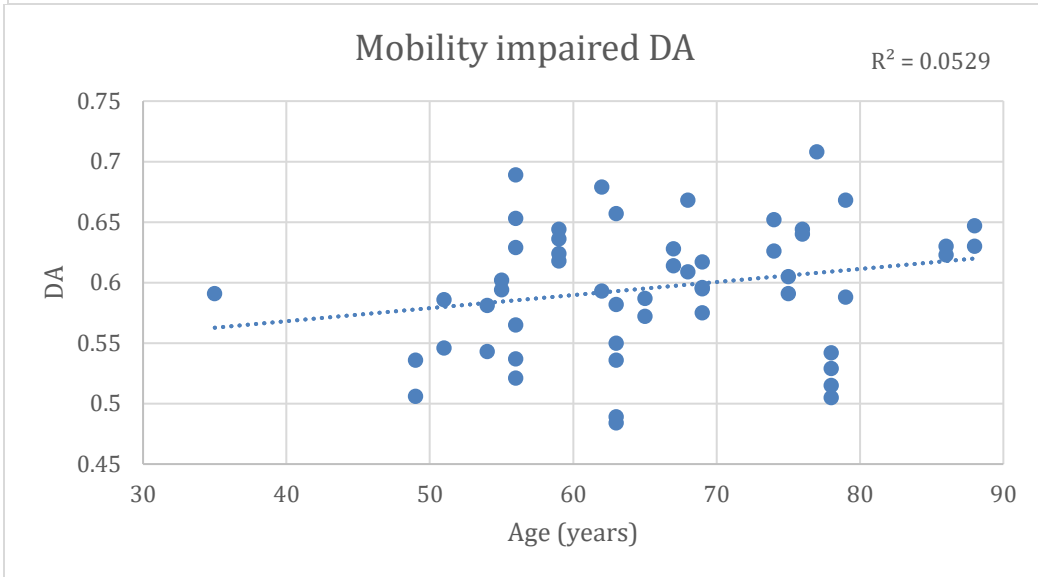
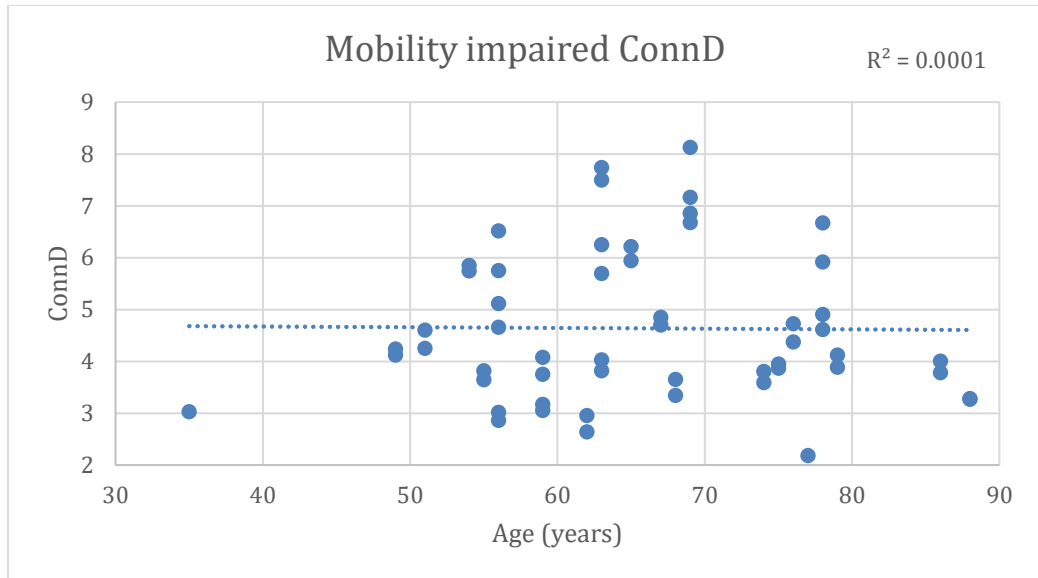


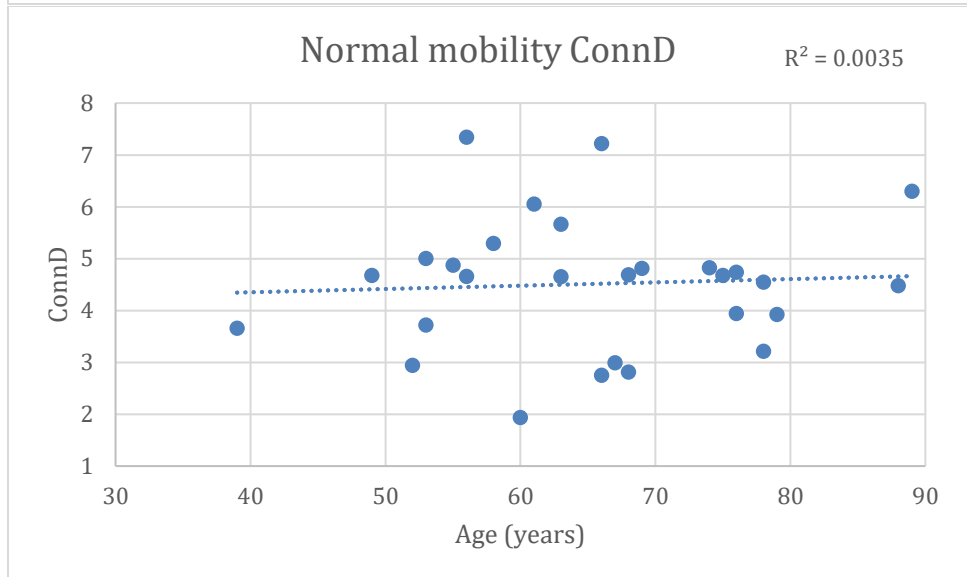
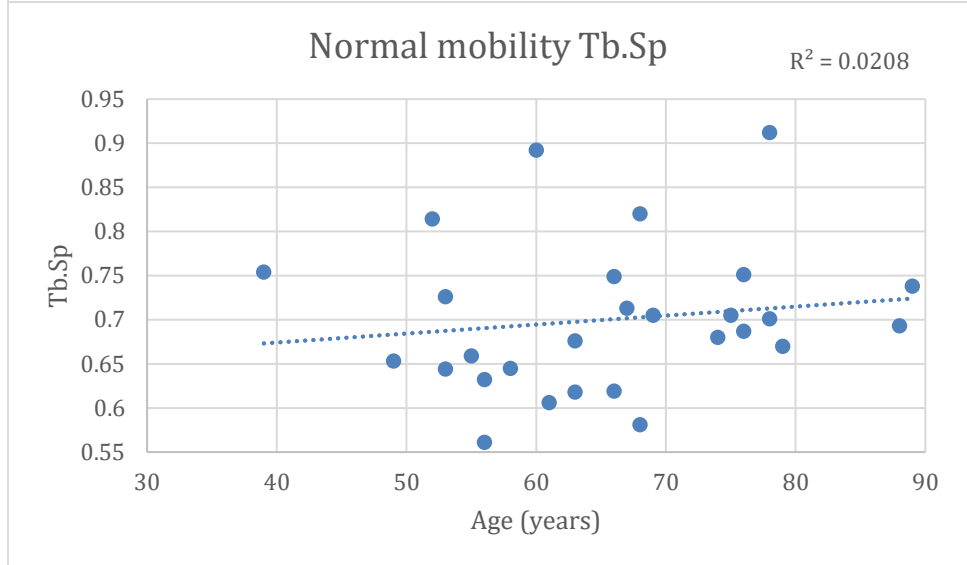
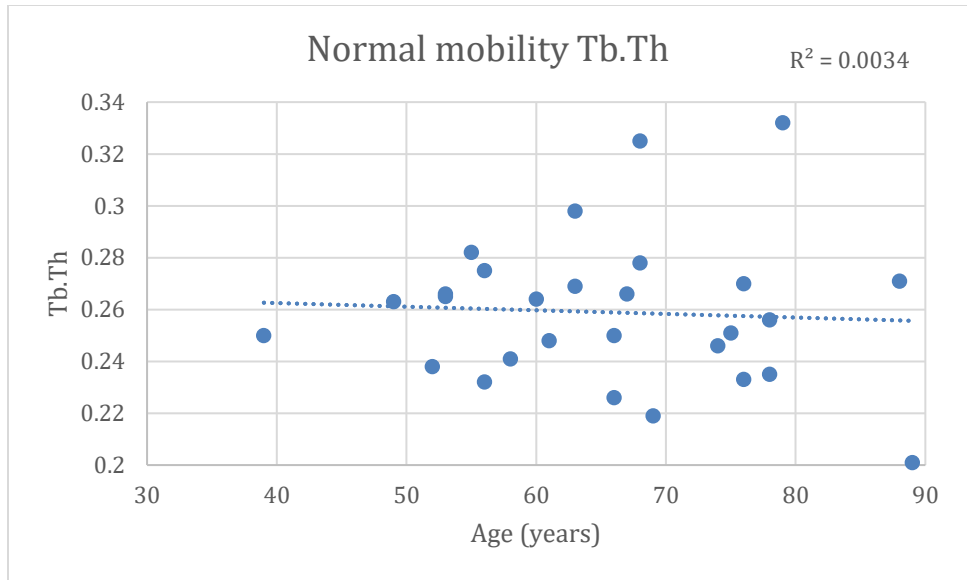


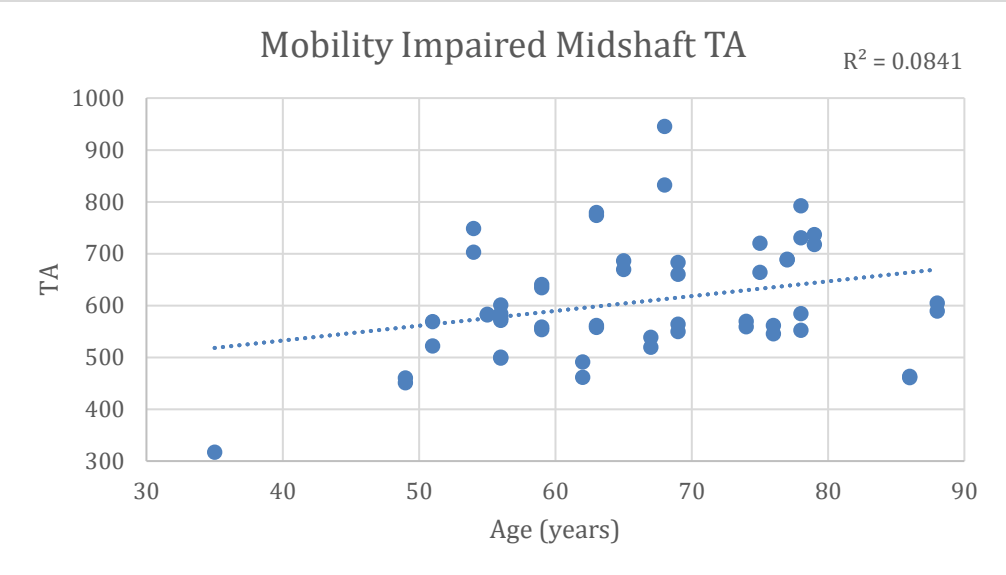
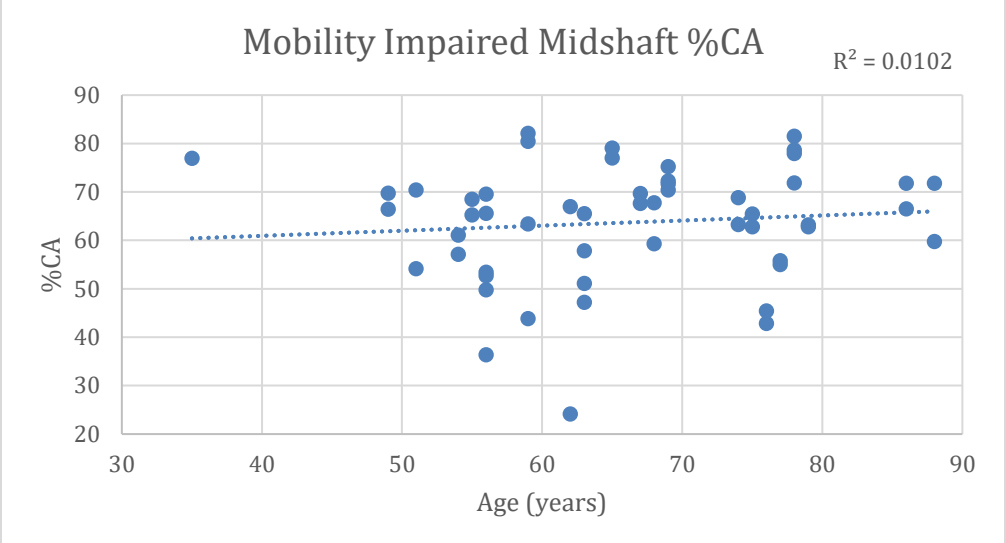
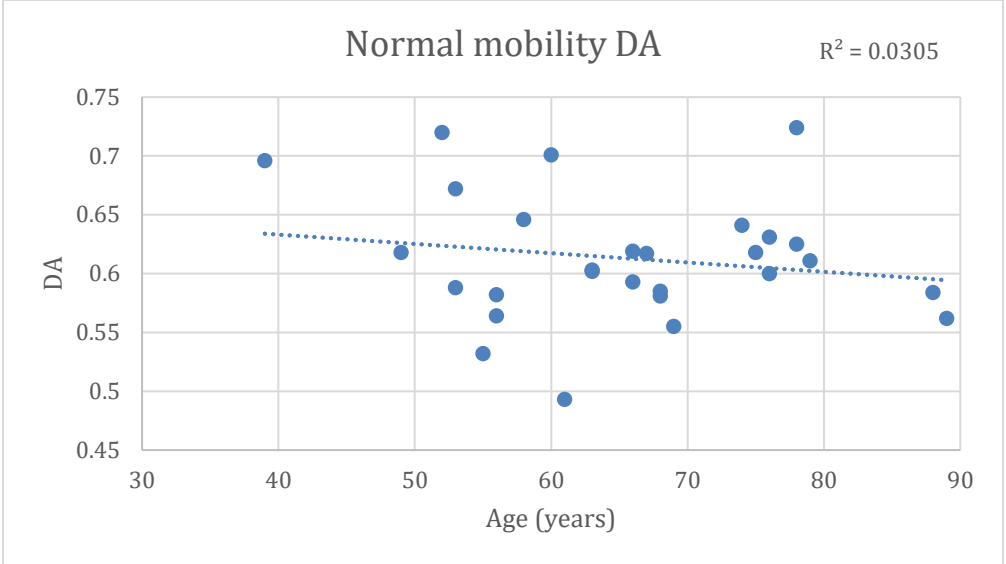


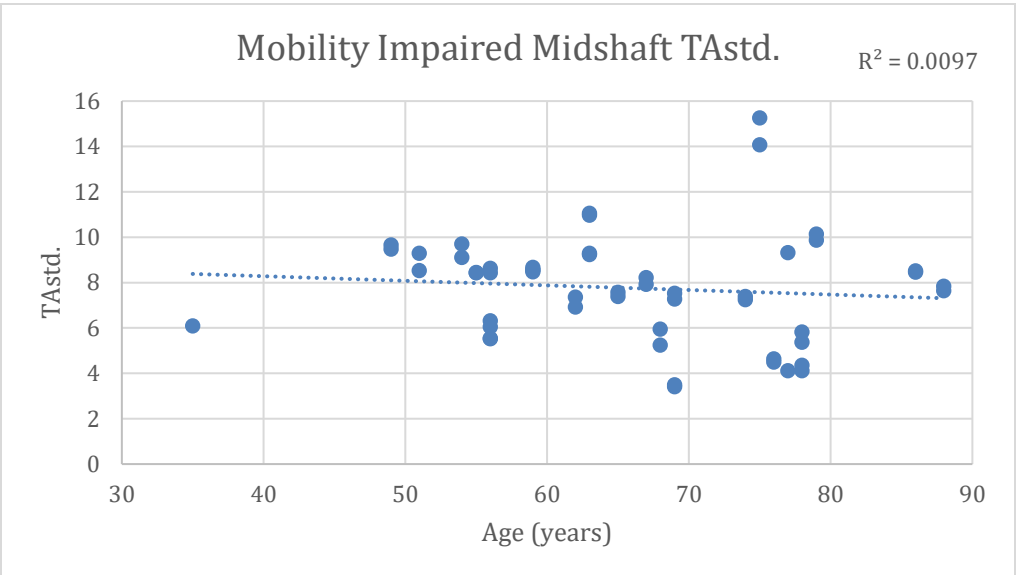
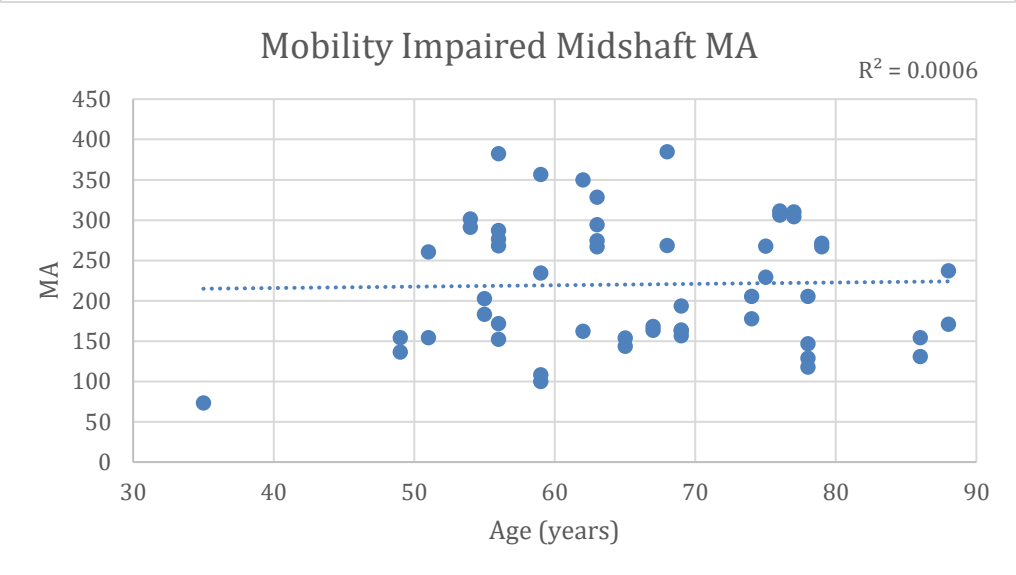
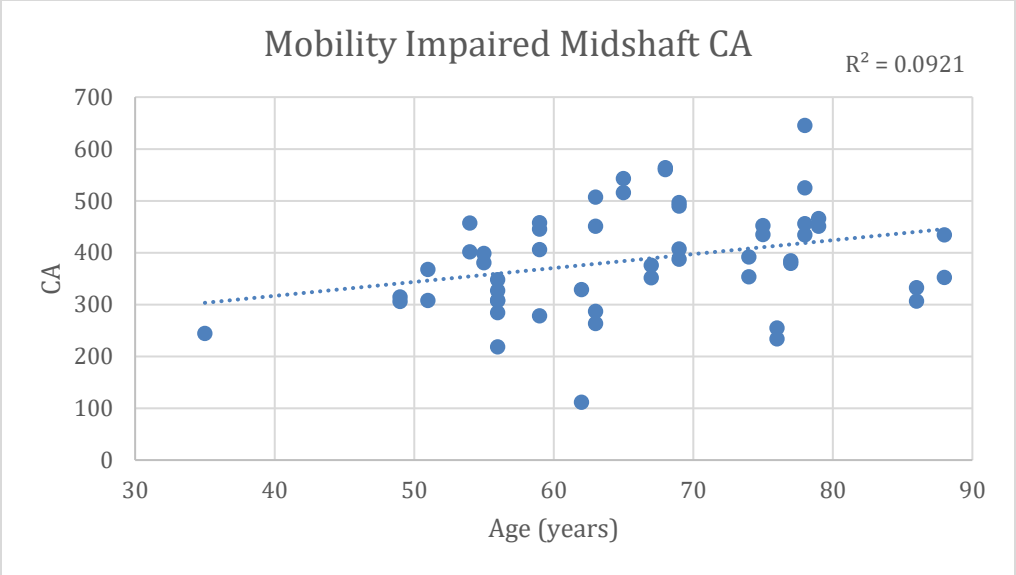
Appendix H. Scatterplots of the trabecular and cortical variables compared to age of the individuals separated by mobility type.

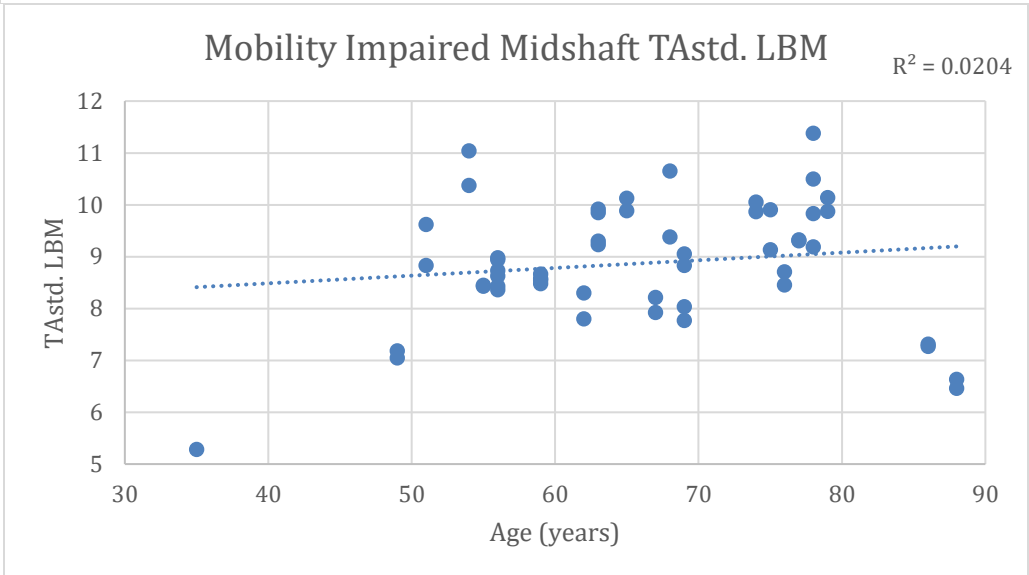
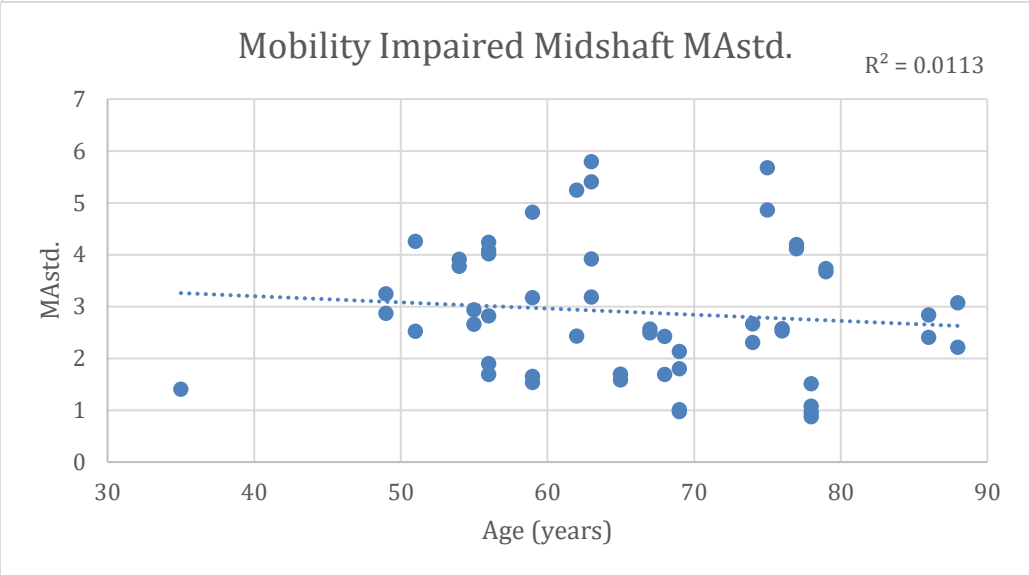
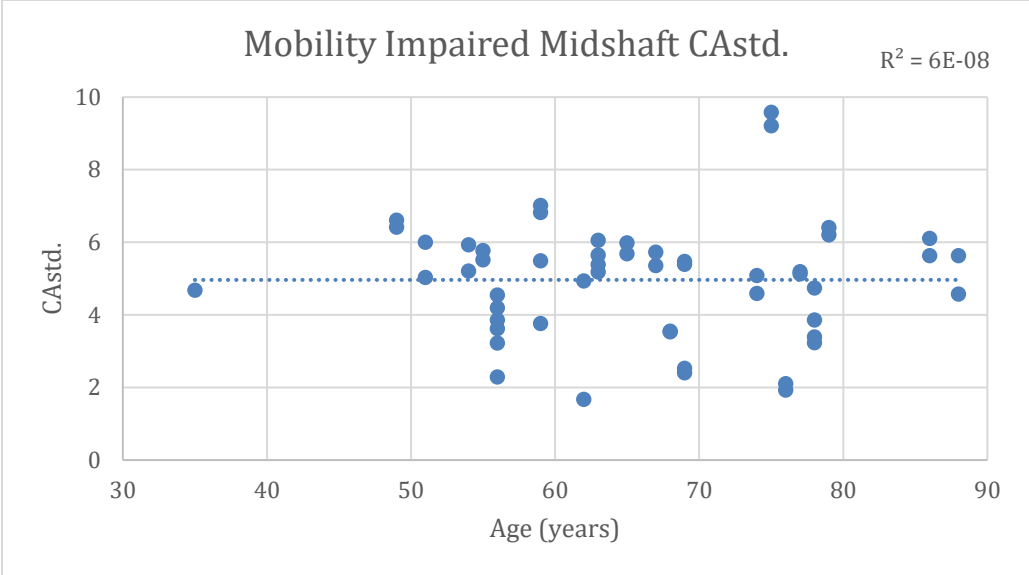


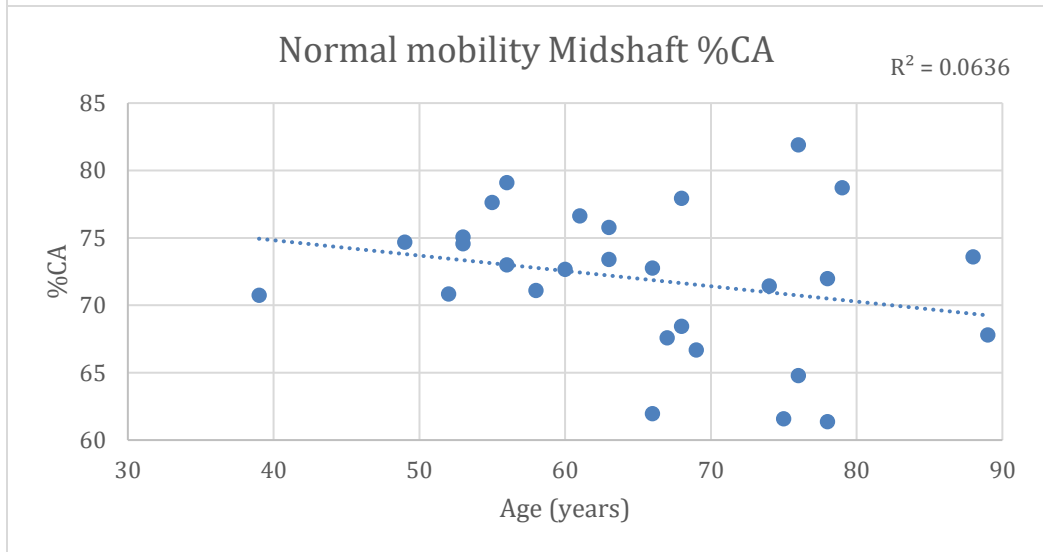
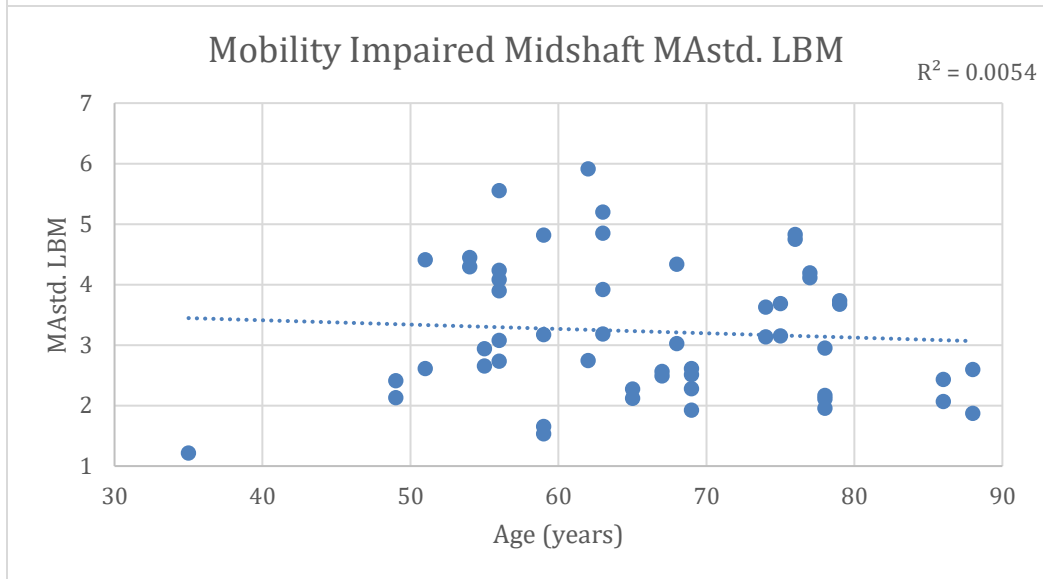
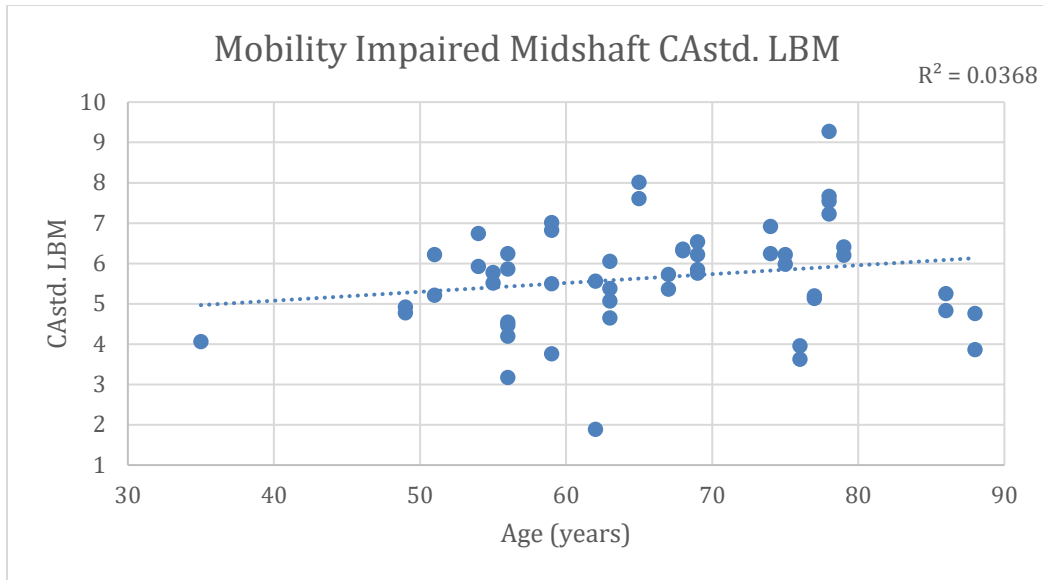


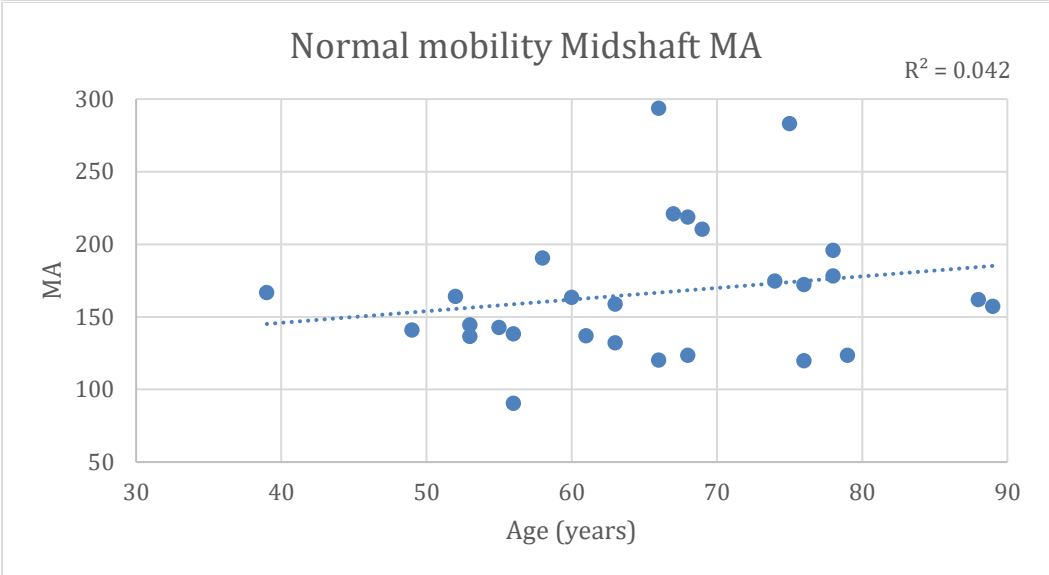
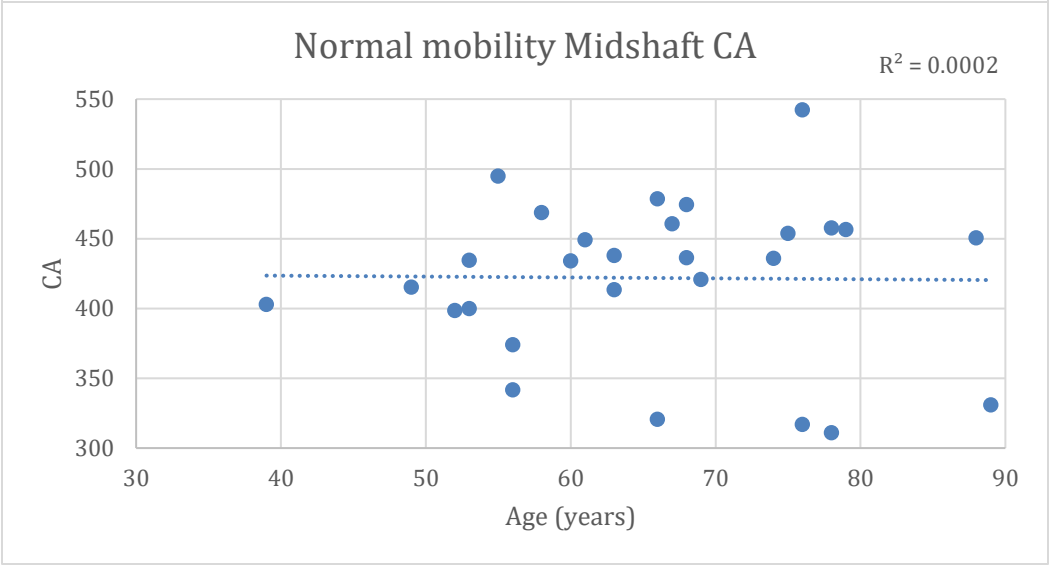
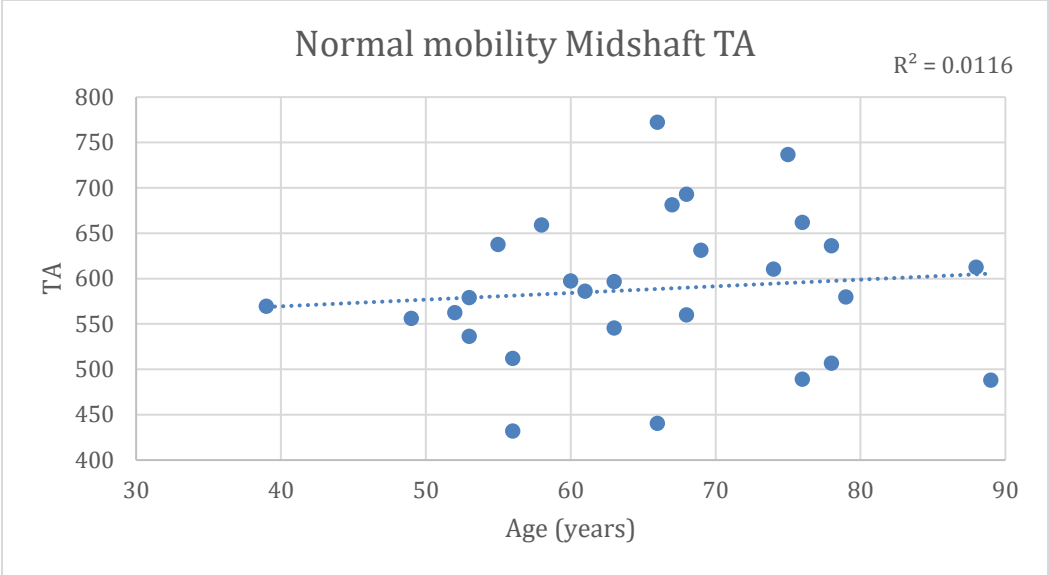


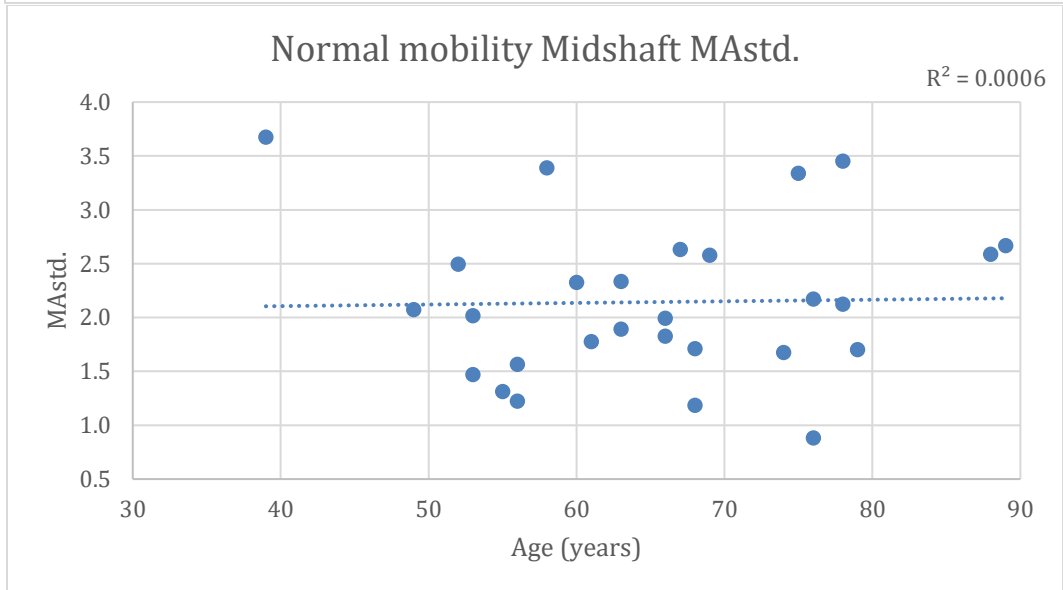
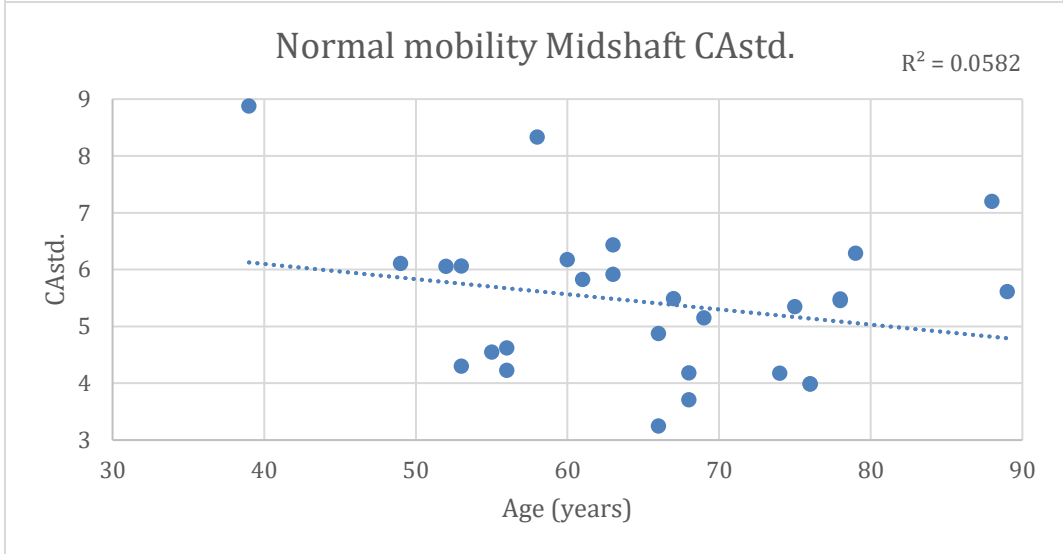
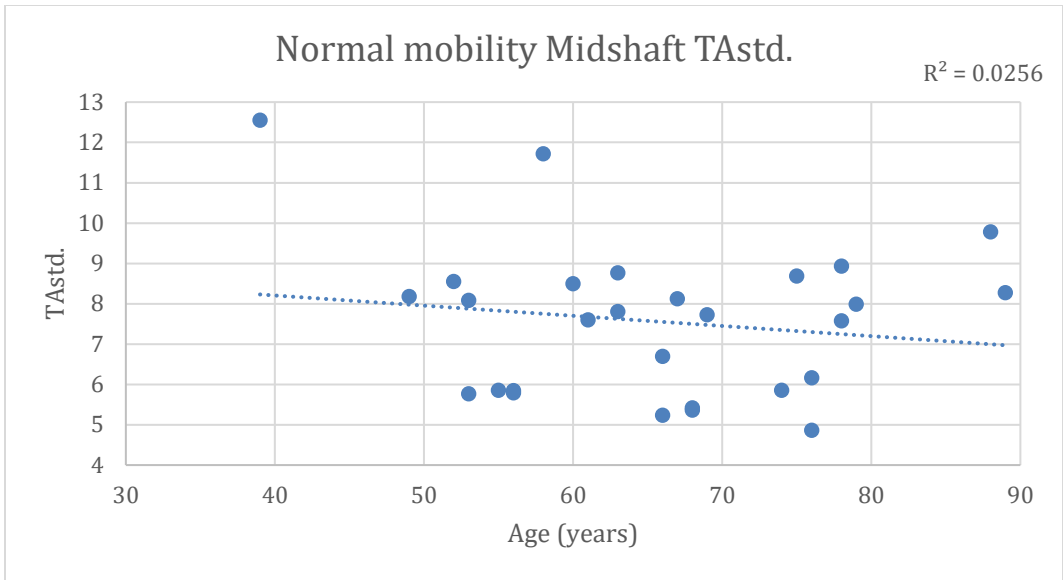


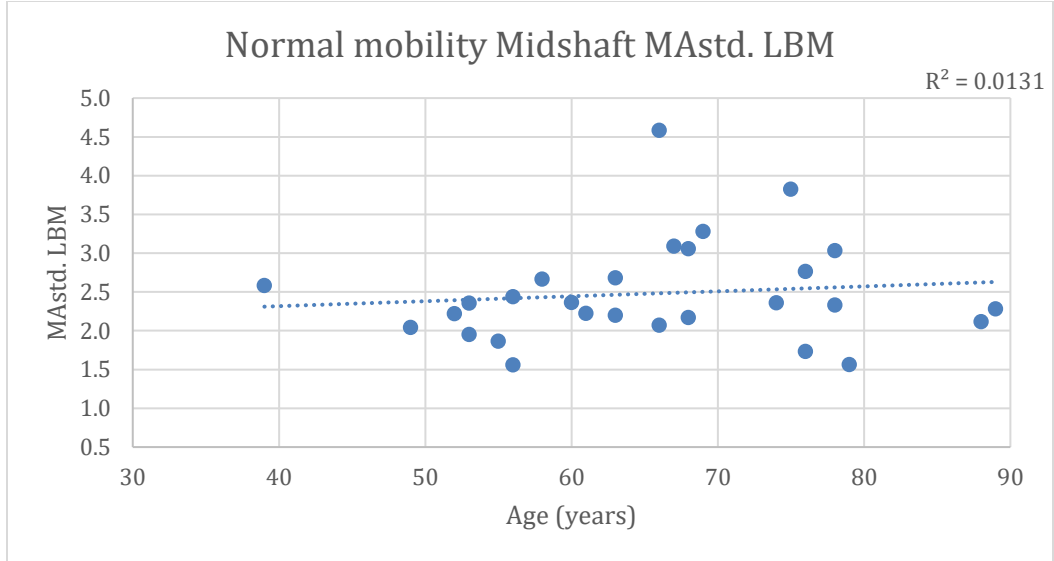
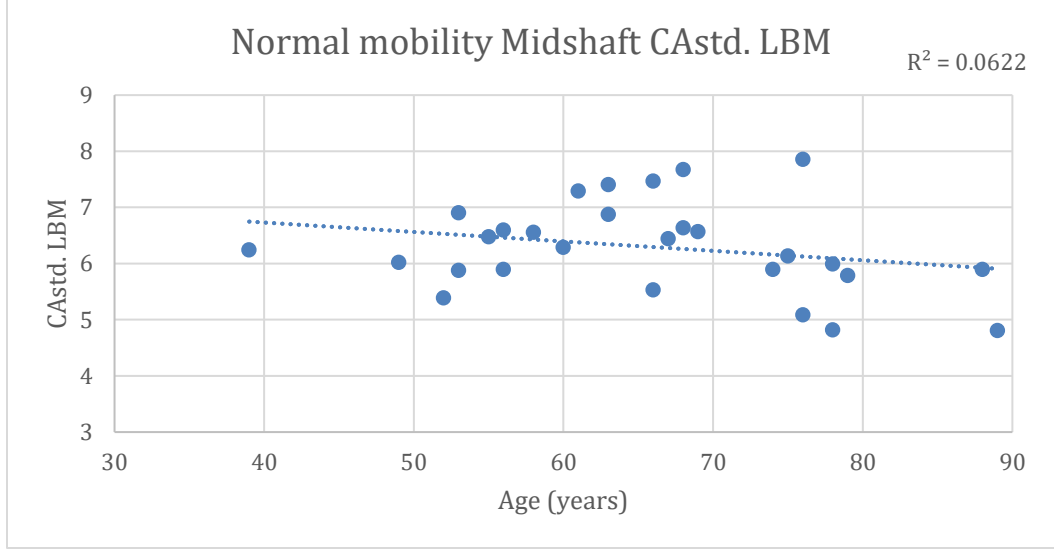
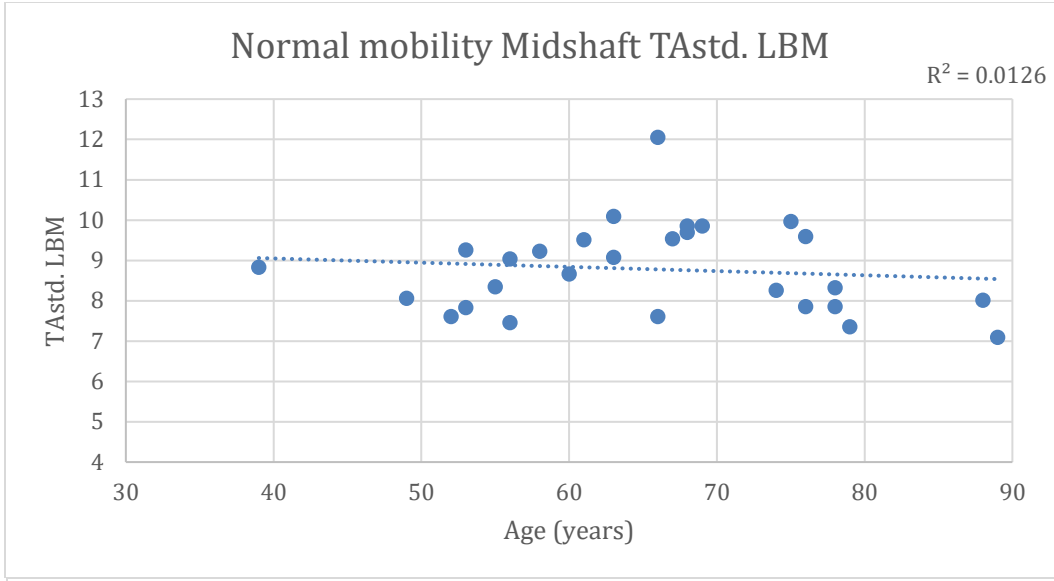


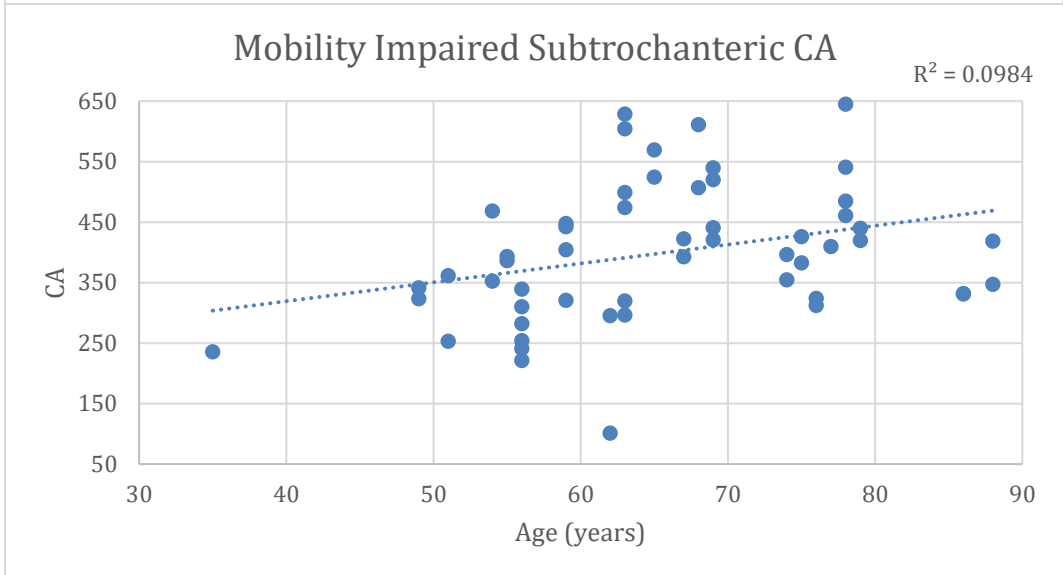
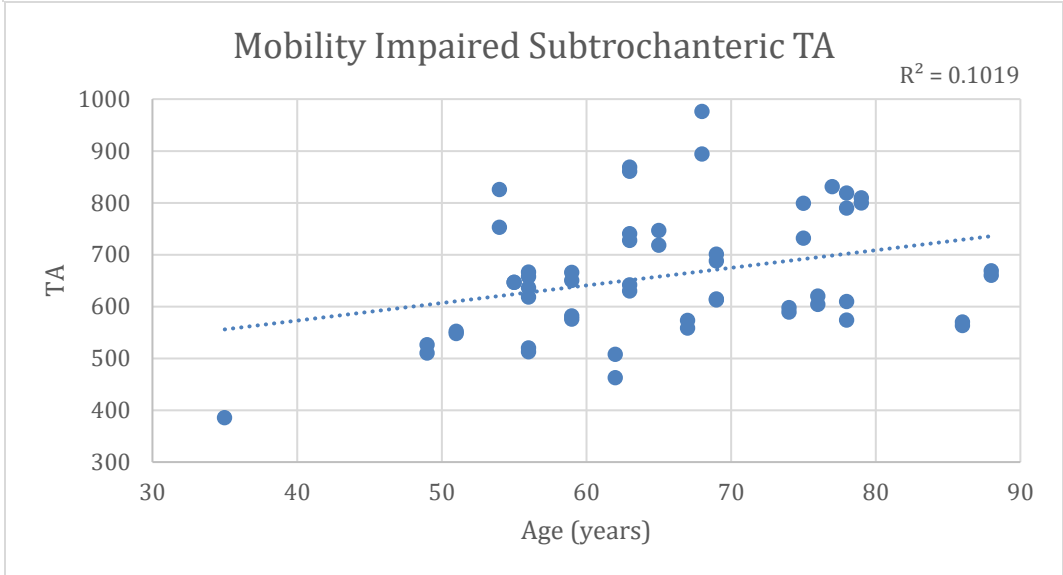
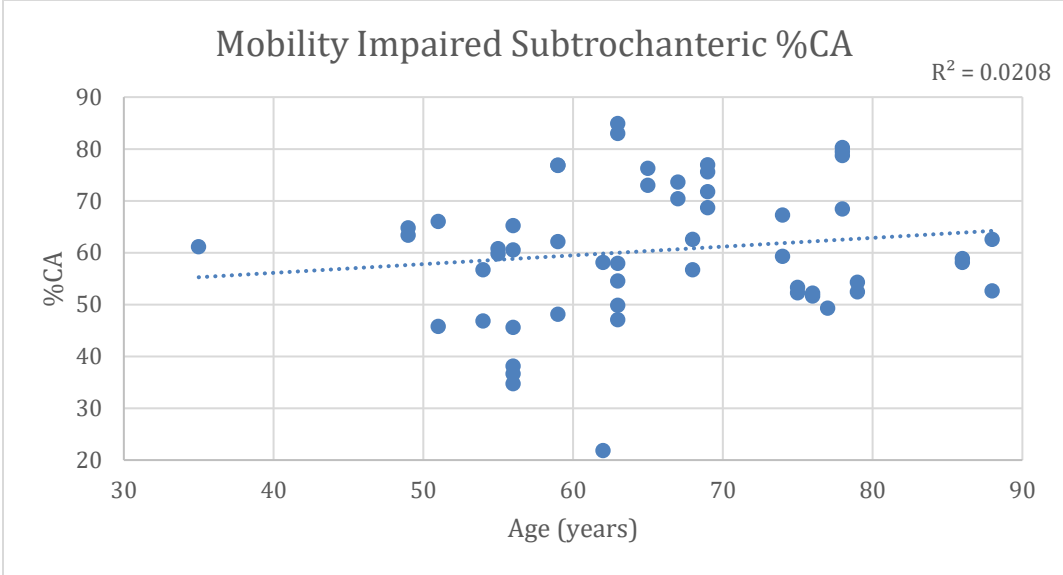


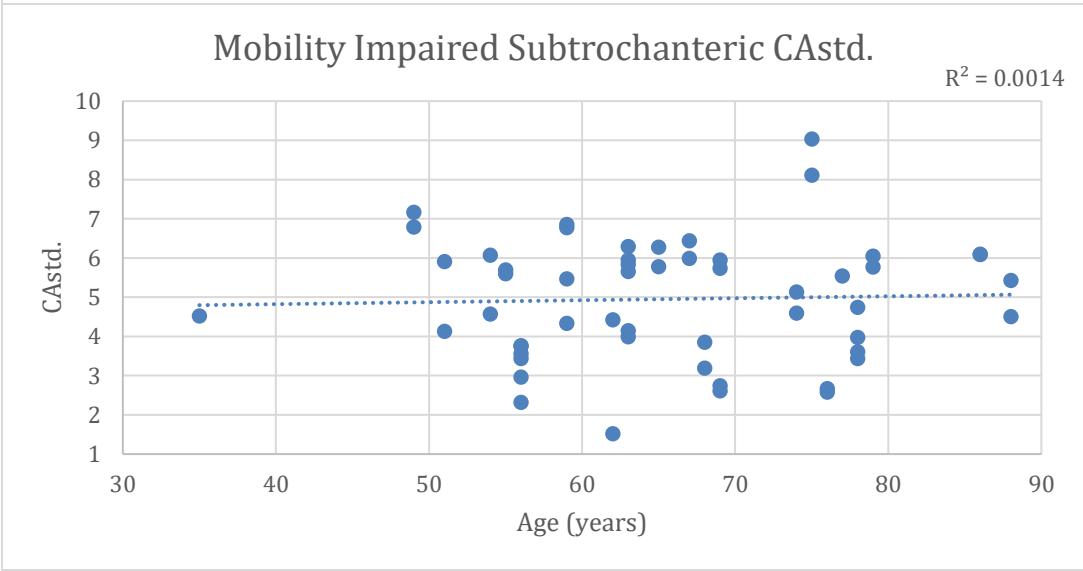
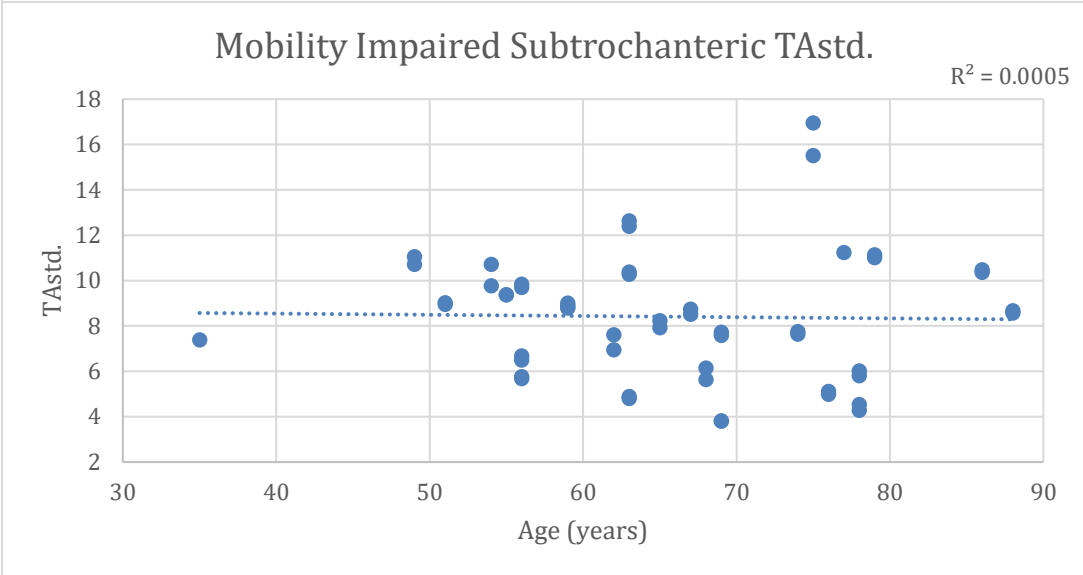
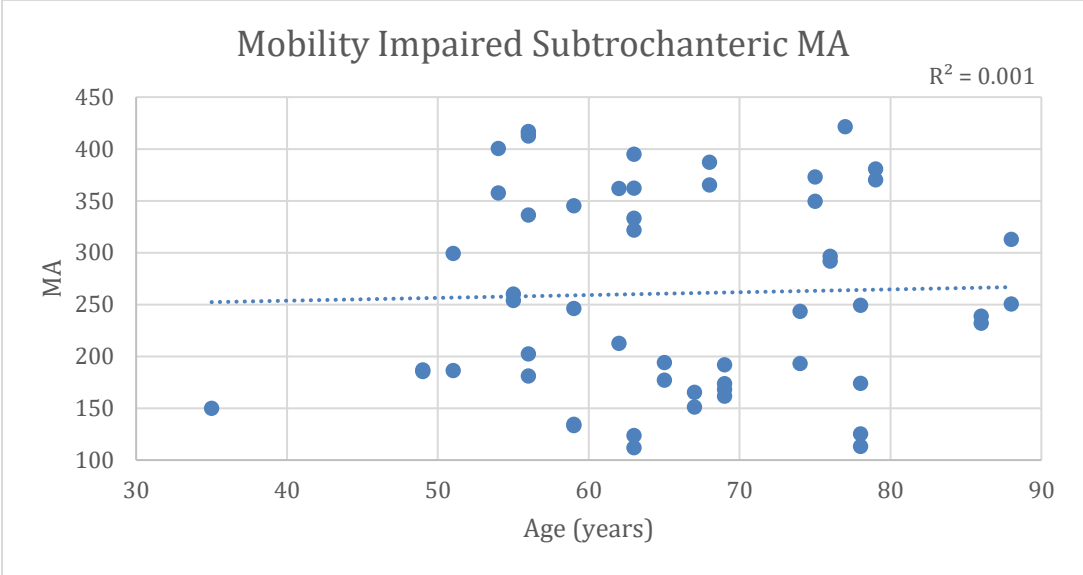


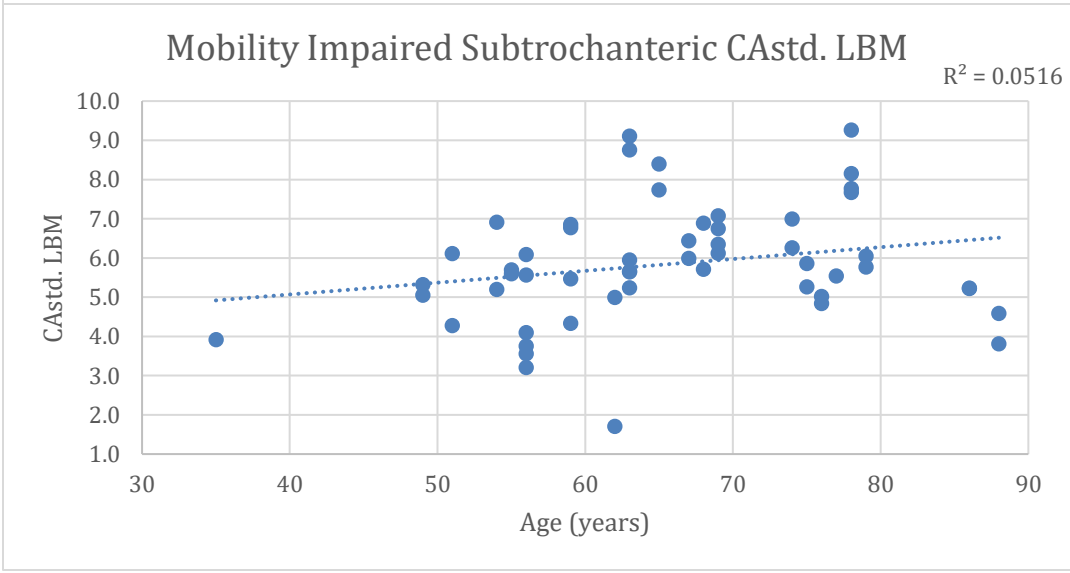
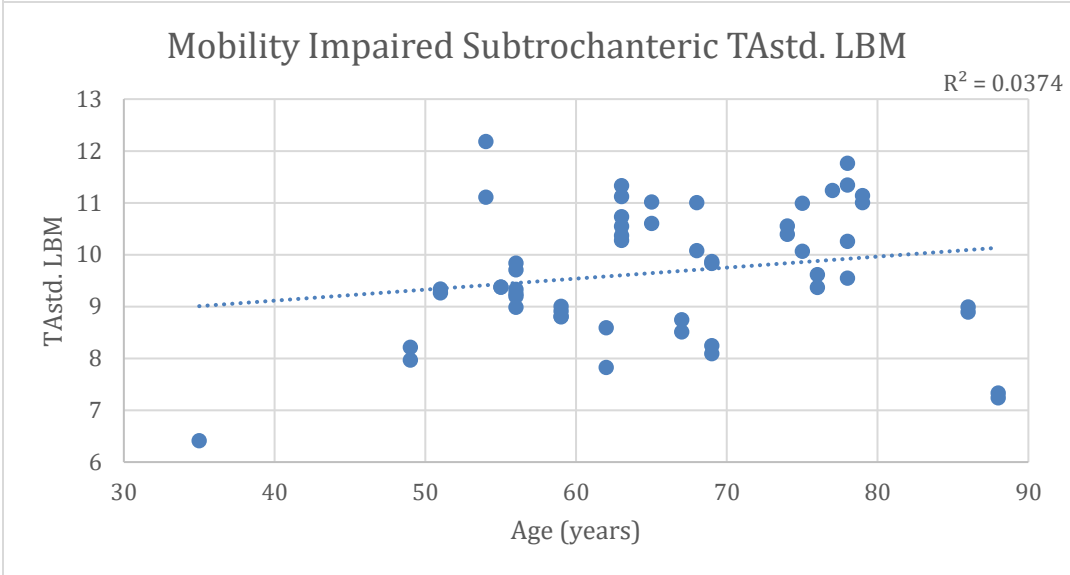
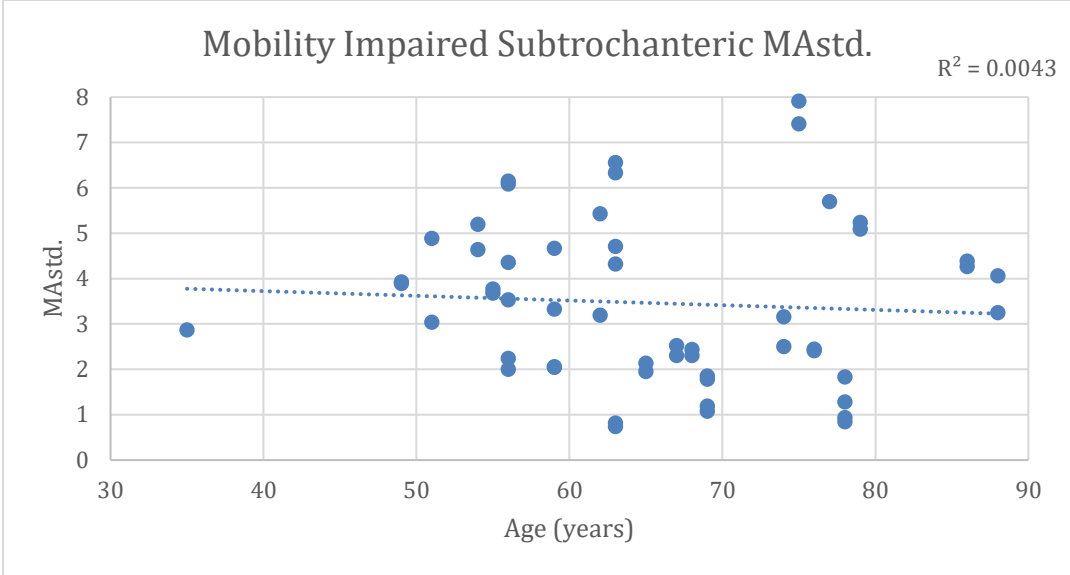




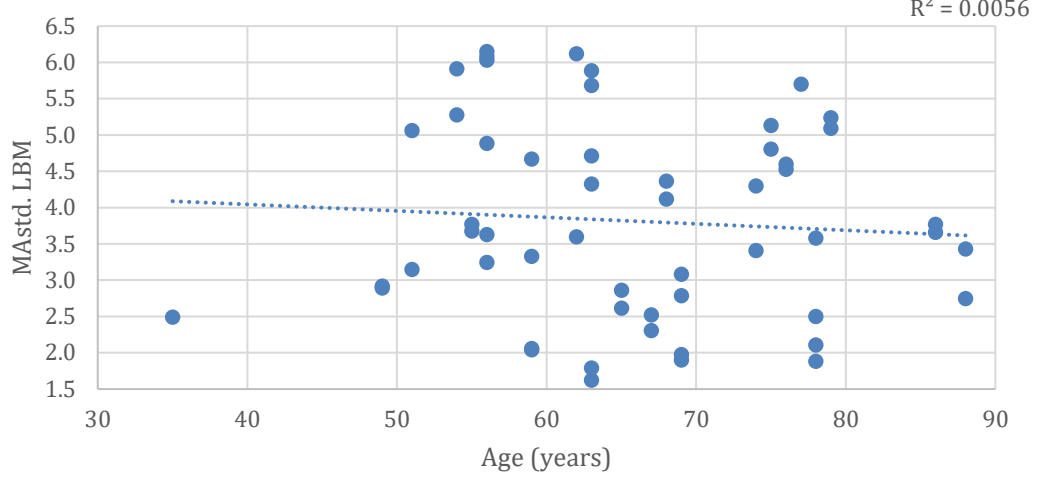




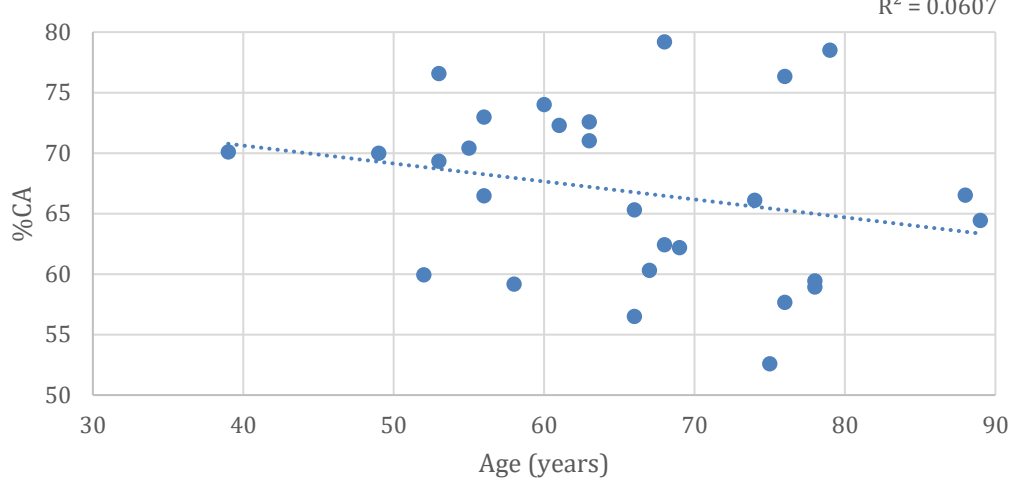




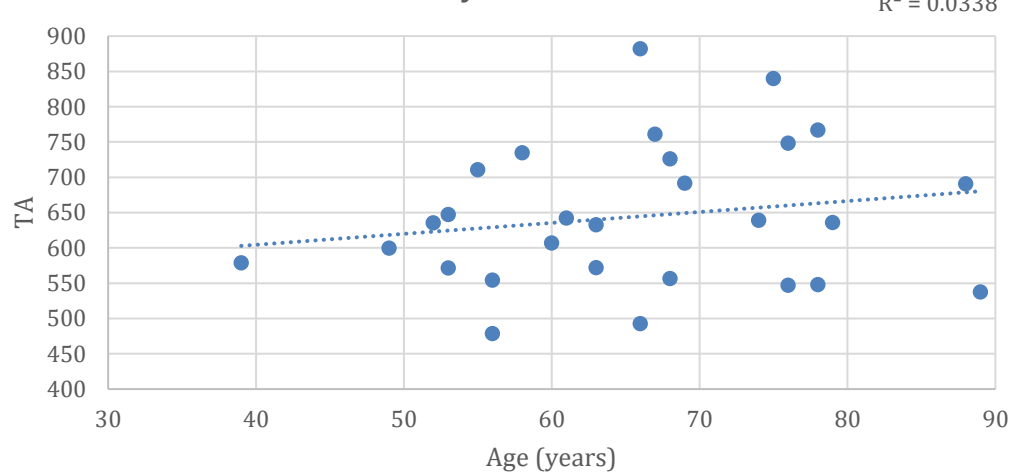
Mobility Impaired Subtrochanteric MAstd. LBM

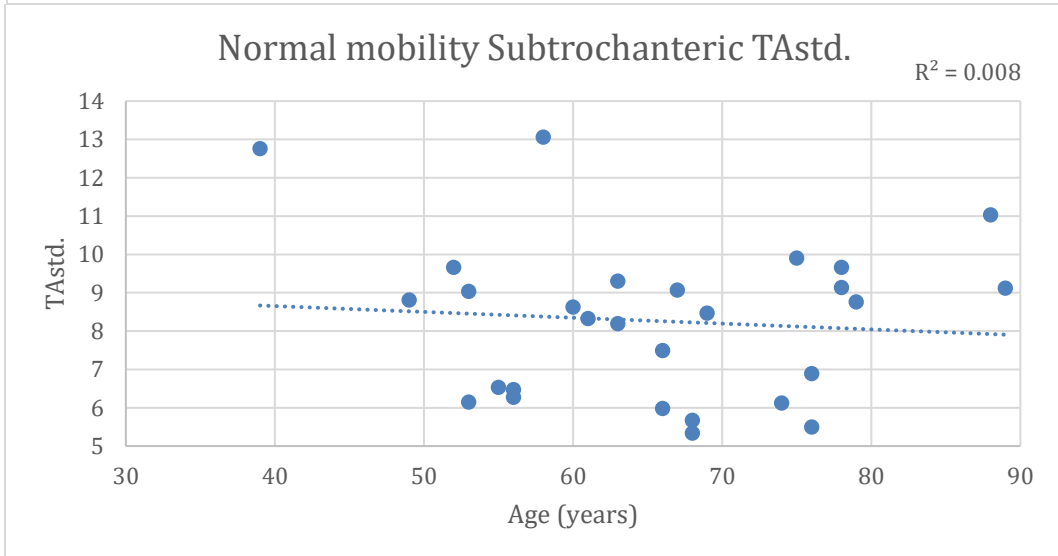
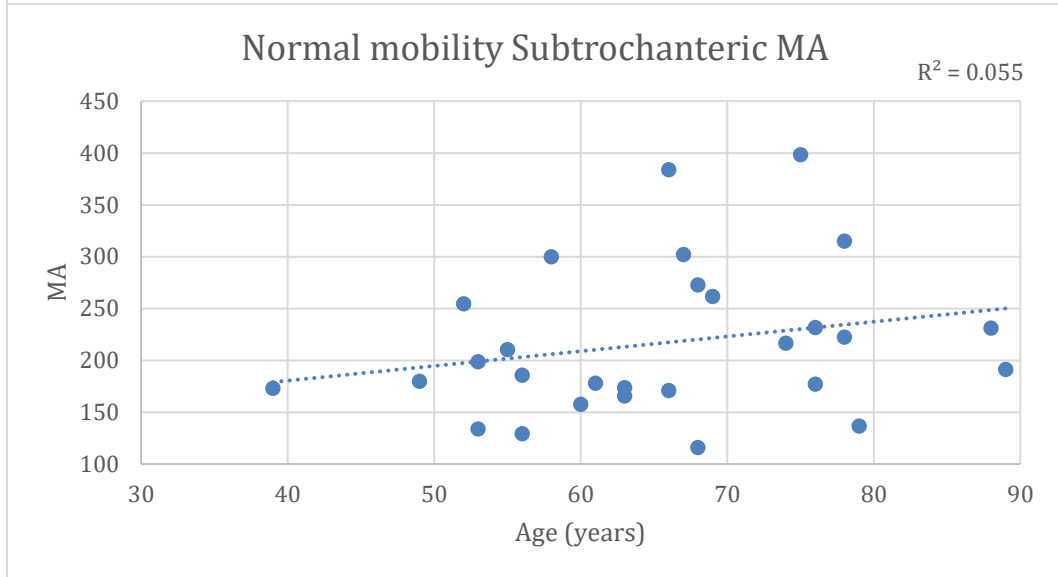
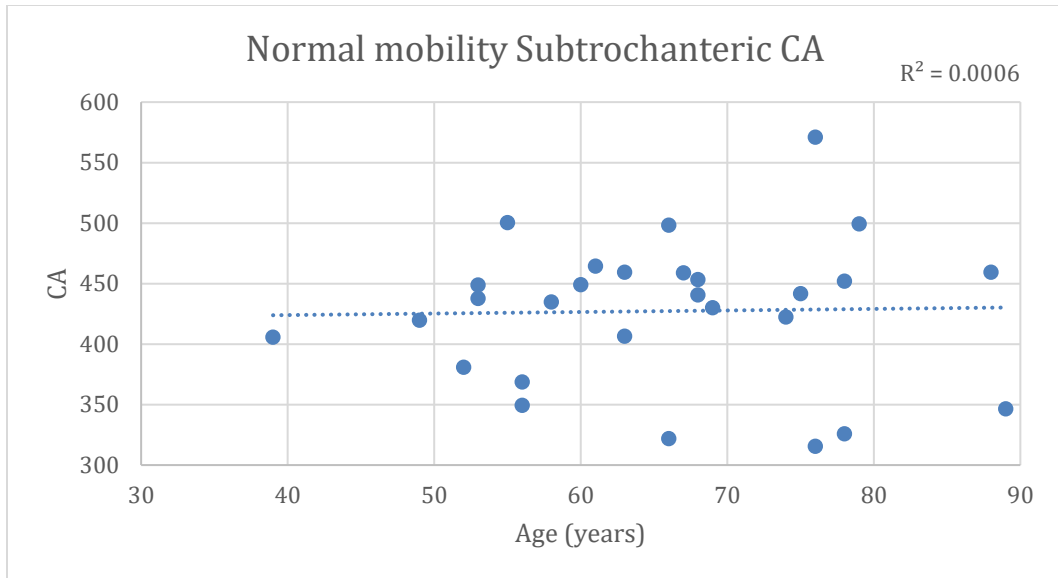


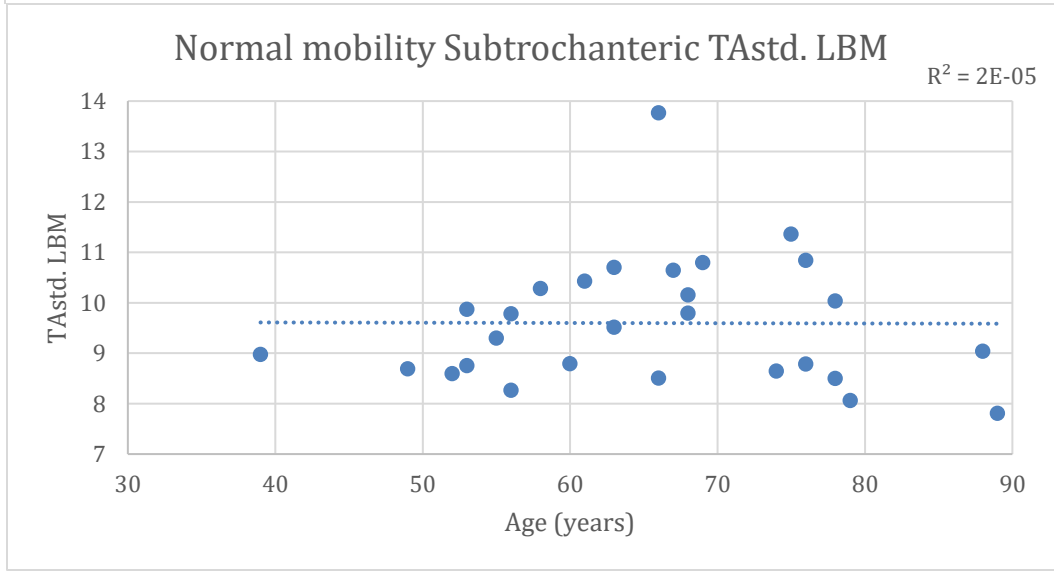
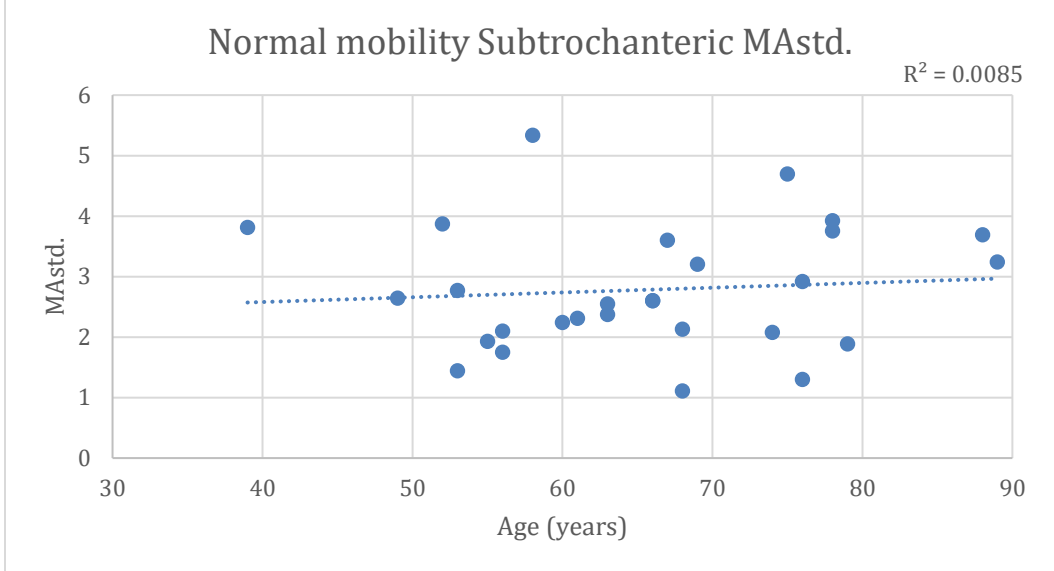
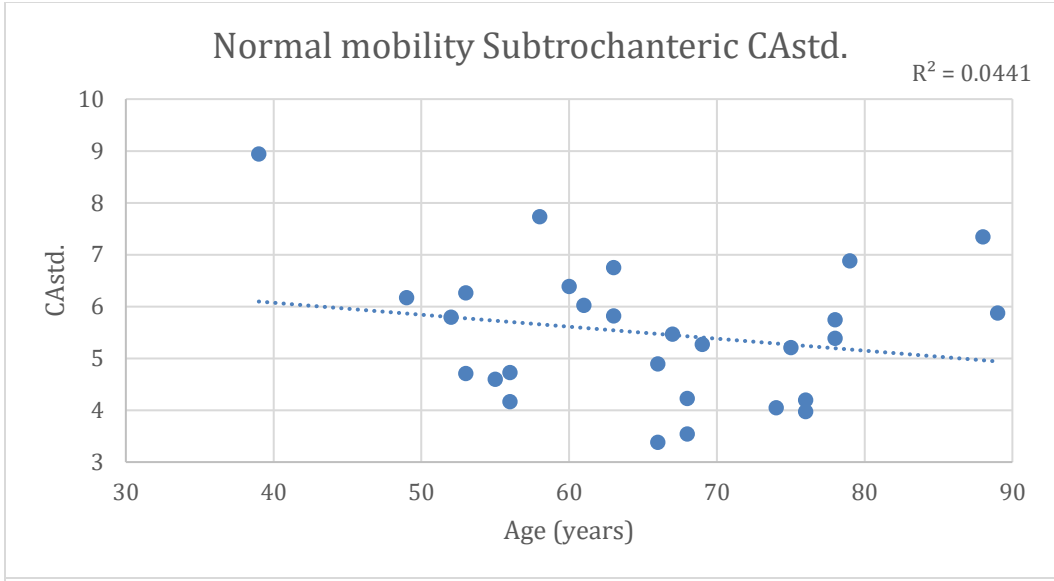
Normal mobility Subtrochanteric %CA

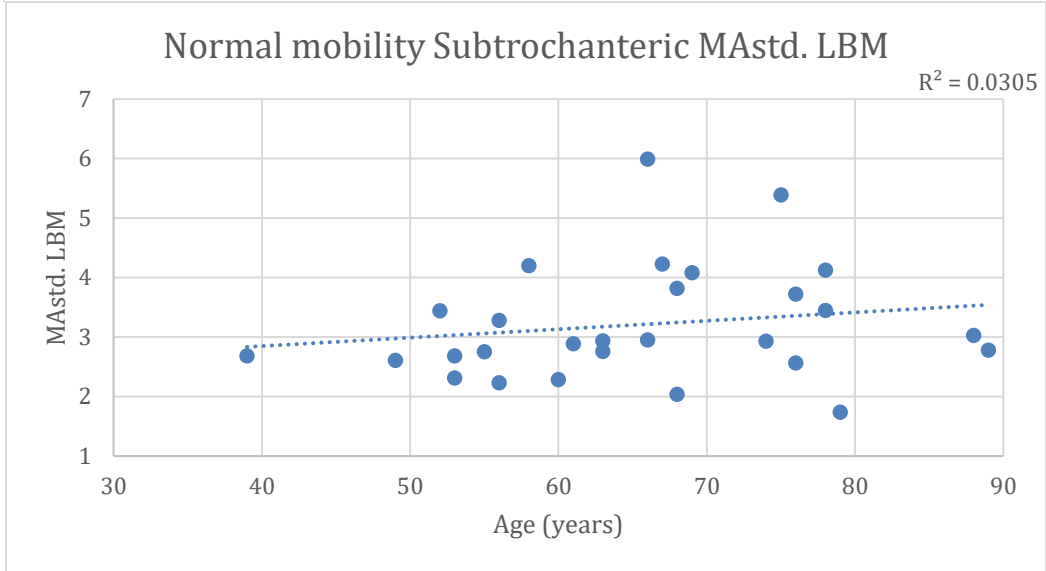
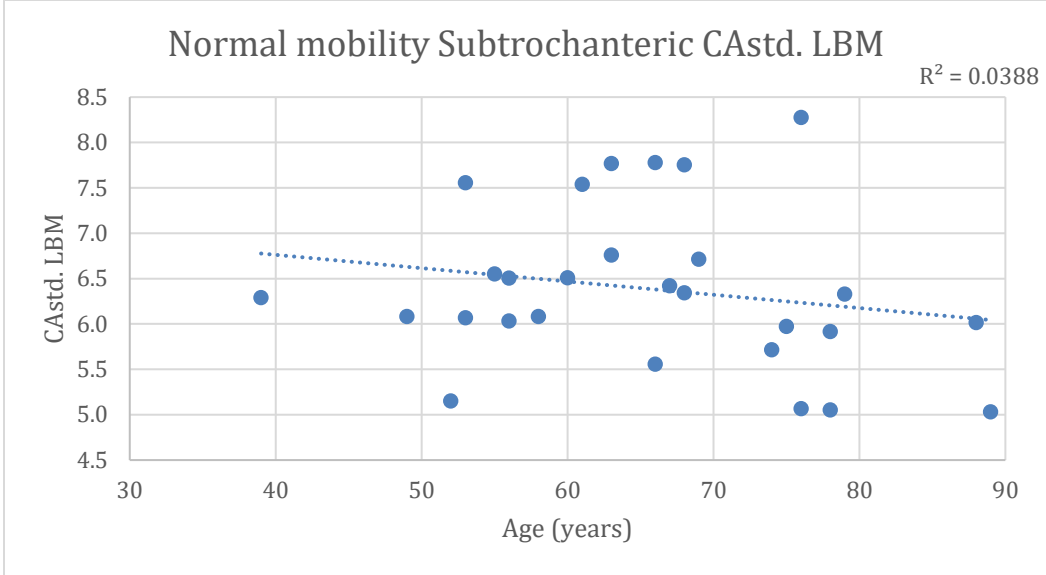


Normal mobility Subtrochanteric TA

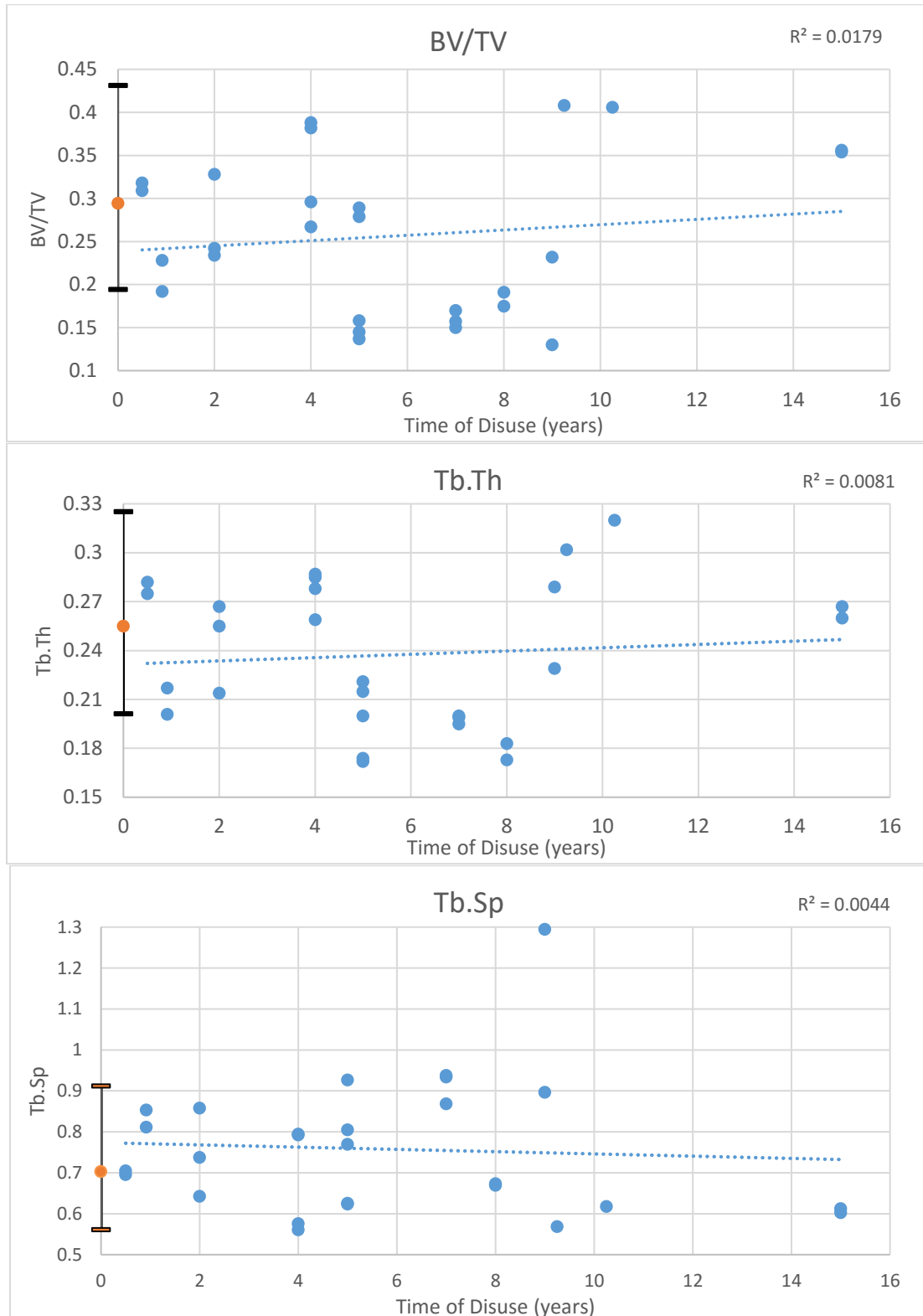


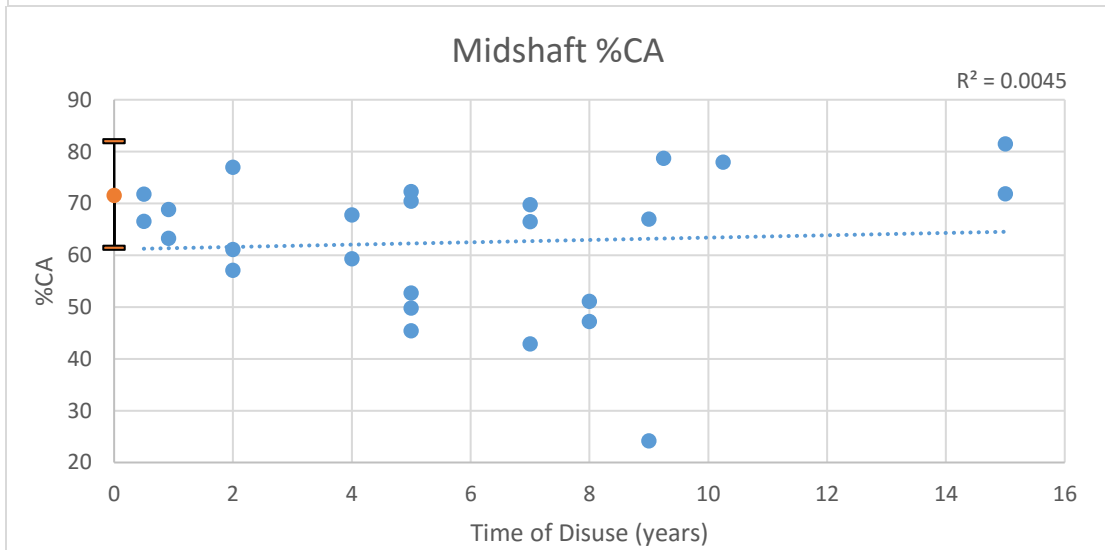
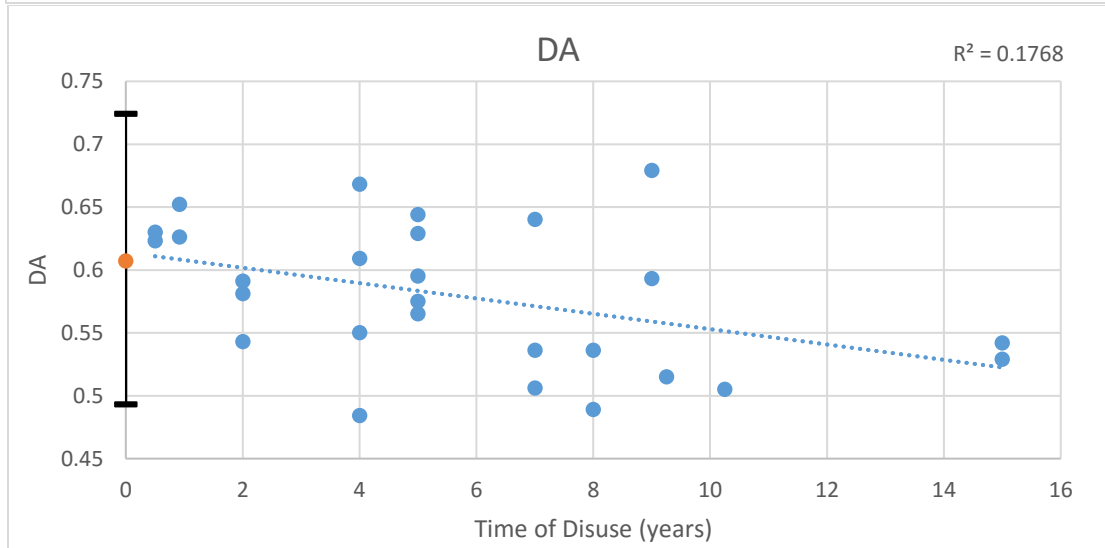
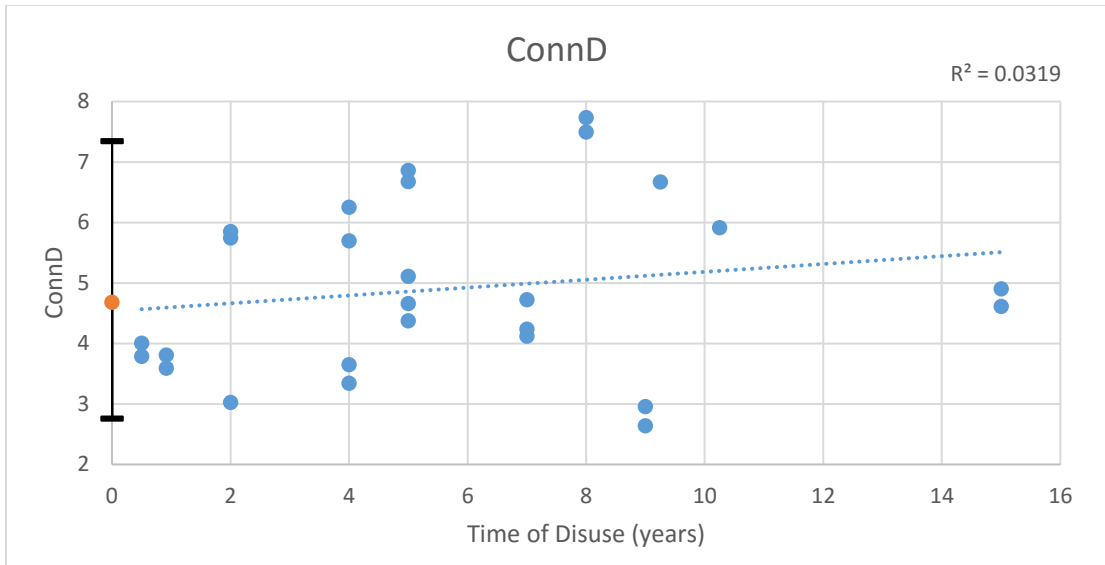


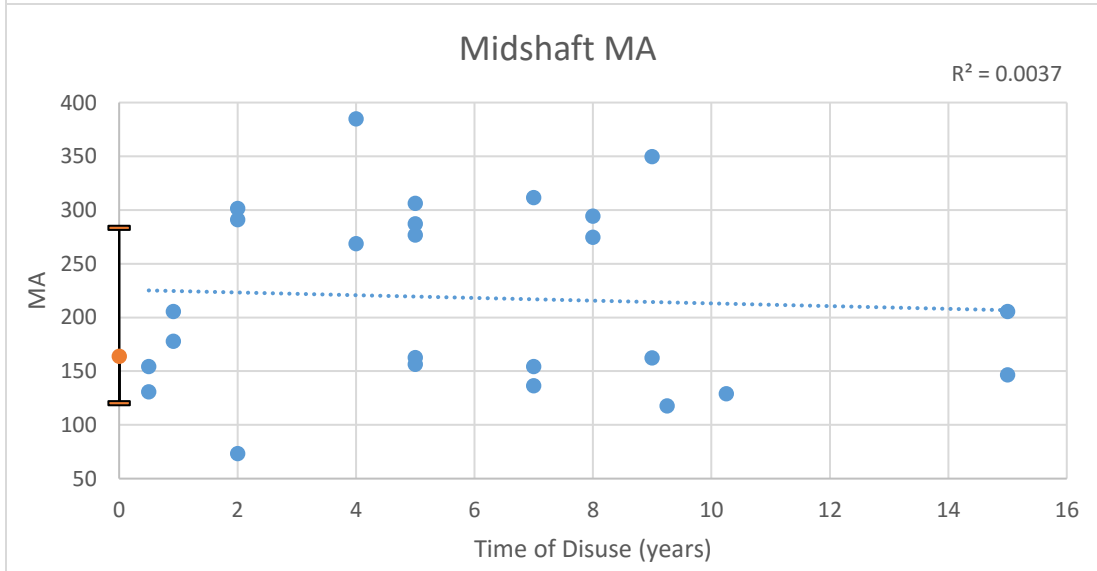
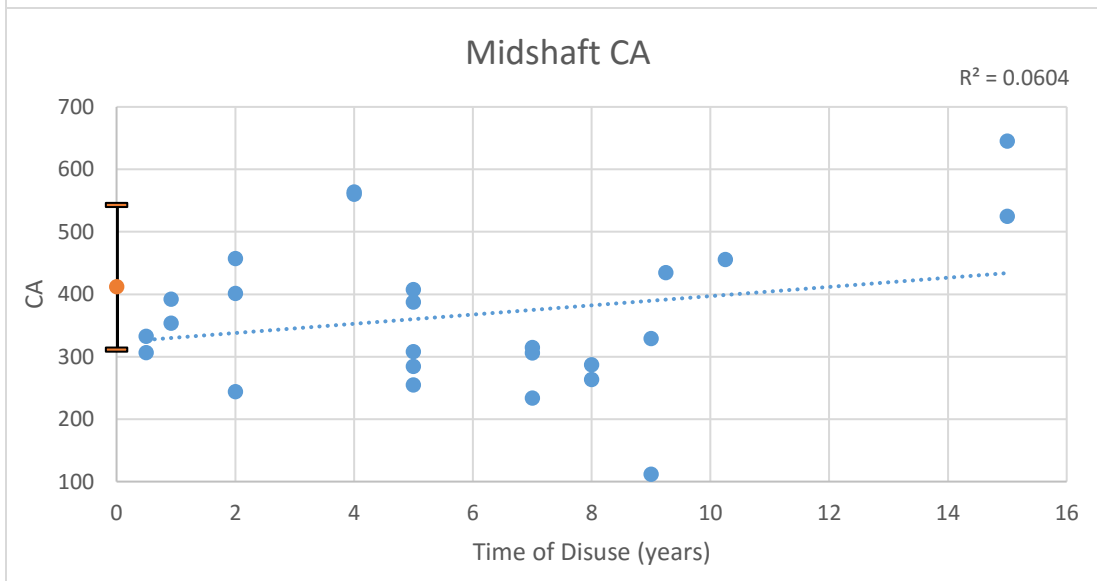
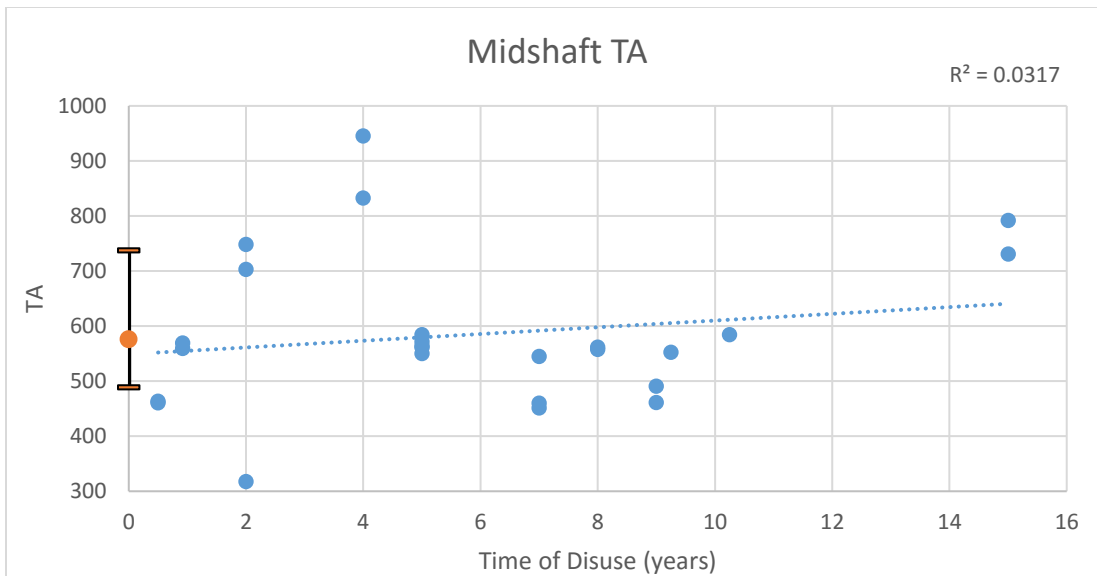


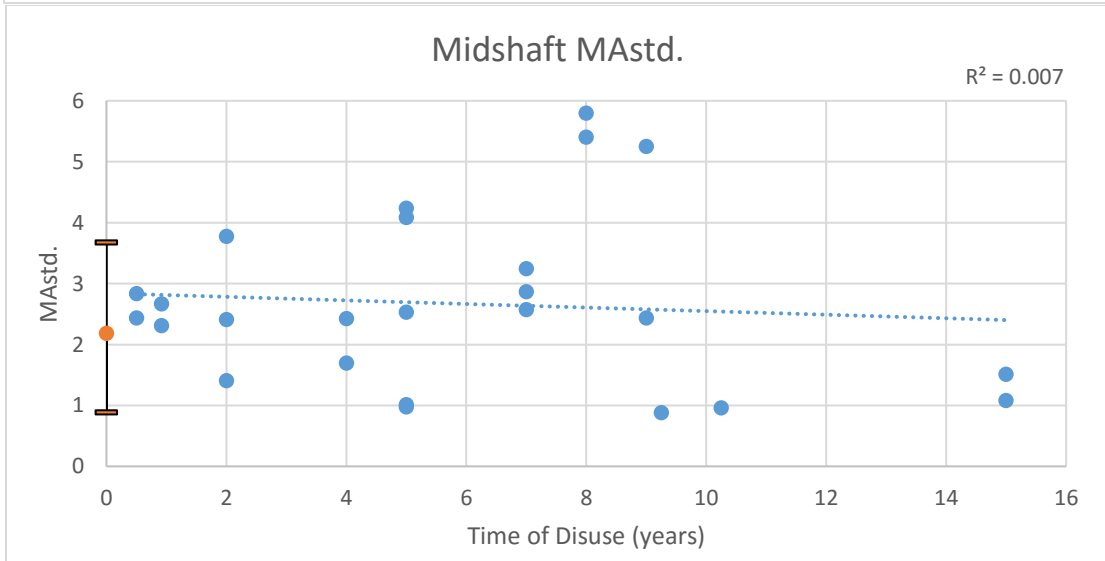
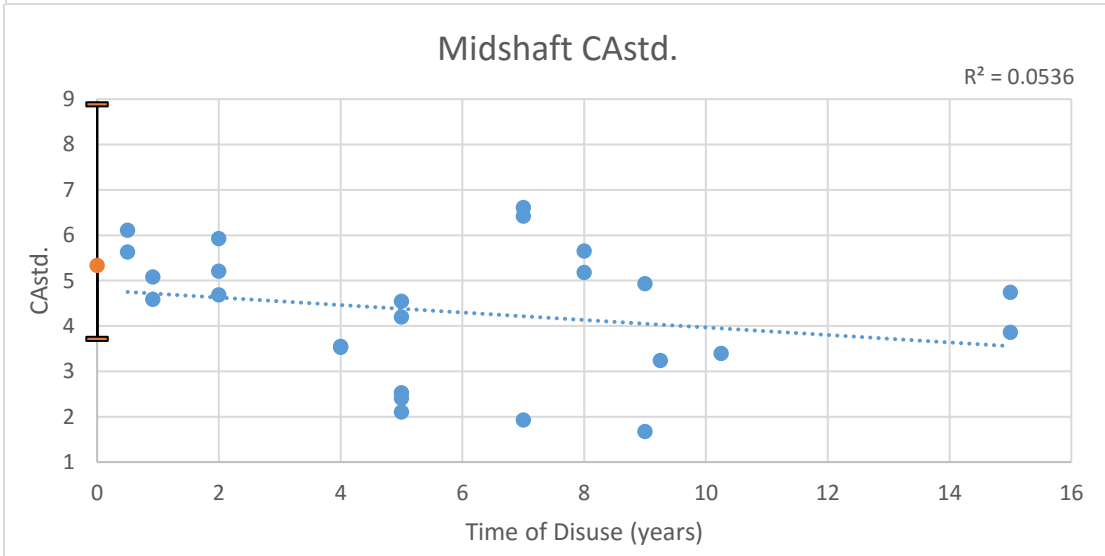
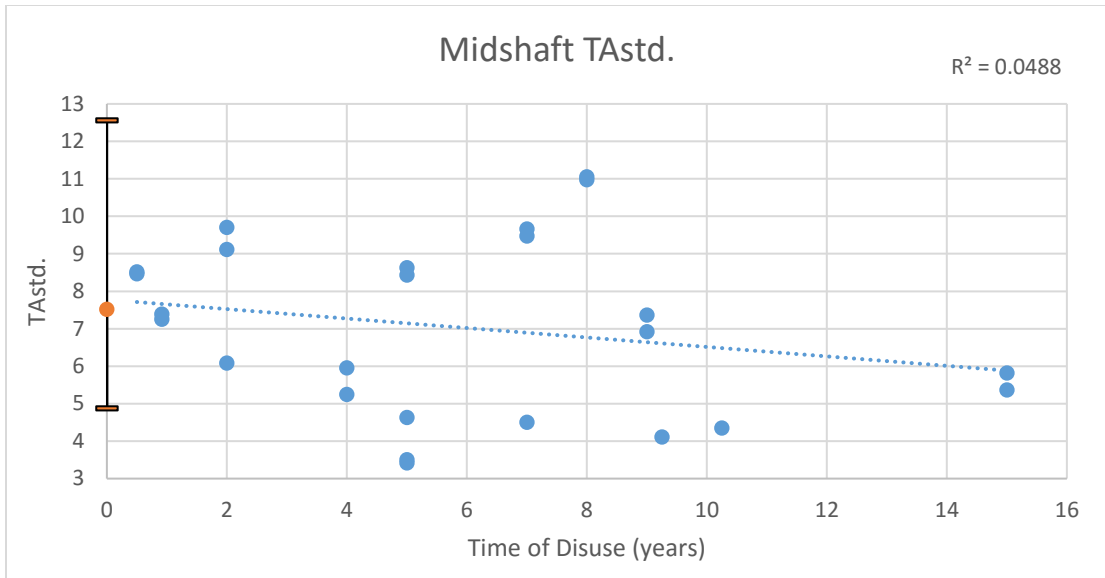


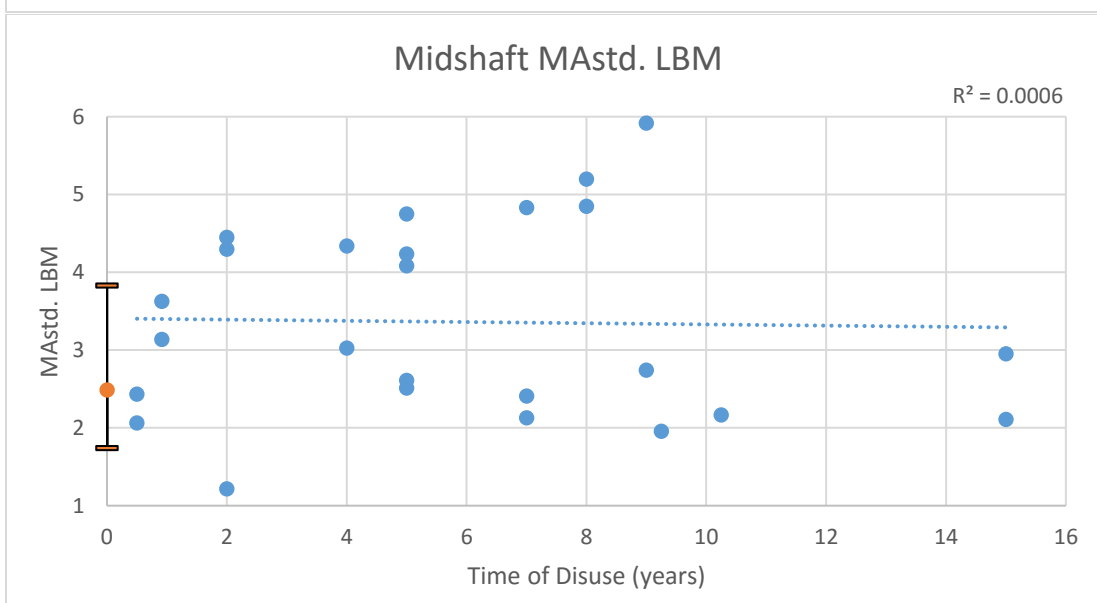
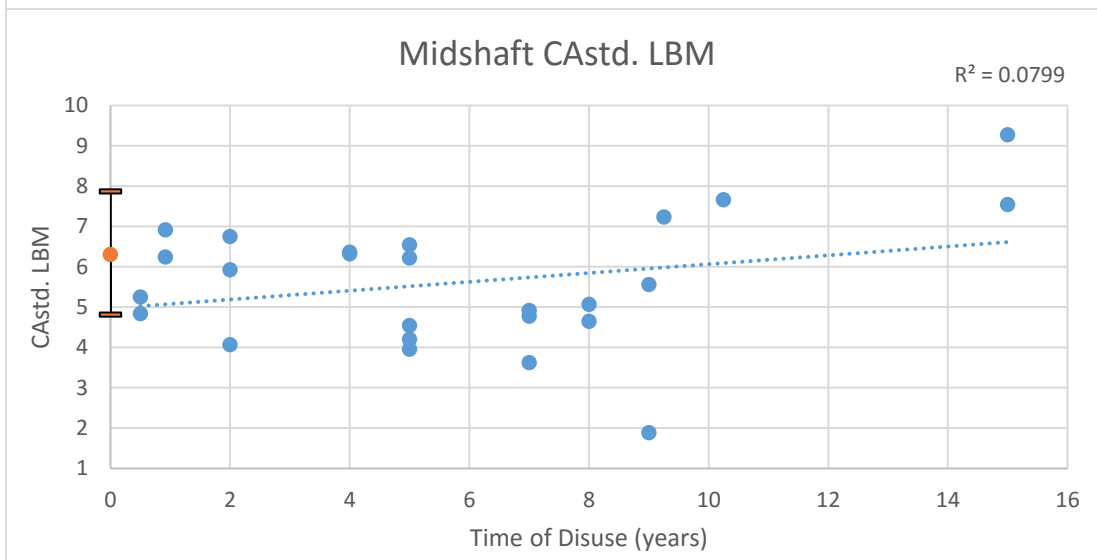
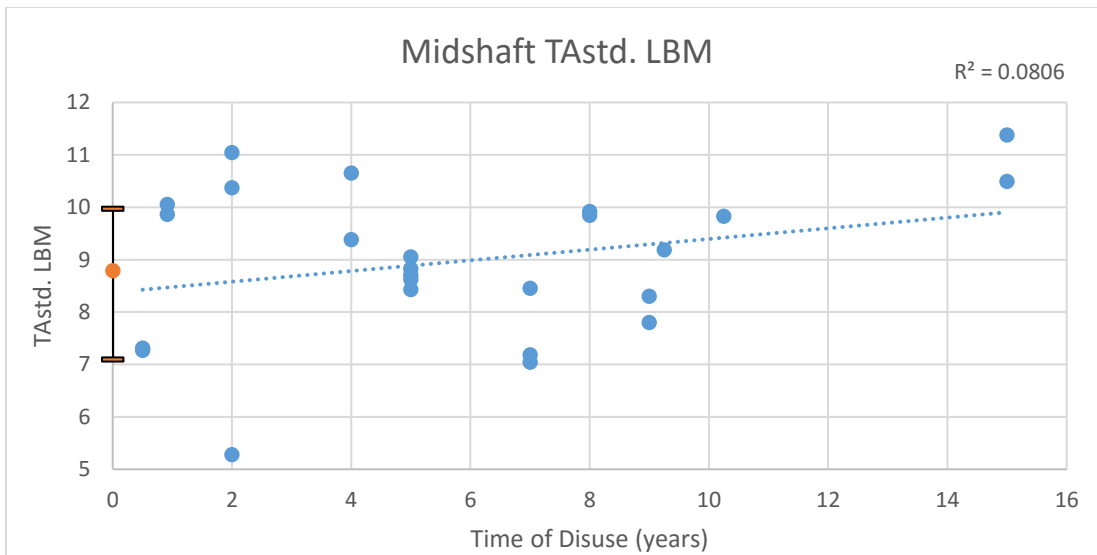
Appendix I. Scatterplots of the trabecular and cortical bone properties regressed against the amount of time of disuse in years. The mean (orange dot) and range (error bars) of the matched normal mobility samples is plotted at 0 years of disuse.

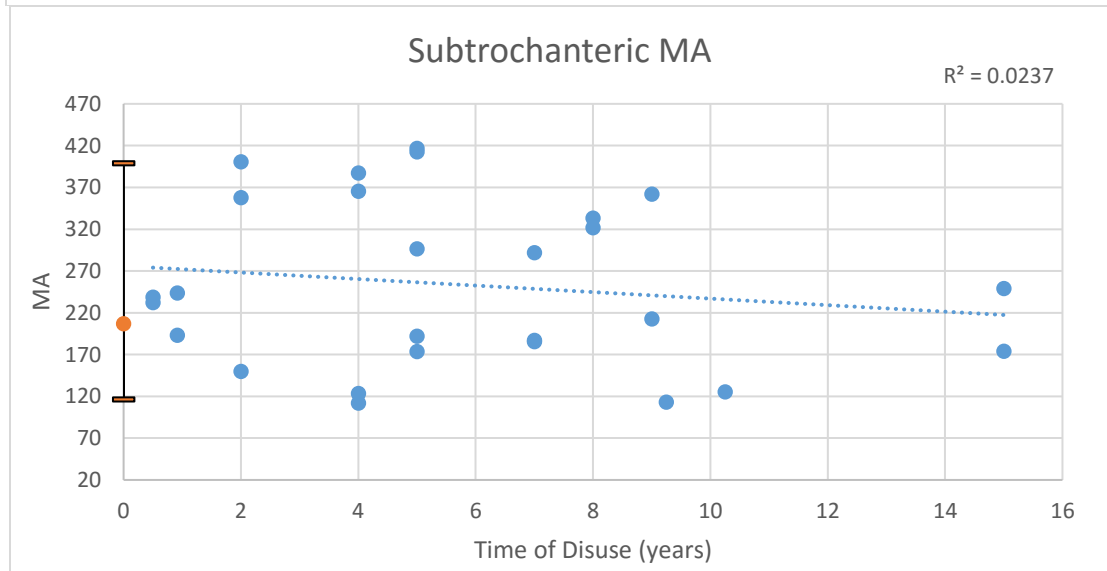
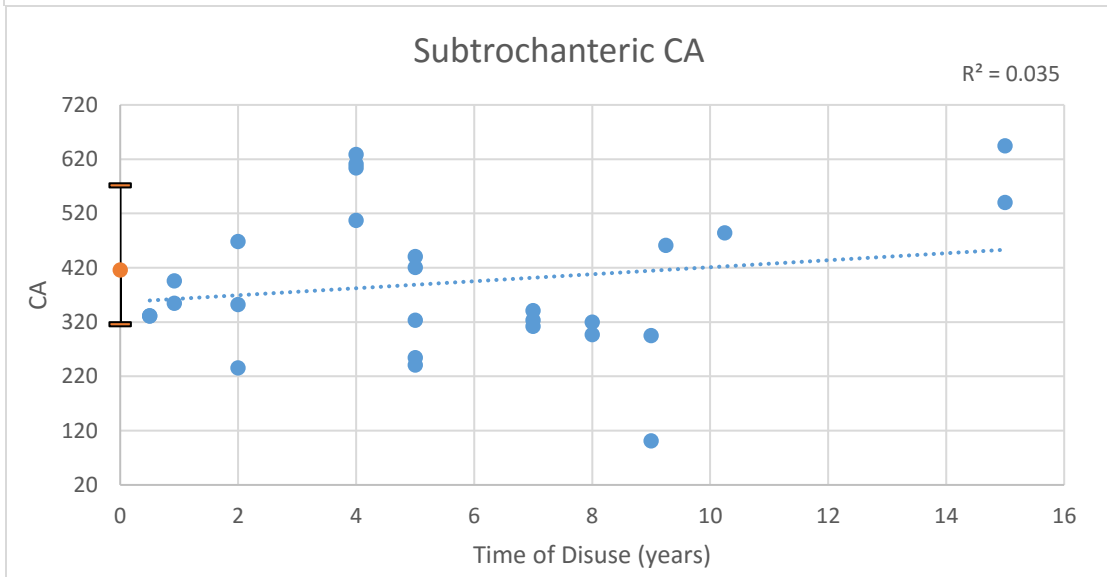
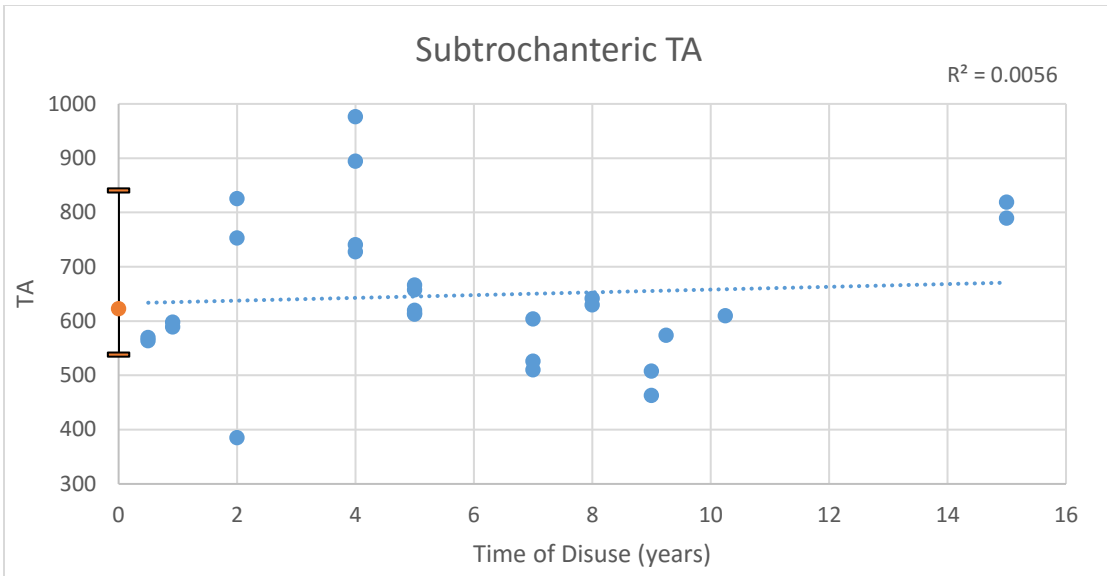


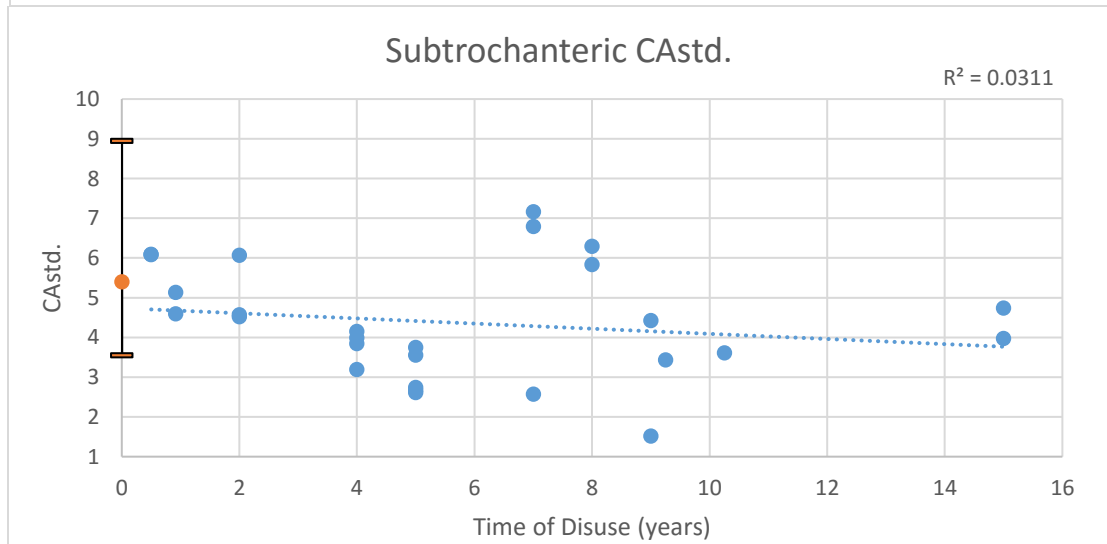
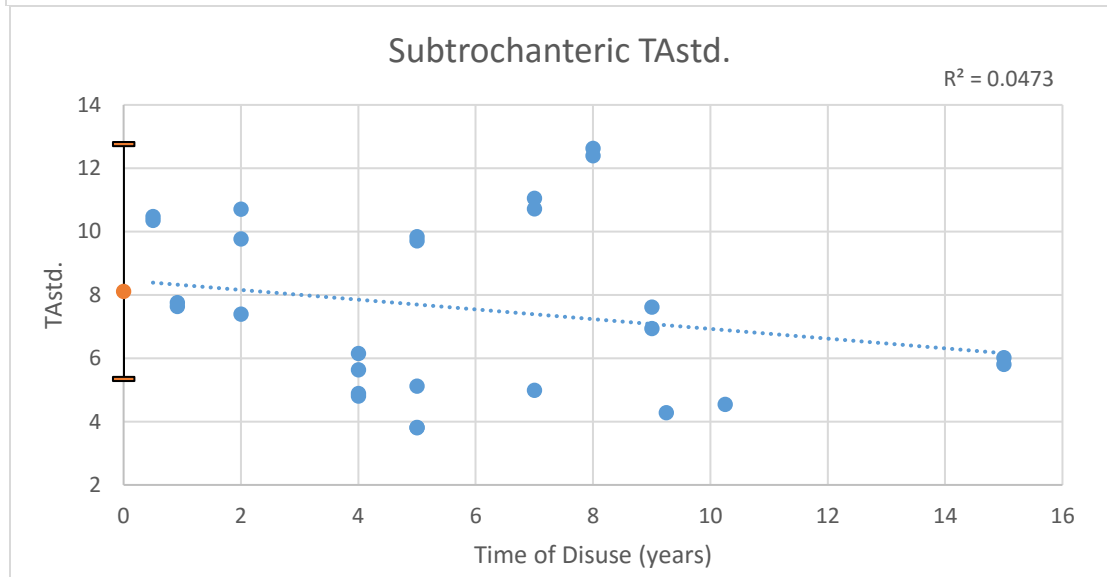
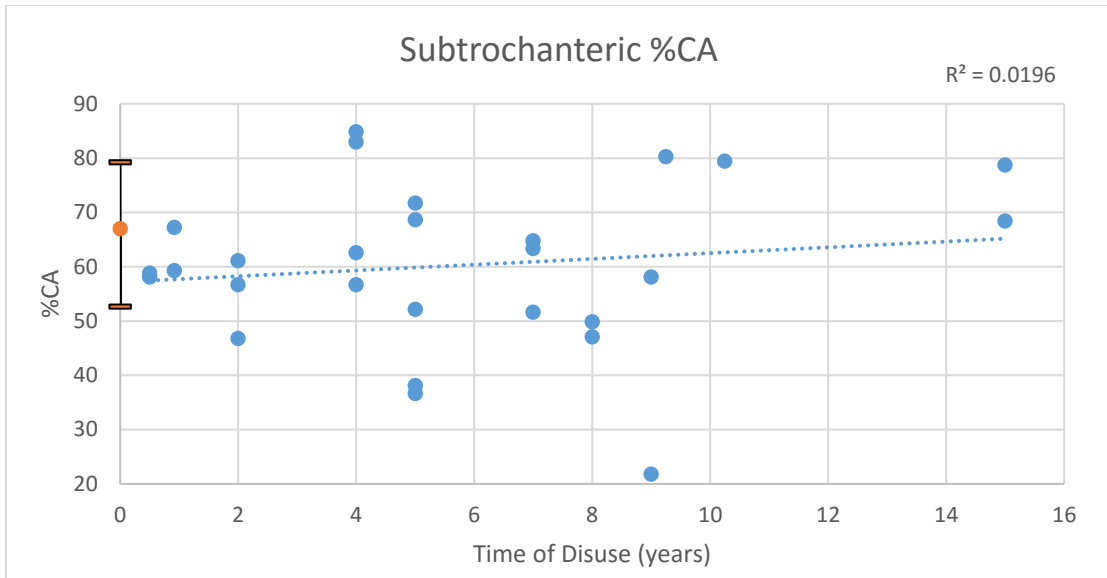


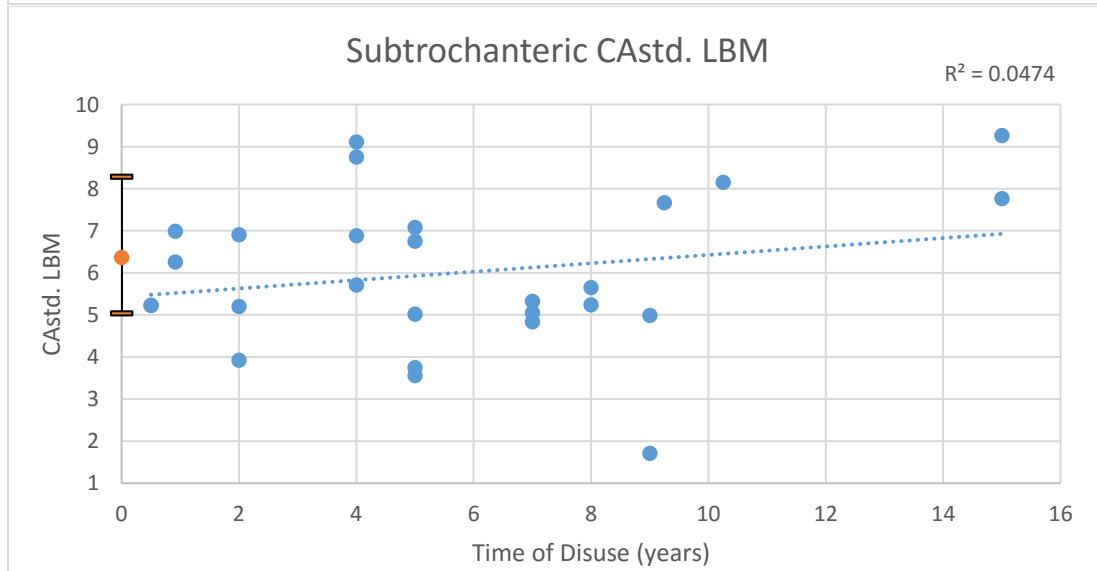
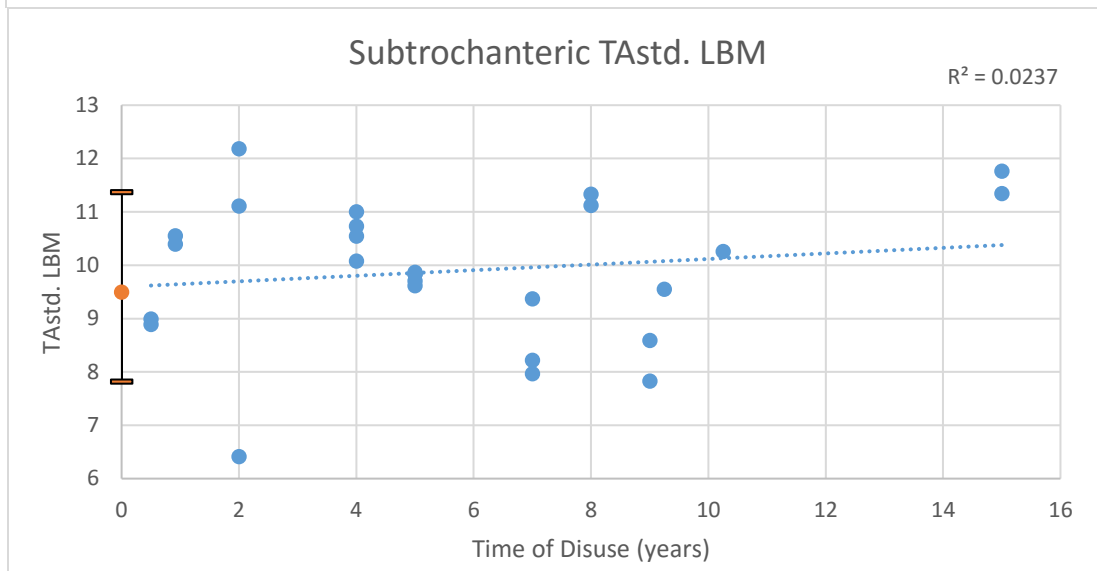
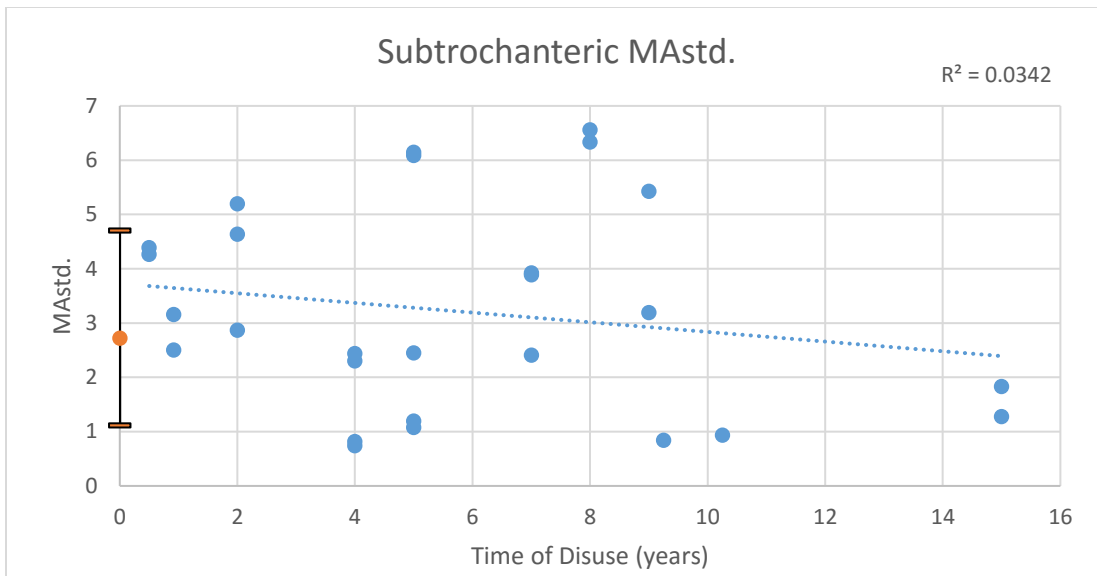


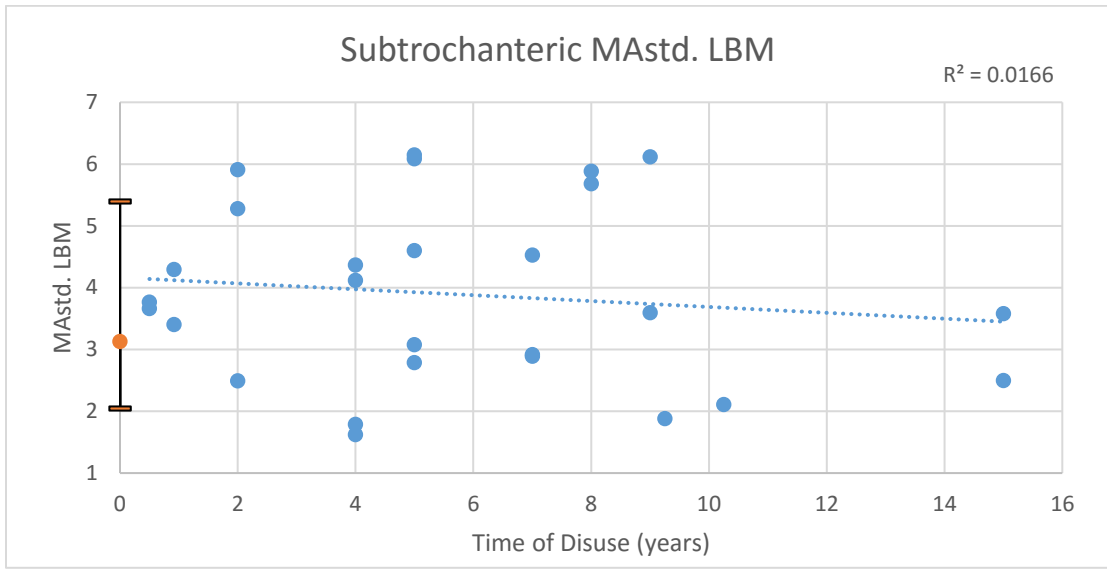




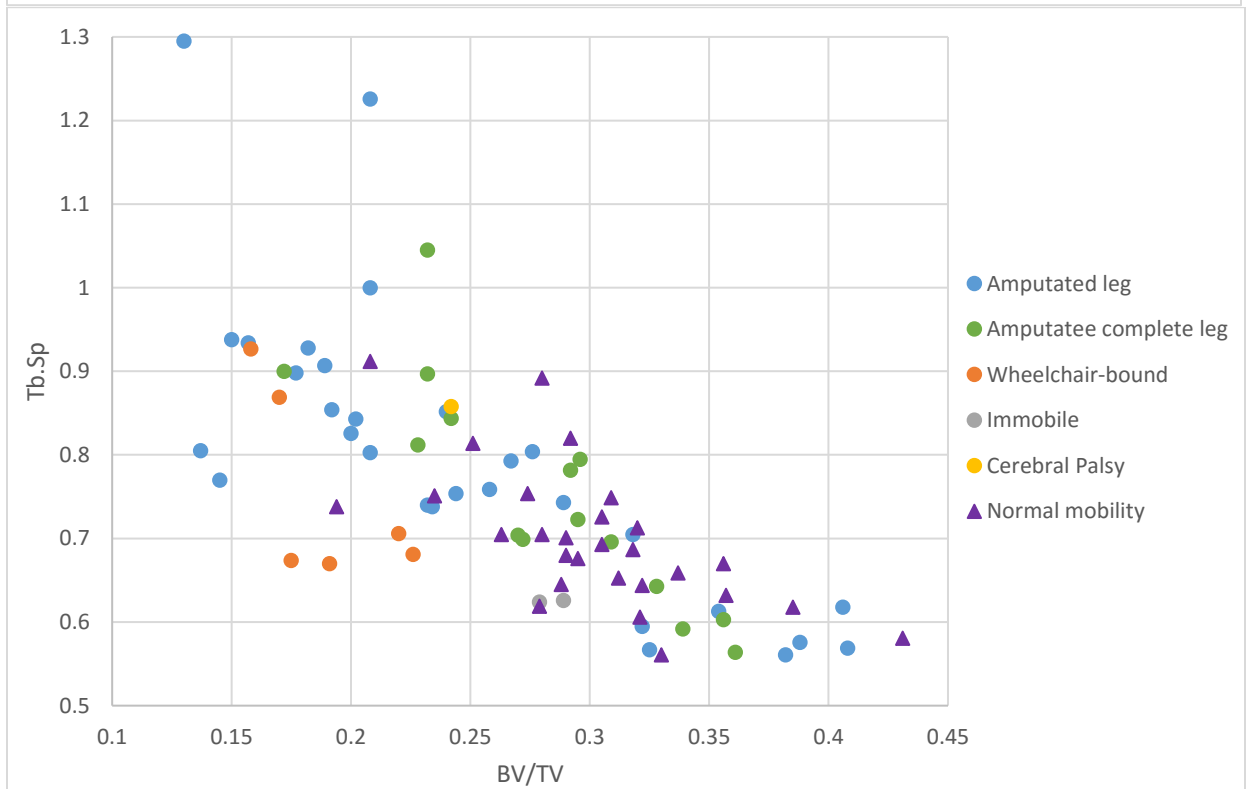
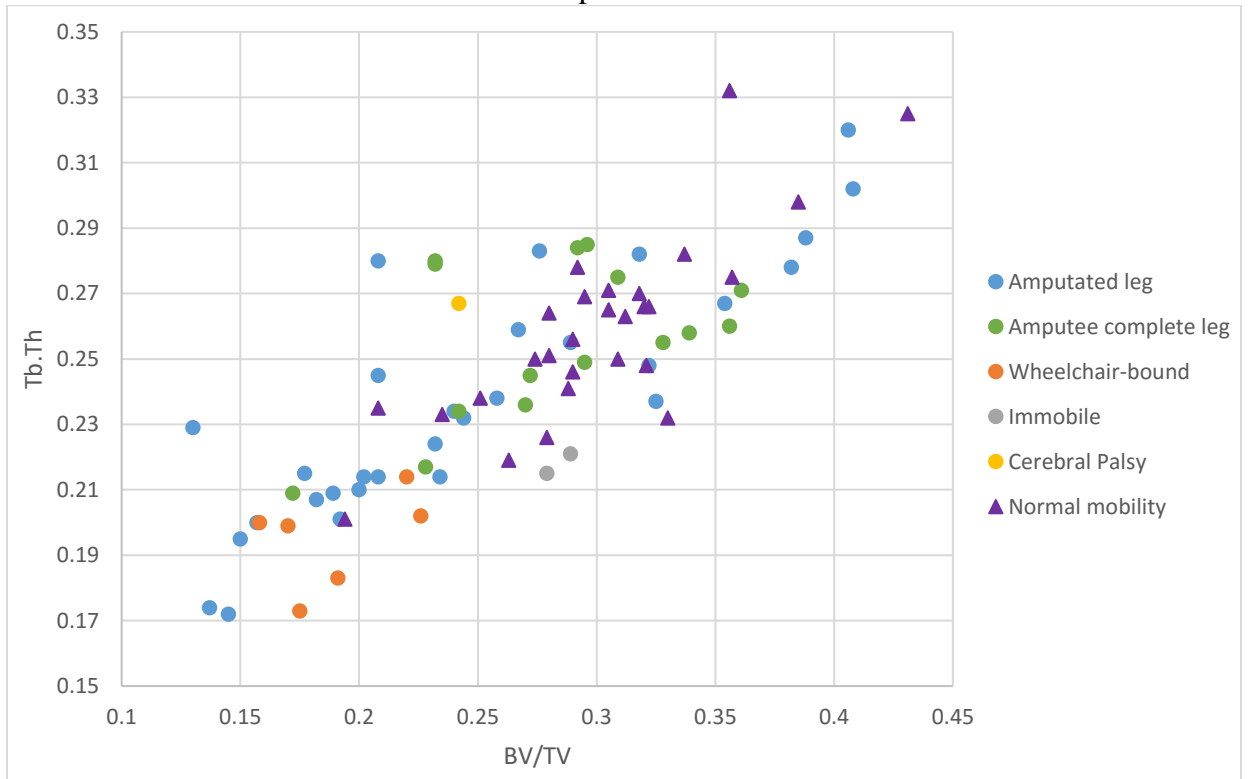


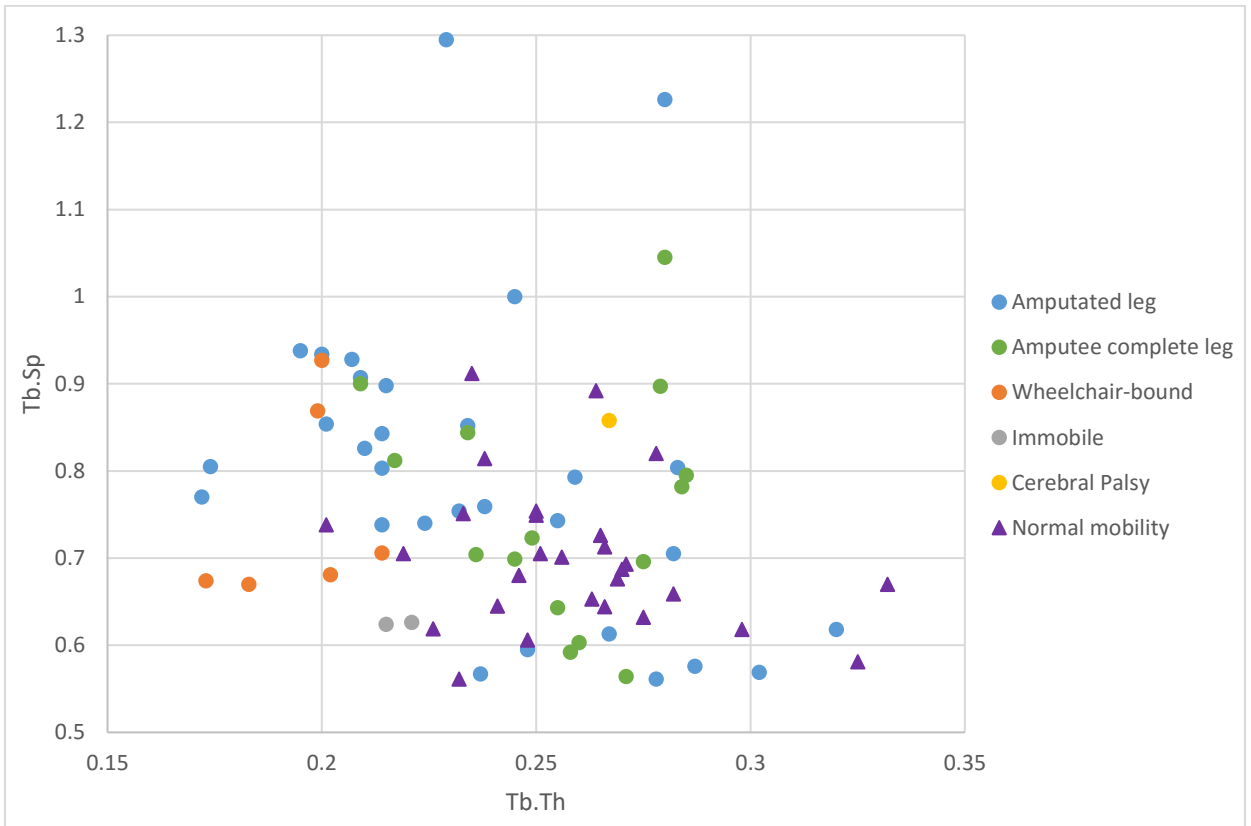






Appendix J. Additional scatterplots regressing the significant trabecular properties against one another: BV/TV and Tb.Th, BV/TV and Tb.Sp, and Tb.Th and Tb.Sp for the mobility impaired samples separated by impairment type and the normal mobility samples.





REFERENCES

- Auerbach BM, Ruff CB. 2004. Human body mass estimation: a comparison of “morphometric” and “mechanical” methods. *Am J Phys Anthropol* 125:331-342.
- Biering-Sørensen F, Bohr HH, Schaadt OP. 1990. Longitudinal study of bone mineral content in the lumbar spine, the forearm and the lower extremities after spinal cord injury. *Eur J Clin Invest* 20:330-335.
- Bouvard B, Mabilieu G, Legrand E, Audran M, Chappard D. 2012. Micro and macroarchitectural changes at the tibia after botulinum toxin injection in the growing rat. *Bone* 50:858-864.
- Bouxsein ML, Boyd SK, Christiansen BA, Guldberg RE, Jepsen KJ, and Müller R. 2010. Guidelines for assessment of bone microstructure in rodents using micro-computed tomography. *J Bone and Miner Res* 25:1468-1486.
- Dionyssiatis Y, Trovas G, Galanos A, Raptou P, Papaioannou N, Papagelopoulos P, Petropoulou K, Lyritis GP. 2007. Bone loss and mechanical properties of tibia in spinal cord injured men. *J Musculoskelet Neuronal Interact* 7:62-68.
- Doube M, Klosowski MM, Arganda-Carreras I, Cordelières F, Dougherty RP, Jackson J, Schmid B, Hutchinson JR, Shefelbine SJ. 2010. BoneJ: free and extensible bone image analysis in ImageJ. *Bone* 47:1076-1079.
- Ericksen MF. 1979. Aging changes in the medullary cavity of the proximal femur in American blacks and whites. *Am J Phys Anthropol* 51:563-570.
- Eser P, Frotzler A, Zehnder Y, Wick L, Knecht H, Denoth J, Schiessl H. 2004. Relationship between the duration of paralysis and bone structure: a pQCT study of spinal cord injured individuals. *Bone* 34:869-880.
- Fajardo RJ, Müller R. 2001. Three-dimensional analysis of nonhuman primate trabecular architecture using micro-computed tomography. *Am J Phys Anthropol* 115:327-336.
- Fajardo RJ, Müller R, Ketcham RA, Colbert M. 2007. Nonhuman anthropoid primate femoral neck trabecular architecture and its relationship to locomotor mode. *Anat Rec* 290:422-436.
- Frey-Rindova P, de Bruin ED, Stussi E, Dambacher MA, Dietz V. 2000. Bone mineral density in upper and lower extremities during 12 months after spinal cord injury measured by peripheral quantitative computed tomography. *Spinal Cord* 38:26-32.
- Frost HM. 2003 Bone's mechanostat: a 2003 update. *Anat Rec* 275A:1081-1101.

- Frost HM. 1996. Perspectives: a proposed general model for the mechanostat (suggestions from a new paradigm). *Anat Rec* 244:139–147.
- Gleiber DS, Skipper CE, Cunningham DL, Wescott DJ. 2016. Variation in the trabecular structure of the proximal tibia between obese and non-obese females. In: Program of the 85th Annual Meeting of the American Association of Physical Anthropologists. *Am J Phys Anthropol* 159:3-346.
- Gocha TP, Agnew AM. 2016. Spatial variation in osteon population density and the human femoral midshaft: histomorphometric adaptations to habitual load environment. *J Anat* 228:733-745.
- Gross TS, Akeno N, Clemens TL, Komarova S, Srinivasan S, Weimer DA, Mayorov S. 2001. Selected contribution: Osteocytes upregulate HIF-1alpha in response to acute disuse and oxygen deprivation. *J Appl Physiol* 90:2514–2519.
- Hazelwood SJ, Martin BR, Rashid MM, Rodrigo JJ. 2001. A mechanistic model for internal bone remodeling in disuse and overload. *J Biomech* 34:299-308.
- Holt BM. 2003. Mobility in Upper Paleolithic and Mesolithic Europe: evidence from the lower limb. *Am J Phys Anthropol* 122:200-215.
- Huiskes R, Ruimerman R, van Lenthe GH, Janssen JD. 2000. Effects of mechanical forces on maintenance and adaptation of form in trabecular bone. *Nature* 405:704-706.
- Huiskes R. 1982. On the modelling of long bones in structural analyses. *J Biomech* 15:65-69.
- Judex S, Donahue LR, Rubin C. 2002. Genetic predisposition to low bone mass is paralleled by an enhanced sensitivity to signals anabolic to the skeleton. *FASEB J* 16:1280–1282.
- Ketcham RA, Ryan TM. 2004. Quantification and visualization of anisotropy in trabecular bone. *J Microsc* 213:158-171.
- Ketcham RA. 2005b. Three-dimensional textural measurements using high-resolution X-ray computed tomography. *J Struct Geol* 27:1217-1228.
- Lerebours C, Buenzli PR. 2016. Towards a cell-based mechanostat theory of bone: the need to account for osteocyte desensitisation and osteocyte replacement. *J Biomech* 49:2600-2606.
- Mullender MG, Hiskes R, Versleyen H, Buma P. 1996. Osteocyte density and histomorphometric parameters in cancellous bone of the proximal femur in five mammalian species. *J Orthop Res* 14:972-979.

North Star Imaging, Inc. efX_{CT}: Computed Tomography Reconstruction and Visualization software version 1.7.97.0.

North Star Imaging, Inc. efX_{DR}: Digital Radiography and CT Acquisition Software version 1.1.97.6.

Odgaard A, Gundersen HJG. 1993. Quantification of connectivity in cancellous bone, with special emphasis on 3-D reconstructions. *Bone* 14:173-182.

Qin Y, Lin W, Mittra E, Xia Y, Cheng J, Judex S, Rubin C, Müller R. 2013. Prediction of trabecular bone qualitative properties using scanning quantitative ultrasound. *Acta Astronaut* 92:79-88.

Robin J, Graham HK, Selber P, Dobson F, Smith K, Baker R. 2008. Proximal femoral geometry in cerebral palsy a population-based cross-sectional study. *J Bone Joint Surg Br.* 90:1372-1379.

Ryan TM, Shaw CN. 2015. Gracility of the modern *Homo sapiens* skeleton is the result of decreased biomechanical loading. *PNAS* 112:372-377.

Rubin C, Rubin J. 2006. Biomechanics and mechanobiology of bone. In: Favus, MJ, editor. *Primer on Metabolic Bone Diseases and Disorders of Mineral Metabolism*. Sixth Edition. Washington D.C.: American Society for Bone and Mineral Research. p 36-42.

Ruff C, Holt B, Trinkaus E. 2006. Who's afraid of the big bad Wolff? "Wolff's law" and bone functional adaptation. *Am J Phys Anthropol* 129:484-498.

Ruff CB. 2008. Biomechanical analyses of archaeological human skeletons. In: Katzenberg MA, Saunders SR, editors. *Biological anthropology of the human skeleton, second edition*. Hoboken: John Wiley & Sons, Inc. p 183-206.

Sanyal A, Gupta A, Bayraktar HH, Kwon RY, Keaveny TM. 2012. Shear strength behavior of human trabecular bone. *J Biomech* 45:2513-2519.

Shaw CN, Ryan TM. 2012. Does skeletal anatomy reflect adaptation to locomotor patterns? Cortical and trabecular architecture in human and nonhuman anthropoids. *Am J Phys Anthropol* 147:187-200.

Sievänen H. 2010. Immobilization and bone structure in humans. *Arch Biochem Biophys* 503:146-152.

Simske SJ, Guerra KM, Greenberg AR, Luttges MW. 1992. The physical and mechanical effects of suspension-induced osteopenia on mouse long bones. *J Biomech* 25:489-499.

Skerry TM. 2008. The response of bone to mechanical loading and disuse: fundamental principles and influences on osteoblast/osteocyte homeostasis. *Arch Biochem Biophys* 473:117-123.

Stock JT. 2006. Hunter-gatherer postcranial robusticity relative to patterns of mobility, climatic adaptation, and selection for tissue economy. *Am J Phys Anthropol* 131:194-204.

Tardieu C. 2010. Development of the human hind limb and its importance for the evolution of bipedalism. *Evol Anthropol* 19:174-186.

Turunen MJ, Prantner V, Jurvelin JS, Kröger H, Isaksson H. 2013. Composition and microarchitecture of human trabecular bone change with age and differ between anatomical locations. *Bone* 54:118-125.

Vico L, Lafage-Proust MH, Alexandre C. 1998. Effects of gravitational changes on the bone system in vitro and in vivo. *Bone* 22:95–100.

Wescott DJ. 2008. Biomechanical analysis of humeral and femoral structural variation in the Great Plains. *Plains Anthropol* 53:333-355.

Wescott DJ. 2014. The relationship between femur shape and terrestrial mobility patterns. In: Carlson KJ and Marchi D, editors. *Reconstructing Mobility*. New York: Springer US. p 111-132.